Design and Application of Nanostructured Flavin Photocatalysts

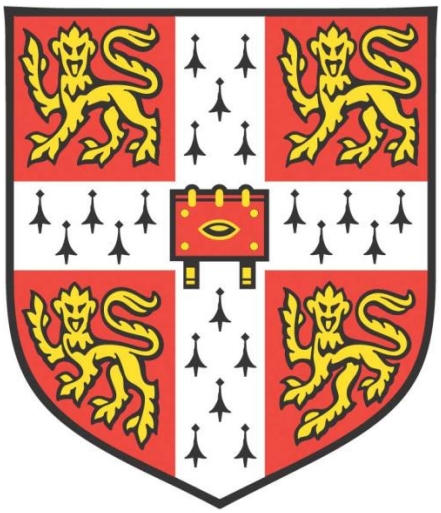

Leander Brian Crocker

Fitzwilliam College

Department of Chemical Engineering & Biotechnology

University of Cambridge

This thesis is submitted for the degree of Doctor of Philosophy

August 2020

DECLARATION

This thesis is the result of my own work and includes nothing which is the outcome of work done in collaboration except where specified in the text. It is not substantially the same as any that I have submitted, or, is being concurrently submitted for a degree or diploma or other qualification at the University of Cambridge or any other University or similar institution except as declared in the Preface and specified in the text. I further state that no substantial part of my dissertation has already been submitted, or, is being concurrently submitted for any such degree, diploma or other qualification at the University of Cambridge or any other University or similar institution except as declared in the Preface and specified in the text.

In accordance with the Department of Engineering guidelines, this thesis does not exceed 65,000 words, and it contains less than 150 figures.

_____

August 2020

Leander Brian Crocker

ABSTRACT

Flavin compounds are found in Nature within a range of flavin-containing enzymes (flavoenzymes) that are responsible for metabolic, antioxidant and photoreception processes across animal, plant and bacteria kingdoms. Their broad redox and photochemistry has seen the field of flavin-based catalysis emerge as a powerful addition to sustainable catalysis thanks to being cheap, non-toxic and highly active. Flavin photocatalysis in particular has shown great promise in a range of synthetic procedures such as benzylic oxidations, sulfoxidations, decarboxylative transformations, isomerisations and [2+2] cycloadditions to name a few. It has been shown that flavin photocatalysts can be tuned to a specific application either through chemical structure modification or by the design of advanced systems through heterogeneous or polymer carrier attachment. The latter has shown encouraging results to widen flavin photocatalyst applicability within organic synthesis but has lacked in displaying characteristics like flavoenzymes which enable highly efficient and selective catalysis of industrially relevant products with precise stereochemical control. This thesis details the design and application of novel flavin photocatalysts through the combination of polydopamine (PDA). It is shown that PDA not only acts as a carrier of the flavin, but actively engages in the catalytic mechanism and improves flavin photostability.

In the first instance, copolymer flavin-polydopamine (**FLPDA**) nanoparticles were synthesised and their photocatalytic activity was characterised through model oxidation and reduction reactions. This study revealed enzyme-like kinetics of the catalysed reactions and improved photostability of the conjugated flavin moieties. Additionally, the biocompatibility of the nanoparticles was assessed through *in vitro* cell studies to ensure applicability to other fields such biomedicine or water remediation. Subsequently, the flavoenzyme specific oxidation of indole to indigo and indirubin dyes was explored using the **FLPDA** photocatalyst. The results showed that the nanoparticle system exhibited higher production of the valuable dyes over a homogeneous flavin photocatalyst. This increase in activity was investigated through reactive oxygen species (ROS) scavenging experiments which revealed that **FLPDA**'s

mechanism of action in this reaction partially resembled natural flavoenzymes and therefore enhanced key product formation.

Finally, reduction reactions catalysed by flavoenzymes were investigated using **FLPDA** and a chiral flavin-polydopamine system (**RCPDA**). The light-driven reduction of azobenzene dyes was first explored using **FLPDA** which provided evidence that hydride could be transferred from PDA-conjugated flavin moieties to a substrate upon irradiation in the presence of an electron donor reagent. Next, the reduction of C=C bonds within α,β-unsaturated ketones and aldehydes was explored by initially screening buffered electron donor reagents and homogeneous flavin photocatalysts with key substrates. The optimal conditions and compatible substrates were then applied to the nanoparticle **RCPDA** system which produced the saturated products in comparable yields to the homogeneous photocatalysts with very low catalyst loading (<1 mol% vs. 10 mol%). The inclusion of a chiral linkage between PDA and flavin and its effect on the stereochemical outcome of the reaction was also explored, with preliminary data showing that adopting such a strategy could enable some enantioselectivity over the product.

In summary, this thesis provides new methodologies to design advanced flavin photocatalysts with enzyme-like characteristics that will help to further develop the field of sustainable catalysis.

ACKNOWLEDGEMENTS

Firstly, I want to thank Dr. Ljiljana Fruk for giving me this opportunity to explore science within her lab and providing endless motivation, support and guidance. I have grown not just as a scientist but also as a person during my time working with you, for which I will be forever grateful. Thank you for your mentorship and belief in my ideas that have allowed my creativity to flourish. I am looking forward to exploring more ideas with you in the future and having more discussions about the crazy world we live in!

I wish to thank Dr. Antonina (Tonya) Kerbs for her endless patience and compassion, selfless dedication to the lab and her little lab brothers. You are an amazing scientist and set the perfect example. You have helped me develop so much as a chemist and I don't think my work would have ever progressed so far without your support. I wish you all the best for the future and hope we can meet again soon.

To Sam Nehme, my brother who I started this roller coaster journey with, thank you for being the friend I could always rely on through thick and thin. Thank you for your honesty and council when life got tough and thank you for the joy and happiness we've had during the good times. I know this is not the end, and I look forward to riding the roller coaster some more with you, hands up, no cares.

Special thanks to Christoph Franck, my German chemist counterpart, for welcoming me to Cambridge and your friendship and support thereafter. I look forward to more special times on the decks with you.

I wish to thank all the other past and present members of the Fruk Lab I have worked with, specifically, Dr. Olatz Guaresti, Dr. Andrea Bistrovic, Dr. Badri Parshad, Dr. Ishtaiq Ahmed, Dr. Hirak Patra, Bill Stockham, Drew Baker, Harry Zhu, Sunniya Iftikhar, Will Etheridge, Swetha Lingamgunta, Suraj Pavagada, Maxime Crebe, Patrick Bernhard and Daniel Heid.

Thanks to my Physics collaborators in the Nanophotonics Centre: Dr. Philipp Koehler, Dr. Alex Gentleman, Dr. Ermanno Miele, Omid Siddiqui, Takashi Lawson and Dr. Tijmen Euser for their amazing ideas, friendship and music tastes.

Special thanks to all the technicians and staff in the CEB department for their help over the years. Thanks also to Duncan Howe and Andrew Mason from the NMR team in Chemistry, as well as Dr. Dijana Matak-Vinkovic, Dr. Roberto Canales and Asha Boodhun from the Mass Spec team in Chemistry. Many thanks to Dr. Richard Langford and Dr. John J. Rickard from the EM facility in Physics.

I also wish to thank the Cambridge University Lacrosse Club which has played a massive role in my life and contributed greatly towards my experience here. All the friends I have made from the club will stay with me forever and I will always be grateful for what the sport has given me.

I am truly grateful to my close friends and family who have supported, loved and believed in me every step of the way.

Finally, the UKRI is acknowledged for funding this work and the Leathersellers' Company and Fitzwilliam College is thanked for additional support.

PUBLICATIONS ARISING FROM THIS THESIS

i. Enzyme-inspired flavin–polydopamine as a biocompatible nanoparticle photocatalyst

   L. Crocker, P. Koehler, P. Bernhard, A. Kerbs, T. Euser, L. Fruk, *Nanoscale Horizons*, **2019**, *4*, 1318-1325.

ii. Flavin-conjugated polydopamine nanoparticles displaying light-driven monooxygenase activity

   L. Crocker, L. Fruk, *Frontiers in Chemistry*, **2019**, *7*, 278.

iii. Flavin-conjugated iron oxide nanoparticles as enzyme-inspired photocatalysts for azo dye degradation

   S. Nehme, L. Crocker, L. Fruk, *Catalysts*, **2020**, *10*, 324.

CONTENTS

List of Tables

List of Figures

List of Abbreviations and Acronyms

A549	Adenocarcinomic human alveolar basal epithelial cells
AR	Amplex Red
ATRP	Atom transfer radical polymerisation
AzoR	Atom transfer radical polymerisation
BLUF	Blue-Light-Utilizing flavin adenine dinucleotide
BNAH	1-Benzyl-1,4-dihydronicotinamide
BVMO	Baeyer–Villiger monooxygenase
CRY	Cryptochrome
cm	Centimetre
DABCO	1,4-Diazabicyclo[2.2.2]octane
DCM	Dichloromethane
DIPEA	Diisopropylethylamine
DLS	Dynamic light scattering
DMEM	Dulbecco's modified Eagle's medium
DMF	*N,N*-Dimethylformamide
DNA	Deoxyribonucleic acid
DOPAC	Dihydroxyphenylacetic acid
ee	Enantioselective excess
EDTA	Ethylendiaminotetracetic acid
ER	Ene-reductase
ESI	Electrospray ionisation
EtOAc	Ethyl acetate
FBS	Foetal bovine serum
FL	Flavin
FLDA	Flavin-DOPAC
FLPDA	Flavin-Polydopamine
FMN	Flavin mononucleotide
FMO	Flavin monooxygenase
FTIR	Fourier transform infrared spectroscopy
g	Gram

GC-MS	Gas chromatography mass spectrometry
HATU	Hexafluorophosphate azabenzotriazole tetramethyl uronium
HEMO	4-(2-Hydroxyethyl)morpholine
HPLC	High pressure liquid chromatography
HRMS	High-resolution mass spectrometry
IPA	Isopropanol
ISC	Intersystem crossing
KPi	Potassium phosphate buffer
LC-MS	Liquid chromatography mass spectroscopy
LDH	Lactate dehydrogenase
LED	Light emitting diode
LOV	Light Oxygen Voltage
M	Molar concentration (mol/L)
MAO	Monoamine oxidase
MCM-41	Mobil Composition of Matter No. 41
MeCN	Acetonitrile
MES	2-(*N*-Morpholino)ethanesulfonic acid
mg	Milligrams
mL	Millilitre
mm	Millimetre
mM	Millimolar
MMO	4-Methylmorpholine
mmol	Millimole
MOPS	3-(*N*-Morpholino)propanesulfonic acid
MTS	3-(4,5-Dimethylthiazol-2-yl)-5-(3-carboxymethoxyphenyl)-2-(4-sulfophenyl)-2H-tetrazolium salt
mW	Milliwatt
MW	Molecular weight
NAD(P)H	Nicotinamide adenine dinucleotide (phosphate)
NHE	Normal hydrogen electrode
nm	Nanometres
nmol	Nanomole

NMR	Nuclear magnetic resonance
NP(s)	Nanoparticle(s)
OYE	Old Yellow Enzyme
PBS	Phosphate buffered solution
PDA	Polydopamine
PDI	Polydispersity index
PEG	Polyethylene glycol
PEI	Polyethyleneimine
RBF	Riboflavin
RCPDA	Riboflavin-Captopril-Polydopamine
RF	Resorufin
RFCPT	Riboflavin-Captopril
ROS	Reactive oxygen species
RTA	Riboflavin tetraacetate
RZ	Resazurin
SCE	Standard calomel electrode
STEM	Scanning tunnelling electron microscopy
TEA	Triethylamine
TEMPO	(2,2,6,6-Tetramethylpiperidin-1-yl)oxyl
TEOA	Triethanolamine
TFA	Trifluoroacetic acid
THF	Tetrahydrofuran
TLC	Thin layer chromatography
TRIS	Tris(hydroxymethyl)aminomethane
UV-vis	Ultraviolet-visible
W	Watt
µg	Microgram
µL	Microlitre
µm	Micrometre
µM	Micromolar

1 INTRODUCTION

1.1 Flavin

Flavins are organic redox cofactors found within enzymes (flavoenzymes) in the form of flavin adenine dinucleotide (FAD) or flavin mononucleotide (FMN) derived from Vitamin B_2, riboflavin (**Figure 1.1**). Flavoenzymes are involved in a wide range of biological metabolic processes thanks to a number of radical and ionic states (**Figure 1.2**) that allow for the catalysis of both one and two electron transfer reactions.[1,2] They can mediate both reduction and oxidation reactions, acting as either a nucleophile or electrophile on a range of substrates including amines, amino acids, dithiols, aldehydes, ketones, and carboxylic acids.[3] Interestingly, although flavoenzymes have been shown to induce oxidative stress through production of superoxide, they are also antioxidative by being involved in the reduction of hydroperoxides.[4,5]

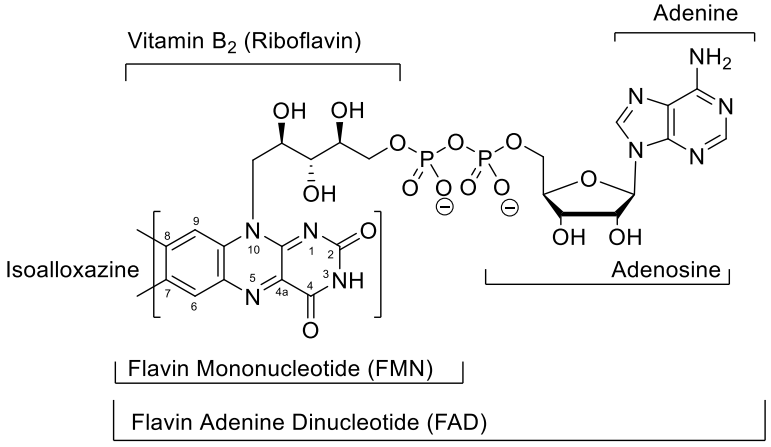

Figure 1.1: Structures and nomenclature of flavins found in nature.

In addition to their catalytic roles, flavins are also found within photoreceptors across bacteria, plant and animal kingdoms. More specifically, BLUF (Blue-Light-Utilising FAD) domains, found primarily in bacteria, control enzyme activity or gene expression in response to blue light,[6] LOV (Light Oxygen Voltage) domains are

crucial to phototropism and adjusting circadian rhythm within many plants,[7] as well as CRY (cryptochrome) domains being mainly responsible for circadian rhythm in animals.[8] Flavins are also crucial to the activity of light activated processes such as DNA repair by photolyase[9] and also the light emission by bacterial luciferase.[10]

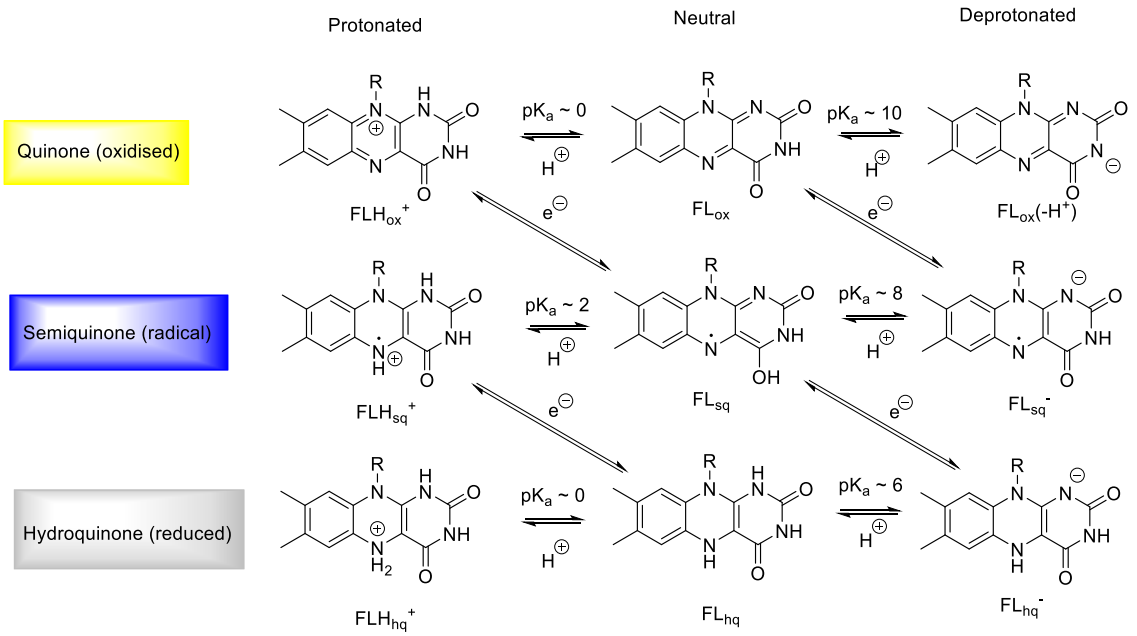

Figure 1.2: Redox and acid-base equilibria of flavins. Adapted from Heelis *et al.*[2]

Their significant biological role has prompted numerous studies of their properties and function.[1,2,11–13] As a result, there have been many applications of flavoenzymes and related flavin compounds within green chemical synthesis and biotechnology. This thesis is mainly concerned with the application of flavins within green chemical synthesis as photocatalysts. Therefore, the following literature review will focus on the recent developments of flavin-based catalysis and their applications within biocatalysis, organocatalysis and photocatalysis.

1.1.1 Flavoenzyme biocatalysis

Flavoenzyme use in biocatalysis is wide-spread due to their extremely varied chemistry that allows for a range of organic transformations to be achieved with regio- and enantiospecific control over the product, which is for the most part almost impossible to achieve by traditional synthetic means.[14] Some of the key catalytically active flavin redox states within flavoenzymes and their related catalytic transformations are

shown in **Figure 1.3** and will be discussed in order to introduce the main flavin redox states relevant to this thesis.

The oxidised flavin cofactor ($FL_{ox,}$ **Figure 1.3A**) can undergo reduction to yield oxidised substrates. A key example of such a reaction is imine formation from amines - a transformation catalysed by monoamine oxidases (MAOs) involved in the neurochemical removal of neurotransmitters.[15] Engineering of this class of enzymes pioneered by the Turner group has seen MAOs being exploited for enantioselective amine resolution and functionalisation to prepare numerous active pharmaceutical ingredients.[16] Recently, the Hyster group discovered the ability of ene-reductase (ER) enzymes to catalyse dehalogenation reactions through the single electron reduction of FL_{ox} to form the anionic radical flavin semiquinone (FL_{sq}^{-}, **Figure 1.3B**). This allowed them to perform enantioselective hydrodehalogenation on a range of α-bromoesters.[17]

Further single electron reduction of flavin semiquinone, FL_{sq} or the direct reduction of FL_{ox} *via* hydride transfer from NAD(P)H results in the fully reduced flavin hydroquinone (FL_{hq}, **Figure 1.3C**). FL_{hq} is responsible for the activity of ene-reductases (ERs), a group of enzymes derived from the Old Yellow Enzyme (OYE) family, that are capable of C=C bond reduction *via* hydride transfer from FL_{hq} to the substrate followed by protonation. These enzymes have been employed in several reaction cascades and industrially relevant processes due to inherent substrate promiscuity and excellent stereoselectivity over products (a more detailed discussion of this enzyme class can be found in **Chapter 4**).[18,19]

Finally, FL_{hq} can react with molecular oxygen to form peroxyflavin, $FLOO^{-}$ (**Figure 1.3D**) which can also be protonated to form the hydroperoxyflavin species, FLOOH (**Figure 1.3E**). These peroxy-flavin species are present in a large group of enzymes known as flavin-containing monooxygenases (FMOs) and have been among the most widely exploited enzymes in biocatalysis. There are several classes (A-F) of FMOs that are generally classified by the type of chemical reaction that is catalysed, the nature of the reducing and oxidising substrates, or the sequence and structural data of the enzyme.[20]

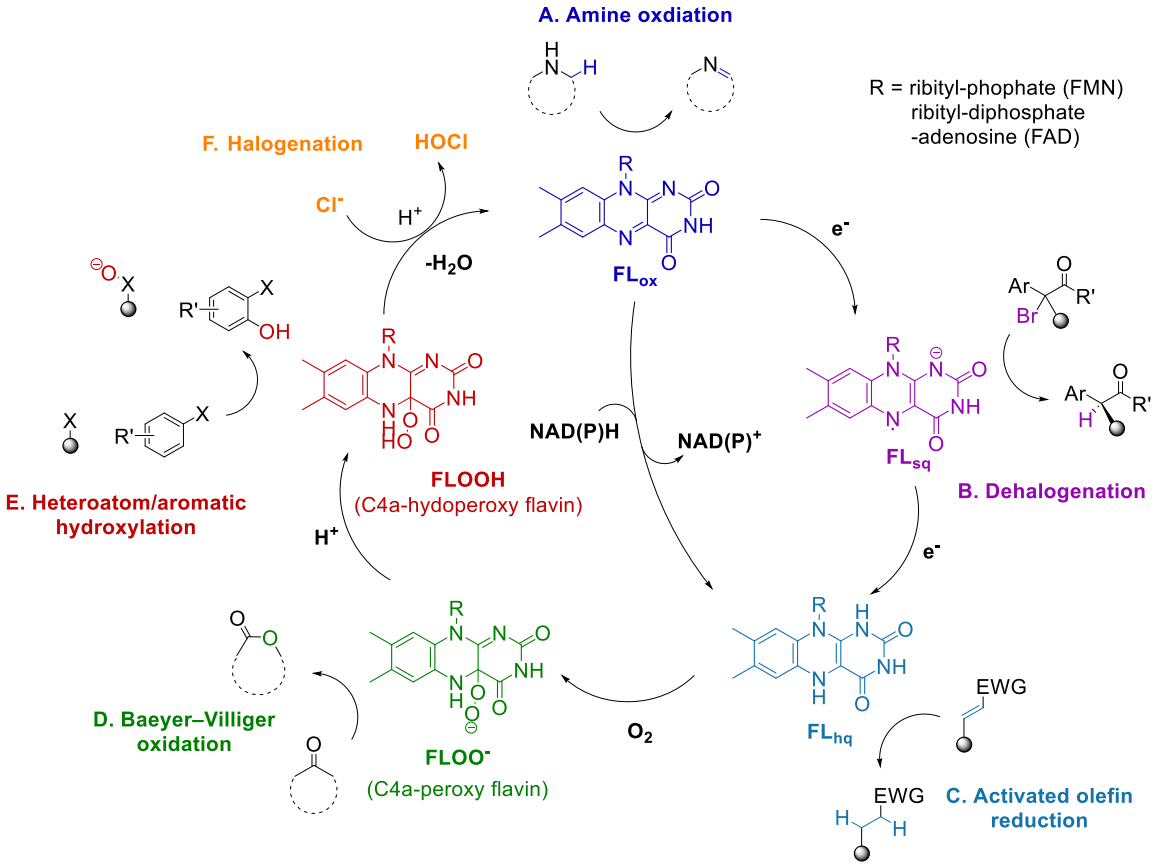

Figure 1.3: Catalytically active species of flavin utilised in biocatalysts. (A) FL_{ox} within MAOs can oxidise amines to imines. FL_{ox} can also act as a one or two electron acceptor to afford either (B) flavin semiquinone (FL_{sq}) that can catalyse dehalogenation reactions, or (C) reduced flavin hydroquinone (FL_{hq}) that can perform two-electron reduction of activated olefins within ERs. FL_{hq} can also react with molecular oxygen to form the C4a-peroxy (D) or hydroperoxy flavin (E) which can undergo Baeyer-Villiger oxidation or hydroxylation of a substrate. Halogenation of a substrate can occur through a chloride anion binding to FLOOH to form hypochlorous acid (F). Adapted from Baker Dockrey *et al.*[21]

Class A FMOs are primarily attributed to the hydroxylation of aromatic species which serves an important biological function in xenobiotic degradation (a more detailed discussion of this topic can be found in **Chapter 2**).[22–25] Within biocatalysis, such FMOs have been employed in natural product synthesis to achieve sorbicilin natural products through site- and stereoselective oxidative dearomatisation steps.[26,27] Hydroxylation of a particular substrate by this class is mediated by the electrophilic hydroperoxyflavin species, FLOOH (**Figure 1.3E**) which has also been

identified in other classes of FMOs such as class B Baeyer-Villiger monooxygenases (BVMOs). Although BVMOs show promiscuous catalytic activity towards epoxidation and heteroatom oxidation reactions, their primary mechanism of action utilises $FLOO^-$ for the nucleophilic oxygenation of carbonyl compounds to form lactones or esters (Baeyer-Villiger oxidation, **Figure 1.3D**).[28] As a result, BVMOs have been used to prepare various enantioenriched pharmaceuticals, fragrance compounds and Nylon precursors, as well as some applications towards large scale industrial processes.[29]

Another industrially relevant class of FMOs are the class F halogenases also employ the hydroperoxyflavin cofactor in their catalytic activity, however, bind halide ions which are oxidized by the C4a-hydroperoxide to form hypochlorous or hypobromous acid. These reactive intermediates then interact with active site residues to enable aromatic halogenation.[30] As a result, halogenases have been widely applied to the production of valuable halogenated tryptphan/indole derivatives for use as agrochemicals and pharmaceuticals.[31]

In general, biocatalytic reactions are carried out using whole-cells or purified enzymes, however the latter suffers from limitations in terms of initial protein purification and external NAD(P)H cofactor recycling. Consequentially, various NAD(P)H recycling strategies have been developed using other enzymes,[32,33] nicotinamide derivatives,[34] electrochemistry[35] or photochemical strategies (discussed in more detail in **Section 1.1.3.1**).[35–39] The wide-ranging catalytic activity of the flavin cofactor has also been exploited in organocatalytic applications within green chemistry, utilising the flavin compound outside of a protein environment. This helps to address some of the other disadvantages associated with biocatalysis such as limited access, stability, and scale-up of protein enzymes whilst providing cheap and environmentally friendly reagents.

1.1.2 Flavin organocatalysis

The most prominent use of flavins in organocatalysis are within oxidation reactions catalysed by an N5-ethyl flavinium cation (**1**, **Figure 1.4**)**.** By the addition of reducing agents to **1** in the presence of air *via* dihydroquinone **2**, or by directly adding H_2O_2 the stabilised hydroperoxyflavin species, **3** can be formed effectively resembling natural

FMO activity. This can then interact with a substrate, such as an aryl sulfide, and finally eliminate water as the only by-product to regenerate **1**.

This methodology was initially developed in the late 20th century by Bruice and coworkers as a model for flavoenzyme activity because hydroperoxyflavins derived from neutral flavins are extremely unstable outside of an enzyme and almost immediately release H_2O_2.[40–42] Since then, a number of synthetic strategies using this methodology have been exemplified such as Baeyer-Villager oxidations,[43–45] *S*- and *N*-oxidations,[46,47] hydroxylations,[48] as well as aryl aldehyde oxidations to carboxylic acids[49] or hydroxyls (Dakin oxidation).[50,51] Another successful route to enable FMO-like activity has been the combination of flavinium cations with inorganic cocatalysts such as OsO_4 or I_2 to perform hydroxylations[52,53] and oxidative sulfenylations respectively.[54–57]

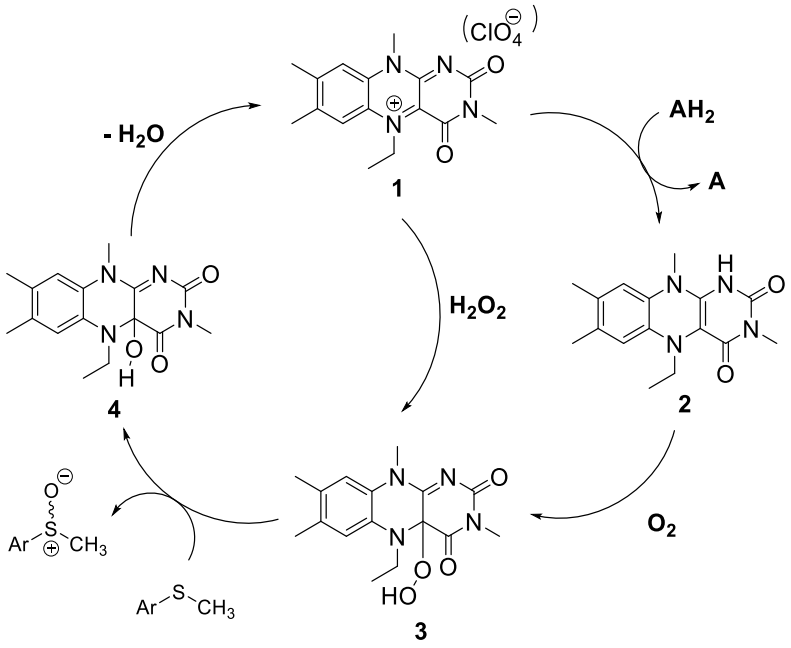

Figure 1.4: General reaction mechanism N5-ethyl flavinium catalysed oxidations using H_2O_2 or air. S = substrate and AH_2 = reducing agent or sacrificial electron donor.

Another interesting approach was taken by Imada and co-workers by designing a neutral flavin-tripeptide conjugate which acted as an effective BVMO mimic through amino acid residue stabilisation of the C4a-hydroperoxyflavin.[58] This conjugate demonstrated efficient sulfoxidation of thioanisole as well as the chemoselective Baeyer–Villiger oxidation of 3-phenylcyclobutanone. The Imada group have also used both neutral and cationic flavins in the presence of hydrazine to

achieve aerobic hydrogenation of C=C bonds.[59,60] As shown in **Figure 1.5**, the flavin (**5**) acts as a catalyst to generate diimide from hydrazine *via* an initial reduction of **5** to form a reduced flavin and diimide complex (**6**). This can then react with olefins to afford hydrogenated products and N_2. Fully reduced flavin **7** can then interact with oxygen to generate the short lived hydroperoxyl flavin **8** that either eliminates H_2O_2 or oxidises another hydrazine species to form an oxidised flavin diimide complex (**9**). A similar reaction with an olefin can then regenerate **5** to complete the catalytic cycle. The mechanism for cationic flavinium is analogous to this, however it is shows faster kinetics for the initial rate determining step of flavin reduction.[60]

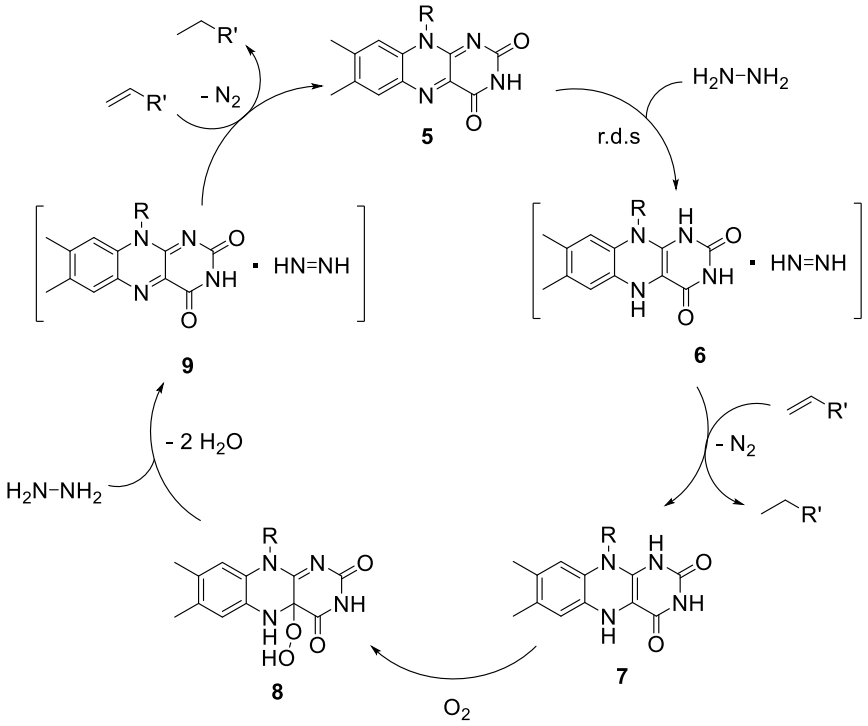

Figure 1.5: Mechanism of aerobic hydrogenation by a neutral flavin catalyst in the presence of hydrazine. R = ribityl tetrabutyrate.

More recently, the Cibulka group introduced an N1-N10 ethylene bridged flavin catalyst with PPh_3 to prepare esters *via* an N5-PPh_3 adduct flavin intermediate similar to the Mitsunobu reaction.[61] Rather than using a conventional dialkyl azodicarboxylate reagent at a stoichiometric amount, this method benefits from using the flavin at 10 mol% without the need for low temperature activation with PPh_3. In addition, this N5-adduct position is rarely observed in natural flavoenzymes as most mechanisms proceed *via* the C4a position, which demonstrates that there is scope for flavin organocatalysts to resemble a range of flavoenzyme activity.

Enantioselective transformations are crucial to the synthesis of many high value pharmaceutical products. Often, this involves several steps and range of complex chiral catalysts, all of which could be replaced by use of flavoenzymes or flavins that contain optically active modifications. Attempts have been made to carry out enantioselective flavin organocatalysis using chiral flavinium derivates, such as the enantiomerically pure flavinophanes, **10** and **11** (**Figure 1.6**) prepared by Shinkai and co-workers for enantioselective sulfoxidation reactions in 1988.[62] These derivates were shown to mediate the enantioselective oxidation of aryl methyl sulfides (*ee* values up to 65%) and methyl 2-naphthyl sulfide (*ee* of 72%), however the reactions were carried out at -20 ^{o}C and over 5 days, which limits any potential for scale-up.[62,63] Later, Murahashi and Imada reported the chiral bisflavin **12** that mediated the enantioselective Baeyer-Villiger oxidation of 3-arylcyclobutanones with ee values up to 67% at -30 ^{o}C after 6 d using H_2O_2.[44] It was found that yields and *ee* values were dependent on the solvent used, favouring a protic aqueous solvent system (CF_3CH_2OH/MeOH/water) in order to maximise hydrophobic π–π stacking interactions between the aromatic ring of the catalyst and that of the substrate. The addition of sodium acetate also improved the *ee* by neutralising perchloric acid formed as a by-product from the reaction of H_2O_2 and the flavinium counter anion.

A series of chiral flavinium catalysts (**13**) were developed by the Cibulka group by installing an phenyl "cap" that covers one face of the isoalloxazinium structure allowing the access of hydrogen peroxide and a substrate to only the uncovered face of the catalyst.[64,65] They performed a range of asymmetric sulfoxidation reactions on *para*-substituted thioanisoles with *ee* values ranging from 15-65%. These values depended on the type substrate functional groups and $R^{3/7/8}$ group substitution on the catalyst, however reaction conditions still required low temperatures (-20 ^{o}C) and long reaction times (72 h).

To further improve optical purity, two-component organocatalytic systems were introduced employing a flavin catalyst and auxiliary chiral co-catalysts. For example, Yahsima *et al.* utilised a chiral triazolium-derived N-heterocyclic carbene (NHC) and N3-benzyl protected riboflavin tetraacetate (**RTA**) to afford asymmetric esterification of aldehydes with various alcohols.[66] More recently, Poudel *et al.* combined a flavinium catalyst with a cinchona alkaloid dimer that enabled the

asymmetric Baeyer-Villiger oxidation of 3-arylcyclobutanones using H_2O_2 with impressive *ee* values up to 98%.[67] The observed enantioselectivity was attributed to ionic pairing and an intermolecular assembly of the flavinium and substrate on the chiral alkaloid dimer through both π–π stacking and ionic pairing.

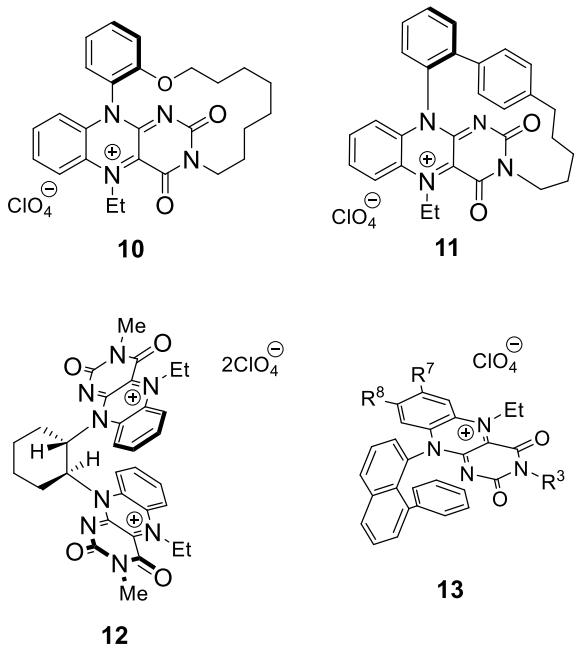

Figure 1.6: Chiral flavinium catalysts used for enantioselective oxidation reactions.

Clearly, flavins can be successfully used to catalyse several flavoenzyme-like reactions and can be employed as green organocatalysts for a variety of organic transformations.[68,69] Another branch of flavin catalysis takes advantage of their photochemical properties. This enables the catalysis of higher potential reactions due to the increased redox potential of excited state flavin (reduction potential of excited state for riboflavin tetraacetate = 1.67 V vs SCE).[70]

1.1.3 Flavin photocatalysis

Visible light photoredox catalysis has gained a lot of momentum over the past decade, providing a mild means of accessing radical chemistry for complex synthesis utilising an energy source which is potentially limitless. The use of organic photosensitisers has developed greatly within the field in order to offer a more sustainable alternative to the classical ruthenium and iridium complexes that are costly and scarce resources.[71] Naturally occurring flavin compounds therefore pose as an even greener addition to organic photoredox catalysis.

Riboflavin (**RBF**) and its derivative, riboflavin tetraacetate (**RTA**) have been shown to mediate a range of organic transformations using visible light (**Figure 1.7**). The most prominent examples of flavin photocatalysis are the aerobic photooxidation of benzyl alcohols,[72–77] benzyl amines,[78] and sulfides[79,80] (**Figure 1.7A-C**). Other substrates include a range of methylbenzenes, styrenes and phenylacetic acids, all forming benzyl aldehydes.[81] More recently, flavoenzymes and other natural systems have been used as inspiration for flavin photocatalysis. For example, aromatic chlorination performed by halogenases was successfully achieved (**Figure 1.7D**),[82] and the catalytic *E*-*Z* isomerisation of activated olefins was inspired by retinal (**Figure 1.7E**).[83–87] The versatility of flavin photocatalysis is further highlighted by their demonstrated photocatalytic ability towards ester formation,[88,89] nitration of protected aniline derivatives (**Figure 1.7F**),[90] the cyclisation of thiobenzanilides (**Figure 1.7G**),[91] as well as a number of aliphatic decarboxylative transformations to yield fluorinated,[92] cyanated[93] and alkylated/arylated products (**Figure 1.7H**).[94,95]

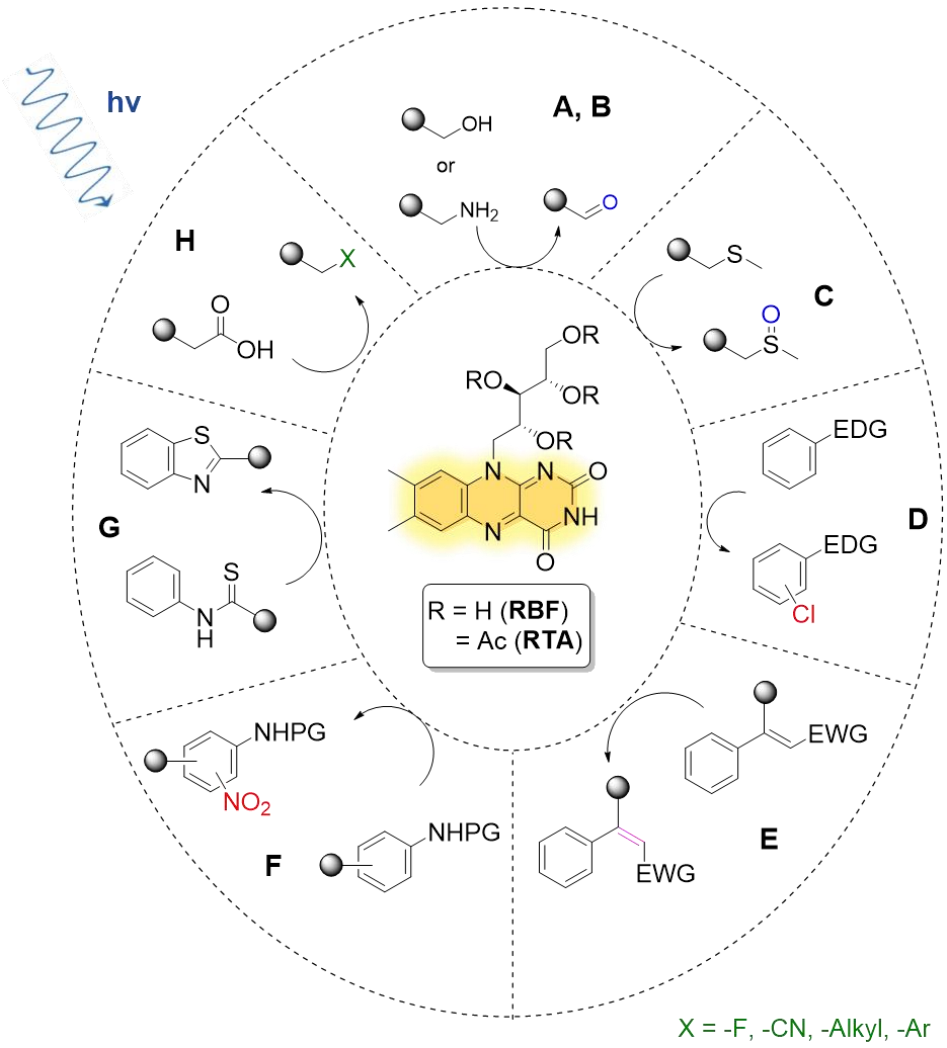

Figure 1.7: Key examples of the organic transformations demonstrated by **RBF** and **RTA** photocatalysts using visible light: (A) benzyl alcohol, (B) amine and (C) sulfide oxidation; (D) aromatic chlorination; (E) E-Z isomerisation; (F) aromatic nitration; (G) thiobenzanilide cyclisation; (H) decarboxylative transformations. EDG = electron donating group, EWG = electron withdrawing group, PG = protecting group.

Such versatility of flavin-mediated photocatalysis can be explained through their photochemical transitions that result in both energy and electron transfer processes, as well as the generation of reactive oxygen species (ROS).[2] As shown in **Figure 1.8**, the excitation of ground state FL_{ox} induces the formation of a singlet excited state flavin ($^1FL^*$) that can then undergo intersystem crossing (ISC) to form the triplet state flavin ($^3FL^*$). This reactive species can then interact with an electron-rich substrate/donor (D) to generate the anionic semiquinone flavin (FL_{sq}^-) and radical cation substrate ($D^{\bullet+}$) *via* a single electron transfer process. Consequently, FL_{sq}^- can interact with O_2 to regenerate FL_{ox}, yielding a superoxide radical species ($O_2^{\bullet-}$). Finally,

superoxide can then react with a substrate of interest in a ***Type I photooxidation*** which is the most common flavin photooxidation mechanism.

FL_{sq}^{-} can also undergo a second electron transfer process with a substrate/donor to yield the fully reduced flavin hydroquinone (FL_{hq}) which is finally reoxidised by O_2 to FL_{ox} producing H_2O_2 as a by-product. This by-product has been shown to be deleterious to flavin photocatalytic activity but can be removed by the use of a scavenging additive such as molecular sieves.[88]

In addition, $^3FL^*$ can undergo an energy transfer process with molecular oxygen to form singlet oxygen ($^1O_2$) and oxidise a substrate within a ***Type II photooxidation***. This has been shown to be the primary mechanism of riboflavin sensitized degradation of amino acids[96] and photooxidation of sulfides to sulfoxides in alcoholic solvent systems.[79] However, this is often occurring in tandem with the free radical mediated Type I process.[80,97] Another advantage of $^3FL^*$ is its ability to undergo energy transfer to a substrate which allows for photoinduced E-Z isomerisation and [2+2] cyclisation events using visible light.[83–87,98–100]

Finally, single electron transfer processes can occur between a substrate and $^3FL^*$ to access radical chemistry mechanisms. This has been utilised to achieve decarboxylative transformations[92–95] and thiobenzanilide cyclisations.[91] Interestingly, photochemically generated FL_{sq}^{-} and an amine electron donor has been utilised in reductive dehalogenation processes,[101] and FL_{hq} has been utilised in the photocatalytic reductive activation of Pt^{IV} prodrugs.[102–105] There are however, no photocatalytic examples of an enzyme-like hydride-transfer from FL_{hq} to a substrate to achieve hydrogenation reactions.

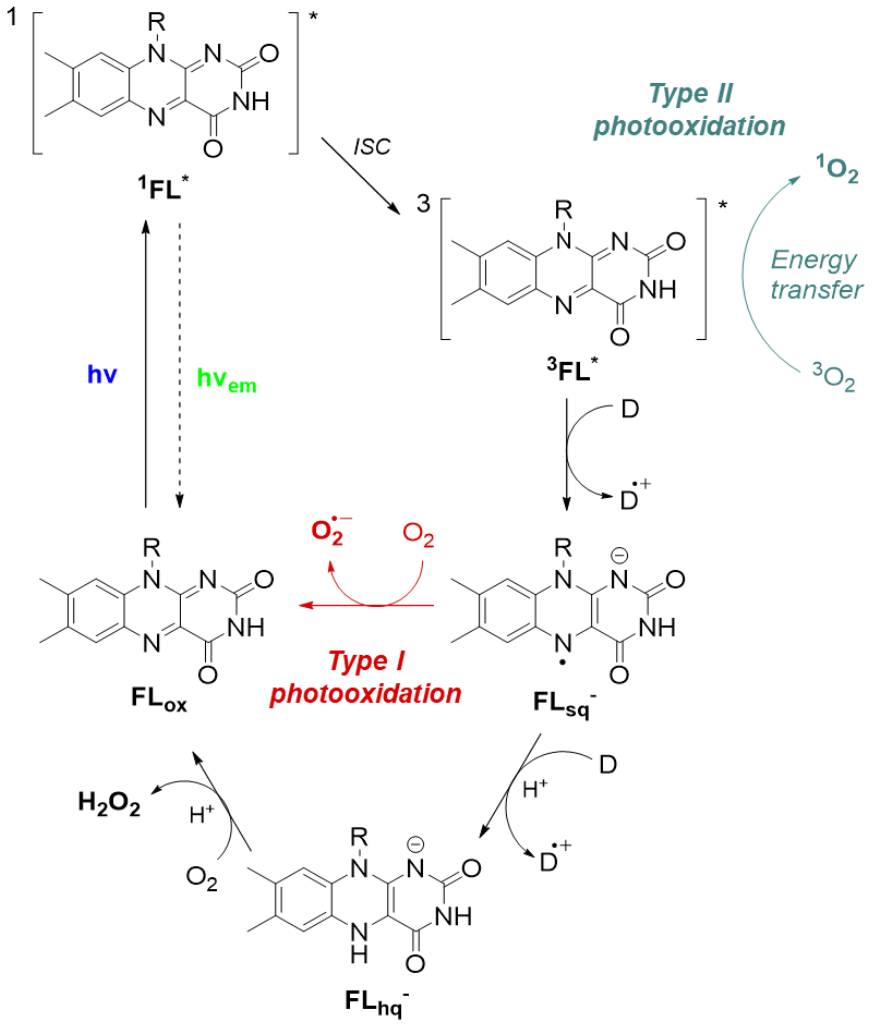

Figure 1.8: Photochemical pathways of flavins in the presence of oxygen that generates ROS species, either by a Type I photooxidation to yield superoxide or a Type II photooxidation to produce singlet oxygen *via* energy transfer. ISC = intersystem crossing, D = electron donating substrate.[2]

In recent years, several strategies have been developed to enhance flavin photocatalysis and allow for more advanced transformations with higher redox potentials. Fukuzumi *et al.* demonstrated that the redox potential of **RTA** can be increased by metal ion coordination,[70,106] and the oxidation of benzylic C–H bonds in the presence of Sc^{3+} ions was achieved which was otherwise not possible using **RTA** alone.[107] This methodology however, was not as effective for electron-deficient benzylic substrates prompting the design of cooperative systems. For example, Wolf *et al.* employed a biomimetic iron co-catalyst which utilised H_2O_2 produced as a by-product from flavin photooxidation to enable further oxidation of electron-deficient substrates.[108] Tang *et al.* improved this strategy by employing cheap ferric chloride

and N-hydroxy succinimide (NHS) to achieve the photooxidation of benzylic C-H bonds in presence of **RTA**.[109] The Lin group have recently advanced this further by use of photoelectrochemistry to enable facile aliphatic C-H oxidation mediated by **RTA** and a thiourea additive.[110]

Other than the use of additives, chemical modification of the flavin chromophore has also proven to be a useful tool to achieve higher level transformations. The Cibulka group have shown that flavin redox potentials and related photoactivity can be tuned through structural modifications to the (iso)alloxazine ring system (**Figure 1.9**). Such modifications have enabled them to achieve the photooxidation of electron-deficient benzylic substrates using flavin derivates **14** and **15** without a co-catalyst.[111,112] Further changes to the core flavin structure obtained deazaflavin **16** and alloxazine **17** that showed enhanced activity towards [2+2] cycloadditions using visible light.[98–100] The group also found that the alloxazinium salt **18** is a useful tool for oxidative [2+2] cyclobutane ring cycloreversion using visible light, which was previously only achievable by the addition of a strong acid to **RTA**.[113]

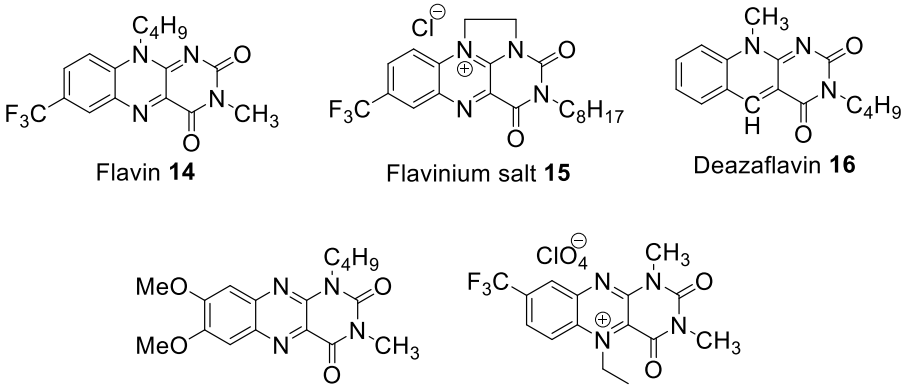

Figure 1.9: Structures of the flavin derivates developed by the Cibulka group utilised for benzylic C-H and alcohol oxidations (**14, 15**),[111,112] [2+2] cycloadditon reactions with visible light (**16, 17**),[98–100] and [2+2] cycloreversion reactions using visible light (**18**).[113]

1.1.3.1 Flavin photobiocatalysis

The combined use of enzymes and photocatalysts has seen great interest in the last decade thanks to the ability of photosensitisers, such as flavins, being able to act as

electron mediators to activate enzyme redox activity upon irradiation in the presence of a sacrificial electron donor.[36,39]

In 1978, Massey reported a protocol which employed flavins as electron mediators to activate several flavoenzymes using visible light in the presence of ethylenediaminetetraacetic acid (EDTA) as the electron donor.[114] This was inspired by Frisell's initial observation of free flavin photoreduction by a variety of amino acids, carboxylic acids, and amines.[115] Since then, the Hollmann group in 2007 applied this methodology to drive enantioselective Baeyer-Villiger oxidations of cyclic ketones using a Baeyer-Villiger monooxygenase (BVMO) enzyme, FAD as the flavin photosensitiser and EDTA as the sacrificial electron donor (**Figure 1.10**).[116] This report showed, for the first time, that light could be employed as an alternative to existing NAD(P)H recycling methods for biocatalysis and the field of photobiocatalysis has since developed significantly.[35–39] This methodology has been applied to various flavoenzymes such as FMOs and ERs,[116–125] as well as a halogenase.[126] A limiting factor in these applications however, is generation of ROS by the flavin photosensitizer that inhibits flavoenzyme activity. To combat this, flavin derivatives such as deazaflavins have been utilised with some success as they exhibit low reactivity with molecular oxygen.[127–129]

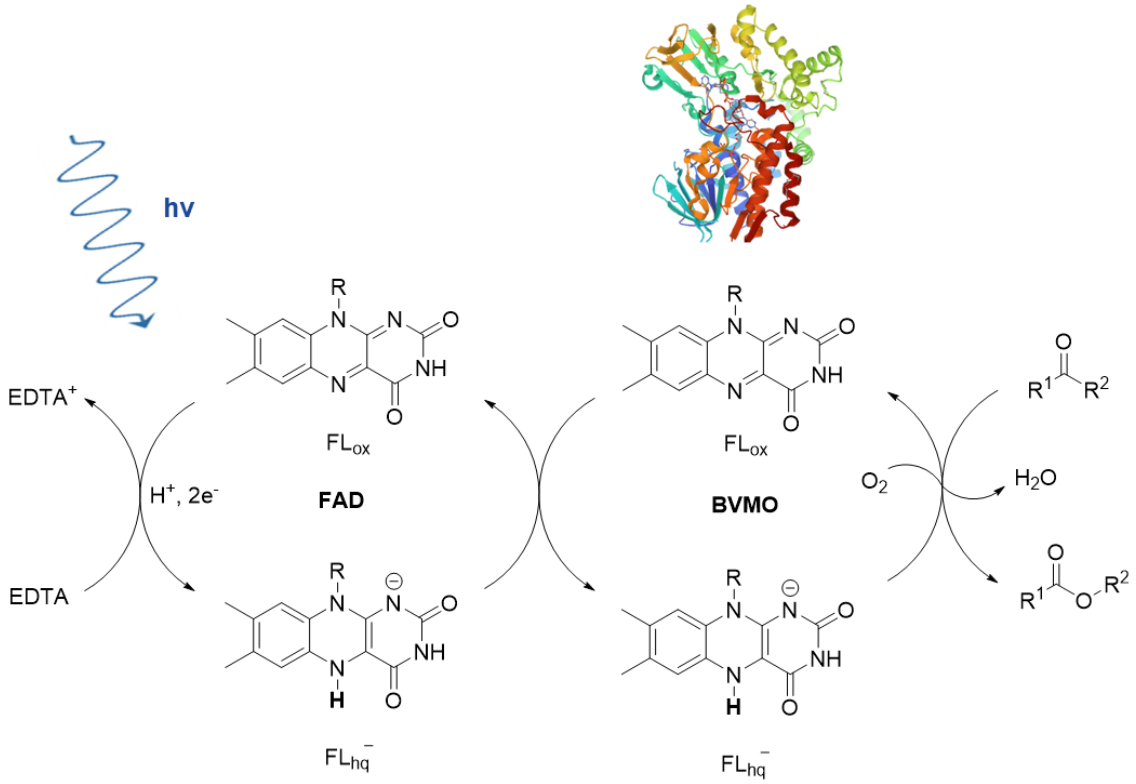

Figure 1.10: Photobiocatalysis using FAD as the photosensitiser and electron mediator for a Baeyer-Villiger monooxygenase (BVMO) enzyme (PDB entry - 4D03) in the presence of EDTA and light. R = adenine dinucleotide.[116]

More recently, morpholine-based buffer systems have been successfully used as sacrificial electron donors for flavin photoreduction in order to activate Pt prodrugs,[102–104] and activate flavoenzymes without damaging side reactions.[130,131] In the context of flavoenzyme activation, buffers such as 3-(*N*-morpholino)propanesulfonic acid (MOPS) show enhanced activity compared to EDTA due to spin ion pair correlation with reduced anionic flavin semiquinone (FL_{sq}^{-}).[130] This formation was shown to prolong the lifetime of FL_{sq}^{-} and reduce ROS generation in an aerobic environment that would otherwise destroy the flavin and/or enzyme.

Besides using free flavins as electron mediators for enzyme activation, innovative examples of direct illumination of a flavoenzyme itself has provided access to chemistry not naturally seen in the dark. In particular, the identification of a flavin-based algal enzyme responsive to blue light to produce hydrocarbons from fatty acids has sparked great interest in utilising flavin-containing 'photoenzymes' for microbial biofuel and feedstock production.[132–136] Additionally, the Hyster group discovered

catalytic promiscuity within ene-reductase (ER) enzymes such that they can perform enantioselective hydrogen atom transfer on a range of α-bromo substituted ethyl esters.[17] This methodology was extended by directly irradiating the flavoenzyme itself with cyan LEDs to access unnatural stereoselective radical cyclisation chemistry *via* an initial electron transfer from the excited semiquinone flavin (FL_{sq}*) to an α-chloro amide substrate.[137] A follow-up study using a different ER enzyme utilised a similar methodology to achieve redox-neutral radical cyclisation of α-halo-β-amidoesters to yield 3,3-disubstituted oxindoles, however the ground state FL_{sq} was found to be responsible for initiating the reaction in this case.[138]

The Hyster group has also combined the use of ERs with ruthenium photocatalysts to achieve synergistic photoenzymatic ketone reduction and hydrogenation of heteroaromatic olefins, however the use of such photosensitisers are unfavourable from a sustainability perspective.[139,140] Hartwig and colleagues on the other hand, developed a cooperative photoenzymatic catalytic system using FMN as the photocatalyst to first carry out the E-Z photoisomerisation of an olefin which is then asymmetrically reduced by an ER enzyme (a glucose dehydrogenase/NADPH recycling system was also used, **Figure 1.11**).[141]

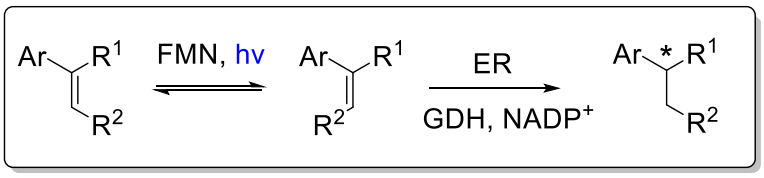

Figure 1.11: Hartwig's combination of photocatalytic isomerization and enzymatic reduction of alkenes. The asterisk indicates the chiral centre. ER = ene-reductase, GDH = glucose dehydrogenase. Adapted from Litman *et al.* [141]

This methodology achieved a variety of biologically active molecules and valuable synthetic intermediates at preparative scale which clearly demonstrates the excellent potential of flavin-based photocatalysis and enzymes in organic synthesis.

1.1.4 Advanced flavin catalyst systems

1.1.4.1 Polymeric and heterogeneous systems

Despite the relative ease and high yields of flavin catalytic reactions either in the dark using cheap oxidants (air/H_2O_2) or under irradiation with LEDs, there are issues relating to their long-term stability, separation of the products from catalyst in a homogeneous reaction mixture and catalyst reuse. In general, the (photo)stability of flavins are significantly reduced when removed from a protein environment due to a lack of H-bonding, aromatic stacking and other electrostatic interactions between amino acid residues, all of which have been shown to stabilise and modulate flavin redox potentials.[142] Model systems for flavoenzyme activity have been developed by the Rotello group and others using cyclodextrins,[143–145] polymers,[146,147] dendrimers,[148,149] peptides,[150] nanoparticles[151–153] and sol-gels[154,155] which has led to the preparation of stable and catalytically active heterogeneous flavin systems (**Figure 1.12**).

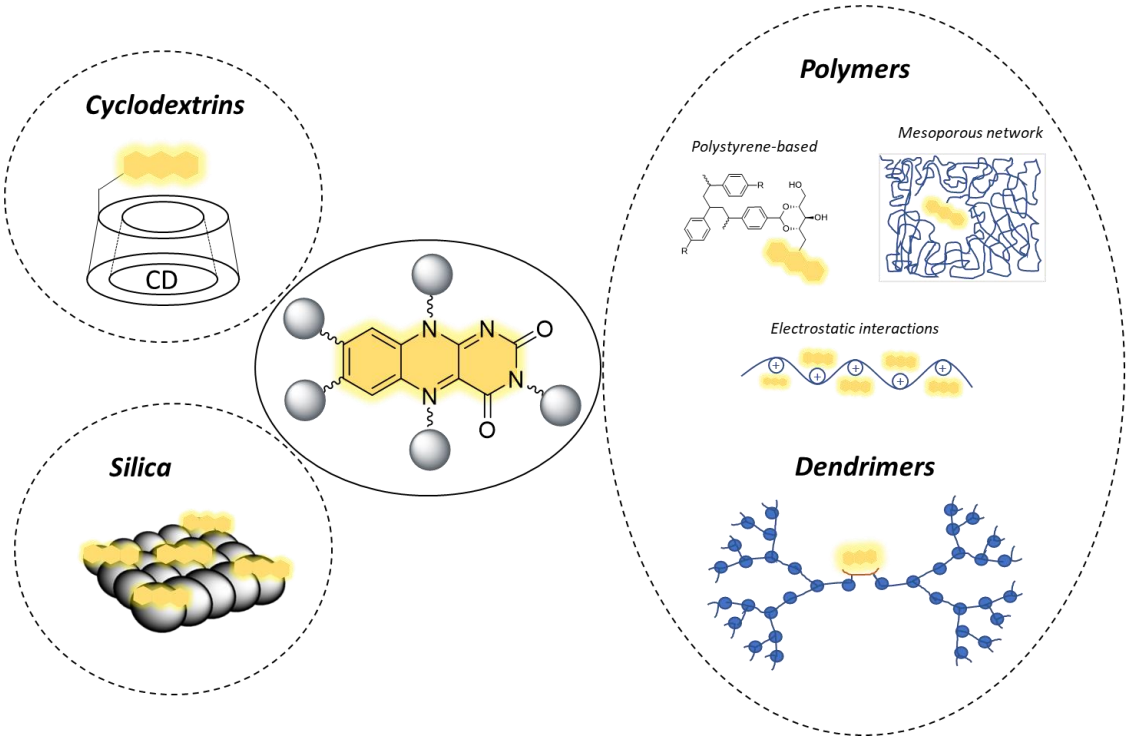

Figure 1.12: Key examples of reported polymeric and heterogeneous flavin catalyst systems: cyclodextrin-flavin conjugates,[156–159] polystyrene-based polymer,[160] mesoporous polymer networks,[161] electrostatically bound flavin polymers,[162–164] dendrimers,[165–167] and heterogeneous silica immobilisation.[75,168,169]

Thanks to their cavity-forming structure, cyclodextrins are a particularly useful scaffold in developing flavoenzyme mimetic catalysts. For example, D'Souza showed that flavin-cyclodextrin conjugates were effective catalysts for benzyl mercaptan oxidation and photooxidation of benzyl alcohols with greater efficiency than riboflavin (**Figure 1.13A**).[158] The Cibulka group later prepared alloxazine- and alloxazinium-cyclodextrin conjugates (**Figure 1.13B** and **C**) that were able to catalyse a range of enantioselective sulfoxidations of aryl methyl sulfides obtaining near-quantitative conversions with *ee* values up to 91% with very little catalyst loading (0.2-1 mol%) at room temperature.[156,157] The rate enhancement and enantioselectivity of these reactions are the consequence of preorganisation of the substrate in the chiral cyclodextrin cavity covalently attached to the flavin.

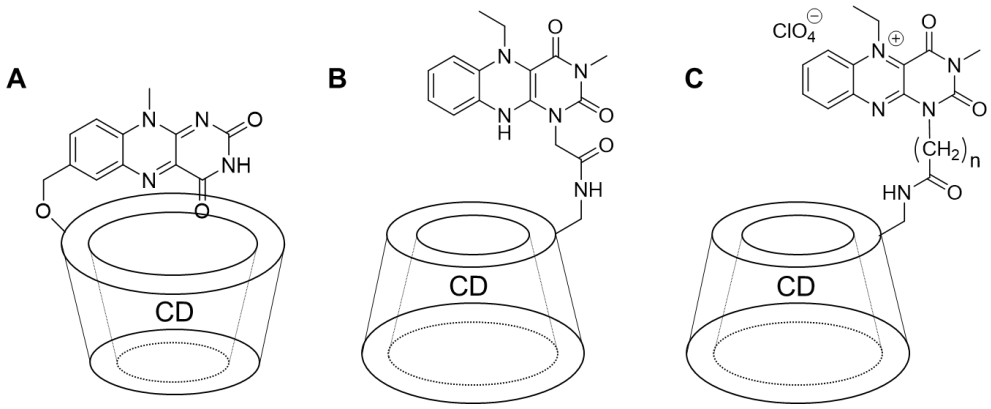

Figure 1.13: Examples of flavocyclodextrin conjugates synthesised by D'Souza (A)[158] and Cibulka (B and C).[156,157] Chirality of the cyclodextrin (CD) cavity enables enantioselectivity of the catalysed oxidations.

Polymeric flavin systems prepared using both covalent and non-covalent strategies have been widely explored for dark organocatalytic transformations.[170] For example, the free radical copolymerisation of styrene derivatives **20** and **21** and styrene-riboflavin monomer, **19** (**Figure 1.14**) resulted in a series of insoluble polystyrene-supported flavin catalysts that showed activity towards aerobic reduction of olefins with hydrazine.[160] It should be noted that this activity was related to the R group of **20** and the type of substrate, such as hydroxyl and carboxylate styrene derivatives showed enhanced activity towards phenolic substrates. Furthermore, the recyclability of these catalysts was demonstrated up to 10 times which highlights their suitability for heterogeneous applications.

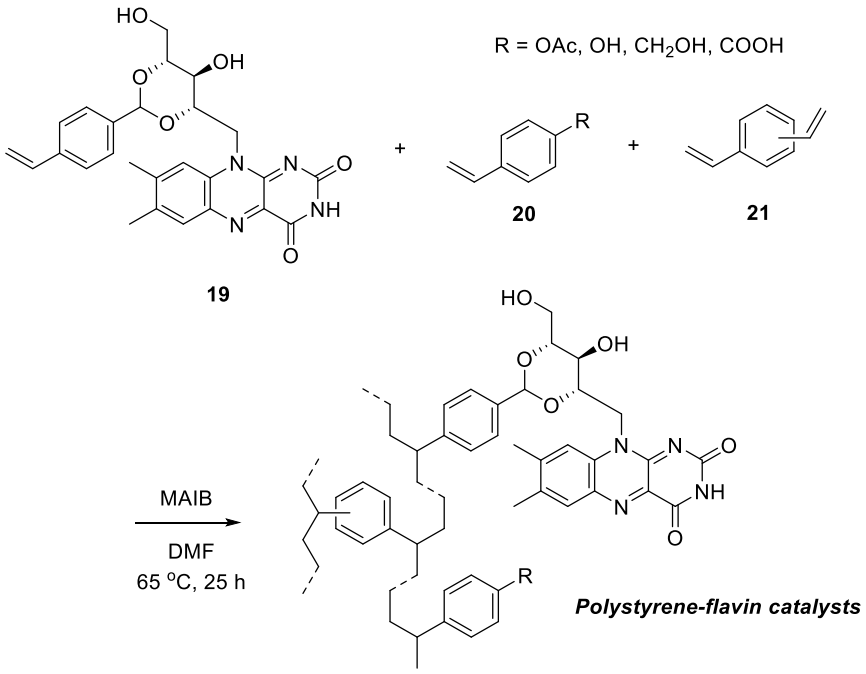

Figure 1.14: Free radical copolymerisation of styrene derivatives, **20** and **21** with styrene-riboflavin monomer, **19** forming polystyrene-based flavin catalysts.[160]

A recent study using a similar radical polymerisation strategy employed the riboflavin derivative, **22** and ethylene glycol dimethacrylate (**EGDMA**) to form a flavin-containing mesoporous network polymer (**Figure 1.15**).[161] This mesoporous catalytic polymer mediated the aerobic reduction of a range of olefins in the presence of hydrazine and was recyclable up to 5 times. The photooxidation of 4-methoxybenzyl alcohol was also demonstrated by the polymeric system at a higher yield than the monomer **22** however recyclability of this reaction was not demonstrated.

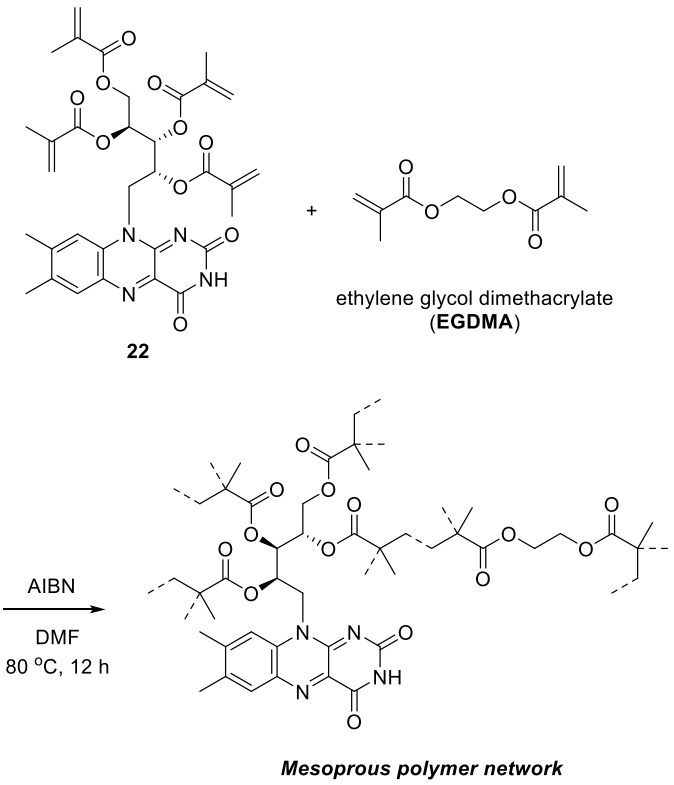

Figure 1.15: Free-radical copolymerisation of methacrylate-riboflavin monomer **22** and EGDMA forming a mesoporous flavin polymer network.[161]

Non-covalent strategies to formulate heterogeneous flavin catalysts have been developed such as the self-assembly of flavinium cations onto anionic cation-exchange resins[162] and sulphated chitin.[164] The latter strategy proved most successful, showing enhanced activity towards Baeyer-Villiger oxidation and sulfoxidation in the presence of alkali metals and H_2O_2. The heterogeneous catalyst was also reusable and showed activity up to 7 runs for the sulfoxidation of aromatic sulfides.

Another non-covalent strategy to formulate artificial flavoenzyme mimetic catalysts employed FMN which was incorporated into a hydrophobic microenvironment utilising a guanidinium and octyl functionalised polyethyleneimine ($PEI_{gaun\text{-}oct}$, **Figure 1.16**).[163] This catalyst mediated the Baeyer-Villiger oxidation of bicylo[3.2.0]hept-2-en-6-one in the presence of O_2 and NADH, however more challenging cyclic ketone substrates (5- and 6-membered rings) were not assessed, nor was the recyclability of the catalyst. Although the discussed non-covalent strategies to form heterogeneous flavin catalysts showed interesting enzyme-like kinetics and

recyclability in some cases, their applicability to larger scale heterogeneous catalysis is limited due to the lack of robust flavin conjugation.

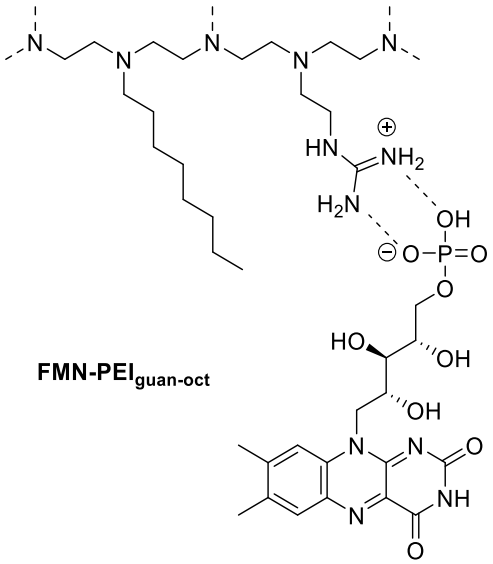

Figure 1.16: Self-assembly of FMN within $PEI_{gaun-oct}$ to form a flavoenzyme mimetic polymer catalyst.[163]

Dendron-based flavin systems were originally developed by the Rotello group using a covalent attachment strategy which showed enhanced catalytic activity compared to homogeneous riboflavin towards the aerobic oxidation of NADH analogue, 1-benzyl-1,4,-dihydronicotinamide (BNAH).[148] In another example, Imada and colleagues utilised the non-covalent assembly between flavin and a diaminopyridine-based poly(benzyl ether) dendrimer (**Figure 1.17**) to obtain a catalytic system for the aerobic reduction of olefins in the presence of hydrazine as well as the oxidation of sulfides using a flavinium cation (**1**).[165–167]

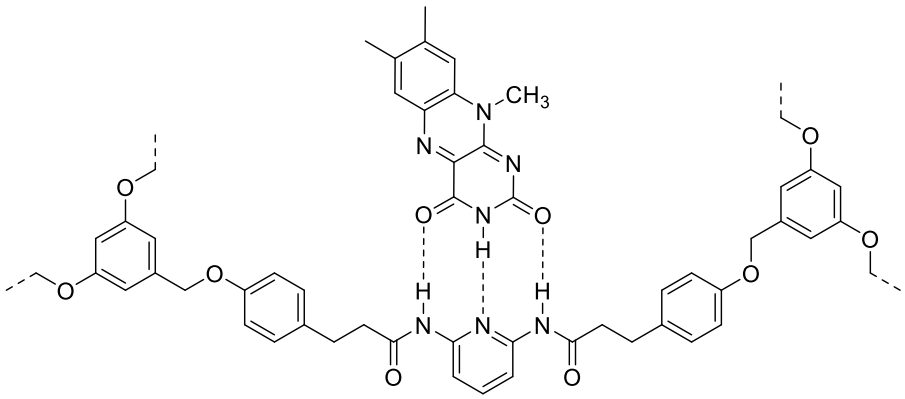

Figure 1.17: Self-assembly of lumiflavin within diaminopyridine-based poly(benzyl ether) dendrimer.[165–167]

To date, there are only a few examples of heterogeneous photocatalytic flavin systems. One of the first examples prepared heterogeneous flavin catalysts capable of benzyl alcohol photooxidation by immobilising flavin derivatives onto fluorous silica gel, reversed phase silica gel and polyethylene pellets *via* physical absorption or mechanical entrapment respectively.[75] Although the photocatalytic activity of the heterogeneous flavin systems was analogous to the equivalent homogeneous flavin system, the reaction rates decreased by a factor of 8-20 for the silica gel derivative and by a factor of 50 for the flavin-containing polyethylene pellets, most likely due to inefficient light absorption. Recyclability of the best performing systems was observed for up to 3 runs without loss of activity.

Recently, the Cibulka group utilised mesoporous silica (MCM-41) to covalently attach flavin derivatives, **23** and **24** (**Figure 1.18**), to perform benzyl alcohol oxidations, sulfoxidation, photoesterification and [2+2] cycloadditions.[168,169] This method showed improved yields and ease of product-catalyst separation, but reuse of the catalyst resulted in drastic decrease of activity due to flavin decomposition.[168] Additionally, it was shown that solvent polarity also played a role in the stability of these heterogeneous systems through cleavage of the flavin moiety from the **24**-derived silica catalyst being observed in aqueous acetonitrile reaction mixtures which was circumvented by the use of alcoholic solvent systems.[169]

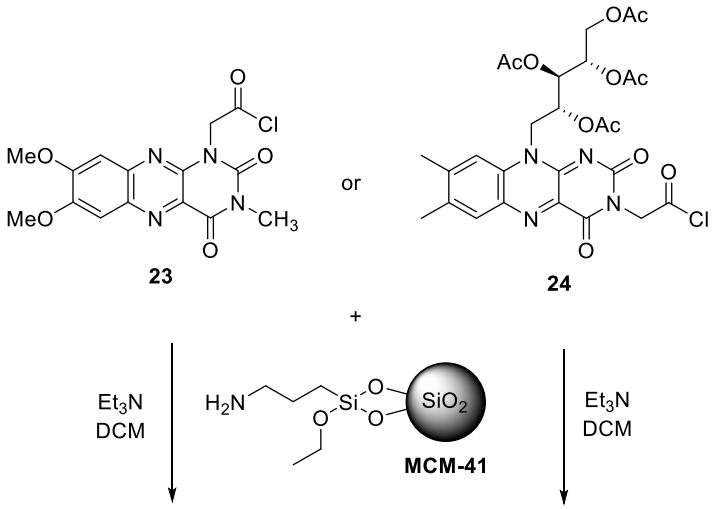

Figure 1.18: Synthesis of heterogeneous flavin-silica catalysts derived from alloxazine 23 and riboflavin-derivate 24 using amino-functionalised MCM-41 silica.[168,169]

1.1.4.2 Micro- and nanostructured flavin catalysts

The rate and efficiency of heterogeneous catalytic systems are well known to be improved using nanoparticles (NPs) or nanostructured elements due to an large increase in surface-to-volume ratio.[171] Examples of flavin-NP conjugates have been known for some time thanks to the work of the Rotello group and others, however the application of this work was aimed at molecular recognition as a model for flavoenzyme activity rather than catalysis.[151–153] Various catalytic flavin-NP hybrids have now been reported (**Figure 1.19**) and riboflavin-NP conjugates were also developed for biomedical applications in order to enable the targeting of overexpressed riboflavin receptors on cancer cells.[172–178]

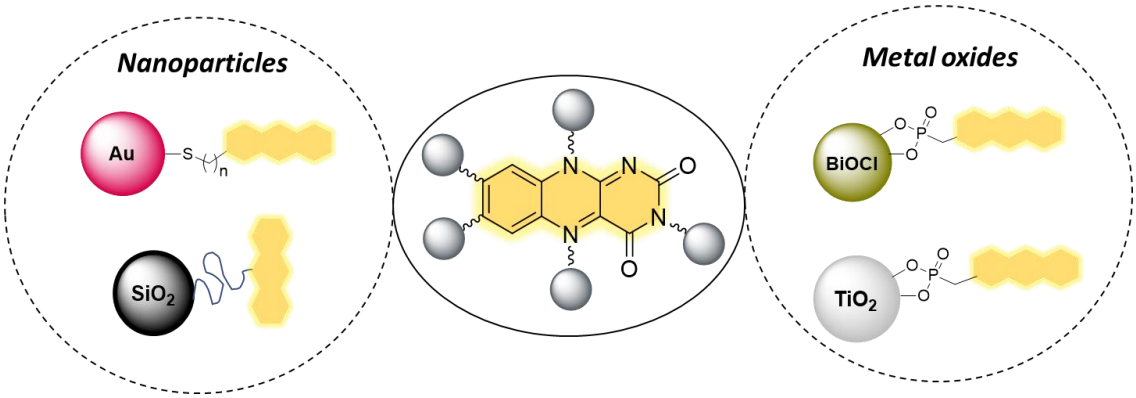

Figure 1.19: Key examples of micro- and nanostructured flavin catalyst systems using nanoparticles[179,180] and metal oxide semiconductors.[181–183]

One of the first examples of flavin-NP conjugates for catalysis was from Imada and Noata using PPh_3 stabilised Au NPs conjugated with octylthiol flavin-derivatives (**Figure 1.20A** and **B**).[179] The system was used for organocatalytic sulfoxidation and olefin reduction in the presence of hydrazine. Interestingly, an increase in the kinetic rates of both reaction was observed for the nanoparticle catalyst over the analogous free flavin catalyst. This was explained using a Michaelis-Menten-type mechanism in which substrates could coordinate into cavities on the Au NP surface through π-stacking and hydrophobic interactions to the PPh_3 layered surface thereby improving reaction efficiency.

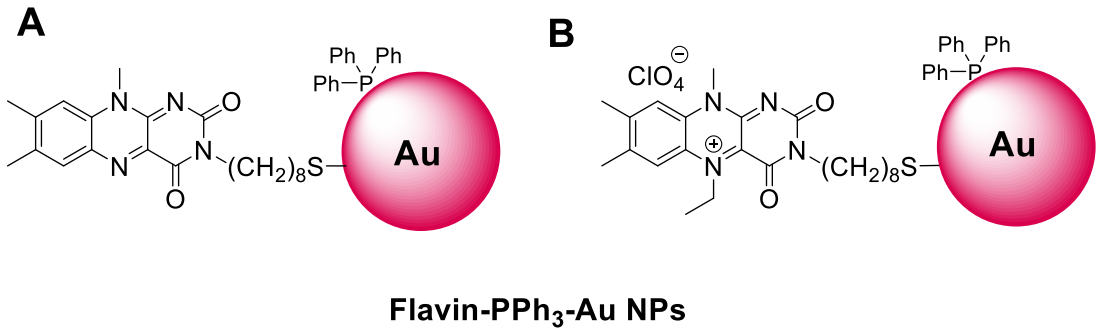

Figure 1.20: Flavin-functionalised gold nanoparticles (stabilised by PPh_3) prepared by Imada and Noata.[179]

Another approach recently reported by Metternich *et al.* was based on the covalent immobilisation of riboflavin (**RBF**) to silica micro- and nanoparticles using an atom transfer radical polymerization (ATRP) strategy (**Figure 1.21**).[180] The silica particles were first functionalised with an ATRP initiator and then copolymerisation of riboflavin-acrylate conjugates and 2-hydroxyethylacrylate successfully immobilised the catalyst to yield the heterogeneous system. This was utilised to mediate the E-Z photoisomerisation of cinnamonitrile, with enhanced rates of reaction observed for the 60 nm particle system compared to 500 nm particle system. However, the system could not be recycled due to decomposition of the photocatalyst, most likely induced by the acidic silica.[180]

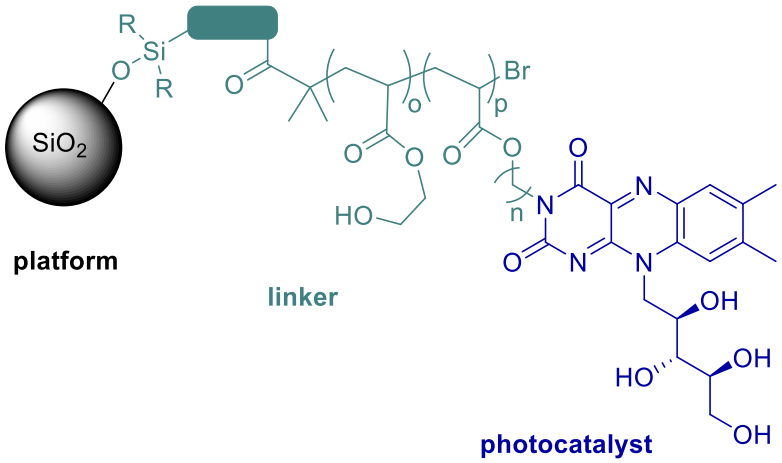

Figure 1.21: Design and structure of riboflavin-functionalised silica nanoparticles *via* an ATRP linker strategy.[180]

Other photocatalytic examples have investigated the combination of flavins with semiconducting nanomaterials primarily for water remediation applications, using

the flavin to sensitise activity in the visible light range (dye-sensitised semiconductor photocatalysis). The Paz group reported two separate flavin-conjugated semiconductor systems in 2016 using BiOCl microparticles[181] and Degussa P25 TiO_2 nanoparticles,[182] to carry out the aerobic photocatalytic degradation of salicylic acid and ethanol respectively. Conjugation of the flavin to the semiconductor was achieved using N3 phosphonic acid-functionalised flavin species **25a-d** (**Figure 1.22**). In the case of BiOCl particles, it was found that aromatic linker **25d** showed the highest photocatalytic activity compared to aliphatic chains (**25a-c**). The reason for this can be derived from its conjugated electronic structure which enhances photo-induced charge transfer to the semiconductor. As a results of this, ROS generation increased and subsequentially more salicylic acid was degraded.[181]

The TiO_2 system showed a relationship between the photoexcitation wavelength of light used and the photostability of the attached flavin. For example, under UV light irradiation, an increase in the photooxidation of ethanol was achieved accompanied by stabilisation of flavin against degradation. In contrast, irradiation of the system with visible light led to flavin degradation. These results were attributed to the propensity for charge transfer from excited flavin moieties to the semiconductor under certain excitation wavelengths. UV light excites the flavin to its S_2 and S_3 electronic states, which can transfer charge to the TiO_2 conduction band whereas excitation with visible light excites the flavin to an S_1 state that is less likely to transfer charge to the semiconductor and induces flavin photodecomposition.[182]

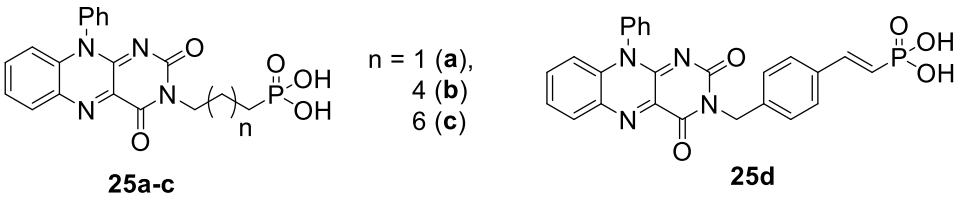

Figure 1.22: Structures of phosphonic acid functionalised flavin derivatives synthesised by the Paz group.[181,182]

Another class of semiconducting material that has been explored in combination with flavin is CeO_2–reduced graphene oxide (RGO).[184] In this example, riboflavin (**RBF**) was non-covalently immobilised within a CeO_2-RGO nanohybrid for use in aerobic photocatalytic degradation of methyl orange and p-nitrotoluene using

visible light (>400 nm).[184] In this case, the photostability of **RBF** was shown to be enhanced through immobilisation within the nanohybrid and was able to be recycled up to 4 runs using TEOA as the sacrificial electron donor.

Other than water remediation, dye-sensitised semiconductor photocatalysis (DSSPC) is widely utilised in solar fuel applications[185] and some of the design strategies developed in this field have now been applied to an example of heterogeneous flavin photocatalysis. Dongare *et al*. prepared photocatalytic glass substrates utilising phosphate-bearing FMN and fluorine-doped indium oxide (FTO) glass featuring mesoporous 4-µm films of 10 nm ZrO_2 or 15–20 nm TiO_2 NPs to efficiently oxidise a range of benzyl alcohol substrates.[183] Atomic layer deposition was used to coat a 1.0 nm overlayer of Al_2O_3 in order to stabilise the system as FMN leaching was observed without an additional layer. Catalytic activity was achieved with very low catalyst loading (<0.1 mol%) in presence of MnO_2 as a H_2O_2 scavenging co-catalyst. The system also benefitted from easy reaction workup which simply involved removing the catalyst-loaded glass from the reaction mixture. However, the recyclability of the system was not explored, so it is hard to conclude whether this system could be suitable for implementation into large scale heterogeneous photocatalytic flow reactors.[186]

In summary, artificial flavin catalysis has shown great promise over the last few decades in providing a green methodology to facilitate several redox reactions, like their natural flavoenzyme counterparts. Flavin photocatalysis poses as an exciting extension to this methodology thanks to the use of a naturally abundant sensitiser with wide ranging capabilities under light irradiation. The development of polymer and other heterogeneous flavin catalysts has demonstrated their applicability to large-scale synthetic process as well as in applications outside of organic synthesis such as energy and environmental applications.

1.2 Polydopamine

Polydopamine (PDA) is a polymer, inspired by the adhesive proteins secreted by mussels, originally developed by the Messersmith group to act as a universal surface coating.[187,188] As such, it has been widely exploited over the past decade in a number of research fields such as biomedicine, environmental remediation and energy thanks to its ease of synthesis in weakly alkaline aqueous conditions from dopamine hydrochloride, strong adhesive properties used to form uniform coatings on organic, inorganic and superhydrophobic surfaces, and its ease of functionalisation through reactive amine, catechol and quinone moieties (see **Figure 1.23**).[189–192] PDA is structurally analogous to naturally occurring melanin pigments (eumelanin) and consequently displays similar optical, magnetic and electrical properties to eumelanin including biocompatibility.[193]

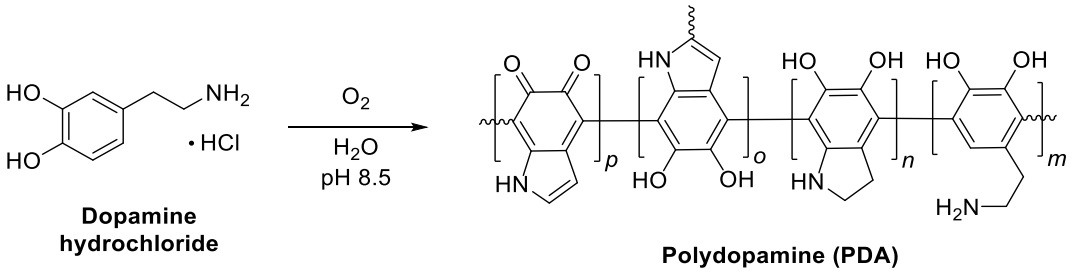

Figure 1.23: Polymerisation of dopamine hydrochloride in basic aqueous conditions to form PDA (general structure of major repeating units).[194]

The mechanism of formation and resulting structure of PDA has been widely debated, however it is agreed that its structure is comprised of conjugated oligomers bound together *via* supramolecular interactions such as H-bonding and π-stacking, analogous to that of eumelanin.[193,194] Ultimately, the synthesis conditions chosen will play a role in the resulting PDA structure and a wide range of synthetic methodologies have been developed to fit the end application.[195–197] Classically, synthetic conditions to achieve film formation on a substrate surface involved the use of TRIS buffer (pH 8.5) in presence of oxygen to initiate the autooxidative polymerisation of dopamine hydrochloride.[188] Since then, polymerisation onto surfaces has been demonstrated using chemical oxidants in acidic conditions[198–200] as well as in neutral conditions by UV-light irradiation.[201,202]

Besides the use of PDA as a surface coating, the synthesis of PDA nanomaterials such as nanoparticles (NPs) and rods have also been developed.[196] Typically, PDA nanoparticles are prepared analogous to the Stöber process used to prepare silica nanoparticles featuring ethanol-water mixtures in the presence of NH_4OH or NaOH as a catalyst.[203–205] Particle size can be tuned according to the amount of base catalyst used, whereby increased pH results in smaller particle size. PDA nanomaterials have been prominently used within biomedicine applications, mainly as drug delivery vehicles and in the design of theranostic agents.[196,206] The nature of their structure allows for loading of aromatic drugs *via* π-π stacking and chelation of metal cations or radionuclides by catechol coordination.[206] The relatively low reduction potential of catechol (dihydroxyindole) moieties within PDA (0.428 V vs. NHE)[207] also allows for *in-situ* metal cation reduction to obtain M^0-PDA NP composites which have been utilised for antimicrobial[208] and energy storage[192] applications as well as catalysis.[209]

The applications and literature surrounding PDA is vast, however the exploitation of PDA within catalysis is less explored. The state-of-the-art surrounding its use in catalysis shall be discussed, focussing on topics relevant to this thesis concerning organo- and photocatalytic behaviour.

1.2.1 Polydopamine in catalysis

PDA within catalysis has primarily been used as a support material for various metal NPs (M^0-PDA). This is due to its ability to chelate and reduce metal cations independent of additional reducing agents, efficient stabilisation of embedded metal NPs and biocompatibility that makes it well suited for green chemistry applications. The most studied reaction using M^0-PDA composites is the reduction of nitroarenes, such as the toxic 4-nitrophenol (R^1 = OH, **Figure 1.24A**), which has been demonstrated using Au,[210–217] Ag,[218–222] Pd,[223–226] and Pt[227] metals using an excess of $NaBH_4$ as the hydrogen source. Most of these formulations utilise M^0-PDA in combination with additional functional materials/supports such as magnetic Fe_3O_4 NPs,[212,214,217,221,227,228] or immobilisation into polymer membranes[218,219,229,230] and cellulose[220] to enhance catalyst recovery and recyclability.

The role of PDA within these reactions has been shown to enhance catalysis by allowing favourable coordination of the substrate to the M^0-PDA surface.[231–233] Furthermore, PDA alone has been shown to mediate the reduction of other pollutant dyes in the presence of $NaBH_4$ *via* redox mediation through catechol/quinone moieties, illustrating PDA's catalytic potential as not just an inert carrier material.[234,235]

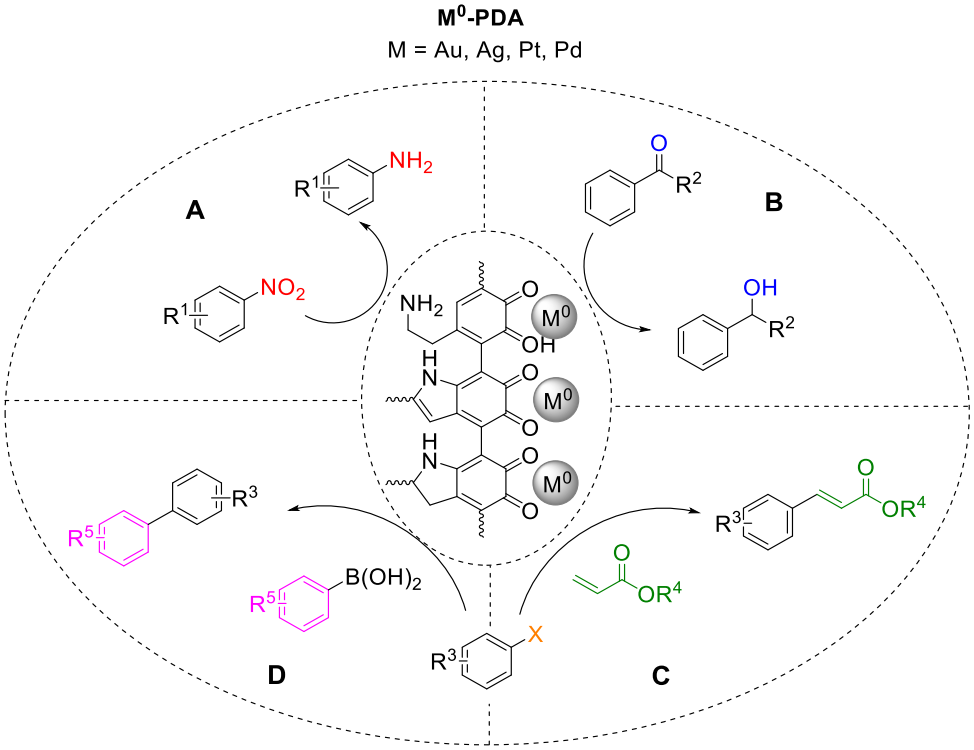

Figure 1.24: Key examples of M^0-PDA catalysis relating to dye degradation and organic synthesis: (A) nitroarene reduction,[236] (B) carbonyl reduction,[236] (C) Heck,[236,237] and (D) Suzuki coupling.[236,238–241]

Pd^0-PDA composites have been employed to achieve a wider range of nitroarene reductions (**Figure 1.24A**),[236] carbonyl reductions (**Figure 1.24B**),[236] and cross-coupling reactions such as the Heck,[236,237] and Suzuki reactions (**Figure 1.24C** and **D**).[236,238–241] Similarly to dye degradation applications, M^0-PDA composites used for organic synthesis are often combined with additional support materials to improve recyclability, such as magnetic Fe_3O_4[238,241], cellulose sponge[239] and within reactor walls through silicone nanofilaments.[237] M-PDA composites have also been employed as catalysts for oxidation reactions such as benzylic C-H oxidation (Au and reduced graphene oxide),[242] benzylic alcohol oxidation (Pd immobilised onto silica gel) [243] and

sulfide oxidation (oxo-vanadium chelated to Fe_3O_4@PDA NPs).[244] In all of these examples, PDA plays a key role in enhancing recyclability and activity of the catalytic system through actively engaging in a synergistic mechanism.

Besides being used as a metal carrier, PDA has also been utilised for enzyme immobilisation to enhance enzyme loading, activity and stability thus potentially decreasing the costs associated with industrial biocatalysis.[245] The Messersmith group demonstrated the ease of biomolecule attachment to PDA films through covalent attachment of amino/thiol-containing residues to quinone moieties in PDA.[246] Since then, lipase enzyme immobilisation onto Fe_3O_4@PDA NPs greatly increased the enzyme loading capacity in reactions, improved thermal and pH stability compared to the free enzyme, and magnetic separation of the catalyst, all of which allowed retention of 70% activity up to 21 cycles.[247] A different approach utilised colloidosomes by inducing interfacial polymerisation of dopamine within the oil/water phase of silica particles to allow covalent attachment of encapsulated lipases. This system demonstrated improved esterification activity compared to the free lipase, as well as efficient recycling which retained 86.6% of enzyme activity after 15 cycles.[248]

Many other enzymes have been immobilised using PDA to various solid supports such as trypsin on silica/titania monoliths,[249] alkaline phosphatase on quartz glass,[250] laccase on halloysite nanotubes,[251] formate dehydrogenase on Fe_3O_4 NPs,[252] and glucose oxidase with a metal-organic framework.[253] PDA has also been involved in the formulation of various multienzyme cascade systems, maintaining a strong adhesion/entrapment of the enzymes without the loss of activity.[254–256] For example valuable isomalto-oligosaccharide (IMO) was produced from starch by immobilisation of glucosidase, α- and β-amylase within PDA microcapsules.[254]

Interestingly, PDA has also been coated on bacterial *Rhodotorula glutinis* cells that led to improved biocatalytic activity towards the asymmetric reduction of acetophenone.[257] A five times increase in catalytic activity (product yield) was observed for the PDA coated cells when compared to native cells, as well as an eight times increase in biocatalyst reusability. The authors propose that the PDA coating acts as a redox shuttle for the transfer of two protons and two electrons, thus accelerating the rate of electron transfer in the reduction or from the cytoplasm to the extracellular environment. Additionally, the PDA coating allowed further

functionalisation with other inorganic components such as Fe_3O_4 for magnetic retrievability and TiO_2 for UV protection.

Overall, the use of PDA in catalysis as a support material has demonstrated a key role in enhancing the catalytic properties of both metal and biological catalysts through interplay of its inherent redox chemistry. The utilisation of this chemistry has been further investigated through organo- and photocatalytic applications within catalysis.

1.2.2 Polydopamine organocatalysis

PDA has demonstrated intrinsic organocatalytic activity towards a small number of organic transformations as a result of reactive catechol, quinone and amino moieties that also enable H-bonding, π-interactions and electrostatic stabilisation of intermediates. For example, in 2014 the Liebscher group reported that PDA could catalyse aldol condensation reactions between aryl aldehydes and cyclohexanone under mild aqueous conditions in both its pure and Fe_3O_4 NP coated forms (**Figure 1.25A**).[258] Aldehydes with electron-withdrawing groups (R^1 = NO_2, Br) reacted well however without activation (R^1 = H, OMe) low or no activity was observed. Mechanistically, the authors proposed a transition state whereby cyclohexanone forms an imine with PDA and undergoes nucleophilic attack to the non-covalently bound aryl aldehyde (**Figure 1.25A**). The PDA catalyst was found to be reusable up to 5 runs however, decreasing activity was apparent and more pronounced when using Fe_3O_4@PDA NPs due to PDA leaching.[258]

In the same year, Yang *et al.* utilised PDA NPs in combination with KI to synthesise cyclic carbonates from a range of epoxides and CO_2 in solvent-free conditions (**Figure 1.25B**).[259] It should be noted that catalysis was only observed in the presence of KI, and recyclability was demonstrated up to six runs. The authors proposed a synergistic mechanism between PDA and KI through H-bonding activation of the epoxide by catechol residues in order to facilitate KI integration, CO_2 addition and cyclisation, similar to that observed with cellulose/KI.[260]

PDA NPs were also used as a catalyst for the formation of disulfide bonds between a range of thiols under aqueous aerobic conditions (**Figure 1.25C**).[261] The catalyst showed excellent recyclability up to five runs with no changes in the

morphology of particles. It was proposed that the thiol conjugates *via* Michael addition to quinone moieties within the PDA polymer and then reacts with another thiol to form the disulfide bond and dissociate from the polymer. It should be noted that thiol conjugation to PDA is a primary way to functionalise the material post synthesis,[188,262] which indicates that anaerobic conditions must be employed to avoid catalytic thiol oxidation.

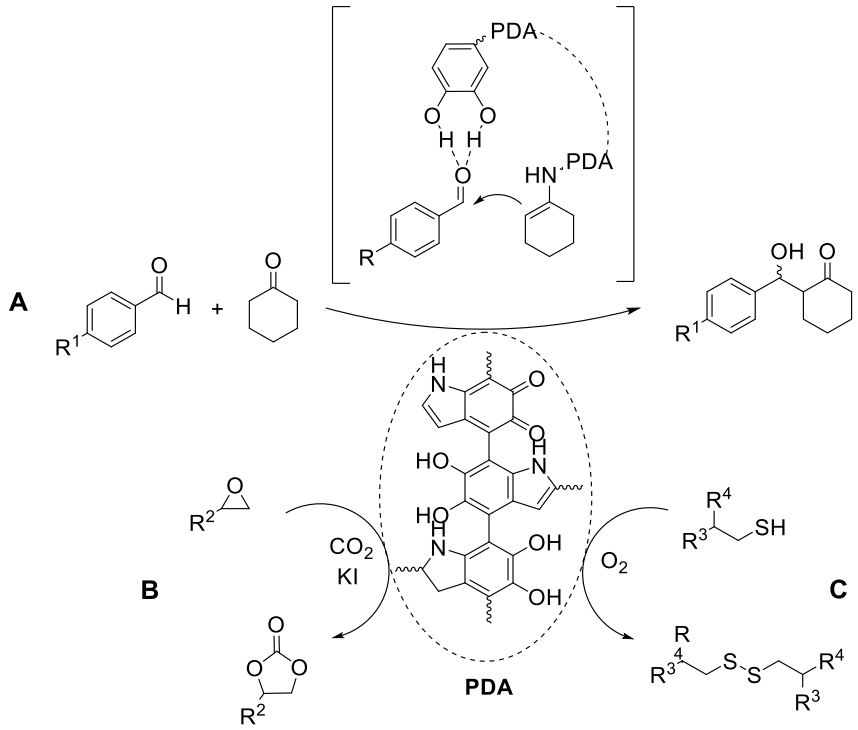

Figure 1.25: Examples of PDA organocatalysis: (A) aldol condensation,[258] (B) synthesis of cyclic carbonates from epoxides using CO_2 and KI,[259] and (C) oxidative thiol coupling.[261]

Recently, the organocatalytic activity of PDA has been extended by taking advantage of the similarity between PDA catechol/quinone moieties and naturally occurring quinone redox cofactors within copper amine oxidases (CuAOs) to synthesise a series of N-heterocycles in aqueous solvent conditions (**Figure 1.26**).[263] PDA particles (100 wt%) were utilised as a heterogeneous catalyst to synthesise a series of benzimidazole and quinoxaline compounds were synthesised at 80 °C in either H_2O or H_2O/EtOH (1:1, v/v) under O_2 atmosphere with yields up to 92% after 6-24h depending on R^1 and $R^{2/3}$ substituents (**Figure 1.26A**). Similarly, quinazolinone derivatives were obtained using analogous conditions but the substrate scope was more limited as electron-withdrawing groups (R^4 = CF_3, **Figure 1.26B**) show no activity. Secondary

amine oxidation was also demonstrated using the same reaction conditions through the dehydrogenation of some tetrahydroquinolines and indole with isolated yields up to 84% over 24h (**Figure 1.26C**). Furthermore, a large-scale reaction (1.5 mmol) and recycling of both pure PDA and Fe_3O_4@PDA was demonstrated up to 3 runs with no considerable loss of catalytic activity, however the magnetic system displayed longer reaction times and lower yields due to less catalytically active PDA being present in the reaction.

The mechanism proposed by the authors for the heterocycle formation involves the formation of PDA-imine adducts with the substrate which then undergoes transamination with the aniline and subsequent cyclisation-oxidation steps to yield the final product. The oxidation of secondary amine substrates was presumed to proceed through a similar imine adduct followed by hydrolysis and oxidation to form the oxidized quinolines and indole.

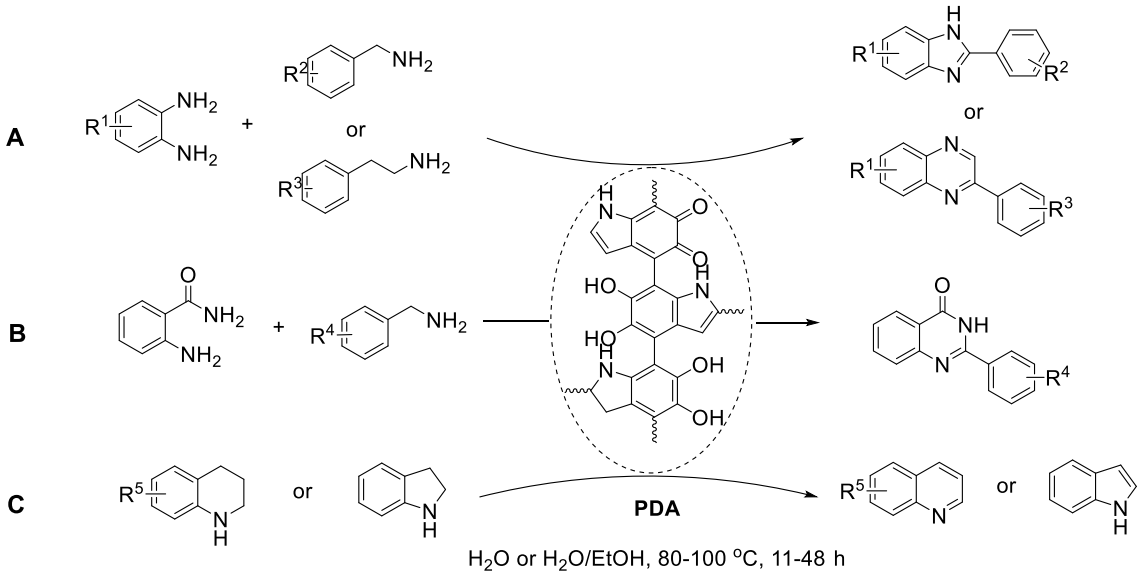

Figure 1.26: Synthesis of N-heterocycles using PDA as an amine oxidase mimetic catalyst: (A) substituted benzimidazole or quinoxaline formation, (B) substituted quinazolinone formation and (C) oxidative aromatisation of substituted tetrahydroquinolines or indoline.

In summary, this work alongside the previously mentioned examples, clearly demonstrate that PDA shows promising biomimetic catalytic activity that has the potential to expand and improve modern green chemistry methodology.

1.2.3 Polydopamine photocatalysis

The structure of PDA features conjugated dihydroxyindole oligomers of varying length and character stacked *via* π-interactions, resembling that of naturally occurring melanins.[193] As a result, melanin has historically been described as an amorphous organic semiconductor due to its broad absorption spectrum, electrical conductivity and photoconductivity,[264,265] however recent reports have shown that melanin acts more as an electronic-ionic hybrid conductor.[266] In either case, PDA has been utilised in a number of photocatalytic applications thanks to its close relation to melanin and related optical and electrical properties.[209,267]

The use of PDA in photocatalysis has mainly been in conjunction with semiconducting metal oxides or related materials to achieve water pollutant dye degradation.[209] Photocatalytic dye degradation using semiconductor-PDA (SC-PDA) composites share many of the same advantages as previous examples of 'dark' M^0-PDA catalysis, whereby PDA helps to immobilise the catalytic metal into an elaborated support material, and also enhances activity through redox mediation and/or improved substrate binding. For wide-band gap semiconductors like TiO_2, PDA is also employed to sensitise visible light activity due to broad absorption over the UV-Vis light spectrum.[268–271] Other examples include the addition of plasmonic metal photocatalysts such as Au,[272,273] and Ag/AgCl,[274–276] as well as other semiconductors such as carbon nitride,[275,277] ZnO,[278] Cu_2O,[279] and β-FeOOH.[280] All these examples however, focus on the degradation of organic dye compounds such as methylene blue, rhodamine B or methyl orange as model substrates for water remediation applications. There are fewer examples however, utilising PDA enhanced photocatalysis to achieve useful organic transformations in synthesis.

Xie *et al.* demonstrated that PDA enhanced the activity of Pd NPs (10-30 nm) towards Suzuki cross-coupling reactions under white LED irradiation.[281] The Pd NPs were supported on an inert carrier material such as carbonised loofah (CL), utilising a PDA nanofilm to attach the Pd NPs after initial *in-situ* reduction of $Pd(OAc)_2$. Without irradiation, the reaction between iodobenzene and phenylboronic acid using the CL supported catalyst gave only trace amounts of product at room temperature after 2h. Using white LED irradiation resulted in an increase up to 96% isolated yield and overall,

very good substrate scope was demonstrated, however amino substituents were not compatible due to interaction with the PDA film. Recyclability of the catalyst system (using CL support) was demonstrated up to five runs with very little loss of activity and Pd NP content. The authors proposed a mechanism to explain their observations whereby charge separation within PDA upon irradiation enables the accumulation of electrons on Pd NPs and positive charge on PDA (**Figure 1.27**). Addition of aryl substrates to PDA *via* π-stacking could subsequently undergo rapid addition to Pd NPs, with Ar-$B(OH)_3^-$ being activated by interaction with h^+ on PDA. Reductive elimination of the aryl-Pd complexes yields the biphenyl products.

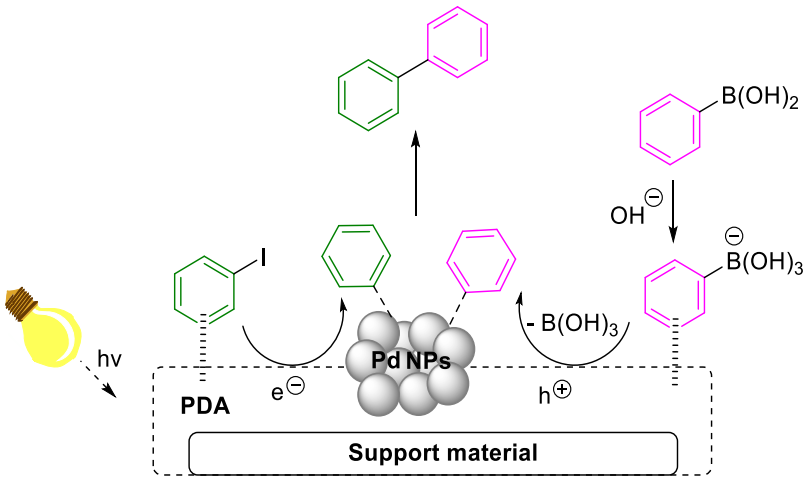

Figure 1.27: Proposed mechanism of the photochemically enhanced Suzuki coupling catalysed by a supported Pd/PDA catalyst. Adapted from Xie *et al*.[281]

In another example, PDA-coated TiO_2 nanotubes have been reported to oxidise benzyl alcohol wherein the PDA coating acts as a visible light sensitiser for TiO_2.[282] The mechanism proposed by the authors involves charge injection from photoexcited PDA to the TiO_2 conduction band which leads to the generation of $O_2^{\bullet-}$ from dissolved O_2. The superoxide radical then oxidises the benzyl alcohol substrate to benzaldehyde. Interestingly, the system showed recyclability up to three runs of 24 h reactions with no decomposition of PDA reported, however quantities of benzaldehyde produced were low at around 30 µmol or 3.2 mg per 24 h run.

It is clear from these examples that the applicability of PDA in photocatalysis for organic synthesis is far from being fully explored but also demonstrates it could be very useful in heterogeneous photocatalyst design. Outside of organic synthesis or

water remediation, the photoactivity of PDA has also shown great potential in artificial photosynthesis,[283,284] dye-sensitised solar cells (DSSCs) [285] and CO_2 reduction.[286–288]

To summarise, the use of PDA within catalysis is broad and despite its use primarily being as a support for metals or other inorganic materials, it has shown the ability to enhance (photo)catalytic processes by synergistic redox chemistry and biomimetic organocatalytic ability. Collectively, these attributes position PDA as a good candidate to advance green heterogeneous catalyst design.

1.3 Aims & Objectives

This thesis aims to develop novel heterogeneous flavin photocatalysts using PDA nanoparticles. So far, the only reported organic (metal-free) heterogeneous photocatalysts systems comprise of carbon nitrides and related materials such as carbon dots.[289,290] The use of PDA as a catalytic support material has already demonstrated interesting synergy between the carried catalyst (metal, semiconductor or biological) and PDA's inherent redox chemistry that enhances activity. This redox chemistry has been further utilised in organocatalytic transformations and within photocatalysis to sensitise semiconductor activity. The use of PDA-based heterogeneous photocatalysts to achieve biomimetic transformations has not yet been reported as well as its combination with an organic photosensitiser such as flavin. It is therefore envisaged that the combination of flavin with nanostructured PDA, which is not just a passive carrier of the photoactive moiety but actively engages in the catalytic process, could yield a system with enhanced photocatalytic activity and give rise to a new class of organic heterogeneous photocatalysts.

Hence, the major objectives of this thesis are to ***rationally design flavin-PDA hybrid nanoparticles and characterise their photocatalytic activity***. There is a distinct lack of reports regarding flavin photocatalysis of reduction reactions as well as efficient heterogeneous/supramolecular systems that can mimic flavoenzyme activity. Therefore, following initial characterisation using model redox substrates, ***photocatalysis of flavoenzyme-specific oxidation and reduction reactions using flavin-PDA will be investigated.*** This therefore extends the current repertoire of catalytic flavin systems towards efficient, biomimetic heterogeneous photocatalysts which could be useful not only in organic synthesis but also in biomedical and energy applications due to its expected biocompatibility.

2 SYNTHESIS AND PHOTOCATALYTIC ACTIVITY OF FLAVIN-POLYDOPAMINE NANOPARTICLES

2.1 Introduction

This chapter details the synthesis and characterisation of flavin-polydopamine (**FLPDA**) copolymer nanoparticles (NPs) as well as their related photocatalytic activity. A flavin-DOPAC monomer (**FLDA**, **Figure 2.1A**) was first designed to mimic flavin adenine dinucleotide (FAD, **Figure 2.1A**) and subsequently copolymerised with dopamine to form self-assembled **FLPDA** NPs (**Figure 2.1B**). Initial characterisation of **FLPDA**'s photocatalytic capabilities was assessed by monitoring both oxidation and reduction reactions using a redox dye system based on resorufin (**RF**). There is far less data available on photoreductions catalysed by flavins when compared to photooxidations, so it was deemed important to establish this ability for **FLPDA** to widen the scope of flavin photocatalysis. By probing the whole spectrum of the photocatalytic action of **FLPDA**, a deeper insight into the mechanism can be gained to help in the design of even more effective catalytic systems useful for industrially relevant organic transformations. In order to demonstrate the green potential of enzyme inspired **FLPDA** and its potential applicability in fields other than photocatalysis, the in vitro cell biocompatibility of the system is also assessed.

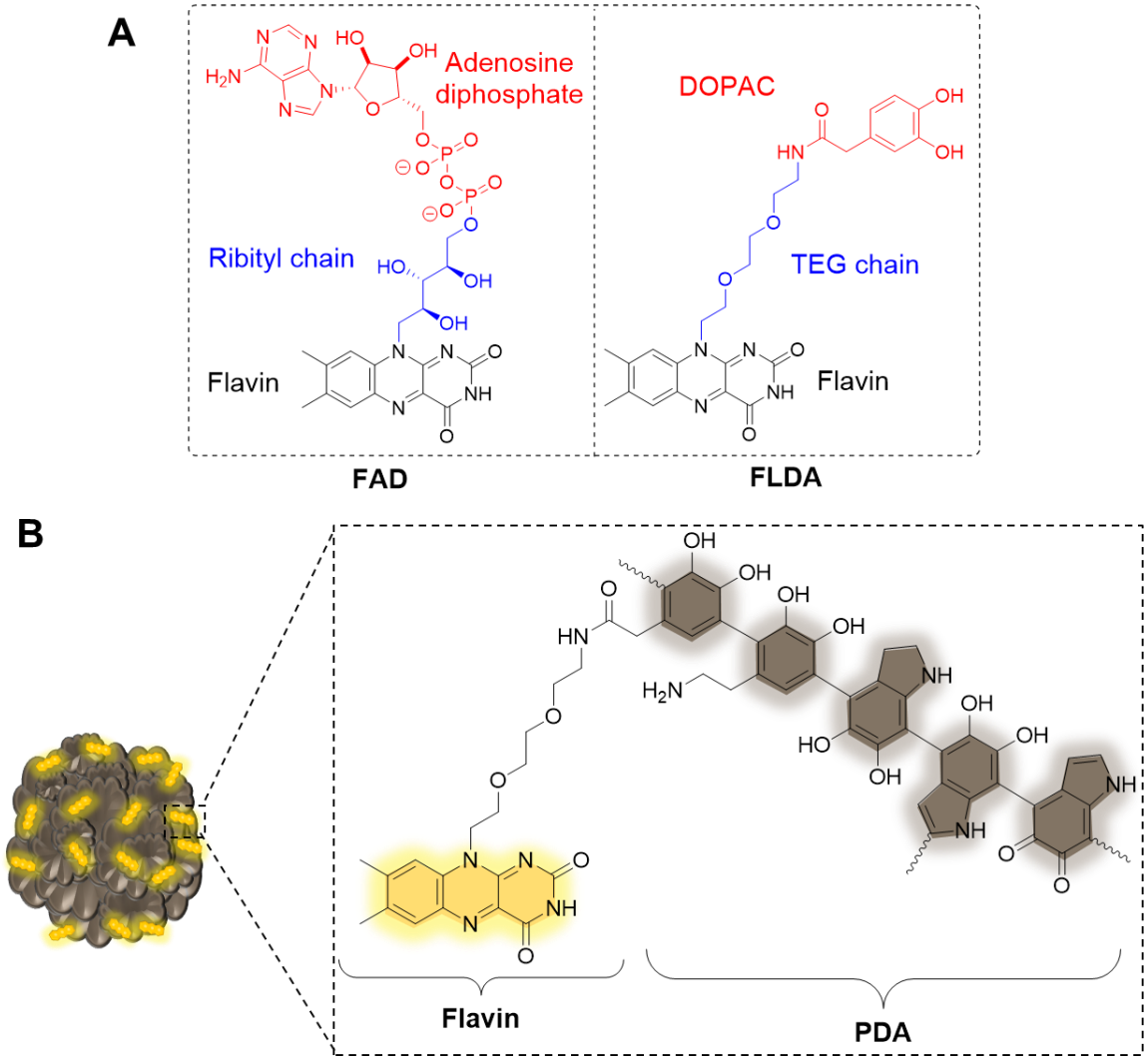

Figure 2.1: Structures of flavin-DOPAC (**FLDA**) monomer and flavin-polydopamine (**FLPDA**) nanoparticles. (A) Comparison of naturally occurring flavin cofactor FAD and **FLDA** synthesized in this work. (B) General structure of **FLPDA** NPs.

2.2 Collaborative Work

Resorufin photocatalytic assays were performed in collaboration with Philipp Koehler in the group of Dr. Tijmen Euser (Nanophotonics Centre, University of Cambridge). Cell culture and biocompatibility assays were performed by Patrick Bernhard in the group of Dr. Ljiljana Fruk (Department of Chemical Engineering and Biotechnology, University of Cambridge).

2.3 Experimental

2.3.1 Materials and Methods

All materials were purchased from either Acros Organics, Alfa Aeser, Sigma-Aldrich or TCI Chemicals in the highest purity available and used without further purification. 1-Azido-2-(2-(2-iodoethoxy)ethoxy)ethane (**1**) was synthesised according to the literature procedure by Deng *et al.*[291] 2-(2,2-Dimethylbenzo[d][1,3]dioxol-5-yl)acetic acid (**5**) was synthesised according to the literature procedure by Geiseler *et al.*[292]

^{1}H and ^{13}C NMR measurements were carried out using a 500 MHz DCH Cryoprobe Spectrometer. HRMS was recorded on a ThermoFinnigan Orbitrap Classic (Fisher Scientific). UV-Vis absorption spectra were obtained with an Agilent Cary 300 Spectrophotometer. Fluorescence emission spectra were obtained using a Varian Cary Eclipse Fluorescence Spectrophotometer using excitation and emission splits of 5 nm or 10 nm. DLS and zeta potential measurements were recorded using a Zetasizer Nano Range instrument (Malvern Panalytical). FTIR spectroscopy was carried out using a Bruker Tensor 27 spectrometer with samples pressed into KBr pellets. STEM images were obtained using a Hitachi S-5500 In-Lens FE STEM (2009) at an acceleration voltage of 1.0 kV. Samples were suspended in water (0.1 mg/mL) and drop cast on lacey carbon copper grids (Agar Scientific).

2.3.2 Synthesis of FLDA

N1-(2-(2-(2-azidoethoxy)ethoxy)ethyl)-4,5-dimethylbenzene-1,2-diamine (2):

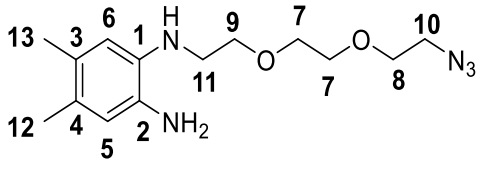

4,5-Dimethylbenzene-1,2-diamine (1.00 g, 7.34 mmol) and K_2CO_3 (2.03 g, 14.68 mmol) were dissolved in anhydrous DMF (30 mL) and heated to 50 °C under Ar atmosphere. 1-Azido-2-(2-(2-iodoethoxy)ethoxy)ethane (2.09 g, 7.34 mmol) dissolved in anhydrous DMF (10 mL) was then added dropwise and the resulting mixture was stirred at 50 °C overnight. DMF was removed under reduced pressure and the resulting residue was re-dissolved in DCM (50 mL) and washed with water (3 x 50 mL) and brine (2 x 50 mL).

The organic layer was then dried over anhydrous Na_2SO_4 and evaporated. The crude product was then purified by silica gel column chromatography using the solvent system DCM/MeOH (99.5:0.5) to give the title compound as a red oil (1.50 g, 5.11 mmol, 70%).

^{1}H NMR (500 MHz, $CDCl_3$): δ = 6.52 (s, 1H, **H-5**), 6.48 (s, 1H, **H-6**), 3.74 (t, 2H, ^3J = 5.2 Hz, **H-9**), 3.70-3.67 (m, 6H, **H-7**, **H-9**), 3.39 (t, 2H, ^3J = 5.1 Hz, **H-10**), 3.27 (br. s, 2H, **H-11**), 2.15 (2 x br. s, 6H, **H-12**, **H-13**) ppm

^{13}C NMR (500 MHz, $CDCl_3$): δ = 134.91 (**C-1**), 132.93 (**C-2**), 127.72 (**C-3**), 126.90 (**C-4**), 118.24 (**C-5**), 115.11 (**C-6**), 70.68 (**C-7**), 70.35 (**C-8**), 70.11 (**C-9**), 50.71 (**C-10**), 44.45 (**C-11**), 19.24 (**C-12**), 18.84 (**C-13**) ppm

HRMS (ESI) m/z: $[M + H]^+$ Calcd for $C_{14}H_{24}O_2N_5$ 294.1925; Found 294.1914.

10-(2-(2-(2-Azidoethoxy)ethoxy)ethyl)-7,8-dimethylbenzo[g]pteridine-2,4(3H,10H)-dione (3):

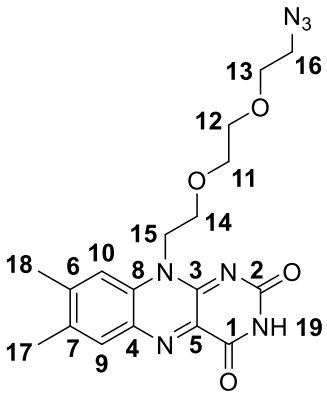

Compound **2** (2.50 g, 8.52 mmol), B_2O_3 (1.19 g, 17.04 mmol) and alloxan monohydrate (1.21 g, 8.52 mmol) were dissolved in glacial acetic acid (25 mL) and left to stir in the dark at room temperature under Ar atmosphere for 2 days. Water was added (25 mL) and extracted with DCM (3 x 50 mL). The organic layer was evaporated and then co-evaporated with toluene (3 x 50 mL) to remove any traces of water and acetic acid. The crude product was purified by silica gel column chromatography using a gradient solvent system of DCM/acetone (4:1 - 1:1) to give the title compound as an orange solid (2.35 g, 5.89 mmol, 69%)

^{1}H NMR (500 MHz, DMSO-d_6): δ =11.30 (s, 1H, **H-19**), 7.82 (s, 1H, **H-9**), 7.81 (s, 1H, **H-10**), 4.76 (t, 2H, ^3J = 5.8 Hz, **H-15**), 3.81 (t, 2H, ^3J = 5.8 Hz, **H-14**), 3.54 (m, 2H, **H-13**),

3.45 (m, 4H, **H-11**, **H-12**), 3.25 (t, 2H, ^{3}J = 5.8 Hz, **H-16**), 2.47 (s, 1H, **H-17**), 2.36 (s 1H, **H-18**) ppm

^{13}C NMR (500 MHz, DMSO-d_6): δ = 160.33 (**C-1**), 155.98 (**C-2**), 150.66 (**C-3**), 146.65 (**C-4**), 137.48 (**C-5**), 136.20 (**C-6**), 134.10 (**C-7**), 131.83 (**C-8**), 131.18 (**C-9**), 117.30 (**C-10**), 70.67 (**C-11**), 70.06 (**C-12**), 69.73 (**C-13**), 67.24 (**C-14**), 50.39 (**C-15**), 44.56 (**C-16**), 21.06 (**C-17**), 19.22 (**C-18**) ppm

HRMS (ESI) m/z: $[M + Na]^+$ Calcd for $C_{18}H_{21}O_4N_7Na$ 422.1547; Found 422.1528.

10-(2-(2-(2-aminoethoxy)ethoxy)ethyl)-7,8-dimethylbenzo[g]pteridine-2,4(3H,10H)-dione (4):

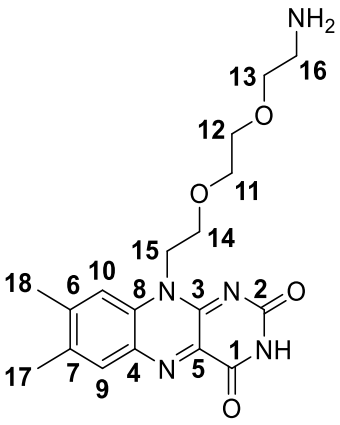

Flavin **3** (0.50 g, 1.25 mmol) was added to a dried 100 mL 3 neck round bottom flask and dissolved in degassed glacial acetic acid (50 mL). The vessel was purged with Ar by water aspiration before adding Pd/C (10 mg), rinsing any residual powder off of the flask walls with degassed acetic acid. The vessel was purged with Ar again before replacing the atmosphere with H_2 from a balloon. The reaction was then left to stir for 18 h at room temperature. The atmosphere was then replaced by Ar and the reaction mixture filtered through celite, washed with methanol and evaporated. The crude residue was subjected to flash silica gel column chromatography using the solvent system DCM/MeOH/AcOH (70:20:10 - 20:70:10) to give the title compound as a red residue (0.43 g, 1.05 mmol, 84%).

^{1}H NMR (500 MHz, CD_3OD): δ = 8.20 (s, 1H, **H-9**), 8.14 (s, 1H, **H-10**), 5.17 (t, 2H, ^{3}J = 5.0 Hz, **H-15**), 4.13 (t, 2H, ^{3}J = 5.0 Hz, **H-14**), 3.68 (m, 2H, **H-13**), 3.64 – 3.59 (m, 4H, **H-11**, **H-12**), 3.08 (t, 2H, ^{3}J = 5.0 Hz, **H-16**), 2.68 (s, 3H, **H-17**), 2.55 (s, 3H, **H-18**) ppm

^{13}C NMR (500 MHz, CD_3OD): δ = 158.9 (**C-1**), 151.6 (**C-2**), 150.8 (**C-3**), 145.9 (**C-4**), 140.6 (**C-5**), 137.1 (**C-6**), 134.4 (**C-7**), 131.3 (**C-8**), 130.5 (**C-9**), 117.3 (**C-10**), 70.4 (**C-11**), 69.8 (**C-12**), 67.7 (**C-13**), 66.4 (**C-14**), 42.8 (**C-15**), 39.2 (**C-16**), 20.3 (**C-17**), 18.2 (**C-18**) ppm

HRMS (ESI) m/z: $[M + H]^+$ Calcd for $C_{18}H_{24}O_4N_5$ 374.1823; Found 374.1828.

N-(2-(2-(2-(7,8-Dimethyl-2,4-dioxo-3,4-dihydrobenzo[g]pteridin-10(2H)-yl)ethoxy)ethoxy)ethyl)-2-(2,2-dimethylbenzo[d][1,3]dioxol-5-yl)acetamide (6):

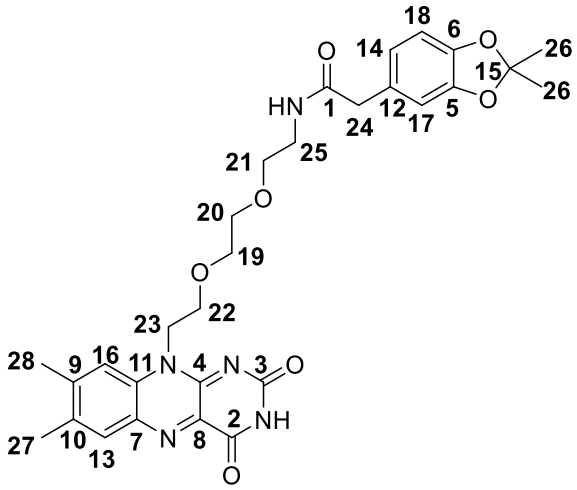

Compound **5** (0.42 g, 2.02 mmol) was dissolved in anhydrous DCM (40 mL) before adding $SOCl_2$ (1.46 mL, 20.17 mmol) and refluxing for 2 h under Ar atmosphere. The reaction mixture was evaporated to remove the solvent and excess $SOCl_2$ was removed by toluene co-evaporation (3 x 20 mL). The resulting dark brown oil was immediately used in the following step without further purification (0.46 g, 2.02 mmol, quant).

Flavin **4** (0.40 g, 0.98 mmol) was dissolved in anhydrous DMF (40 mL) under Ar atmosphere and protected from light. Et_3N (0.27 mL, 1.95 mmol) was added and the solution turned form dark red to dark green. The mixture was then cooled to 0 °C before adding the acyl chloride activated **5** (0.44 g, 1.95 mmol) dissolved in anhydrous DMF (10 mL) dropwise over 20 minutes. The resulting dark red reaction mixture was left to stir and warm to room temperature over 18 h. The solvent was then removed *in vacuo* and the crude residue purified by silica gel column chromatography using the solvent system DCM/MeOH/AcOH (98.5:1:0.5 – 90:6:4) to give the title compound as an orange solid (0.355 g, 0.63 mmol, 64%).

^{1}H NMR (500 MHz, CD_3OD): δ = 7.94 (s, 1H, **H-13**), 7.91 (s, 1H, **H-16**), 6.64 (m, 2H, **H-17**, **H-18**), 6.59 (d, 1H, ^3J = 8.1 Hz, **H-14**), 4.97 (t, 2H, ^3J = 5.4 Hz, **H-23**), 3.98 (t, 2H, ^3J = 5.4

Hz, **H-22**), 3.58 (m, 2H, **H-19**), 3.46 (m, 2H, **H-20**), 3.36 (t, 2H, ^{3}J = 5.6 Hz, **H-21**), 3.34 (s, 2H, **H-24**) 3.21 (t, 2H, ^{3}J = 5.6 Hz, **H-25**), 2.56 (s, 3H, **H-27**), 2.46 (s, 3H, **H-28**), 1.58 (s, 6H, **H-26**) ppm

^{13}C NMR (500 MHz, CD_3OD): δ = 173.0 (**C-1**), 157.8 (**C-2**), 150.6 (**C-3**), 147.8 (**C-4**), 147.5 (**C-5**), 146.4 (**C-6**), 137.5 (**C-7**), 137.2 (**C-8**), 136.2 (**C-9**), 135.7 (**C-10**), 134.8 (**C-11**), 132.2 (**C-12**), 130.9 (**C-13**), 121.3 (**C-14**), 117.6 (**C-15**), 117.1 (**C-16**), 108.7 (**C-17**), 107.5 (**C-18**), 70.5 (**C-19**), 69.9 (**C-20**), 69.0 (**C-21**), 67.5 (**C-22**), 45.0 (**C-23**), 42.1 (**C-24**), 39.0 (**C-25**), 24.5 (**C-26**), 20.0 (**C-27**), 18.0 (**C-28**) ppm

HRMS (ESI) m/z: [M + H]+ Calcd for $C_{29}H_{34}O_7N_5$ 564.2453; Found 564.2448.

2-(3,4-Dihydroxyphenyl)-N-(2-(2-(2-(7,8-dimethyl-2,4-dioxo-3,4-dihydrobenzo[g]pteridin-10(2H)-yl)ethoxy)ethoxy)ethyl)acetamide (FLDA):

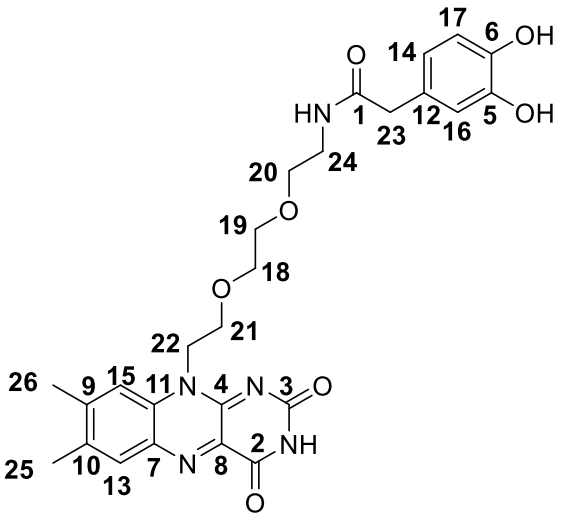

Flavin **6** (0.20 g, 0.35 mmol) was dissolved in DCM (20 mL) and TFA (4 mL) was added dropwise at 0 °C. The reaction mixture was then left to stir at room temperature until TLC analysis showed completion (2 h). The solvent and excess TFA were removed under reduced pressure and co-evaporated with toluene (3 x 20 mL) to give the title compound as a red solid (0.184 g, 0.35 mmol, 99%)

^{1}H NMR (500 MHz, CD_3OD): δ = 7.84 (s, 1H, **H-13**), 7.82 (s, 1H, **H-15**), 6.67 (d, 1H, ^{4}J = 2.1 Hz, **H-16**), 6.64 (d, 1H, ^{3}J = 8.0 Hz, **H-17**), 6.54 (dd, 1H, ^{3}J = 8.0 Hz, ^{4}J = 2.1 Hz, **H-14**), 4.90 (t, 2H, ^{3}J = 5.5 Hz, **H-22**), 3.94 (t, 2H, ^{3}J = 5.5 Hz, **H-21**), 3.55 (m, 2H, **H-18**), 3.44 (m, 2H, **H-19**), 3.36 (t, 2H, ^{3}J = 5.5 Hz, **H-20**), 3.29 (s, 2H, **H-23**) 3.21 (t, 2H, ^{3}J = 5.5 Hz, **H-24**), 2.52 (s, 3H, **H-25**), 2.42 (s, 3H, **H-26**) ppm

^{13}C NMR (500 MHz, CD_3OD): δ = 174.8 (**C-1**), 162.3 (**C-2**), 151.7 (**C-3**), 149.4 (**C-4**), 146.4 (**C-5**), 145.3 (**C-6**), 138.9 (**C-7**), 138.7 (**C-8**), 137.3 (**C-9**), 136.1 (**C-10**), 133.5 (**C-11**), 132.2 (**C-12**), 128.2 (**C-13**), 121.5 (**C-14**), 118.5 (**C-15**), 117.2 (**C-16**), 116.4 (**C-17**), 71.9 (**C-18**), 71.3 (**C-19**), 70.5 (**C-20**), 68.8 (**C-21**), 46.4 (**C-22**), 43.3 (**C-23**), 40.4 (**C-24**), 21.4 (**C-25**), 19.4 (**C-26**) ppm

HRMS (ESI) m/z: [M + H]+ Calcd for $C_{26}H_{29}O_7N_5Na$ 546.1959; Found 546.1948.

2.3.3 Synthesis of DOPAC-free flavin (FLOH)

2-(2-(2-((2-Amino-4,5-dimethylphenyl)amino)ethoxy)ethoxy)ethan-1-ol (7):

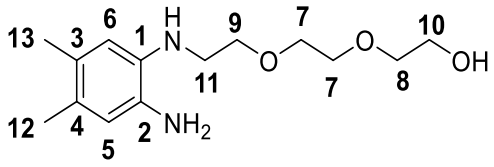

4,5-dimethylbenzene-1,2-diamine (1.41 g, 10.32 mmol) and TEA (2.40 mL, 17.20 mmol) were dissolved in dry THF (40 mL) and heated to 60°C before adding an excess of NaI (5.16 g, 34.40 mmol) and the dropwise addition of 2-(2-(2-chloroethoxy)ethoxy)ethan-1-ol (1.00 mL, 6.88 mmol) dissolved in THF (5 mL). The resulting heterogeneous mixture was then stirred overnight under inert atmosphere at 60°C. After cooling, the mixture was diluted with water (100 mL) and extracted with DCM (5 x 50 mL). The combined organic layers were dried over anhydrous Na_2SO_4 and reduced under reduced pressure. The resulting dark red residue was purified by silica gel column chromatography in DCM-methanol (98:2) to yield a red oil (1.242 g, 4.63 mmol, 67%).

^{1}H NMR (500 MHz, $CDCl_3$): δ = 6.52 (s, 1H, **H-5**), 6.47 (s, 1H, **H-6**), 3.76 (t, 2H, ^{3}J = 5.1 Hz, **H-10**), 3.70 (t, 2H, ^{3}J = 5.1 Hz **H-9**), 3.67 (br. s, 4H, **H-7**), 3.59 (m, 2H, **H-8**), 3.26 (t, 2H, ^{3}J = 5.1 Hz, **H-11**), 2.16 (s, 3H, **H-12**), 2.12 (s, 3H, **H-13**) ppm

^{13}C NMR (500 MHz, $CDCl_3$): δ = 135.15 (**C-1**), 132.44 (**C-2**), 128.01 (**C-3**), 126.71 (**C-4**), 118.45 (**C-5**), 114.82 (**C-6**), 72.79 (**C-7**), 70.36 (**C-7**), 70.00 (**C-8**), 69.63 (**C-9**) 50.71 (**C-10**), 44.2 (**C-11**), 19.27 (**C-12**), 18.82 (**C-13**) ppm

HRMS (ESI) m/z: [M + H]+ Calcd for $C_{14}H_{24}O_3N_2Na$ 291.167914; Found 291.16703.

10-(2-(2-(2-Hydroxyethoxy)ethoxy)ethyl)-7,8-dimethylbenzo[g]pteridine-2,4(3H,10H)-dione (FLOH):

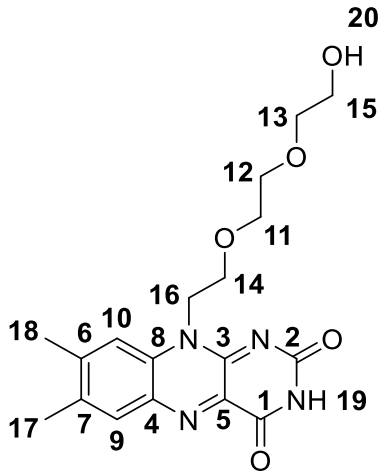

Compound **7**, B_2O_3 (0.778 g, 11.18 mmol) and alloxan monohydrate (0.894 g, 5.59 mmol) were dissolved in glacial acetic acid (17 mL) and left to stir in the dark at room temperature under Ar atmosphere for 2 days. Water was added (25 mL) and the mixture extracted with DCM (3 x 50 mL). The organic layer was evaporated and then co-evaporated with toluene (3 x 50 mL) to remove any traces of water and acetic acid. The crude product was purified by silica gel column chromatography using a gradient solvent system of DCM/acetone (4:1 - 1:1) to give the title compound as a yellow solid (1.49 g, 3.98 mmol, 71%)

^{1}H NMR (500 MHz, DMSO-d_6): δ =11.19 (s, 1H, **H-19**), 7.84 (s, 1H, **H-9**), 7.82 (s, 1H, **H-10**), 4.79 (t, 2H, ^3J = 5.9 Hz, **H-15**), 4.40 (t, 1H, ^3J = 5.5 Hz, **H-20**), 3.85 (t, 2H, ^3J = 5.9 Hz, **H-14**), 3.56 (t, 2H, ^3J = 5.9 Hz, **H-13**), 3.45 (m, 4H, **H-11**, **H-12**), 3.34 (m, 2H, **H-16**), 2.47 (s, 1H, **H-17**), 2.36 (s 1H, **H-18**) ppm

^{13}C NMR (500 MHz, DMSO-d_6): δ = 160.12 (**C-1**), 155.76 (**C-2**), 150.58 (**C-3**), 146.56 (**C-4**), 137.34 (**C-5**), 136.05 (**C-6**), 134.05 (**C-7**), 131.74 (**C-8**), 131.14 (**C-9**), 117.18 (**C-10**), 72.74 (**C-11**), 70.59 (**C-12**), 70.10 (**C-13**), 67.13 (**C-14**), 60.60 (**C-15**), 44.56 (**C-16**), 20.91 (**C-17**), 19.05 (**C-18**) ppm

HRMS (ESI) m/z: $[M + Na]^+$ Calcd for $C_{18}H_{22}O_5N_4Na$ 397.1482; Found 397.1467.

2.3.4 Synthesis of Flavin-Polydopamine

General Procedure: A mixture of ammonia solution (0.1 mL, 28%), ethanol (1.5 mL) and Milli Q water (4.5 mL) was stirred at room temperature for 30 minutes in reaction vessels protected from direct sunlight. Dopamine hydrochloride* dissolved in Milli-Q water (0.5 mL) and **FLDA**** dissolved in ethanol (0.5 mL) were mixed before being added dropwise to the reaction mixture. The resulting dark brown/black mixture was left to stir in the presence of air for 24 h. The mixture was then centrifuged at 25000 x *g* for 30 min and the supernatant was removed. The precipitate was washed with Milli-Q water (3 x 40 mL) and then suspended in Milli-Q water (20 mL), frozen in liquid N_2 and lyophilised to yield a dark brown/black powder.

Sample	*Dopamine Hydrochloride / mg	**FLDA / mg	Molar Ratio (DA·HCl:FLDA)
FLPDA- 5	15.80	8.73	5:1
FLPDA-10	17.24	4.76	10:1
FLPDA-20	18.06	2.49	20:1
PDA	18.96	-	-

2.3.5 Fluorescence Calibration Curve

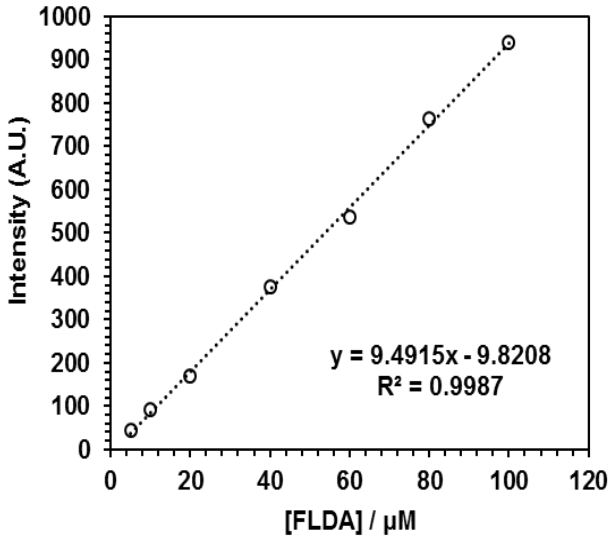

Figure 2.2: Fluorescence calibration curve of **FLDA** at λ_{527} in 0.05 M KPi buffer pH 7.4 (ex/em slits = 10 nm). All measurements were carried out in 200 µL total volume.

Table 2.1: Correlation data obtained from the calibration curve. All measurements were carried out in 0.05 M KPi buffer pH 7.4 and 200 µL total volume (ex/em slits = 10 nm).

Sample	Monomer molar ratio (DA:FLDA)	Intensity @ λ_{527} (50 µg/mL)	Absorbance Corrected Intensity (50 µg/mL)	Relative [FLDA] (µM)	Approximate FLDA content (µmol/mg FLPDA)
FLPDA-5	5:1	325.35	536.73	55.51	1.11
FLPDA-10	10:1	248.16	409.39	42.10	0.84
FLPDA-20	20:1	210.82	347.79	35.61	0.71

2.3.6 Laser Diode Emission Spectrum and Experimental Setup

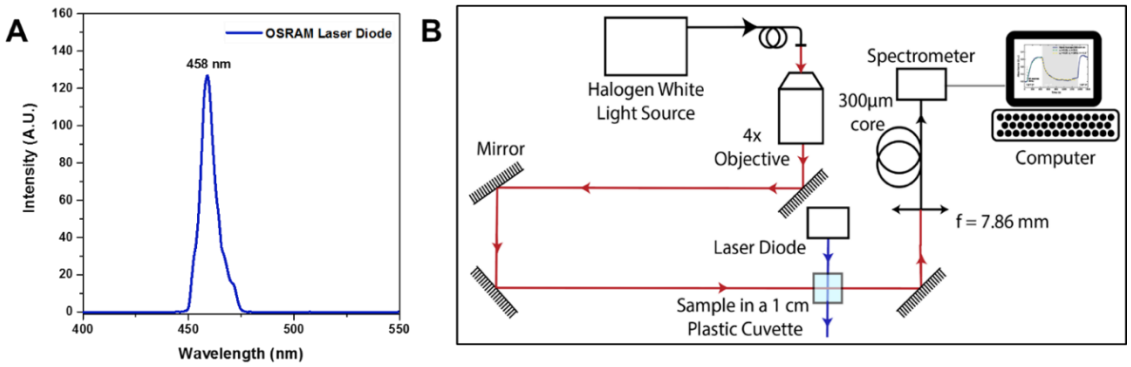

Figure 2.3: (A) Intensity spectrum of the OSRAM laser diode used in the setup (B) Experimental setup of laser diode and fibre-optics.

The time-dependent sample concentrations and reaction rates during excitation with an OSRAM laser diode (**Figure 2.3A**) were measured with a custom-built modular absorption spectroscopy setup as shown in **Figure 2.3B**. A fibre-coupled white light halogen light source (Ocean Optics DH-2000) was collimated with a 4x Olympus Plan N objective and penetrates the sample in a clear 1x1 cm plastic cuvette. The outgoing beam is coupled with a 7.86mm focal length lens into a 300 µm multimode fibre, which was connected to an Ocean Optics QE65000 spectrometer. The reaction is driven with

an OSRAM 458 nm laser diode, spectrum shown in **Figure 2.3A**, through the cuvette perpendicular to the spectroscopy beam.

2.3.7 Photooxidation of Amplex Red

General Procedure: **FLPDA** catalyst (1-10 μg/mL) and Amplex Red (100 μM) were added to a cuvette containing KP_i buffer (2 mL, 10 mM, pH 7.4) under stirring in the dark. The cuvette was then irradiated with a laser diode (458 nm) and spectra were recorded over time. Absorbance values were converted to molar equivalents using the molar extinction coefficient of resorufin at pH 7.4 (67 700 $M^{-1}cm^{-1}$).[293]

2.3.8 Photoreduction of Resazurin

General Procedure: **FLPDA** catalyst (1-10 μg/mL), EDTA (100 μM) and resazurin (25 μM) were added to a cuvette containing KP_i buffer (2 mL, 10 mM, pH 7.4) with stirring. The mixture was purged with N_2 in the dark for 15 minutes. It was then irradiated with a laser diode (458 nm) under N_2 atmosphere and spectra were recorded over time. Absorbance values were converted to molar equivalents using the molar extinction coefficient of resorufin at 572 nm (67 700 $M^{-1}cm^{-1}$, pH 7.4)[293] and for resazurin at 602 nm (35 510 $M^{-1}cm^{-1}$, pH 7.4) which was calculated using known concentrations of resazurin.

Recycling experiments were carried out by irradiating **FLPDA-5** (50 μg/mL) in the presence of **RZ** (0.2 mM) and EDTA (1 mM) in KPi buffer (0.1 M, pH 7.4) for 1 hour under Ar atmosphere. The catalyst was then removed by centrifugation (4000 rpm, 30 min) and washed with MilliQ water (2 x 10 mL).

2.3.9 Cell studies

2.3.9.1 Cell Culture

A549 cells were cultured within 25, 75 or 175 cm^2 flasks in Dulbecco's Modified Eagle's medium (DMEM) supplemented with 10 % (v/v) sterile filtrated (0.2 μM CA membrane filter) fetal bovine serum (FBS), 100 U/mL penicillin and 100 μg/mL streptomycin sulphate (PS) at 37 °C and 5 % CO_2 in a humidified incubator and sub-cultured at 80 % confluency. For passaging cells, the medium was removed, cells were washed with 2-5 mL Dulbecco's Phosphate buffered saline (PBS) before incubating the adherent cells

for 5 min with 2-5 mL trypsin-EDTA solution (0.25 % v/v) in order to detach the adherent cells from the culture flask. After stopping trypsinization by adding at least the same volume of DMEM, the cells were separated from the medium by centrifugation (5 min, 100 x g, RT). Subsequently, the cell pellet was resuspended and diluted in DMEM according to the desired size and cell density of the following cell passage.

2.3.9.2 LDH release cytotoxicity assay

To evaluate the *in vitro* cytotoxicity of **FLPDA** NP treatment on A549 cells, the activity of the cytosolic enzyme lactate dehydrogenase (LDH) present in the culture media was determined by using the commercially available fluorometric LDH assay kit in a 96-well plate format (abcam, UK) monitoring with an excitation of 535 nm and emission at 587 nm.

2.3.9.3 MTS viability assay

To evaluate the *in vitro* viability of **FLPDA** NP treatment on A549 cells, the metabolic activity of the cells was determined by using the commercially available MTS viability assay kit in a 96-well plate format (Promega, USA) monitoring with colorimetric detection between 450-540 nm.

2.3.9.4 Superoxide detection assay

To evaluate the level of oxidative stress on A549 cells by **FLPDA** NPs treatment, the amount of intracellular ROS was detected using the commercially available superoxide detection kit in a 96-well plate format (Enzo Life Sciences Ltd., UK) monitoring with an excitation of 550 nm and emission at 620 nm.

2.4 Results and Discussion

2.4.1 Synthesis and Characterisation

The **FLDA** monomer was synthesised according to the route shown in **Figure 2.4**. First, the functionalised triethylene glycol, **1** was used in a mono-substitution reaction with 4,5-dimethylbenzene-1,2-diamine to form compound **2**. Isoalloxazine formation was achieved through the double condensation reaction with alloxan monohydrate to obtain flavin derivative **3**. The azide functionality was then reduced *via* catalytic hydrogenation to yield the amine-bearing flavin derivative **4**. Conjugation of this compound to the activated catechol-protected dopamine analogue **6** resulted in protected **FLDA** derivative **7**, which was subsequently deprotected to afford the target **FLDA** monomer. Copolymerisation of dopamine and **FLDA** was carried out following a room temperature procedure adapted from Ai *et al.* and using ammonia addition to a water/ethanol solvent system in the presence of air (**Figure 2.4**).[204] The reaction vessels were protected from direct light exposure to avoid any possible side reactions through the excitation of flavin moieties.

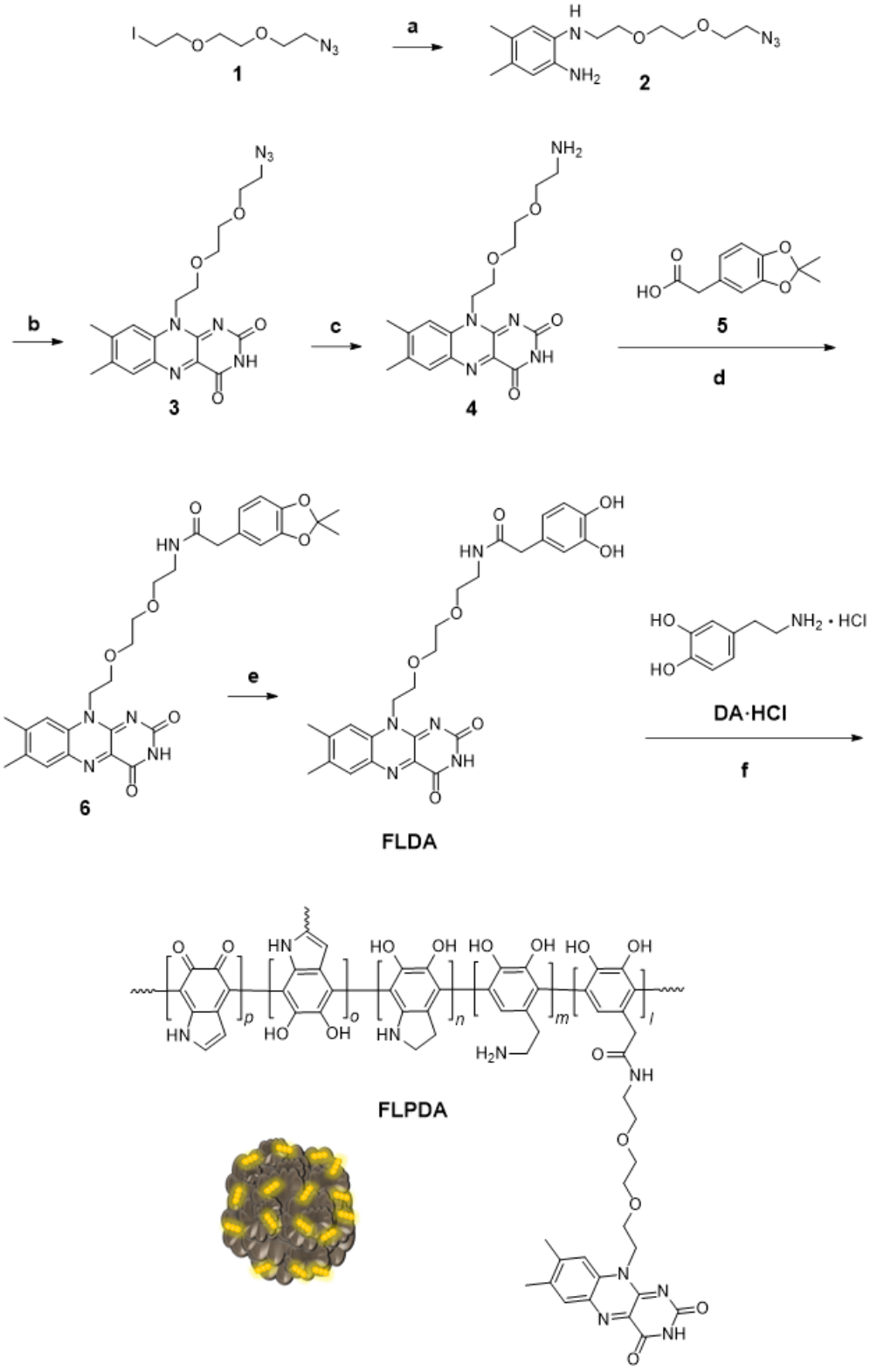

Figure 2.4: Synthesis of **FLDA** and **FLPDA**. Reaction conditions: a) 4,5-dimethylbenzene-1,2-diamine, K_2CO_3, DMF, 50 ^oC, 12 h (70%); b) alloxan monohydrate, B_2O_3, AcOH, RT, dark, 48 h (69%); c) Pd/C, H_2, AcOH, RT, dark, 18 h (84%); d) i) **5**, $SOCl_2$, DCM, reflux, Ar, 2h then ii) **4**, TEA, DMF, RT, dark, 18 h, (62%) e) TFA/DCM, RT, dark, 2 h (99%); f) dopamine hydrochloride, NH_4OH, $EtOH/H_2O$, RT, 24 h.

In order to explore the effect of the amount of the **FLDA** monomer on the copolymerisation and formation of NPs, different molar ratios of dopamine to **FLDA** were used (5:1, 10:1 and 20:1) resulting in NPs referred to as **FLPDA-5**, **FLPDA-10**, **FLPDA-20** respectively. Prepared samples were washed extensively and lyophilized to avoid any thermal decomposition of the polymer that could occur through vacuum heating. Flavin modified NPs were noticeably browner in colour when compared to black unmodified PDA NPs. The zeta potential values ranged from -35.7 mV for **FLPDA-5** to -41.5 mV for **FLPDA-20** indicating good colloidal stability and dispersibility (see **Table 2.2**). The size and shape of **FLPDA** particles were further investigated by STEM (**Figure 2.5**) showing that all samples contained spherical NPs of similar size (approx. 200 nm) with relatively large size distribution (± ~50 nm). Some conjoined particles and the largest size distribution were observed in **FLPDA-5** (see **Figure 2.5A/B** and **Table 2.2**). In contrast, PDA NPs synthesized under the same conditions displays a narrow size distribution with an average size of 110 ± 18 nm (see **Figure 2.5G/H**), which indicates that the presence of flavin moieties affects the polymerization mechanism and oligomer aggregation leading to particle formation. This change in shape and size is most likely a consequence of H-bonding and electrostatic interactions between the flavin group and oligomeric units.

Table 2.2: Size and zeta potential measurements of **FLPDA** samples.

Sample	Monomer molar ratio (DA:FLDA)	Hydrodynamic size (nm)[a]	PDI[a]	Zeta potential (mV)	Particle size (nm)[b]
FLPDA-5	5:1	577.3 ± 37.32	0.448	-35.7 ± 0.3	202 ± 110
FLPDA-10	10:1	495.5 ± 23.05	0.382	-37.7 ± 0.8	207 ± 53
FLPDA-20	20:1	389.4 ± 16.83	0.334	-41.5 ± 0.8	201 ± 58
PDA	1:0	155.0 ± 1.12	0.044	-55.0 ± 1.2	110 ± 18

[a] Measured by DLS
[b] Measured by STEM

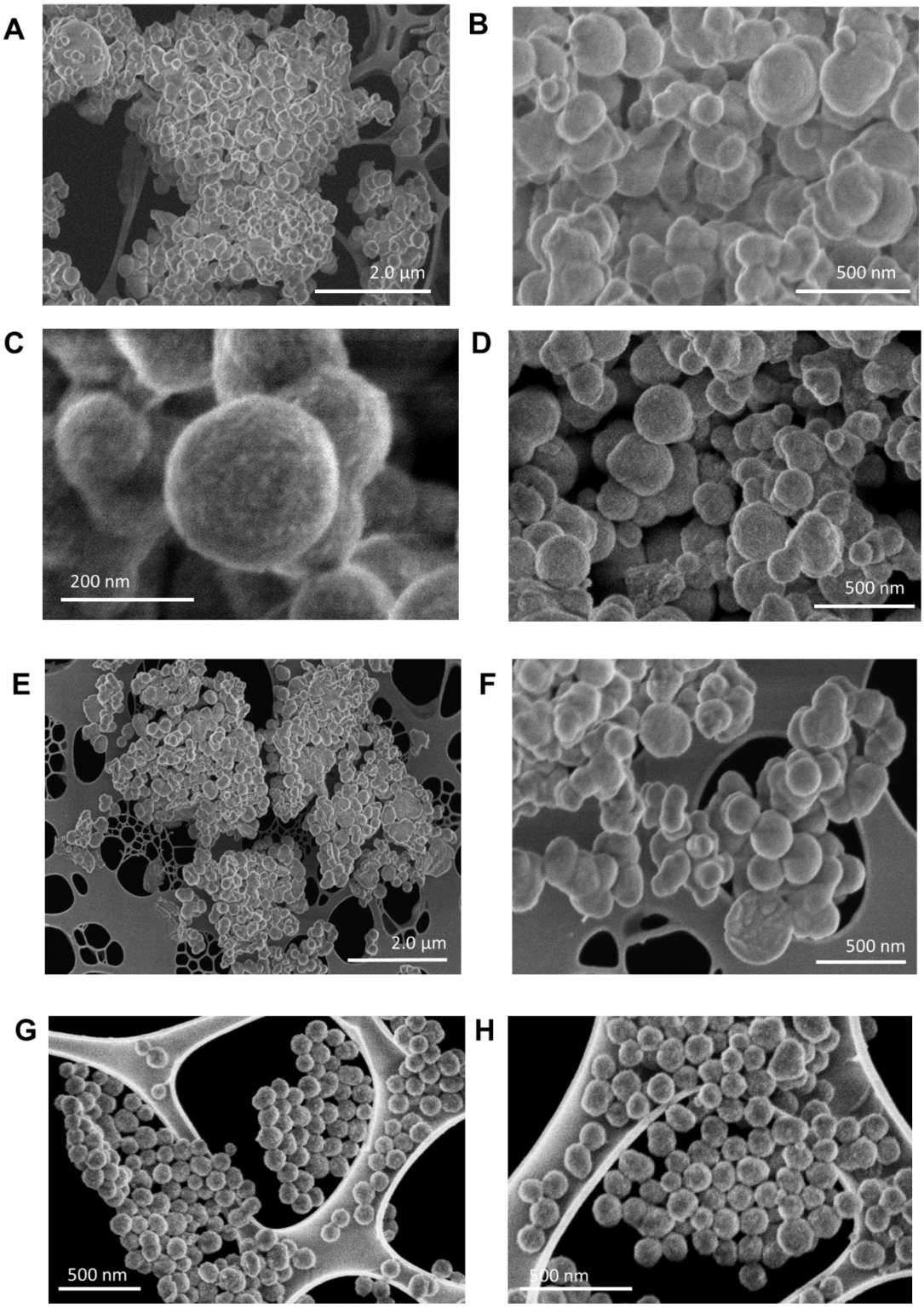

Figure 2.5: STEM images of **FLPDA** NPs prepared with different molar ratios of dopamine to **FLDA** monomer. (A and B) **FLPDA-5** (5:1), (C and D) **FLPDA-10** (10:1), (E and F) **FLPDA-20** (20:1), (G and H) PDA (1:0).

To validate the presence of flavin moieties, particles were first analysed by UV-Vis absorption and fluorescence spectroscopy. The UV-Vis spectrum of the **FLDA**

monomer shows absorption bands at λ_{max} = 445 nm and 373 nm corresponding to the transitions from the ground state (S_0) to the S_1 (λ_{max} ~ 442–450 nm) and S_2 (λ_{max} ~ 360–375 nm) excited states (see **Figure 2.6A**).[2] These bands are red-shifted to ~ 456 nm for the $S_0 \rightarrow S_1$ transition and ~ 376 nm for the $S_0 \rightarrow S_2$ transition in **FLPDA** (**Figure 2.6B**). This can be explained by an increase in proton donation from PDA,[294] and by electron-withdrawing inductive effects on the flavin moieties due to incorporation into the highly conjugated PDA system.[295]

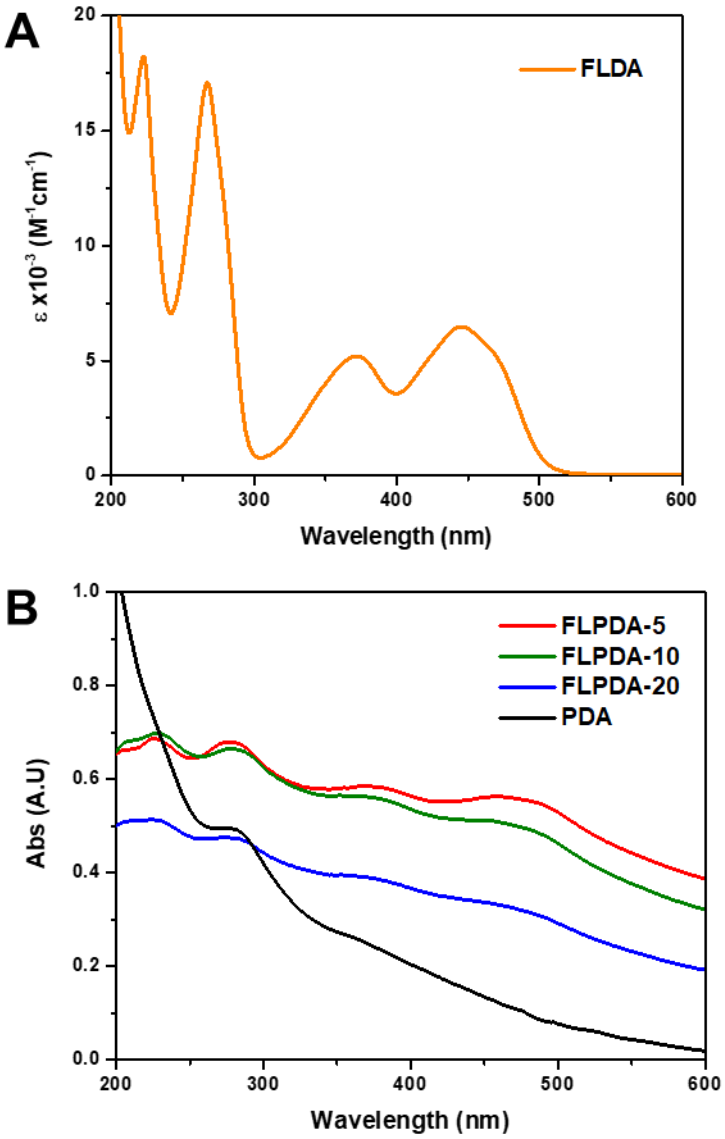

Figure 2.6: UV-Vis absorption spectra of (A) **FLDA** (80 µM in H_2O) and (B) **FLPDA** samples with PDA reference (50 µg/mL in 0.05 M KPi buffer pH 7.4).

The fluorescence emission spectrum of **FLDA** is characterized by emission maxima at ~ 527 nm (λ_{ex} = 450 nm) which correlates well to other known flavin compounds (see **Figure 2.7A**).[296] **FLPDA** samples also exhibit this signal, as shown in **Figure 2.7B**, confirming the presence of flavin moieties in the particles. An earlier study in which flavin compounds were incubated with melanin (structurally analogous to PDA) showed that the fluorescent properties of flavins did not change upon binding and there was no significant fluorescence quenching by the polymer.[297] That study, however, focussed on the non-covalent binding of flavin derivatives to melanin, and not on the covalent attachment used in this work.

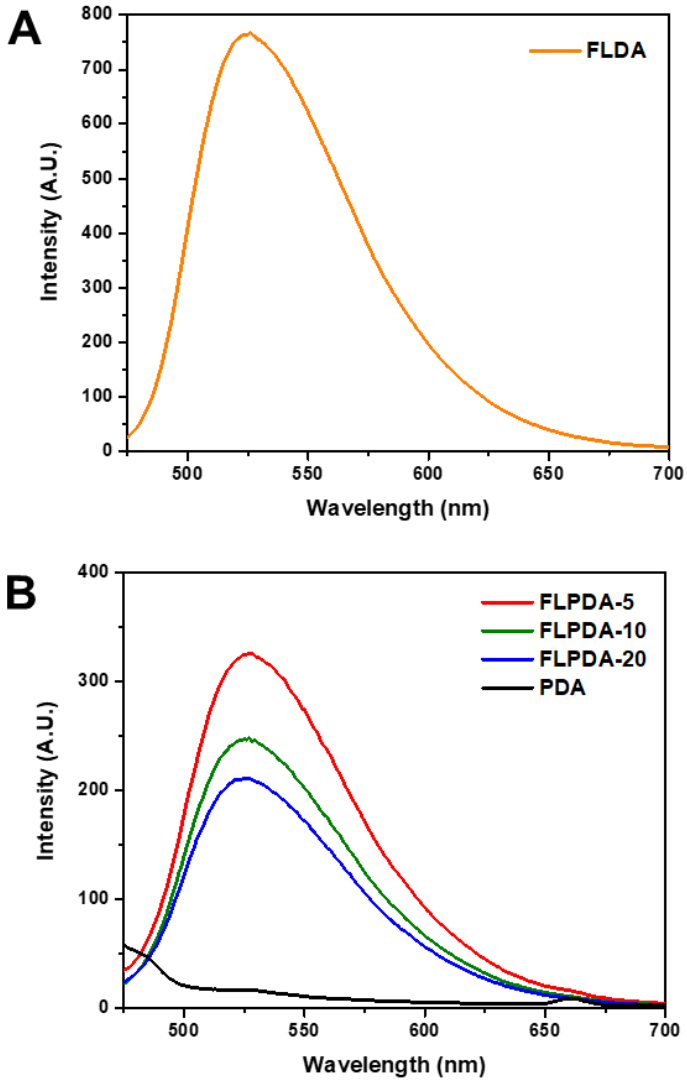

Figure 2.7: Fluorescence emission spectra of (A) **FLDA** (80 µM in H_2O) and (B) **FLPDA** samples with PDA reference (50 µg/mL in 0.05 M KPi buffer pH 7.4).

In order to validate the assumption that flavin content can be indeed quantified *via* fluorescence measurements of particles, a DOPAC-free flavin analogue, **FLOH** was prepared and compared to the DOPAC conjugated monomer **FLDA** (**Figure 2.8**). Despite the UV-vis absorption of **FLDA** being only slightly weaker in signal that **FLOH** (**Figure 2.8**), the fluorescence intensity is much lower for **FLDA** when compared to same concentration of **FLOH** (**Figure 2.9A**) This observation indicates some intramolecular isoalloxazine-catechol fluorescence quenching similar to that found for FAD and adenosine due to a possible formation of a 'closed' structure.[298] Kozik *et al*. suggested that the key phenolic and indolic groups in the melanin polymer do not incur any fluorescence quenching due to their inability to form charge-transfer complexes with the isoalloxazine ring.[297] Although it was initially observed that there was a fluorescence decrease when **FLOH** was incubated with PDA NPs, this was no longer valid after correcting for the absorbance of PDA at the excitation and emission wavelengths. A correction factor was therefore applied by multiplying the λ_{max} intensity value at 527 nm by the percentage absorbance of PDA (50 μg/mL) at λ = 450 nm (41%) followed by the percentage absorbance of PDA at λ = 527 nm (17%). As a result, a representative emission spectrum of **FLOH** was obtained showing negligible quenching by PDA and indicates that any attenuation in intensity is absorbance dependent (**Figure 2.9B**). Additionally, it can be observed that the emission of the absorbance corrected **FLOH** + PDA spectrum exhibits a red-shift to 527 nm. This is the same value as **FLDA** and **FLPDA** but in this case, the emission has the same intensity as **FLOH** alone. It can therefore be assumed that there is negligible fluorescence quenching of the flavin moiety bound covalently to the PDA backbone and the only appreciable quenching is derived from the catechol moiety attached to the monomer **FLDA**.

A fluorescence calibration curve was subsequently obtained using known concentrations of **FLDA** to approximate flavin concentration within the NPs. As expected, **FLPDA-5** contains a higher proportion of flavin than **FLPDA-10** and **FLPDA-20**; approximately 1.11, 0.84, 0.71 μmol/mg **FLPDA** respectively (see **Section 2.3.5** for full details). Clearly, the relative amounts of flavin do not exactly match the initial monomer ratios used for the synthesis. This could be explained by base-catalysed

cleavage and/or hydrolysis of some flavin moieties during the polymerization, which was previously reported for other flavins.[299,300]

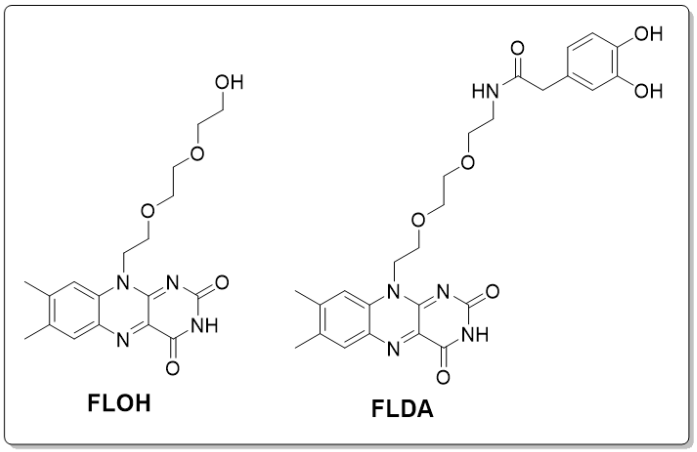

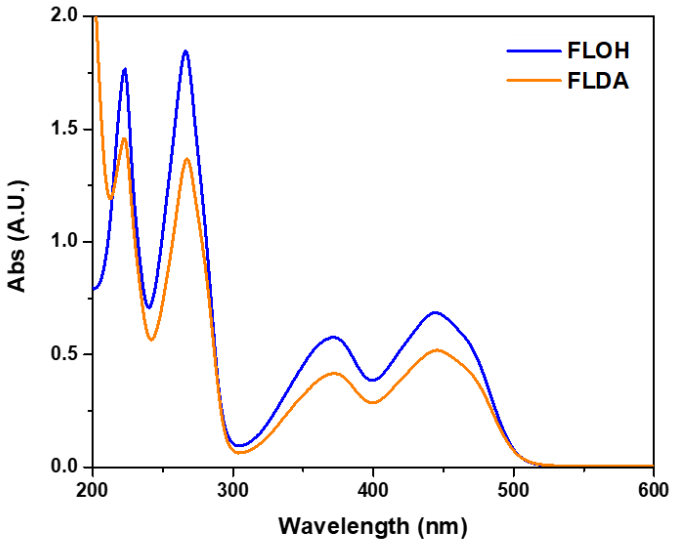

Figure 2.8: Comparison of **FLOH** and **FLDA** structures and their corresponding UV-Vis spectra (100 µM in H_2O).

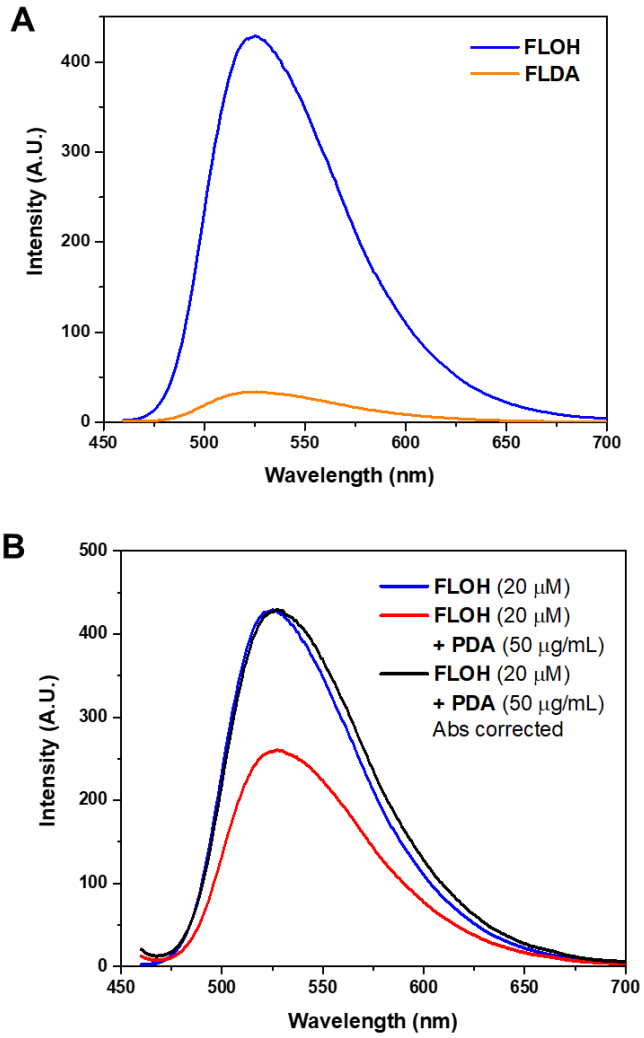

Figure 2.9: Fluorescence emission spectra of (A) **FLDA** and **FLOH** (20 μM in H_2O) and (B) the effect of PDA (50 μg/mL) incubation which decreases fluorescence emission intensity that can be corrected by factoring in the absorbance of PDA.

Flavin presence within nanoparticles was additionally confirmed by Fourier transform infrared (FTIR) spectroscopy by comparing **FLPDA** samples with **FLDA** and **PDA.** As shown in **Figure 2.10**, the FTIR spectrum of PDA (**Figure 2.10A**) contains characteristic bands at 3356 cm^{-1} relating to O-H and N-H stretching vibrations. The spectrum of **FLDA** has a much broader band at 3414 cm^{-1} relating to these vibrations, and as a result, **FLPDA** samples show very similar bands through the contributions of both modes. Unlike PDA, the spectra of **FLPDA** samples clearly contain C-H stretching vibration bands at 2924 and 2855 cm^{-1} that correlate well to the spectrum of **FLDA**. As seen in **Figure 2.10B**, the main characteristic bonds corresponding to the flavin

moieties in the polymer can clearly be observed when compared to the monomer **FLDA**, from the sharp bands at 1545 cm^{-1} and 1580 cm^{-1} relating to ν(C=N) modes in the isoalloxazine ring.[301] Contributions from the flavin carbonyl ν(C=O) (1711 and 1680 cm^{-1}) and ν(C=C) be seen in **FLPDA** samples in combination with C=O and C-O vibrational modes of PDA, seen at 1610 and 1512 cm^{-1} respectively in its spectrum. Further C=N and C=C combined contributions can also be observed at lower wavenumbers in the spectra of **FLPDA** (1292 cm^{-1}).

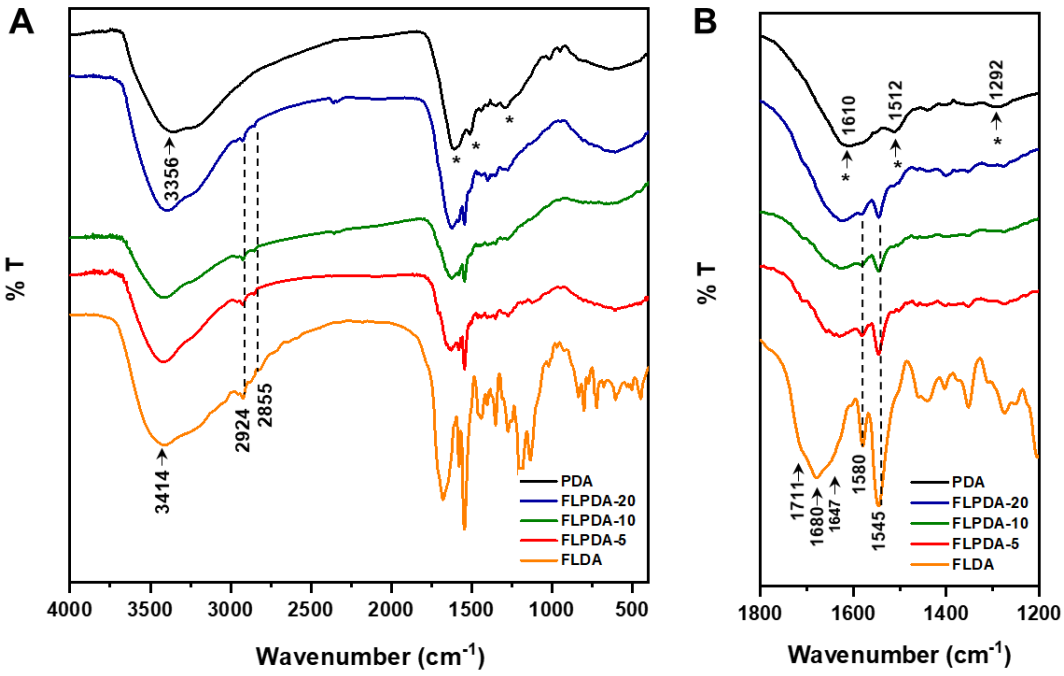

Figure 2.10: FTIR spectra of **FLPDA** samples including PDA and **FLDA** references at (A) full scale and (B) zoomed scale. All samples were measured as KBr discs.

2.4.2 Photocatalytic Assays

Following the preparation and characterization of the **FLPDA** NPs, their photocatalytic activity was initially investigated using model chromogenic dyes to explore both oxidation and reduction reactions (**Figure 2.11**). Amplex Red (**AR**), a common peroxidase enzyme substrate and marker for oxidation[302–304] was chosen as a suitable substrate to monitor **FLPDA** photooxidation activity. The fluorescent product, resorufin (**RF**, absorption λ_{max} = 572 nm) can also be produced by the reduction of blue dye resazurin (**RZ**, absorption λ_{max} = 602 nm), a commonly utilised marker for enzymatic reduction activity.[305] Thanks to the differences in characteristic absorption bands of the substrates and product, monitoring the reaction progress can easily be achieved using real-time UV-Vis absorption spectroscopy (see **Section 2.3.6** for full custom set-up).

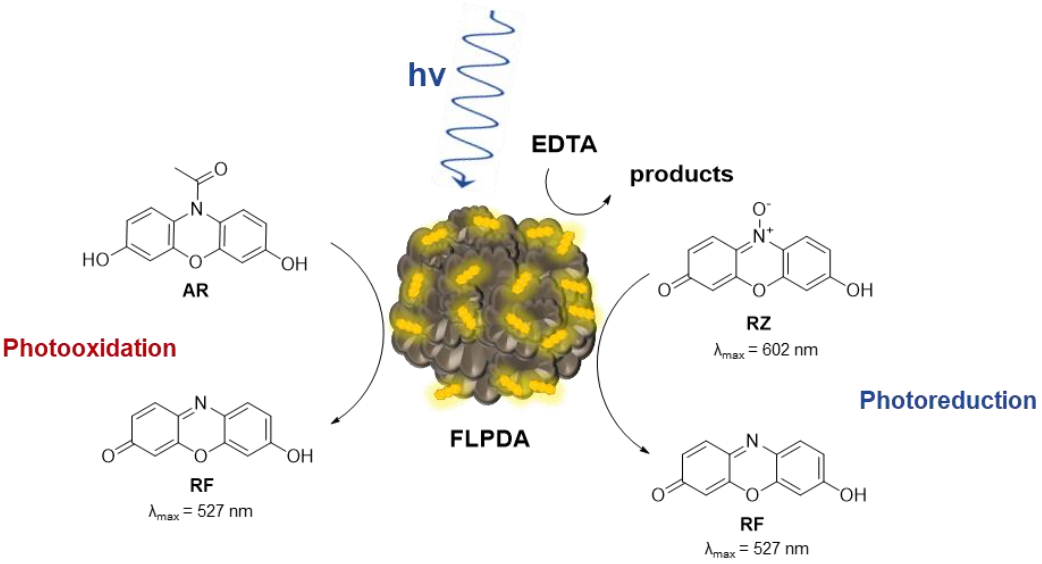

Figure 2.11: Schematic of photo-redox catalytic cycles of resorufin (**RF**) production from Amplex Red (**AR** photooxidation) and resazurin (**RZ** photoreduction) in presence of **FLPDA**.

2.4.2.1 Amplex Red Photooxidation

Initially, 10 µg/mL **FLPDA-5** NPs (~10 mol% flavin) were incubated with **AR** (100 µM) in KPi buffer at pH 7.4 (10 mM, 2 mL) and then irradiated with a blue laser diode (458 nm). Clear oxidative conversion of **AR** to **RF** was observed upon irradiation evidenced by a rapid increase in absorption at 572 nm (**Figure 2.12A**). **FLPDA-5** showed the highest reaction rate of 3.69 µM/h using an excitation intensity of 1.19 mW/cm^2, when

compared to the other **FLPDA** samples, which can be correlated to the higher concentration of flavin moieties within the particles.

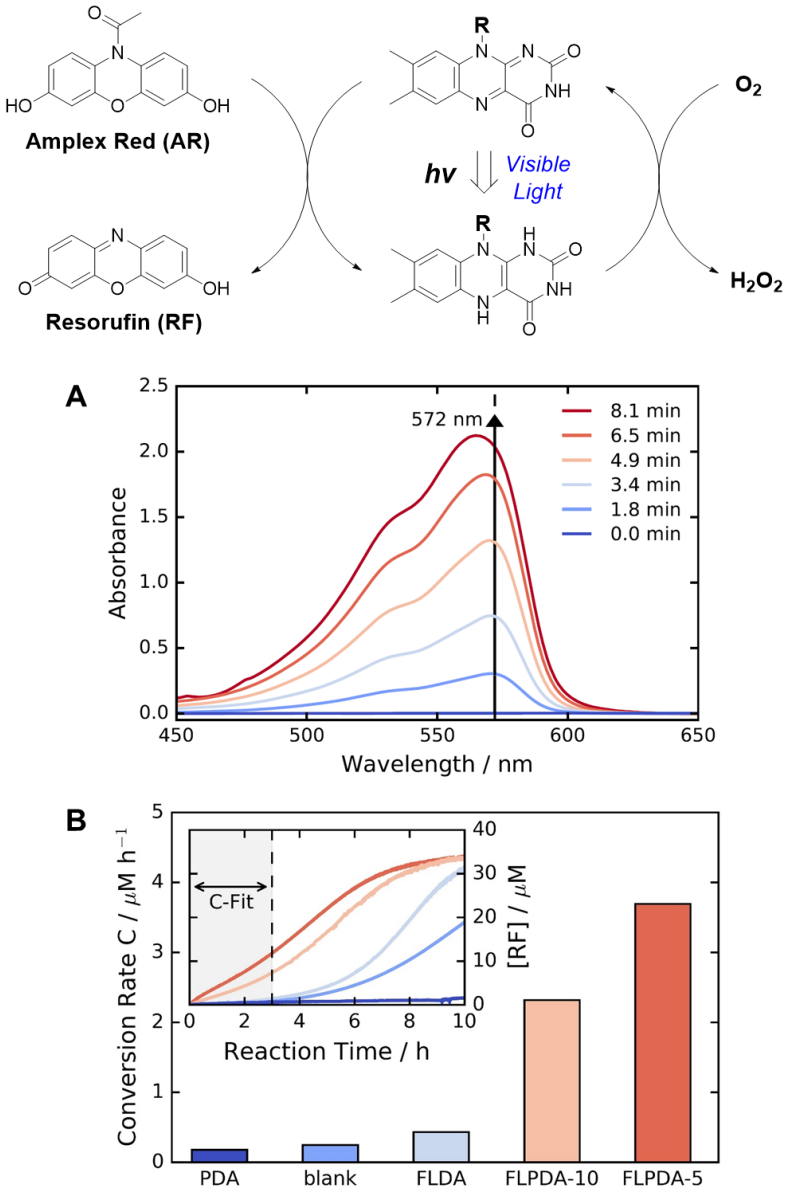

Figure 2.12: FLPDA catalysed photooxidation of Amplex Red (**AR**) to resorufin (**RF**). A) Plot of the absorbance changes observed for the photooxidation of **AR** to **RF** by **FLPDA-5** (10 µg/mL) in KPi Buffer (10 mM, pH 7.4, 2 mL) using 6.40 mW/cm^{2,} excitation intensity. (B) Comparative plot of **AR** photooxidation in presence of **FLPDA** photocatalysts and controls (10 µg/mL, [**FLDA**] = 10 mol%) using 2.95 mW/cm^2 excitation intensity.

Control experiments were performed using **FLDA** (10 mol%) which showed that in comparison to **FLPDA**, the reaction was far less efficient with only 0.43 µM **RF** being produced per hour. Such as significant difference between the monomer and

polymer NP indicates a potential synergistic relationship between PDA and flavin within the hybrid particles, which results in stabilization of reactive intermediates and/or enhancement of charge transfer. Further control experiments using PDA (10 µg/mL) and without any catalyst exhibited no or very little activity. The blank control experiment without any catalyst was carried out as it has been previously reported that trace amounts of excited state **RF** can catalyse the oxidation of **AR**.[306] Indeed, there was some conversion, however, it was at a significantly slower rate (0.24 µM/h vs. 3.69 µM/h for **FLPDA-5**). In addition, the reaction displayed a dependence on laser power indicated by accelerated conversion at higher laser powers, as shown in **Figure 2.13**. This clearly demonstrates the photocatalytic character of **FLPDA** as one would expect more absorbed photons would to lead to higher activity. Furthermore, no reaction occurred between the catalyst and substrate in dark (0 mW) over a period of >10 hours.

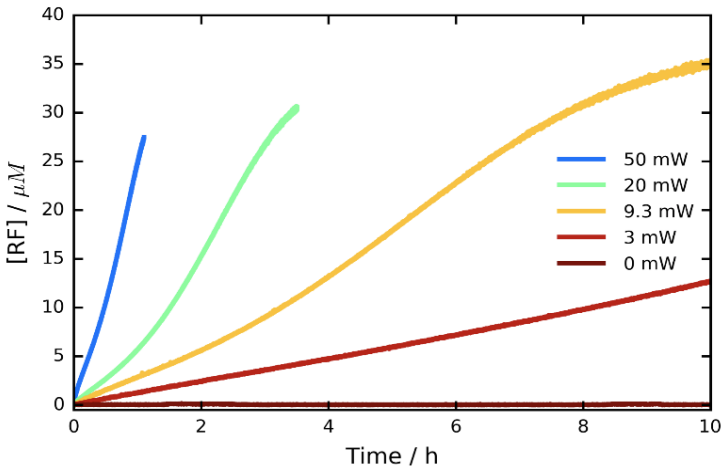

Figure 2.13: Plot of laser diode power (458 nm) dependence (including dark measurement at 0 mW) on the photooxidation of **AR** (100 µM) in KPi buffer (10 mM, pH 7.4, 2 mL) with **FLPDA-5** (10 µg/mL).

Following these experiments, the temporal control of the photooxidation reaction was investigated by performing intermittent ON/OFF irradiation cycles over a period of 9 h as shown in **Figure 2.14**. A clear increase in absorption of the product **RF** at 572 nm is observed when the system is irradiated (ON state) and no further reaction takes place when the laser is switched off for 30 min (OFF state) as evidenced by the absorption plateau. Such behaviour demonstrates that the catalytic activity of **FLPDA** towards substrate oxidation is light-dependent and has excellent capacity for temporal

control, a feature that is widely sought after in green chemistry to minimize the cost and maximize the efficiency of a reaction.[307]

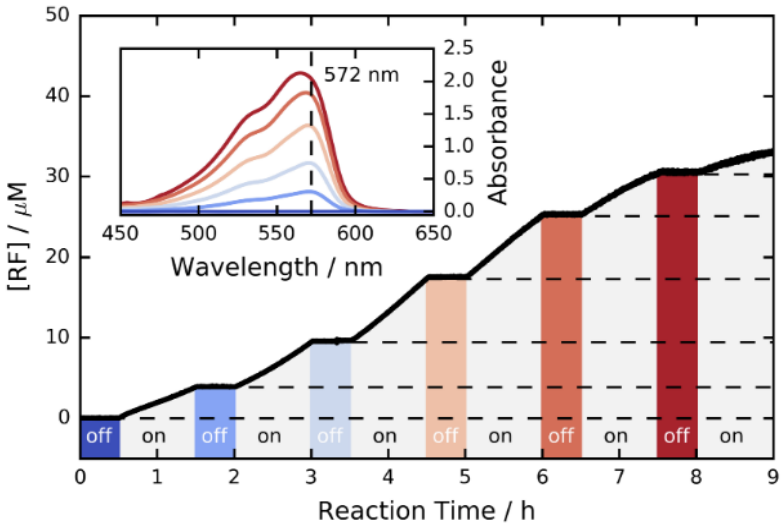

Figure 2.14: Photooxidation of **AR** by **FLPDA-5** under intermittent ON/OFF irradiation cycles. Reaction conditions: **AR** (100 μM), **FLPDA-5** (10 μg/mL) in KPi Buffer (10 mM, pH 7.4, 2 mL) using 2.95 mW/cm^2 excitation intensity (458 nm).

To gain a better understanding into **FLPDA**'s oxidative mechanism, the kinetic profile of **AR** photoxidation by **FLPDA-5** was modelled using Michaelis-Menten theory. As seen in **Figure 2.15**, the catalyst's kinetic behaviour fits the model well over the majority of substrate concentrations indicating a possible enzyme-like mechanism involving substrate binding, followed by reaction and product dissociation. However, as these data do not fit perfectly, a deeper investigation into the modelling the kinetic profile of the catalyst should be investigated in future work as this model may not be the best for this system. The K_m value obtained from the Michaelis-Menten fit was 166.7 μM and a V_{max} of 1.66 μM/min (**Figure 2.15A** and **B**). Compared to enzymes with high specificity to Amplex Red, such as horseradish peroxidase (HRP), these values indicate less specificity and efficiency (6.4 μM and 2.2 μM/min for HRP respectively), but still in a range to be considered as an effective enzyme mimic.[308]

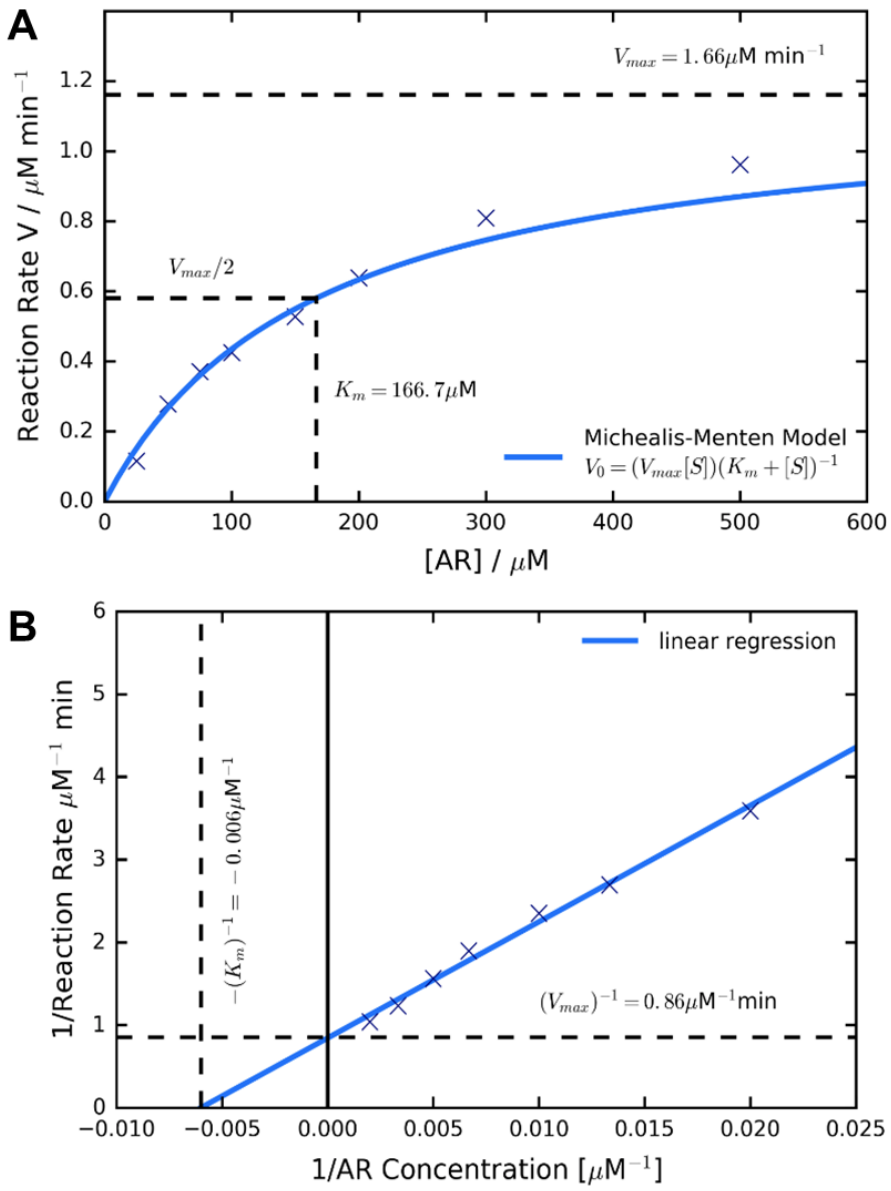

Figure 2.15: Michaelis-Menten plot (A) and reciprocal Lineweaver-Burke plot (B) for the photooxidation of **AR** by **FLPDA-5** (10 µg/mL) in KPi buffer (10 mM, pH 7.4, 2 mL) using 50.3 mW laser diode (458 nm).

The enhanced photocatalytic activity of **FLPDA** compared to the **FLDA** monomer can therefore be attributed to aromatic stacking and other intermolecular interactions between **AR**, PDA and flavin, similar to previously reported flavin-PPh_3-functionalised gold nanoclusters,[179] which allows for favourable orientation for catalysis to occur (**Figure 2.16**). It is also possible that non-specific binding of **AR** to the PDA surface is responsible for a decrease in activity for **FLPDA-10** (less flavin, more PDA) when compared with **FLPDA-5** (less PDA, more flavin).

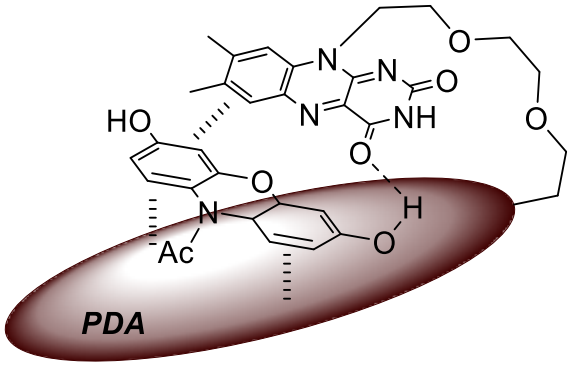

Figure 2.16: Possible intermolecular interactions between **AR**, PDA and flavin moiety that could enhance catalytic activity.

2.4.2.2 Resazurin Photoreduction

After successful demonstration of efficient photocatalytic activity of **FLPDA** towards oxidation, the photoreduction of resazurin (**RZ**) was then investigated. In this case, EDTA was utilised as the electron donor to first reduce flavin moieties within **FLPDA** to afford **RF**.[114,309] As with previous experiments, 10 μg/mL **FLPDA-5** NPs (~10 mol% flavin) were irradiated with a blue laser diode (458 nm) at different excitation intensities now in the presence of **RZ** (25 μM) and EDTA (100 μM) in degassed 10 mM KPi buffer at pH 7.4 (2 mL) under N_2 atmosphere. The spectral changes were then monitored in real time, following the decrease of **RZ** absorption at 602 nm and the increase of **RF** absorption at 572 nm (**Figure 2.17A**). Fast reduction of **RZ** substrate and production of **RF** was observed showing complete conversion after 4 min of irradiation (**Figure 2.17B**). Further decrease in **RF** concentration after 4 min can be attributed to the product bleaching.

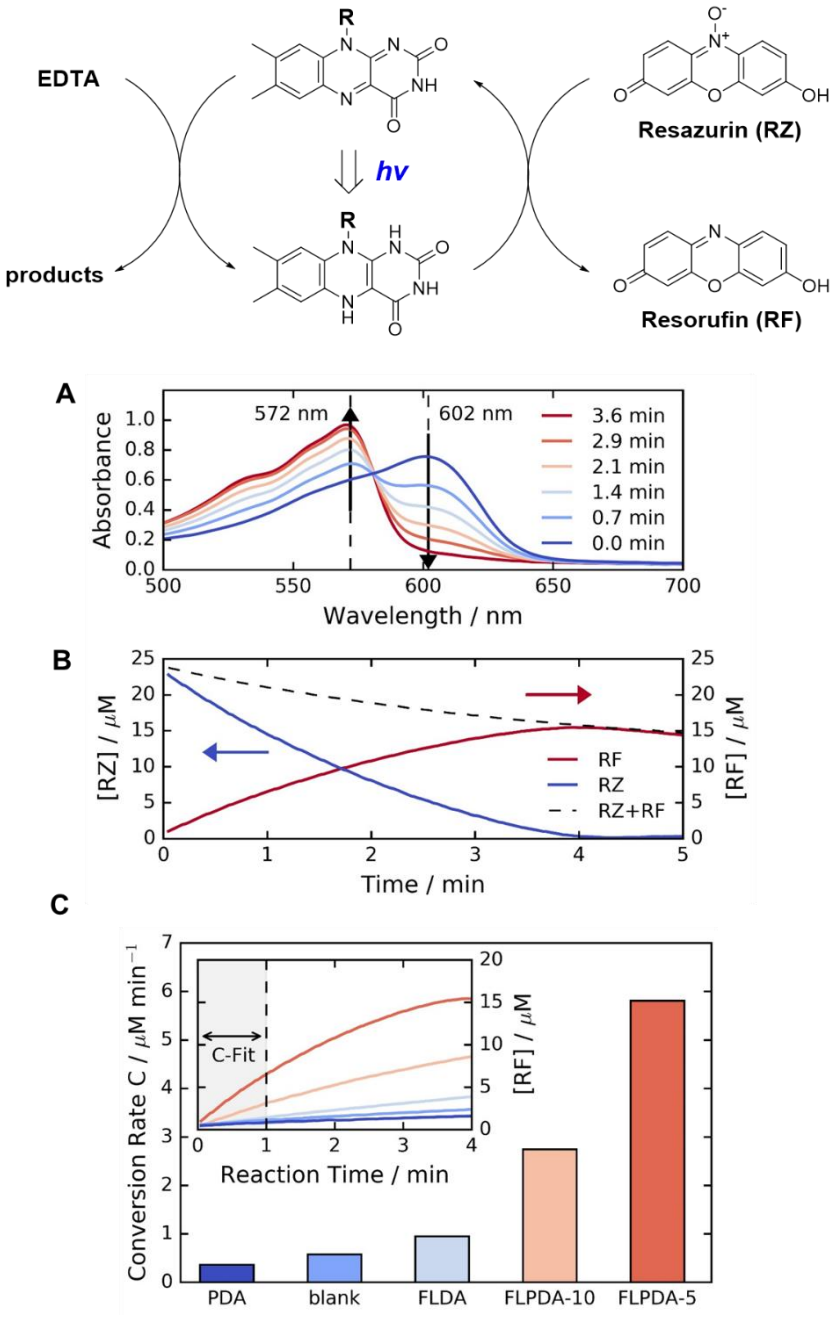

Figure 2.17: Photoreduction of resazurin (**RZ**) to resorufin (**RF**) in the presence of **FLPDA** and EDTA. (A) Plot of the absorption changes observed for the photoreduction of **RZ** to **RF** by **FLPDA-5** (10 µg/mL) in the presence of EDTA (100 µM) in KPi Buffer (10 mM, pH 7.4, 2 mL). (B) Plot showing the relative consumption of **RZ** and production of **RF** by **FLPDA-5** (10 µg/mL) in the presence of EDTA (100 µM) in KPi Buffer (10 mM, pH 7.4, 2 mL). (C) Comparative plot of **RZ** photoreduction in presence of **FLPDA** photocatalysts and controls (10 µg/mL, [**FLDA**] - 10 mol%). All experiments were carried out under N_2 atmosphere and using 458 nm light source with 6.40 mW/cm^2 excitation intensity.

Control runs were also performed (**Figure 2.17C**) showing that PDA (10 μg/mL) displayed almost no activity whereas, some conversion of **RZ** to **RF** (0.58 μM/min compared to 5.7 μM/min for **FLPDA-5**) was observed in the blank measurement containing EDTA, but no catalyst. Such behaviour has been previously reported and is attributed to the interaction of triplet state **RZ** and electron dense tertiary aliphatic amines.[310] Irradiation of **RZ** without EDTA led to **RZ** bleaching and no conversion to **RF**. Following the trend observed in the photooxidation assay, the conversion was doubled for **FLPDA-5** compared to **FLPDA-10** due the larger number of flavin active sites. 10 mol% of **FLDA** showed 6 times lower reaction rate (0.95 μM/min) providing further evidence of the enhanced activity of **FLPDA** through substrate-PDA-flavin interactions.

Finally, the recyclability of **FLPDA-5** was explored by removing the catalyst post-reaction *via* centrifugation. The catalyst was then washed and reused in subsequent reactions, maintaining good activity for up to 4 runs (see **Figure 2.18**). Note that increases in **RF** concentration for runs 2 and 3 are as a result of random experimental error. Due to the inherent losses experienced during catalyst recovery by washing/centrifugation future work should look at developing a continuous flow system using immobilised films of **FLPDA**.

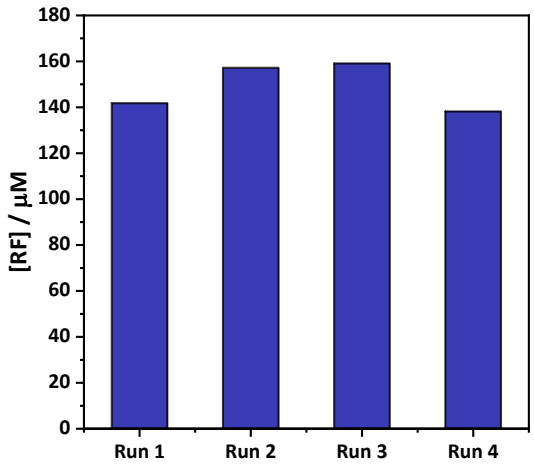

Figure 2.18: Recycling experiments for **RZ** photoreduction using **FLPDA-5** (50 μg/mL) in the presence of **RZ** (0.2 mM) and EDTA (1 mM) in KPi buffer (0.1 M, pH 7.4) for 1 hour runs under Ar atmosphere.

2.4.3 Photostability and decomposition

In order to fully characterise the photocatalytic activity of **FLPDA** NPs, the decomposition of the system under irradiation was explored due to the photostability issues of flavin compounds. Namely, upon irradiation the absorbance of flavin at ~445 nm decreases due to dealkylation to either lumichrome or lumiflavin as well as scission of the isoalloxazine ring.[311]

As an initial assessment of the prepared flavin system's stability, the photodegradation of monomer **FLDA** and its analogue **FLOH** was analysed to observe the effect of a catechol functionality. Homogeneous solutions of **FLDA** and **FLOH** were irradiated using 458 nm light (50.3 mW) under N_2 atmosphere and in air over 30 mins at pH 7.4. Remarkably, in both air and under N_2 atmosphere, **FLDA** exhibits almost no photodecomposition (**Figure 2.19A** and **B**) when compared to **FLOH** (**Figure 2.19C** and **D**). This could be explained by a stabilising charge-transfer process between isoalloxazine and catechol in a 'closed' conformation akin to FAD as rationalised based on the previous fluorescence quenching data (**Figure 2.9**). This process can stabilise the flavin by limiting the amount of degrading ROS formed in an aerobic environment which is clearly seen in the case of **FLOH** in air (**Figure 2.19C**).

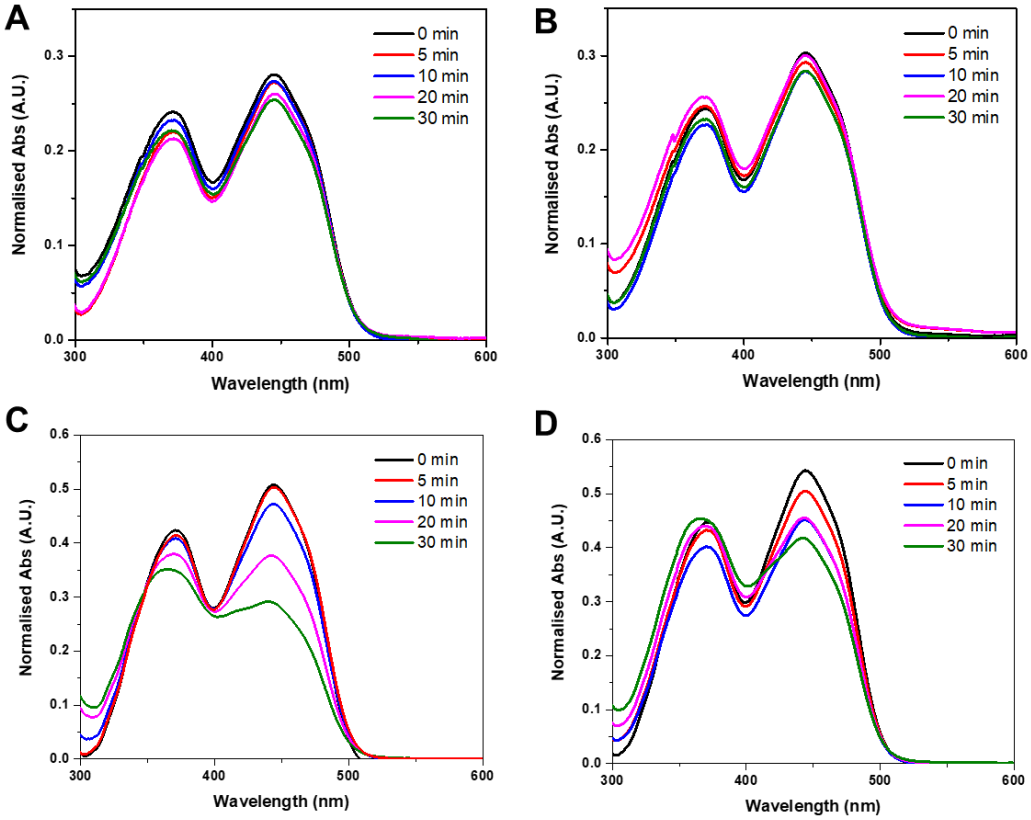

Figure 2.19: Photostability of flavin compounds investigated by UV-Vis absorption. (A) **FLDA** in air (B) **FLDA** under N_2 atmosphere, (C) **FLOH** in air, (D) **FLOH** under N_2 atmosphere. All experiments contained 0.5 mM flavin, 50 mM KPi buffer (pH 7.4) using 458 nm light source with 6.40 mW/cm^2 excitation intensity.

The same study was also performed for **FLPDA-5** by recording the UV-Vis absorption and fluorescence spectra of the particles before and after 30 minutes irradiation, as well as the supernatant after centrifugation of washed particles (see **Figure 2.20**). The absorption spectra of the washed particles in both air and nitrogen still showed presence of characteristic flavin bands (**Figure 2.20A**) but the fluorescence of the particles after irradiation had decreased (**Figure 2.20B**). Analysis of the supernatant revealed an emission at ~524 nm that most likely indicates the presence of lumiflavin[311] or another detached flavin species (**Figure 2.20A**). The cleavage of flavin moieties from the particles could be remedied by the inclusion of a sacrificial electron donor, such as EDTA, which very effectively limited the extent of this degradation (**Figure 2.20A** and **B**).[102]

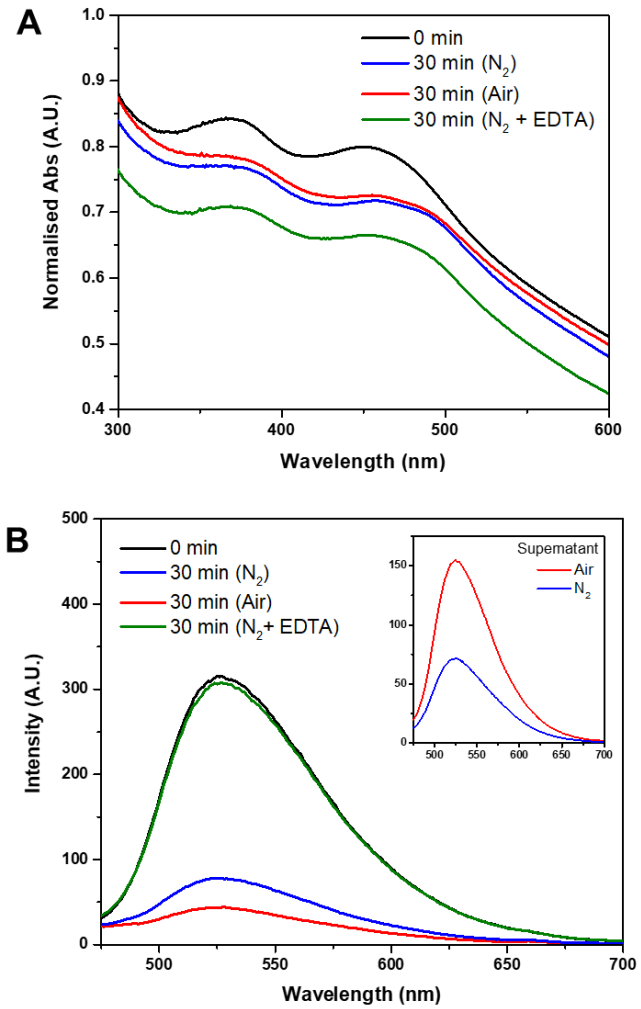

Figure 2.20: Changes in UV-Vis absorption and fluorescence of **FLPDA-5** (50 µg/mL) after 30 min irradiation (50 mW, 458 nm) in KPi buffer (50 mM, pH 7.4) with or without EDTA (5 mM). (A) UV-Vis spectra of **FLPDA-5** in air and under N_2 atmosphere. (B) Fluorescence spectra of **FLPDA-5** after irradiation in air and under N_2 atmosphere and respective supernatants after centrifugation of particles (inset).

Despite the loss of some flavin species, analysis of **FLPDA-5** particles by STEM showed no considerable changes to their size and shape after both photooxidation (**Figure 2.21C** and **D**) or photoreduction (**Figure 2.21E** and **F**).

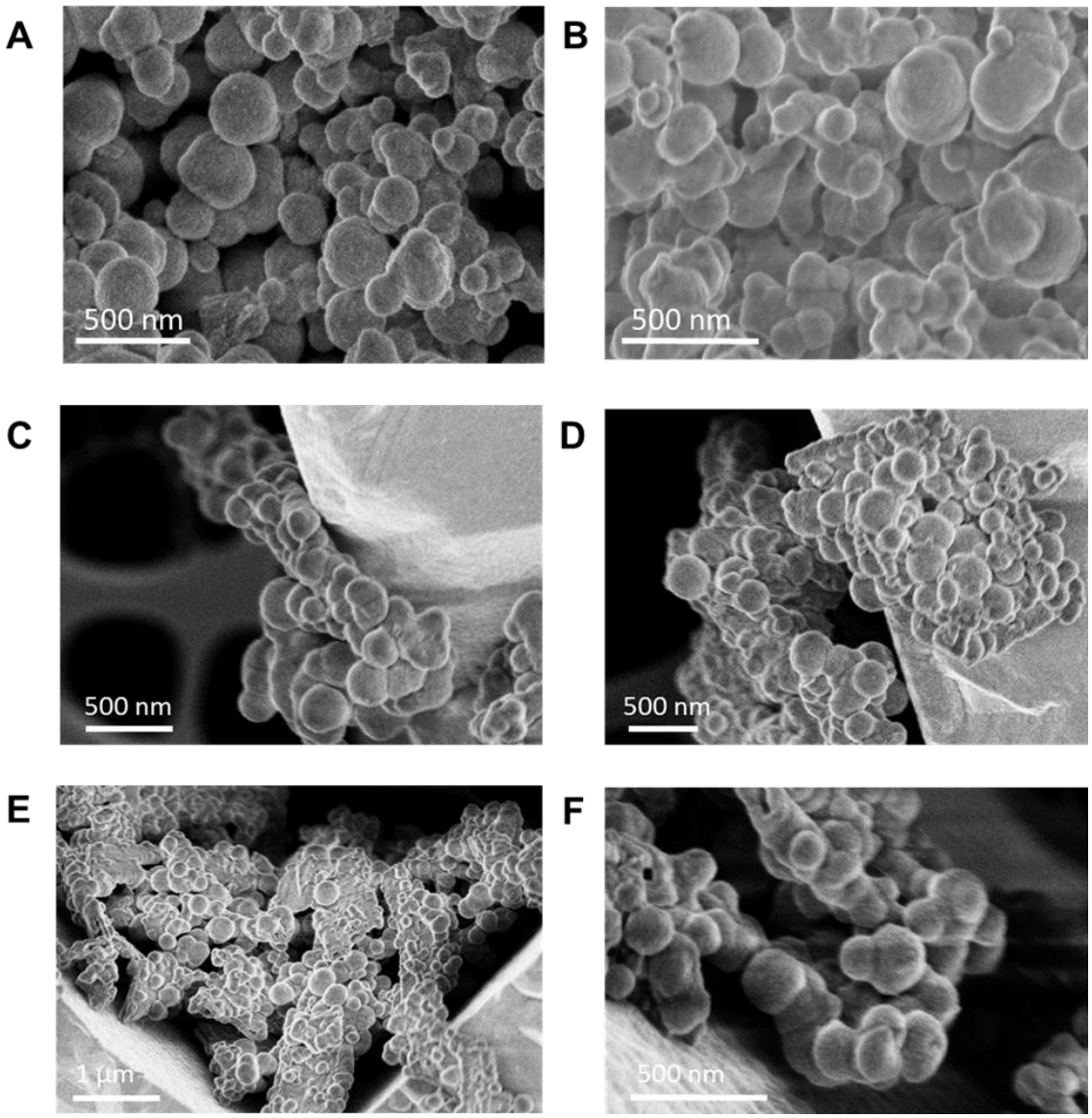

Figure 2.21: STEM images of **FLPDA-5** (A and B) before, (C and D) post photooxidation reaction and (E and F) post photoreduction reaction.

Overall, it is clear from these data that the incorporation of PDA does enhance photostability of the flavin moieties through the formation of charge-transfer complexes that increase its recyclability.

2.4.4 Biocompatibility studies

Finally, a preliminary investigation of the inherent toxicity of **FLPDA** nanoparticles using three *in vitro* assays was performed. First, **FLPDA** was PEGylated to increase the stability in cell culture media (DMEM) and to reduce immunogenicity when applied to future *in vivo* experiments.[312] This was achieved through the covalent attachment of amino terminated $mPEG_{5000}$ to **FLPDA** by incubation in TRIS buffer (10 mM) at pH 8.5

for 18 h. Cell viability was investigated *via* MTS assay after 24 h of incubation with the particles. As shown in **Figure 2.22** (black diamonds), **PEG-FLPDA** has a negligible effect on cell proliferation over a wide dosage range until the concentration of particles is significantly increased (to 1.0 mg/mL) at which point the viability is reduced to 54.6%. The cytotoxicity of **PEG-FLPDA** was also investigated using a lactate dehydrogenase (LDH) assay, which measures release of LDH and signals significant cell damage. This was only observed for very high concentration dosages of 1.0 mg/mL after incubation for 24 h (**Figure 2.22**, blue dots), correlating well to the MTS assay.

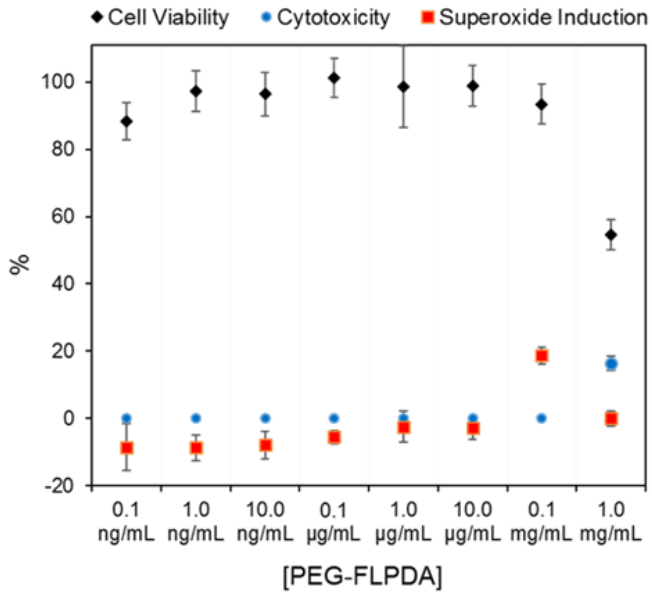

Figure 2.22: Summary of *in vitro* assay data for A549 cells showing the MTS assay data for cell viability (black diamonds), LDH assay data for cytotoxicity (blue dots) and superoxide generation (red squares) in the presence of **PEG-FLPDA** after 24 h.

To compliment these assays, the effect of **PEG-FLPDA** on cell oxidative stress using a superoxide detection assay was explored to monitor the induction or scavenging of superoxide within the cells due to the presence of the particles. The data in **Figure 2.22** (red squares) show that amount of superoxide decreases (relative to untreated controls) upon incubation with up to 10.0 µg/mL **PEG-FLPDA** . This indicates that **FLPDA** has antioxidant properties similar to PDA and melanin.[193,203,313] However, at a concentration of 0.1 mg/mL, incubated cells showed an increased accumulation of superoxide, although this seems not to impact the viability of the cells. Decrease of the superoxide production again at 1.0 mg/mL is correlated to widespread cell death at

this high concentration. However, these three assays clearly indicate that **FLPDA** NPs are non-toxic below concentrations of 1.0 mg/mL, and even show an antioxidative effect below 0.1 mg/mL. This initial study indicates that flavin-polydopamine systems could be useful not only for photocatalysis, but for potential use in nanomedicine as antioxidant drug carriers or photosensitisers for photodynamic therapy and water remediation.

2.5 Conclusion

Hybrid flavin-polydopamine (**FLPDA**) nanoparticles were prepared by the copolymerisation of a flavin-catechol monomer (**FLDA**) and dopamine yielding a system displaying versatile photocatalytic activity. Using model redox substrates, it was shown that **FLPDA** is capable of efficient oxidative and reduction catalysis upon irradiation. The hybrid catalyst was significantly more efficient than the flavin-catechol monomer, **FLDA** which was rationalised by enzyme-like kinetic mechanism that is enabled by PDA. Excellent temporal control was achieved for the photooxidation of Amplex Red (**AR**) through the demonstrated ON and OFF activity upon irradiation. In addition, fast and efficient photoreduction of resazurin (**RZ**) was achieved in presence of EDTA as the electron donor, and the catalyst could be reused over 4 cycles without significant loss of activity. Furthermore, the photodecomposition of the catalyst was investigated showing that catechol conjugation improves flavin photostability through a charge-transfer process which was evidence by fluorescence quenching measurements. Finally, *in vitro* assays demonstrated the non-toxicity of the system and indicated some antioxidative properties. Combined, these data show that flavin-polydopamine is a promising candidate for photocatalysis applications as well as in biomedical applications.

3 Light-Driven Monooxygenase Activity of Flavin-Polydopamine

3.1 Introduction

This chapter will discuss the application of flavin-polydopamine to a flavoenzyme-specific oxidation reaction which has not been reported in flavin photocatalysis. The investigation will also explore the system's ability to access key reactive flavin intermediates upon irradiation through the cooperation of polydopamine and flavin.

Flavin-containing monooxygenases (FMOs) are an important group of xenobiotic-degrading enzymes present in both eukaryotic and prokaryotic organisms. They can add molecular oxygen to the lipophilic xenobiotic compounds, thereby increasing their solubility to allow excretion. As a result, organisms are protected from potentially toxic exogenous compounds derived from natural sources and, particularly important for humans, the metabolism of drugs and pollutants.[314,315] One of the substrates for FMOs, which is also widespread in nature is the *N*-heterocycle indole. Indole is considered to be an aromatic pollutant due to its toxicity and potential mutagenicity,[316] but it is also a versatile intermediate species and signalling molecule across families of organisms.[317–320] FMOs, as well as the other xenobiotic-degrading enzymes such as cytochrome P450s, have been shown to convert indole to the blue indigo dye through initial oxidation to indoxyl and subsequent dimerization to form the dye as shown in **Figure 3.1**.

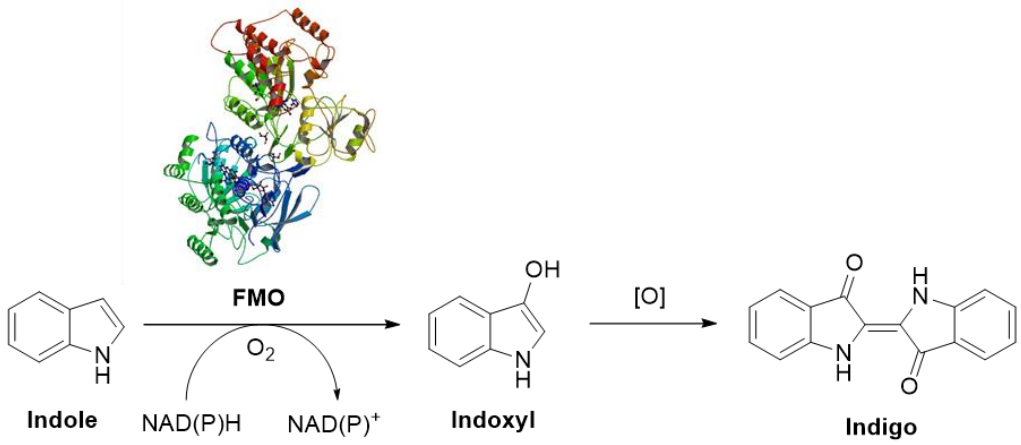

Figure 3.1: Indole oxidation to indoxyl by flavin-containing monooxygenase (FMO from *S. pombe*, PDB Entry - 2GVC) and subsequent oxidation by O_2 and dimerization to indigo.[321,322]

This transformation has been utilized as an enzymatic assay to screen for oxygenases,[323–326] but also as a greener alternative to the industrial manufacture of indigo and related indigoid dyes.[327–329] Indigo dyes are currently commercially produced starting from aniline, formaldehyde, and hydrogen cyanide to form phenylglycinonitrile. This is subsequently hydrolysed to yield phenylglycine and finally indigotin.[330] This chemical synthesis involves use of toxic chemicals and extensive purification steps, limiting the environmental viability and has prompted the design of greener synthetic strategies.[331] For example, whole cell biocatalysis relying on intracellular FMOs within *E. Coli* has hence been utilised to achieve more sustainable production of indigo and indirubin dyes.[327–329] However, some major challenges in whole cell biocatalysis are complex product separation and catalyst inhibition, which incurs large costs and reactor downtime periods.[332] An alternative strategy is use the isolated enzyme, however this suffers from limited amounts of the enzyme that can be isolated, low stability under non-physiological conditions, sensitivity to organic solvents, as well as challenging post-reaction isolation and reuse, hence limiting large scale industrial applications.[333,334]

Taken out of a protein environment, flavin analogues derived from flavin mononucleotide (FMN), flavin adenine dinucleotide (FAD) and riboflavin cofactors have shown huge potential in FMO-like organocatalytic oxidation reactions, however few photocatalytic examples of FMO mimetic reactions exist.[68,69,335,336] Despite the

relative ease of visible-light driven flavin photocatalysis, high yielding reactions, and low toxicity, there are still challenges related to their photostability and stabilisation of reactive intermediates, as well as the separation of the catalyst from the products and subsequent catalyst reuse. To address these issues, attempts have been made to immobilize flavins onto various solid carriers such as silica beads or resins to achieve a heterogeneous catalytic systems, although limited success has been reported in relation to recyclability and activity.[75,168,170] Taking this into account, we have rationalised that the use of PDA - an active polymeric carrier - which not only permits immobilization of flavin but also displays some intrinsic properties similar to proteins such as H-bonding and electron transfer, could significantly improve both the activity and post-reaction recovery of the hybrid catalytic system.

To that end, the FMO-like activity of flavin-polydopamine (**FLPDA**) towards the oxidation of indole to form indigo dye was investigated using blue light irradiation to excite the flavin moieties, bypassing the use of external reducing agents or cofactors such as NAD(P)H (**Figure 3.2**). It is envisaged that PDA will not only act as the flavin carrier but will also play an active catalytic role resulting in improved product selectivity and photocatalyst stability.

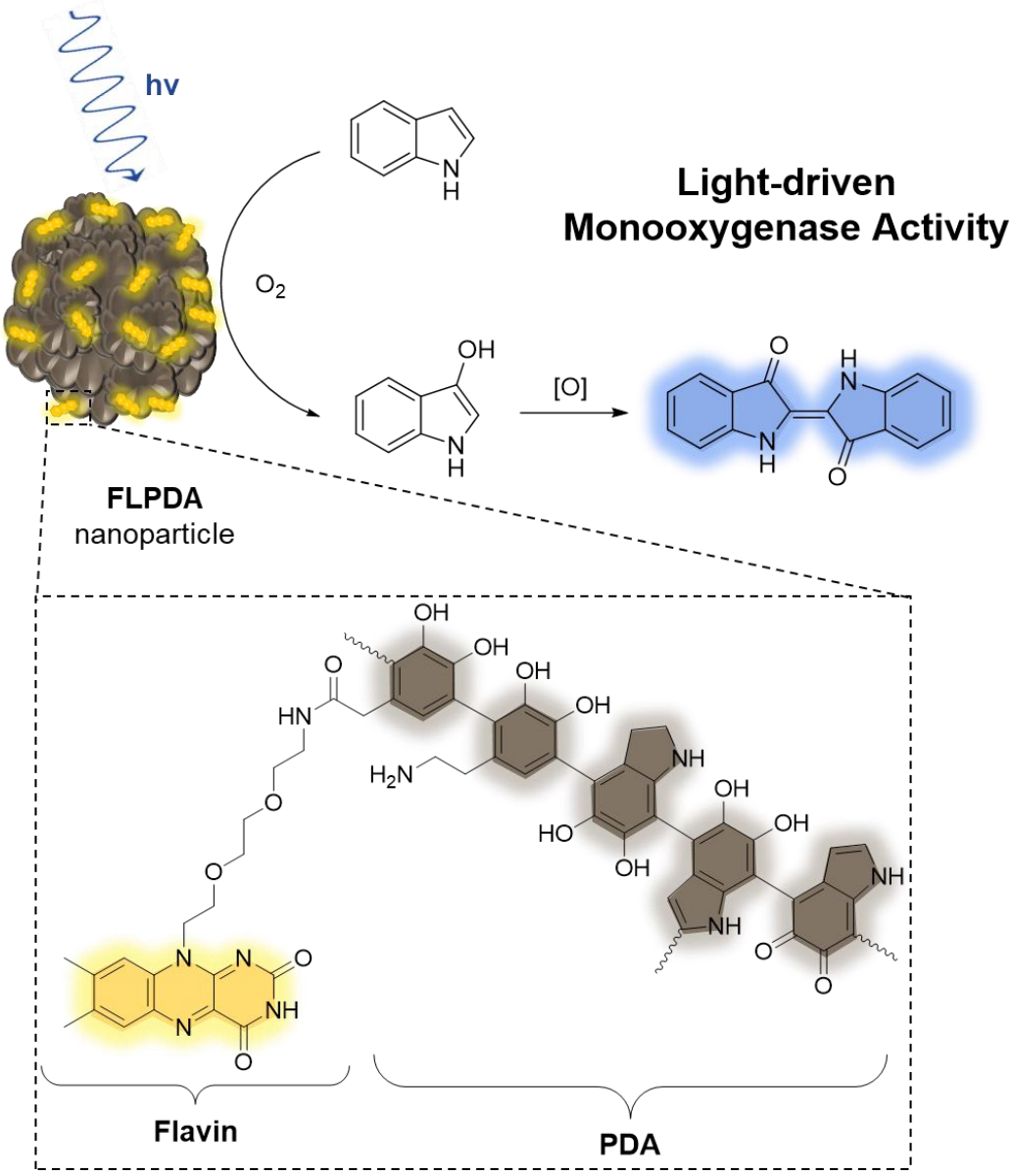

Figure 3.2: Structure of flavin-polydopamine (**FLPDA**) units and the reaction scheme illustrating explored light-driven oxidation of indole to indigo in presence of **FLPDA** nanoparticles.

3.2 Experimental

3.2.1 General information

All materials were purchased from either Acros Organics (UK), Alfa Aeser (UK), Sigma-Aldrich (UK) or TCI Chemicals (BE) in the highest purity available and used without further purification. UV-Vis absorption spectra were obtained with an Agilent Cary 300 Spectrophotometer. Fluorescence emission spectra were obtained using a Varian Cary Eclipse Fluorescence Spectrophotometer using excitation and emission slits of 10 nm.

DLS and Zeta Potential measurements were recorded using a Zetasizer Nano Range instrument (Malvern Panalytical). FTIR spectroscopy was carried out using a Bruker Tensor 27 spectrometer with samples pressed into KBr pellets. STEM images were obtained using a Hitachi S-5500 In-Lens FE STEM (2009) at an acceleration voltage of 1.0 kV. Samples were suspended in water and drop cast on lacey carbon copper grids (Agar Scientific). HPLC was carried out on an Agilent 1260 Infinity Quaternary LC equipped with a Zorbax Eclipse Plus C18 column (5 µm, 4.6 mm x 1.5 mm, Agilent) and diode array detector (monitoring at 270 nm). The mobile phase consisted of Solvent A (water + 0.1% formic acid) and solvent B (ACN/MeOH, 50:50, v/v) running along the following gradient: 0-8 min 85% A and 15% B at a flow rate of 1 mL/min, 8-15 min 65% A and 35% B at a flow rate of 2 mL/min. Indole (99%), isatin (97%) and oxindole (98%) were purchased from Sigma-Aldrich (UK) and calibration curves were obtained from 0 - 1.0 mM stock solutions in order to estimate product concentrations and % conversions. LC-MS was performed on an Agilent G6550 QTof mass spectrometer coupled to an Agilent 1200 Series Infinity LC system using a Zorbax Eclipse Plus C18 column (5 µm, 4.6 x 150 mm, Agilent). The mobile phase consisted of Solvent A (water + 0.1% formic acid) and solvent B (ACN + 0.1% formic acid) running along the following gradient: 0-14 min 85% A and 15% B to 5% A and 95% B at a flow rate of 0.8 mL/min. The electrospray source was operated with a capillary voltage of 3.0 kV and a nozzle voltage of 1.0 kV. Nitrogen was used as the desolvation gas at a total flow of 14 L/min. All m/z values stated are that of the $[M+H]^+$ molecular ion.

3.2.2 Synthesis of FLDA

Synthesis of **FLDA** was carried out as described in **Chapter 2**, **Section 1.5.2**.

3.2.3 Synthesis of FLPDA

FLPDA was synthesised as described in **Chapter 2**, **Section 1.5.4** for **FLPDA-5:** A mixture of ammonia solution (0.1 mL, 28%), ethanol (1.5 mL) and Milli Q water (4.5 mL) was stirred at room temperature for 30 minutes in reaction vessels protected from direct sunlight. Dopamine hydrochloride (15.80 mg, 0.083 mmol) dissolved in Milli-Q water (0.5 mL) and **FLDA** (8.73 mg, 0.017 mmol) dissolved in ethanol (0.5 mL) were mixed before being added dropwise to the reaction mixture. The resulting dark brown/black

mixture was left to stir in the presence of air for 24 h. The mixture was then centrifuged at 25000 x *g* for 30 min and the supernatant was removed. The precipitate was washed with Milli-Q water (3 x 40 mL) and then suspended in Milli-Q water (20 mL), frozen in liquid N_2 and lyophilized to yield a dark brown/black powder (5.5 mg, ρ = 22% where ρ is the percent weight conversion of monomers).[337] Characterisation of the particles by UV-Vis absorption spectroscopy, fluorescence spectroscopy, FTIR, DLS, zeta potential and STEM matched with previously described results for **FLPDA-5** (**Chapter 2**, **Section 2.3.1**). Flavin content was approximated using the same method as described in **Chapter 2, Section 2.5.5** to give an approximate **FLDA** content of ~ 1.0 μmol/mg **FLPDA**.

3.2.4 Photooxidation of indole

General procedure: **FLPDA** (50 μg/mL, ~5 mol%) and indole (1.0 mM) were added to H_2O/MeCN (1:1, v/v, 2 mL) and the mixture was saturated with O_2 gas for 10 minutes before irradiating with a custom-made blue LED strips setup (12 V) with cooling fan to maintain a temperature of ~25 ^oC. 100 μL aliquots were taken from the reaction mixture and diluted to 1 mL (H_2O/MeCN, 1:1) for analysis by UV-Vis absorption spectroscopy. Post-irradiation (2 – 6 h), the reaction mixture was either diluted in H_2O/MeCN (1:1, 10 mL) and the catalyst removed by centrifugation and washed with water (3 x 12 mL) for further use, or the catalyst was removed by centrifugation and the supernatant was concentrated under reduced pressure. The residue was then either diluted in H_2O/MeCN and analysed by HPLC-UV and LC-MS or dissolved in DMF and analysed by ESI-MS and UV-Vis absorption spectroscopy to quantify indigoid dye amounts.

3.2.5 LED reactor setup

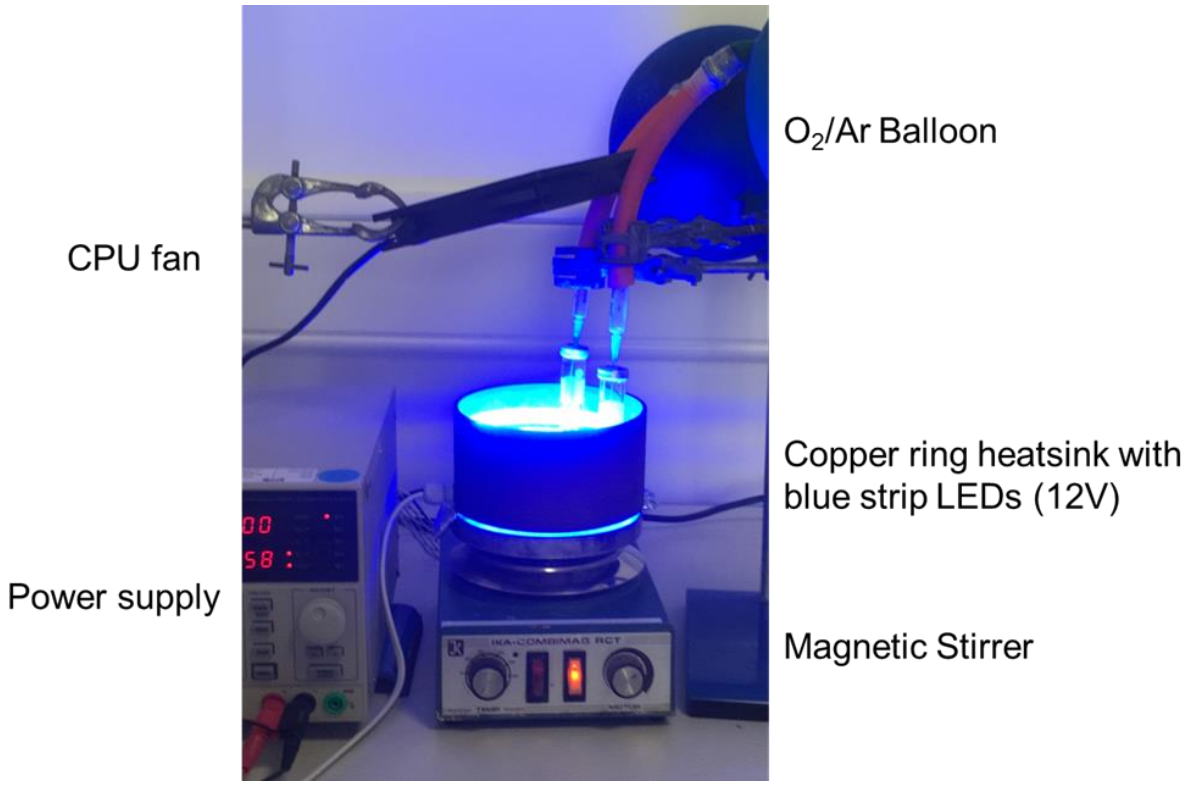

Figure 3.3: The setup was built drawing influence from the LED strips setup described by the MacMillan group.[338] Blue LED strips (12 V) were sourced from a commercial retailer and around 3 strips were stuck into the inside of a 15 cm diameter copper ring. This was then placed on top of a magnetic stirrer with a small gap to allow a vent for cooling which was supplied by a CPU fan. Vials were placed ~1 cm from the LED strips.

3.2.6 Hydrogen peroxide assay

H_2O_2 assay was carried out by first creating a standard calibration curve using Amplex Red (Ampliflu Red, Sigma-Aldrich, 100 µM), horseradish peroxidase (HRP, 0.25 µM) and H_2O_2 (0-100 µM). Phosphate buffer (pH 7.4) was used to adjust final well volumes to 100 µL. A microplate reader (Tecan Spark) was used to record the fluorescence signals of the resorufin product (λ_{ex} = 540 nm, λ_{em} = 585 nm). To determine H_2O_2 amounts after irradiation, an aliquot (50 µL) of a reaction mixture was taken and used under the same conditions as above, comparing the fluorescent intensity of resorufin to the calibration curve. All error bars are the standard deviation of triplicate data.

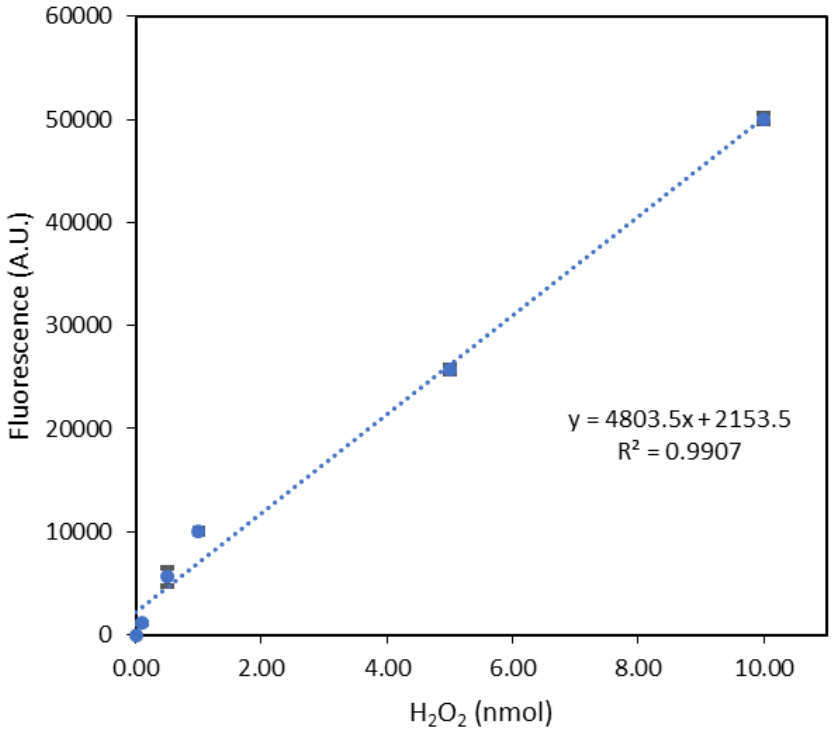

Figure 3.4: H_2O_2 calibration curve using Ampliflu Red + HRP assay. All error bars are the standard deviation of triplicate data. To exemplify the size of the error bars, an example data point is given at $[H_2O_2]$ = 5.00 nmol whereby the fluorescence (A.U.) is 25770 ± 393.15.

3.3 Results and Discussion

3.3.1 Synthesis and characterisation of FLPDA

FLPDA was synthesised as described in **Chapter 2**, **Section 1.5.4** for **FLPDA-5.** Characterisation of the particles by UV-Vis absorption spectroscopy, fluorescence spectroscopy, FTIR, DLS, zeta potential and STEM matched with previously described results for **FLPDA-5** (**Chapter 2**, **Section 2.3.1**). Flavin content was approximated using the same method as described in **Chapter 2, Section 2.5.5** to give an approximate **FLDA** content of ~ 1.0 µmol/mg **FLPDA**.

3.3.2 Indole photooxidation

The light-driven monooxygenase activity of **FLPDA** nanoparticles (NPs) was initially investigated by irradiating an O_2 saturated mixture of indole (1.0 mM) and **FLPDA** (50 µg/mL, ~5 mol% flavin) in H_2O/MeCN (1:1, v/v). This particular solvent system was chosen to guarantee high flavin photooxidation efficiency (quantum yield), which is known to be optimal in aqueous acetonitrile mixtures.[339,340] The reaction was monitored by UV-Vis absorption spectroscopy by taking aliquots (100 µL) of the reaction mixture at specific time intervals. As shown in **Figure 3.5A** the absorption spectrum of indole (0 h) has a characteristic absorbance band at λ_{max} = 287 nm. After 0.5 h irradiation, this peak decreases in intensity and a new band appears at λ_{max} ~ 380 nm which is consistent with the consumption of indole and the production of 2 and 3-position hydroxylated indole species.[341–343] These bands increase in intensity with time and a shoulder replacing the characteristic band belonging to indole at 2 h indicates its consumption.[341] The fluorescence emission (λ_{ex} = 365 nm) of the reaction was also monitored as shown in **Figure 3.5B** and observed the formation of fluorescent indoxyl species (λ_{em} = 465 nm) at 0.5 h and 1 h.[344,345] After 1 h the signal disappears most likely due to indoxyl dimerization into the fluorescent, water-soluble leuco-indigo (λ_{em} = 523 nm).[344,346]

Control experiments without **FLPDA** in the reaction mixture, under Ar atmosphere and using PDA instead of **FLPDA**, and in the dark over 18 h, all showed negligible changes in indole's characteristic absorption band (**Figure 3.6A-D**). Collectively, this data confirms that **FLPDA** is responsible for the oxidation of indole

and the reaction proceeds only in the presence of oxygen and light. In addition, the substrate shows good photostability under the reaction conditions employed. Note that increases in absorption prior to indole's characteristic absorption band around 300-700 nm are the result of light scattering phenomena caused by the presence of nanoparticles.

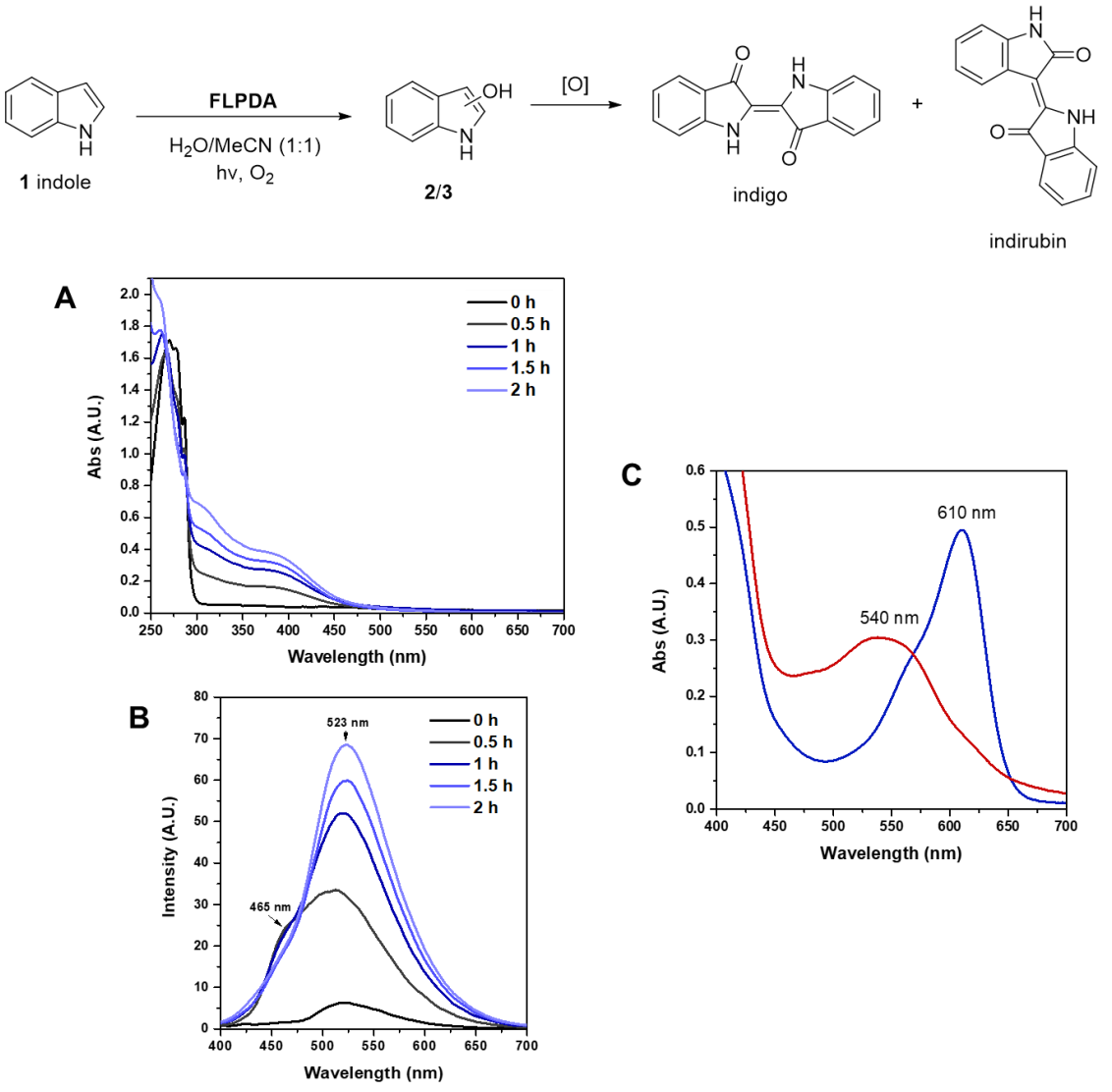

Figure 3.5: Spectroscopic data of indole (1.0 mM) photooxidation by **FLPDA** (50 µg/mL) in O_2 saturated H_2O/MeCN (1:1, v/v, 2 mL). (A) UV-Vis absorption spectra over 2 h, (B) Fluorescence emission spectra (λ_{ex} = 380 nm) over 2 h, (C) UV-Vis absorption spectra of produced indirubin (λ_{max} = 540 nm) and indigo (λ_{max} = 610 nm) in DMF.

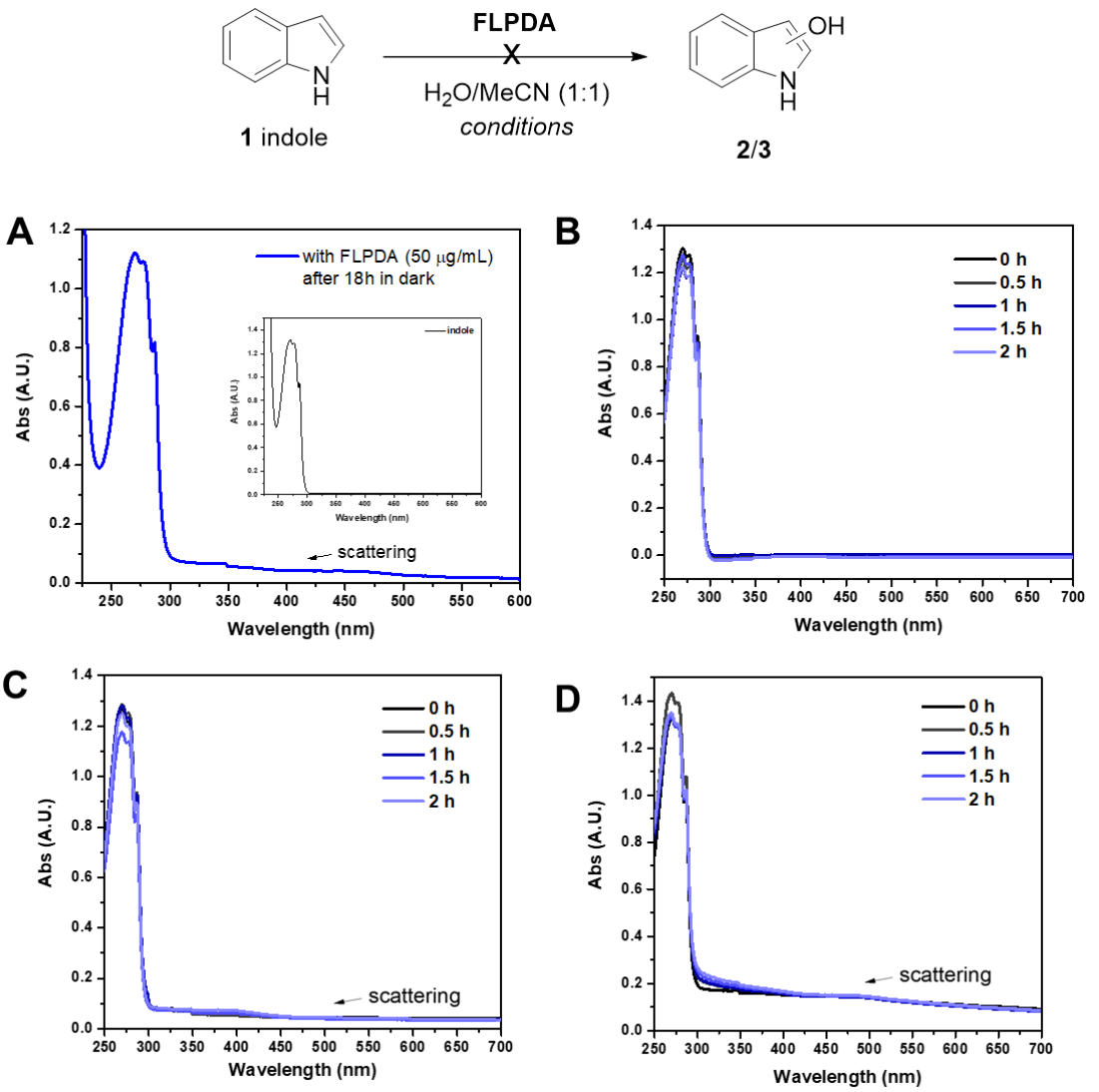

Figure 3.6: UV-Vis spectra of indole photooxidation control experiments over 2 h. Conditions: (A) reaction without irradiation (inset: spectrum of indole), (B) without **FLPDA** catalyst, (C) under Ar atmosphere, and (D) in the presence of PDA NPs (50 μg/mL) instead of **FLPDA**. Scattering occurs due to presence of nanoparticles in samples.

Further analysis of the reaction mixture after photooxidation with **FLPDA** revealed multiple indole oxidation products. Three major oxidation products were identified by HPLC and LC-MS (**Figure 3.7**): isatin **4** (7.07 min, *m/z*: 148), 2-oxindole **2** (7.69 min, *m/z*: 134) and indoxyl **3** observed as its more stable keto-form **3a** (4.23 min, *m/z*: 132). Other products with higher *m/z* values were also identified, including indigo/indirubin (two signals with *m/z*: 263) and two others with m/z values of 249 and 281. The structures of these products are proposed in **Figure 3.7** and labelled as

species **5** and **6**. Their formation is particularly interesting as they have been observed in reactions catalysed by enzymes such as laccases and cytochrome P450s, that contain inorganic cofactors such as copper and iron (heme) respectively.[342,347,348]

The formation of indigo and indirubin were first observed by thin layer chromatography (TLC) of the reaction mixture and were then isolated after reaction workup and characterized by UV-Vis (indirubin λ_{max} = 540 nm and indigo λ_{max} = 610 nm as seen in **Figure 3.5C**). It should be noted that theses dyes were not observed to form during the reaction itself, but could be obtained either upon removal of the solvent, which initiated precipitation, or with the addition of weak acid to the reaction mixture and supernatant which increased the rate of their formation.[349] Yields of the dyes were measured by UV-Vis spectroscopy using published extinction coefficients,[346] but were generally low (≤5%) when precipitated out of solution during solvent removal *in vacuo*. However, these low values are comparable to other biomimetic systems such as Fe(II) and Mn(III) porphyrin complexes used in the presence of H_2O_2.[342,350] Such low yields are most likely the consequence of the non-specific binding to the surface of the **FLPDA** catalyst as the active site of FMO, which ensures specific binding and increases the product selectivity.[327] It was observed that the addition of weak acid to the reaction mixture after irradiation gave better yields of dye, but results in the formation of indirubin rather than indigo. Indigo was only found to precipitate from the reaction mixture upon solvent removal *in vacuo* (see **Figure 3.5C**).

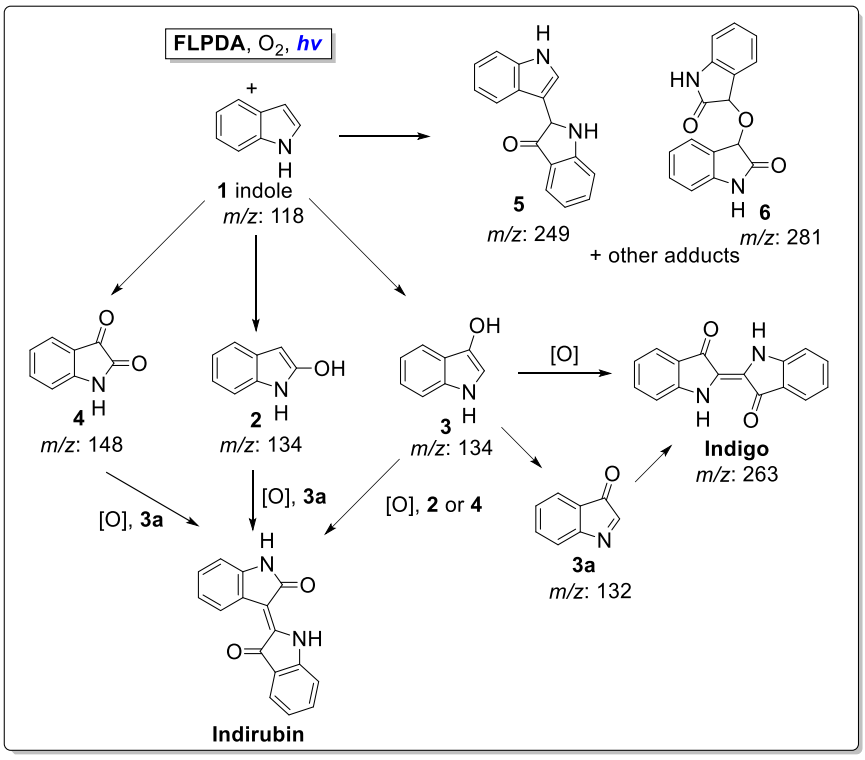

Figure 3.7: Proposed reaction scheme for indole photooxidation in presence of **FLPDA** nanoparticles.

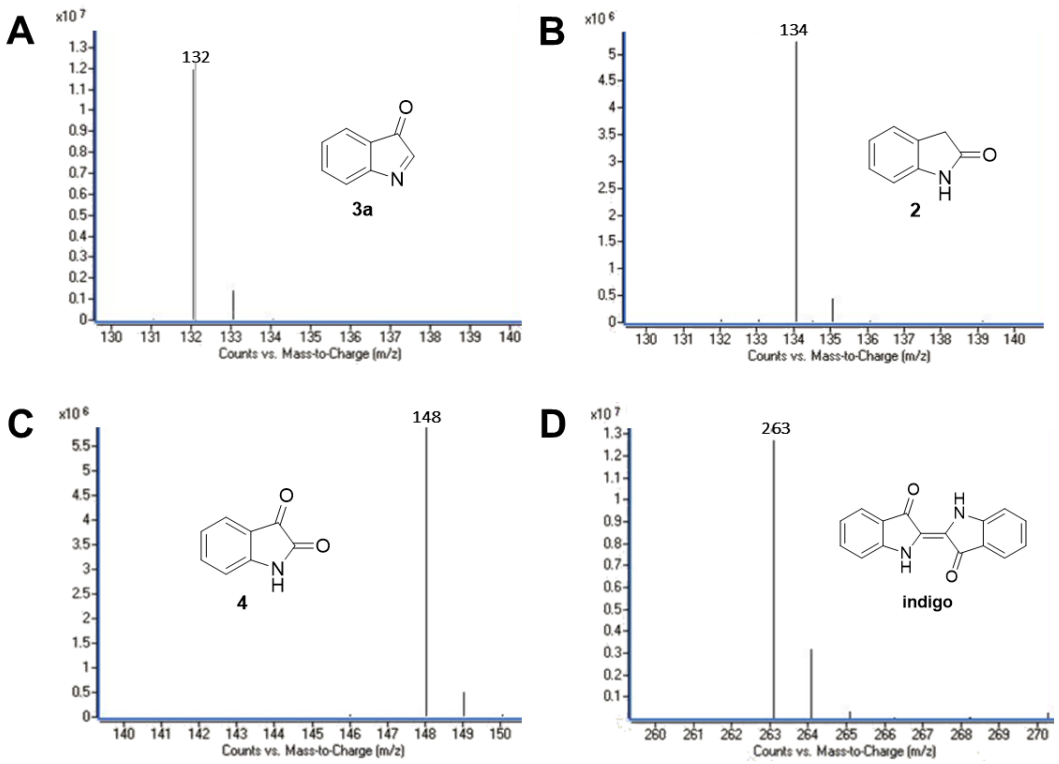

Figure 3.8: LC-MS chromatograms of major photooxidation products of indole in the presence of **FLPDA** nanoparticles. (A) **3a**, (B) **2**, (C) **4** and (D) indigo.

The light-driven oxidation of indole by **FLPDA** is clearly non-specific due to the range of identified oxidation products, however, these main products resemble those formed by FMOs and other xenobiotic degrading enzymes. This work provides the first example of an organic nanoparticle-based photocatalyst that shows such activity. In addition, the only other example of photocatalytic oxidation of indole to form indigo and related compounds are CdS quantum dots, the use of which has serious implications in terms of toxicity.[351,352]

The apparent FMO-like activity of **FLPDA** was then compared to a homogeneous flavin photocatalyst, riboflavin (**RBF**). Flavin loading in the reactions were decreased in order to avoid excess light scattering by the heterogeneous NP system to give a more valid comparison between reactions. UV-Vis analysis of the reaction mixture containing **RBF** showed an increased rate of indole consumption (shoulder formation at ~ 280 nm) after 0.5 h (**Figure 3.9A**). HPLC analysis (**Figure 3.10** and **Table 3.1**) confirmed that there is greater conversion of indole in presence of **RBF** (97%) compared to **FLPDA** (79%). As seen in both **Figure 3.10** and **Table 3.1**, similar oxidation products were observed for both reactions however the selectivity of product formation differs between the two catalysts. **RBF** showed higher selectivity for compound **4** than **FLPDA**, whereas compound **2** was found in higher concentration with **FLPDA** than **RBF**. After addition of 2 drops of 1M HCl to each reaction supernatant to initiate dimerization of hydroxylated indole species to form indigoid dyes, the resulting yield of the dyes also differed. As shown in **Figure 3.9B**, there was more indirubin obtained from the reaction conducted in the presence of **FLPDA** than **RBF**, which was expected as 2.5 times more precursor **3a** can be detected in HPLC profile (**Figure 3.10**). Clearly, despite the decreased indole conversion, **FLPDA** appears to be more selective towards dye formation than the homogeneous counterpart.

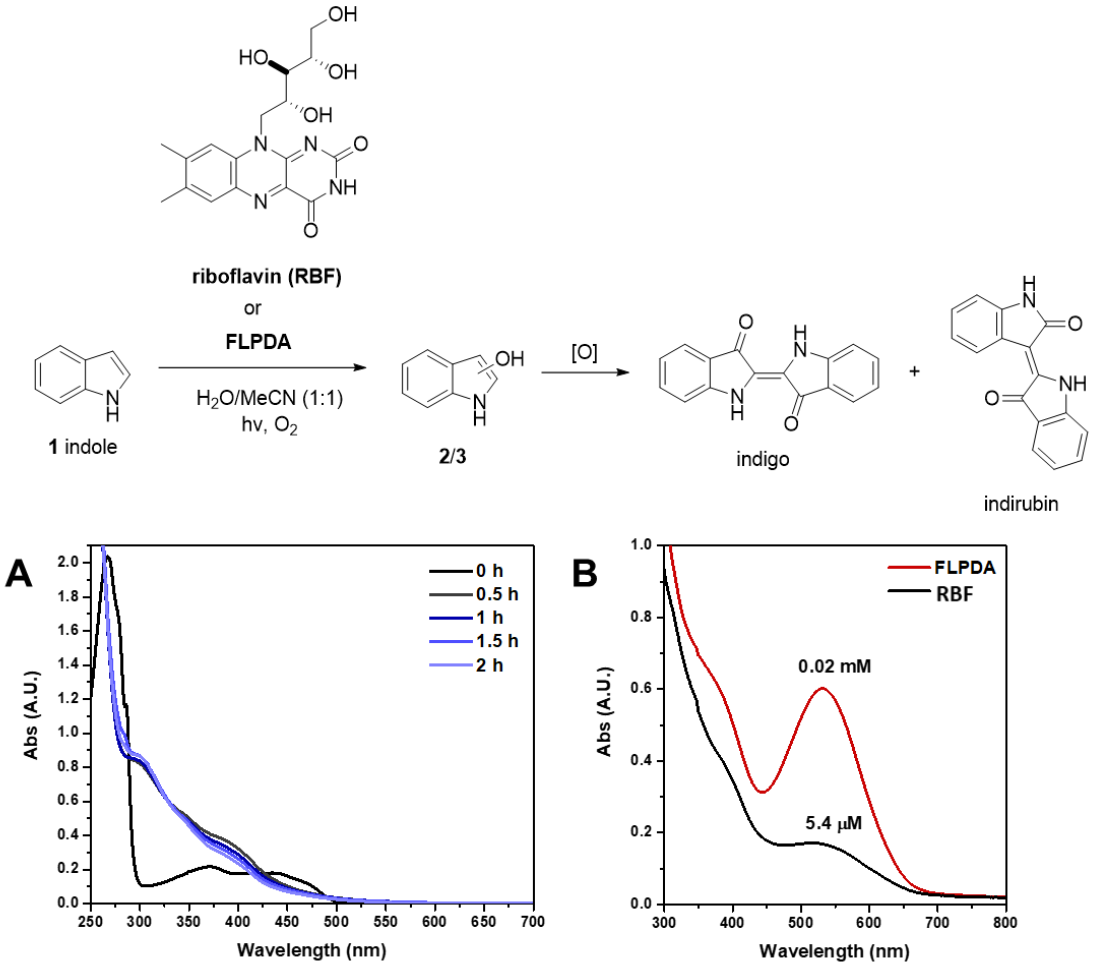

Figure 3.9: Spectroscopic data for indole (1.0 mM) photooxidation in the presence of riboflavin (**RBF**, 20 μM) in O_2 saturated H_2O/MeCN (1:1, v/v, 2 mL). (A) UV-Vis absorption spectra over 2 h, (B) Plot comparing the concentrations of indirubin from **RBF** and **FLPDA** catalysed indole photooxidations post acid workup.

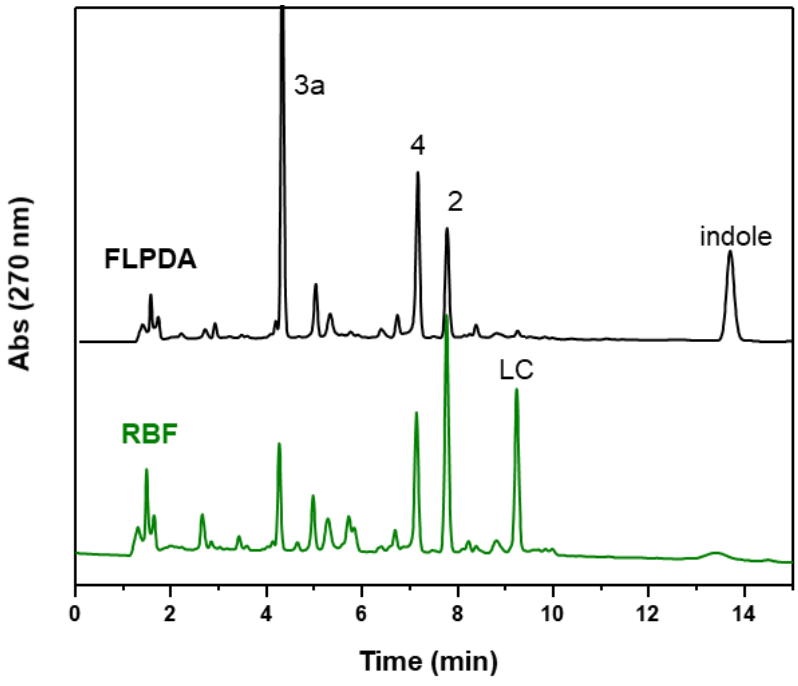

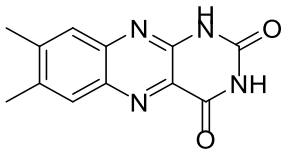

lumichrome (LC)

Figure 3.10: HPLC chromatograms of reaction mixture after 2h irradiation of indole (1.0 mM) in the presence of **FLPDA** (20 µg/mL) or **RBF** (20 µM) in H_2O/MeCN (1:1, v/v, 2 mL). LC = lumichrome.

Table 3.1: Amounts and conversions of major compounds identified by HPLC after acidification of reaction mixture using commercial standards as external calibration references.

Catalyst	Indole (1) (µM)	Oxindole (2) (µM)	Isatin (4) (µM)	Indole conversion	Indigoid yield[a]
FLPDA (20 µg/mL)	213	22	60	79%	5%
RBF (20 µM)	24	16	80	97%	1%

[a] $([indigoid] \times 2/[consumed\ indole])$ [353] with [indigoid] being determined by UV-Vis spectroscopy.

It is also worth noting that after the irradiation, **RBF** could no longer be identified by TLC analysis within the reaction mixture and had degraded to lumichrome (LC), which was confirmed both by HPLC and LC-MS (9.22 min, *m/z*: 243) (**Figure 3.10**). Lumichrome is one of the major photodecomposition products of **RBF** that is photocatalytically inactive.[311] Although lumichrome was also observed in the **FLPDA** catalysed reaction, its concentration was 5 times lower compared to **RBF** (based on

HPLC integration), indicating that the PDA-based catalyst offers more protection toward photodecomposition of active flavin centres, and mitigates the loss of the catalysts observed in homogeneous systems.

3.3.3 Recyclability

The reusability of **FLPDA** in the photooxidation reaction was examined as this is a desirable property for scale up and industrial applications enhancing the green chemistry potential of the system. Previous work on a heterogeneous flavin-based photocatalytic system using mesoporous silica to immobilize flavin moieties suffered from a severe loss of activity after the first reuse, and a complete inactivation upon second and third attempt.[168] For our nanoparticle-based system, the catalyst was easily removed from the reaction mixture *via* centrifugation and maintained activity for 4 cycles. As a proof of concept study, activity was monitored by irradiation of **FLPDA** particles (50 μg/ml) with indole (1.0 mM) for 1.5 h and measuring the changes in absorption of the reaction mixture between 300-600 nm as shown in **Figure 3.11**. The area within this region was integrated and used as a measure for oxidized indole species production. The first run showed a decrease in relative activity compared to the initial run only by a factor of 1.36 (**Figure 3.11B**) and the subsequent three runs stayed within a similar range before minimum activity, although not a complete loss, was observed by run 6.

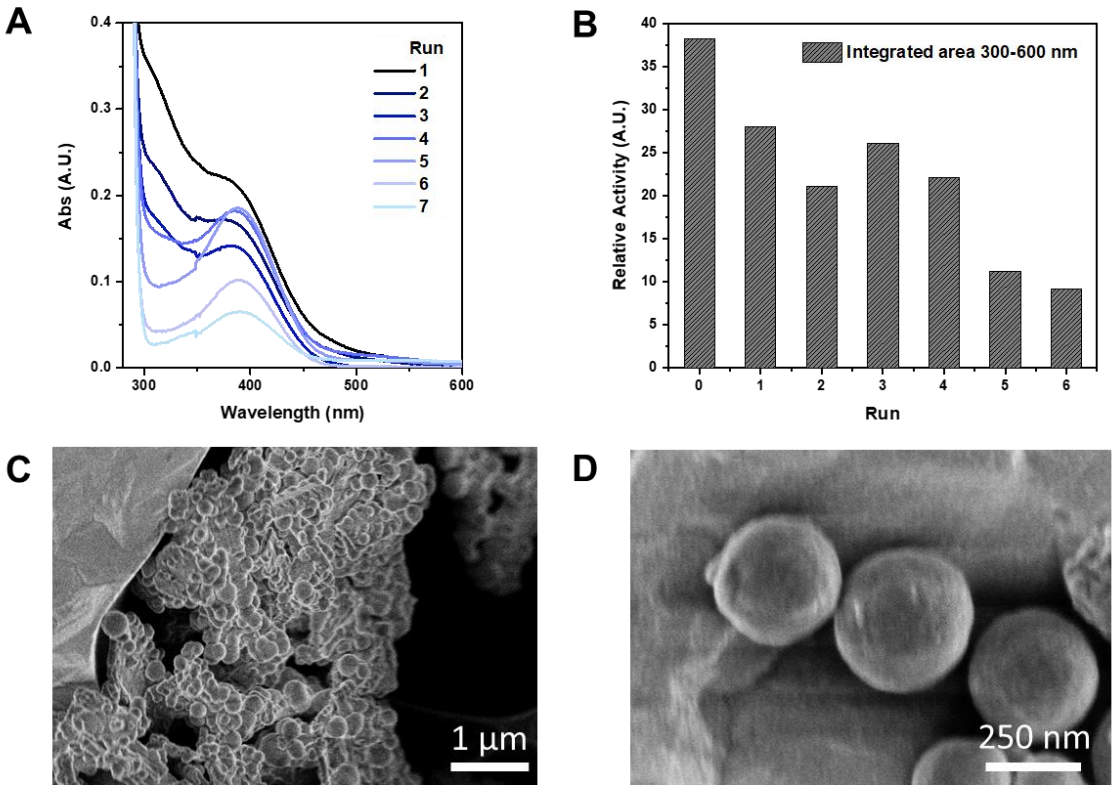

Figure 3.11: Study of **FLPDA** catalyst recyclability. Reaction conditions: indole (1.0 mM), **FLPDA** (50 µg/mL) in O_2 saturated H_2O/MeCN (1:1, v/v, 2 mL) and irradiation for 1.5 h. (A) UV-Vis absorption spectra of different runs using recycled catalyst and (B) the relative activity plot using the integrated area between 300-600 nm of each run. (C) and (D) STEM images of **FLPDA** particles after 2 h irradiation.

The enhanced stability of flavin-polydopamine has already been demonstrated in **Chapter 2** through charge-transfer processes, which has now been proved to be an asset in this enzyme-specific transformation. As mentioned previously (**Section 3.3.2**), HPLC analysis of the reaction mixture catalysed by **FLPDA** showed the formation of lumichrome. This indicates that N10-dealkylation of flavin from PDA occurs and hence, decreases the catalytic activity of the nanoparticles. Loss of activity during recycling can therefore be in part attributed to this process. It was also observed that less particles were retrieved after each centrifugation step which could be due to the inherent inefficiencies of the centrifugation process and/or the degradation of PDA similar to the reported photodecomposition of melanin.[354] However, no considerable differences in particle size and morphology were observed after 2 h of irradiation as seen in **Figure 3.11C** and **D** which disputes this argument –

indicating that loss of particles during centrifugation procedures is the main proponent for this observed decrease in material retrieval. It is envisioned that the reusability of **FLPDA** could be improved by addition of magnetic iron oxide nanoparticles to enable magnetically aided retrieval, which has already proven effective in various application using PDA.[210,211,216,355]

3.3.4 Further control experiments and possible mechanism of action

The photocatalytic mechanism of indole photooxidation by **FLPDA** was investigated by the addition of reactive oxygen species (ROS) scavengers**.** Flavins are well known to produce singlet oxygen and superoxide ROS upon photoexcitation and it can be assumed that one or a combination of these species is responsible for **FLPDA**'s oxidative activity towards indole.[356,357] (2,2,6,6-Tetramethylpiperidin-1-yl)oxyl (TEMPO) was employed as a superoxide scavenger and 1,4-diazabicyclo[2.2.2]octane (DABCO) was used to quench singlet oxygen species. As can be seen from the HPLC chromatograms of the reactions (**Figure 3.12**), the addition of these quenchers did not appear to inhibit the reaction completely. In fact, it was observed that in the case of DABCO, the basic character of the species may have played a role in lowering the activity of **FLPDA** as flavins and PDA are less stable within a basic environment.[358,359] In terms of product selectivity, compound **3a** was not detected most likely due to further oxidisation to isatin **4** which was present at a high concentration of 252 µM as a result of the more basic environment (**Table 3.2**). Based on these observations it could be assumed that singlet oxygen plays a minimal role in **FLPDA** activity as both compounds **2** and **4** are obtained in the presence of singlet oxygen quencher.

The addition of the superoxide scavenger TEMPO had no deleterious effect on **FLPDA** activity either and in fact, it enhanced the production of **2, 3a** and **4** when compared to **FLPDA** alone. TEMPO most likely acts as a redox mediator and co-catalyst in the reaction as previously shown for the synthesis of isatin derivatives in the presence of hypervalent iodine.[360] TEMPO's participation in the reactions was additionally proved by appearance of the by-product 2,2,6,6-tetramethylpiperidine (TMP) at a retention time of 2.49 min, *m/z*: 142 (LC-MS analysis). It should be noted that melanin, which is closely related to PDA, is capable of superoxide radical

quenching and it can therefore be assumed that any superoxide radical generated by flavin would be quickly quenched by PDA in its immediate proximity.[361]

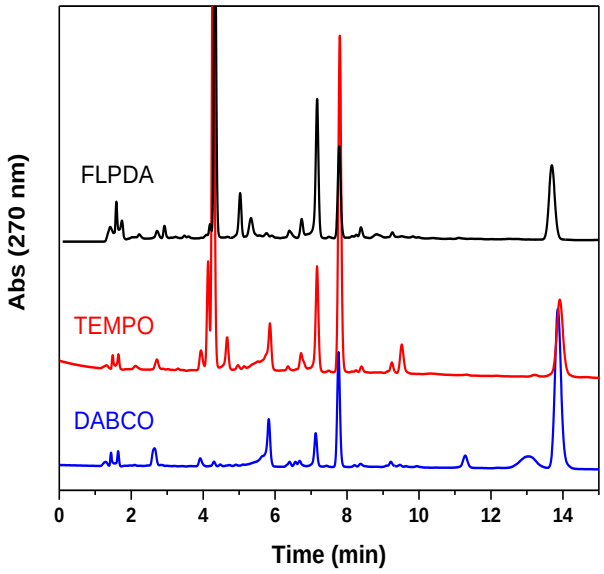

Figure 3.12: Effect of ROS scavengers on indole photooxidation by **FLPDA**. HPLC chromatograms of reactions irradiated for 2 h in the presence of **FLPDA** (50 µg/mL) and indole (1.0 mM) with singlet oxygen scavenger DABCO (1.0 mM) or superoxide scavenger TEMPO (1.0 mM) in H_2O/MeCN (1:1, v/v, 2 mL).

Table 3.2: Amounts and conversions of major compounds identified by HPLC after acidification of reaction mixture using commercial standards as external calibration references.

Quencher	Indole (1) (µM)	Oxindole (2) (µM)	Isatin (4) (µM)	Indole conversion
TEMPO	177	278	121	82%
DABCO	326	143	252	67%

The mechanism of **FLPDA**'s photocatalytic activity was further investigated by using a fluorescence-based assay to monitor the release of H_2O_2 in the reaction. H_2O_2 is released from the unstable C4a-hydroperoxy-flavin species that forms when reduced flavins interact with oxygen.[362] It can therefore be assumed that the concentration of

H_2O_2 detected in the reaction indicates the amount of stabilisation the C4a-hydroperoxy-flavin species receives. Therefore, the concentration of H_2O_2 was determined for the **FLPDA** and **RBF** catalysed photooxidation of indole to be 3.62 ± 0.18 nmol and 5.13 ± 0.04 nmol respectively (**Figure 3.13**). The lower value obtained for **FLPDA** suggests potential stabilisation of the C4a-hydroperoxy flavin species by PDA, however, this would need to be further characterised by *in-situ* EPR or NMR spectroscopy.

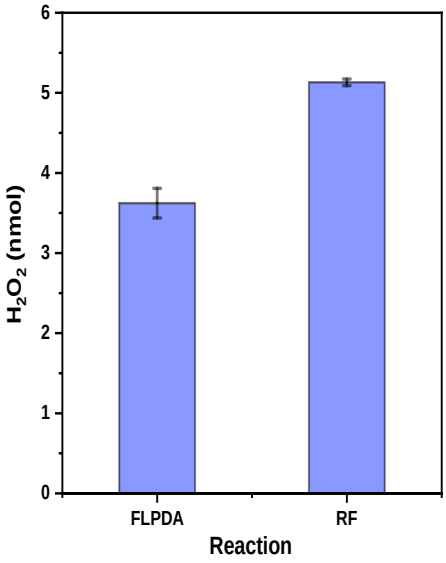

Figure 3.13: H_2O_2 concentrations from **FLPDA** and **RBF** photooxidation of indole. Reaction conditions: indole (1.0 mM), **FLPDA** (20 µg/mL) or **RBF** (20 µM) in H_2O/MeCN (1:1, v/v, 2 mL) irradiated for 1h. Error bars are the standard deviation of triplicate data.

Based on these data, the mechanism shown in **Figure 3.14** is proposed. Photoexcitation of flavin moieties generates a singlet state flavin that undergoes intersystem crossing (ISC) to form the reactive triplet state flavin. PDA features tryptophan and tyrosine mimetic residues that have been shown to play a crucial role in biological signalling pathways through electron transfer to flavin. It is therefore likely that $^3FL^*$ can interact with indole and/or PDA resulting in electron transfer to flavin. Reduced flavin hydroquinone (FL_{hq}) can then interact with molecular oxygen to form C4a-hydroperoxy flavin (FLOOH). Our data suggests that this species is most likely stabilised by H-bonding from neighbouring PDA residues (catechol/amino) and is

therefore able to hydroxylate indole that is favourably adhered to the **FLPDA** surface *via* π-interactions. It is noteworthy to mention that the stabilisation of such (hydro)peroxy flavin species has also been achieved using H-bonding residues in dark catalytic flavin systems.[58,163] Finally, water is eliminated to regenerate oxidized flavin. Additionally, it is expected that Type 1 photosensitisation reactions take place in a similar fashion to that observed between lumiflavin and indole,[363] as well as **RBF** and tryptophan.[364] In this scenario, radical oxidised indole species (neutral or radical cation) are formed that can undergo further oxygenation by ROS or molecular oxygen and can also explain the formation of adducts **5** and **6**.

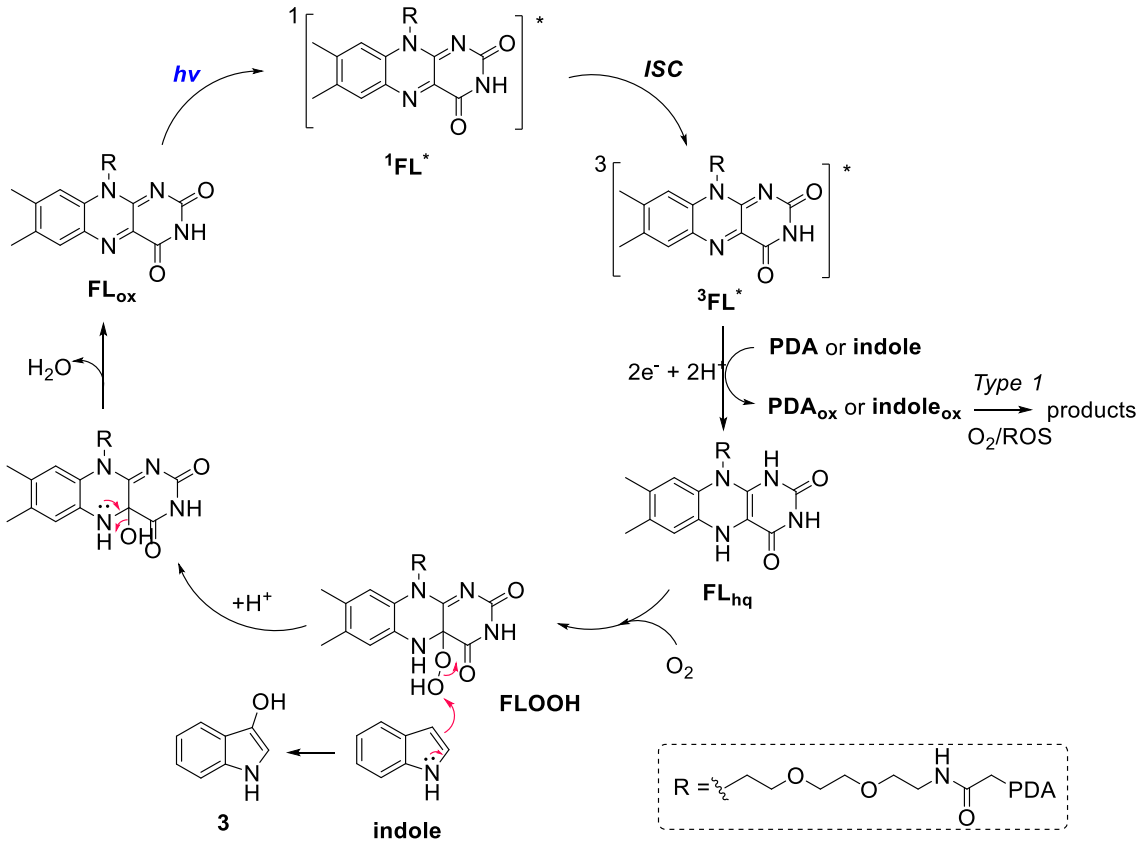

Figure 3.14: Proposed mechanism of action involving electron transfer process between flavin (FL) and PDA moieties within **FLPDA** catalyst.

3.4 Conclusion

Flavin-polydopamine (**FLPDA**) has been shown to effectively display activity analogous to xenobiotic-degrading enzymes such as FMO evidenced by the oxidation reaction of indole to form indigo dye. It is the first time that a flavin photocatalytic system has

demonstrated this activity. Interestingly, the nanoparticle **FLPDA** system displayed five times higher selectivity towards indigoid dye formation than homogeneous riboflavin photocatalyst, and enhanced photostability demonstrated by a decrease in lumiflavin formation. In addition, **FLPDA** displays recyclable activity up to four cycles. ROS scavenging experiments were carried out to identify key species involved in **FLPDA**'s photooxidation mechanism, revealing that neither superoxide nor singlet oxygen were solely responsible for indole oxidation. Subsequently, an H_2O_2 assay discovered that **FLPDA** released less H_2O_2 in the reaction when compared to homogeneous riboflavin. This points towards the stabilisation of C4a-hydroperoxy-flavin as a reactive intermediate in the reaction mechanism and rationalises **FLPDA**'s higher product selectivity towards indigo dye formation. The formation of this reactive intermediate is usually conserved for natural FMOs due to H-bonding stabilisation by amino acid residues. Our hypothesis that polydopamine would enable flavin activity similar to its natural enzyme counterpart has therefore been successfully demonstrated.

4 INVESTIGATING THE LIGHT-DRIVEN REDUCTASE ACTIVITY OF FLAVIN-POLYDOPAMINE

4.1 Introduction

The diversity of flavoenzyme activity is enabled by their ability to undergo one- or two-electron transfer processes with substrates, ranging from oxidations, halogenations, C-C bond formation, as well as a range of reduction reactions.[365–369] Two distinct flavoenzyme classes involved in the catalysis of reduction reactions are the azoreductases (AzoRs) and ene-reductases (ERs).[18,19,370–374] Photocatalytic examples of reduction reactions using artificial flavin systems are very limited, so this chapter aims to develop a methodology to utilise flavin-polydopamine as a photocatalyst for reductase type reactions.

4.1.1 Azoreductase activity and applications

AzoRs have been identified within various microorganisms as critical enzymes in the biotransformation and detoxification of carcinogenic azo dyes, nitro-aromatic and azo-containing drugs (**Figure 4.1**). Consequentially, such microorganisms have been applied to wastewater treatment processes.[375] They are most commonly characterised by a flavin cofactor (FMN/FAD), NAD(P)H dependency, operating in a range of pH, temperatures and in aerobic and anaerobic environments. Their substrate scope is broad and are not conserved to just reducing azo bonds, also displaying the ability to reduce nitro bonds in some cases.[376] With these factors in mind, the usefulness of AzoR containing microorganisms for wastewater treatment is very clear, however they are limited by running costs, contamination, nutrient addition/recycling and often the aromatic amine products from azo dye degradation are more toxic than the azo dye

itself.[377] The latter can be avoided by the addition of laccase-containing microbes that provide further detoxification *via* free-radical oxidation.[377,378]

The reduction of aromatic azo and nitro bonds is also very useful in synthetic organic chemistry and widely employed reactions to access primary aromatic amines for further functionalisation towards drugs and other compounds of commercial interest. This has historically been catalysed by metals such as Pd and Pt,[379] but biocatalytic,[374] and photocatalytic examples provide a greener methodology to achieve such transformations.[380,381] There are however almost no examples of flavin photocatalysis for azo or nitro bond reduction, with the exception of the photoreduction of 4-nitrophenyl phosphate.[382] We therefore saw the demonstration of AzoR activity as a crucial assay to initially highlight the reductive capacity of flavin-polydopamine and identify potential application in water remediation and photocatalysis.

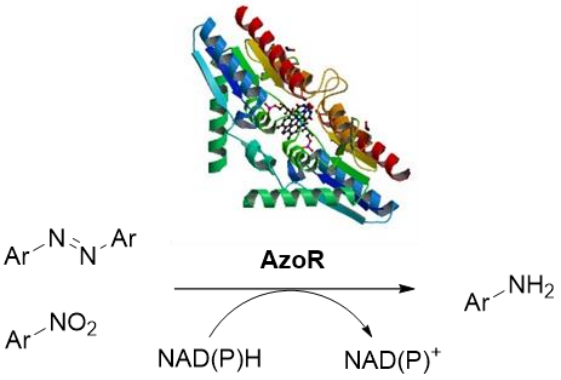

Figure 4.1: General reaction scheme of characteristic azoreductase (AzoR from *E. Coli,* PDB Entry - 1V4B) transformations of aromatic azo and nitro containing compounds to aromatic amine products.

4.1.2 Ene-reductase activity and applications

Ene-reductases (ERs) are flavin and NAD(P)H dependent enzymes found in Nature within the 'Old Yellow Enzyme' (OYE) family widely distributed in bacteria, fungi and plants. In fact, OYE from Baker's Yeast was the first flavin-dependent enzyme to be identified in 1932 by Warburg & Christian and since then, the OYE family has been revitalised in the literature of the 21st century thanks to their new-found role in biocatalysis by providing green methodology to asymmetric olefin reduction.[18,19,383]

ERs are characterised by the ability to reduce activated C=C bonds such as α,β-unsaturated carbonyl species with excellent enantioselectivity (**Figure 4.2**). The mechanism of substrate reduction by ERs follows an overall *trans*-addition of [H_2] through hydride transfer from the reduced anionic flavin hydroquinone (FL_{hq}^-) to the substrate's β-C position *via* a Michael-type addition. Protonation occurs at the α-C position by a tyrosine residue leaving the reduced product and oxidised flavin moiety. A new catalytic cycle is then initiated by NAD(P)H reduction of the oxidised flavin.[384,384]

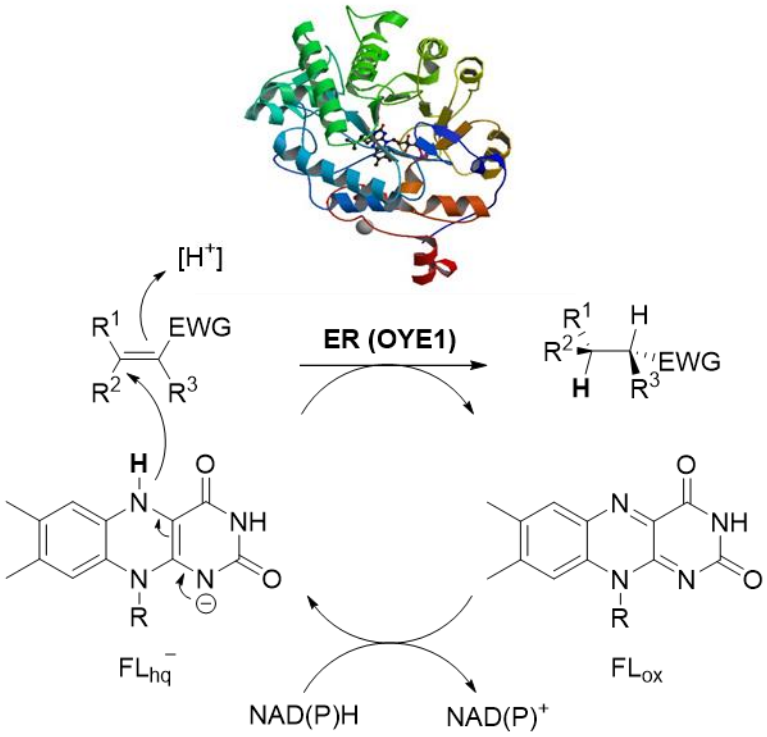

Figure 4.2: General reaction scheme and mechanism of characteristic ene-reductases (ER - OYE1 mutant, PDB Entry - 3TXZ) transformations of activated C=C bonds to chiral saturated products. R = ribityl phosphate, EWG = electron withdrawing group (aldehyde, ketone carboxylic acid, ester, nitrile, nitro *etc.*)[18,19]

This dependency on NAD(P)H however, is one of the major limitation for ERs (and many enzymes in general) to achieve efficient and sustainable biocatalytic reductions. Consequentially, the need for NAD(P)H has been removed through light-driven activation of ERs (photobiocatalysis) using sensitizers such as flavins, transition metal complexes or nanoparticles.[119,121,122,124,385–388] Poor flavin photostability within the enzyme has unfortunately limited the scale-up of these methodologies.[389] Despite

this, direct illumination of ER enzymes has granted access to unnatural asymmetric radical chemistry, a strategy recently developed by the Hyster group.[137–139]

It has yet to be shown whether enzyme-free flavin photocatalysis can effectively display ER activity in a biomimetic fashion, whereby FL_{hq} is accessed to transfer hydride following flavin photoreduction by a sacrificial electron donator species as depicted in **Figure 4.3**. Our aim was to develop a flavin-polydopamine nanoparticle system that could effectively display ER activity under irradiation utilising sacrificial electron donors to reduce the flavin groups and undergo hydride transfer to a substrate akin to the enzymatic mechanism. Additionally, the possibility of achieving enantioselective transformations - a hallmark in biocatalysis - would be an extremely powerful methodology, avoiding the use of NAD(P)H and need of a specific protein make-up. To that end, a chiral riboflavin-polydopamine nanoparticle conjugate (**RCPDA**) was prepared in order to investigate ER activity.

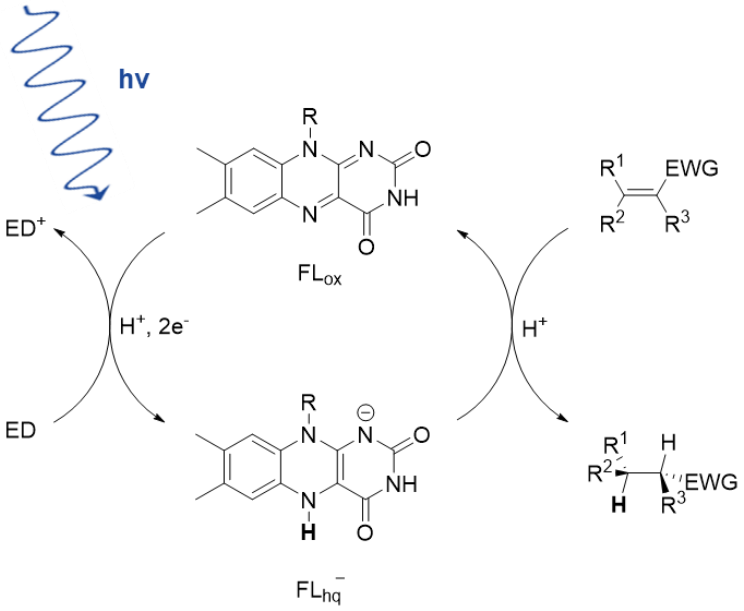

Figure 4.3: Proposed reaction mechanism of light-driven ene-reductase (ER) activity. ED = electron donor.

4.2 Experimental

4.2.1 General information

All materials were purchased from either Acros Organics (UK), Alfa Aeser (UK), Sigma-Aldrich (UK) or TCI Chemicals (BE) in the highest purity available and used without further purification. **RTA** was synthesised from (-)-riboflavin (from Eremothecium ashbyii, ≥98%, Sigma-Alrich, UK) according to the literature procedure by Metternich *et al.*[180] tert-Butyl (2-bromoethyl)carbamate (**4**) was prepared according to the literature procedure by Luescher *et al.*[390] *S*-Acetyl protected Captopril (**7**) was prepared according to the literature procedure by Li *et al.*[391] PDA NPs were prepared according to the literature procedure by Ai *et al.*[204] *rac*-**1b** was prepared by Pd/C hydrogenation according to the literature procedure by Hall *et al.* and used for GC-MS calibration.[392] *rac*-**2b** was prepared by Pd/C hydrogenation according to the literature procedure by Gonçalves *et al.* and used for GC-MS calibration.[131]

^{1}H and ^{13}C NMR measurements were carried out using a 500 MHz DCH Cryoprobe Spectrometer. HRMS was recorded on a ThermoFinnigan Orbitrap Classic (Fisher Scientific). UV-Vis absorption spectra were obtained with an Agilent Cary 300 Spectrophotometer. Fluorescence emission spectra were obtained using a Varian Cary Eclipse Fluorescence Spectrophotometer using excitation and emission splits of 5 nm or 10 nm. DLS and zeta potential measurements were recorded using a Zetasizer Nano Range instrument (Malvern Panalytical). SEM images were obtained using a FEI Helios SEM at an acceleration voltage of 2.0 kV. Samples were suspended in water and drop cast on lacey carbon copper grids (Agar Scientific). GC-MS (Agilent Technologies 7890B GC, 5977A MSD) was performed using an HP-Innowax Agilent column (19091N-133, 30 m x 0.25 mm, 0.25 µm): split 20, flow 40.0 mL min^{-1}, injector: 220°C, detector: 250°C. Temperature programme: 110°C hold for 2 min, to 240°C at 20°C min^{-1}, hold for 10 min. Retention times: **1a** = 9.433 min, **1b** = 10.615 min; **2a** = 4.786 min, **2b** = 5.332 min. Chiral HPLC analysis was carried out using an Agilent 1260 Infinity Quaternary LC equipped with a Chiralcel OD column (10µm, 4.6 mm x 250 mm, Diacel) and diode array detector (monitoring at 254 nm). The mobile phase consisted of hexane/i-PrOH (9:1) with retention times: (R)-**1b** and (S)-**1b** at 20.0 min and 22.0 min, respectively.[393]

4.2.2 Synthesis of RFCPT

(2*S*,3*R*,4*R*)-5-(3-(2-((*tert*-Butoxycarbonyl)amino)ethyl)-7,8-dimethyl-2,4-dioxo-3,4-dihydrobenzo[*g*]pteridin-10(2*H*)-yl)pentane-1,2,3,4-tetrayl tetraacetate (5):

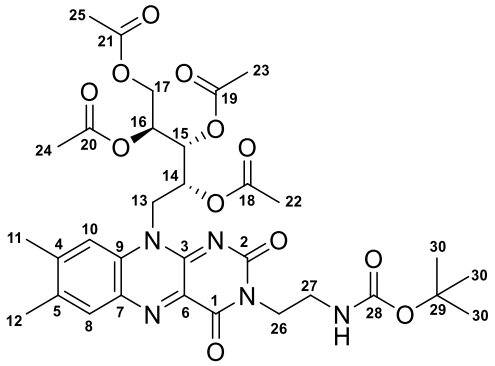

RTA (1.0 g, 1.84 mmol, 1.0 equiv.) and **5** (2.06 g, 9.18 mmol, 5.0 equiv.) were dissolved in dry DMF (18.4 mL) before Cs_2CO_3 (897.5 mg, 2.75 mmol, 1.5 equiv.) was added. The resulting suspension was stirred at room temperature under Ar atmosphere and in the dark for 18 h. The reaction mixture was then diluted with water (20 mL) and EtOAc (20 mL), the aqueous phase was extracted with EtOAc (3x 20 mL) and the combined organic phases were dried over Na_2SO_4 before the solvent was removed *in vacuo*. Purification by silica gel column chromatography (1% MeOH/DCM) yielded the product 2 as an orange sticky solid (1.07 g, 1.55 mmol, 84%).

^{1}H NMR (500 MHz, $CDCl_3$) δ = 7.86 (s, 1H, **H8**), 7.45 (s, 1H, **H10**), 5.51 (br. m, 1H, **H14**), 5.34 (br. m, 1H, **H15**), 5.27 (br. m, 1H **H16**), 5.18 (br. s, 1H, -**NH**-), 4.92 (br. s, 2H, **H13**), 4.31 (dd, *J* = 12.4, 2.7 Hz, 1H, **H17**), 4.11 (m, 3H, **H17**, **H26**), 3.34 (br. m, 2H, **H27**), 2.44 (s, 3H, **H11**), 2.31 (s, 3H, **H12**), 2.14 (s, 3H, **H22**/**23**/**24**/**25**), 2.09 (s, 3H, **H22**/**23**/**24**/**25**), 1.94 (s, 3H, **H22**/**23**/**24**/**25**), 1.62 (s, 3H, **H22**/**23**/**24**/**25**), 1.23 (s, 9H, H**30**) ppm.

^{13}C NMR (500 MHz, $CDCl_3$) δ = 170.6 (**C18**/**19**/**20**/**21**), 170.2 (**C18**/**19**/**20**/**21**), 169.8 (**C18**/**19**/**20**/**21**), 169.7 (**C18**/**19**/**20**/**21**), 160.0 (**C2**), 156.0 (**C28**), 155.1 (**C1**), 149.0 (**C3**), 147.8 (**C4**), 136.7 (**C5**), 135.4 (**C6**), 134.6 (**C7**), 132.6 (**C8**), 131.3 (**C9**), 115.5 (**C10**), 78.9 (**C29**), 70.2 (**C15**), 69.3 (**C14**), 69.0 (**C16**), 61.7 (**C17**), 44.4 (**C13**), 41.4 (**C27**), 39.7 (**C26**), 28.2 (**C30**), 21.4 (**C11**), 20.9 (**C22**/**23**/**24**/**25**), 20.7 (**C22**/**23**/**24**/**25**), 20.6 (**C22**/**23**/**24**/**25**), 20.3 (**C22**/**23**/**24**/**25**), 19.4 (**C12**) ppm.

HRMS (ESI) m/z: $[M + H]^+$ Calcd for $C_{32}H_{42}O_{12}N_5$ 688.2824; Found 688.2830.

(2*S*,3*R*,4*R*)-5-(3-(2-Aminoethyl)-7,8-dimethyl-2,4-dioxo-3,4-dihydrobenzo[*g*]pteridin-10(2*H*)-yl)pentane-1,2,3,4-tetrayl tetraacetate (6):

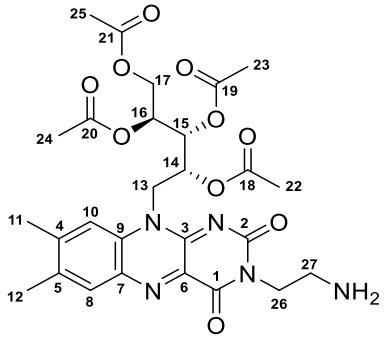

Trifluoroacetic acid (4 mL) was added dropwise to a solution of **2** (1.03 g, 1.50 mmol) in DCM (20 mL) at 0 °C. The resulting mixture was left to warm to room temperature and stirred for 4 h. The solvent was then removed *in vacuo* and residue co-evaporated with toluene (3 x 20 mL) to remove excess trifluoracetic acid, yielding an orange oil (871.2 mg, 1.48 mmol, 99%).

^{1}H NMR (500 MHz, $CDCl_3$) δ = 7.94 (s, 1H, **H8**), 7.50 (s, 1H, **H10**), 5.57 (dt, *J* = 9.7, 2.8 Hz, 1H, **H14**), 5.47 (dd, *J* = 7.7, 2.2 Hz, 1H, **H15**), 5.39 (br. m, 3H **H16,** -**NH_2**), 4.98 (br. s, 2H, **H13**), 4.50-4.33 (m, 3H, **H17**, **H26**) 4.23 (dd, *J* = 12.5, 5.1 Hz, 1H, **H17**), 3.52 (br. m, 2H, **H27**), 2.50 (s, 3H, **H11**), 2.39 (s, 3H, **H12**), 2.19 (s, 3H, **H22**/**23**/**24**/**25**), 2.17 (s, 3H, **H22**/**23**/**24**/**25**), 2.05 (s, 3H, **H22**/**23**/**24**/**25**), 1.65 (s, 3H, **H22**/**23**/**24**/**25**) ppm.

^{13}C NMR (500 MHz, $CDCl_3$) δ = 171.5 (**C18**/**19**/**20**/**21**), 170.8 (**C18**/**19**/**20**/**21**), 169.7 (**C18**/**19**/**20**/**21**), 169.6 (**C18**/**19**/**20**/**21**), 160.8 (**C1**), 156.1 (**C2**), 149.0 (**C3**), 147.9 (**C4**), 137.2 (**C5**), 135.3 (**C6**), 134.9 (**C7**), 132.5 (**C8**), 131.5 (**C9**), 115.7 (**C10**), 70.0 (**C15**), 69.5 (**C14**), 69.0 (**C16**), 61.6 (**C17**), 44.4 (**C13**), 39.6 (**C26**), 39.1 (**C27**), 21.5 (**C11**), 21.0 (**C22**/**23**/**24**/**25**), 20.7 (2C, **C22**/**23**/**24**/**25**), 20.3 (**C22**/**23**/**24**/**25**), 19.3 (**C12**) ppm.

HRMS (ESI) m/z: $[M + H]^+$ Calcd for $C_{27}H_{34}O_{10}N_5$ 588.2300; Found 588.2287.

(2*S*,3*R*,4*R*)-5-(3-(2-((*S*)-1-((*S*)-3-(acetylthio)-2-methylpropanoyl)pyrrolidine-2-carboxamido)ethyl)-7,8-dimethyl-2,4-dioxo-3,4-dihydrobenzo[*g*]pteridin-10(2*H*)-yl)pentane-1,2,3,4-tetrayl tetraacetate (5):

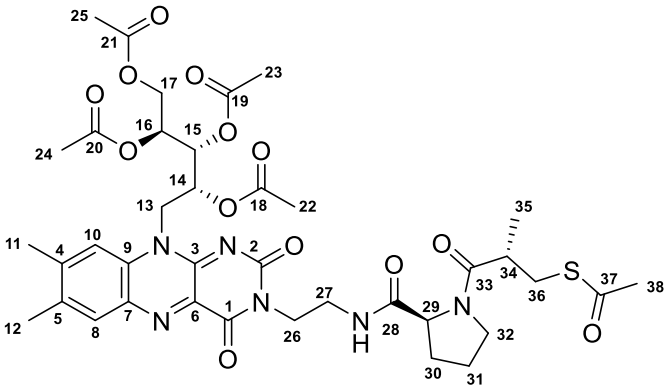

4 (450 mg, 1.74 mmol, 1.0 equiv.), **3** (1.22 g, 2.08 mmol, 1.2 equiv.) and HATU (1.32 g, 3.47 mmol, 2 equiv.) were dissolved in dry DMF (20 mL) under Ar atmosphere. A solution of DIPEA (0.60 mL) in dry DMF (5 mL) was added dropwise and the reaction was left to stir at room temperature for 18 h in the dark. The reaction was then diluted with water (30 mL) and EtOAc (30 mL) the aqueous phase was extracted with EtOAc (3x 30 mL) and the combined organic phases were dried over Na_2SO_4 before the solvent was removed *in vacuo*. Purification by silica gel column chromatography (1-3% MeOH/DCM) yielded the product **5** as a yellow waxy solid (1.07 g, 1.55 mmol, 84%).

^{1}H NMR (500 MHz, $CDCl_3$) δ = 7.96 (s, 1H, **H8**), 7.51 (s, 1H, **H10**), 7.05 (br. t, *J* = 5.4 Hz, -**NH**-), 5.61 (br. m, 1H, **H14**), 5.42 (br. m, 1H, **H15**), 5.38-5.35 (m, 3H **H16**), 4.89 (br. s, 2H, **H13**), 4.41-4.38 (m, 2H, **H17**, **H29**), 4.27-4.13 (m, 3H, **H17**, **H26**), 3.71-3.66 (m, 1H, **H32**), 3.61-3.57 (m, 1H, **H32**), 3.49-3.40 (m, 2H, **H27**), 3.06-2.89 (m, 1H, **H36**), 2.85-2.75 (m, 2H, **H36**, **H34**), 2.52 (s, 3H, **H11**), 2.40 (s, 3H, **H12**), 2.26-2.14 (m, 10H, **H22**/**23**/**24**/**25**, **H30**/**31**), 2.03 (s, 3H, **H22**/**23**/**24**/**25**), 1.84 (br. m, 3H, **H30**/**31**), 1.70 (s, 3H, **H22**/**23**/**24**/**25**), 1.21-1.16 (m, 3H, **H35**) ppm.

^{13}C NMR (500 MHz, $CDCl_3$) δ = 196.1 (**C37**), 174.5 (**C33**), 171.8 (**C18**/**19**/**20**/**21**), 170.7 (**C18**/**19**/**20**/**21**), 170.3 (**C28**), 169.8 (**C18**/**19**/**20**/**21**), 169.7 (**C18**/**19**/**20**/**21**), 160.2 (**C1**), 155.3 (**C2**), 149.2 (**C3**), 147.7 (**C4**), 136.7 (**C5**), 135.7 (**C6**), 134.7 (**C7**), 132.8 (**C8**), 131.2 (**C9**), 115.4 (**C10**), 70.4 (**C15**), 69.3 (**C14**), 69.0 (**C16**), 61.9 (**C17**), 59.9 (**C29**), 47.2 (**C32**), 44.5 (**C13**), 41.3 (**C26**), 38.8 (**C27**), 38.3 (**C34**), 32.2 (**C36**), 30.6 (**C38**), 27.9 (**C30**), 24.8

(**C31**), 21.4 (**C11**), 21.1 (**C22**/**23**/**24**/**25**), 20.8 (**C22**/**23**/**24**/**25**), 20.7 (**C22**/**23**/**24**/**25**), 20.4 (**C22**/**23**/**24**/**25**), 19.5 (**C12**) 16.9 (**C35**) ppm.

HRMS (ESI) m/z: $[M + H]^+$ Calcd for $C_{38}H_{49}O_{13}N_6S_1$ 829.3073; Found 829.3073.

(*S*)-*N*-(2-(7,8-dimethyl-2,4-dioxo-10-((2*R*,3*R*,4*S*)-2,3,4,5-tetrahydroxypentyl)-4,10-dihydrobenzo[*g*]pteridin-3(2*H*)-yl)ethyl)-1-((*S*)-3-mercapto-2-methylpropanoyl)pyrrolidine-2-carboxamide (RFCPT):

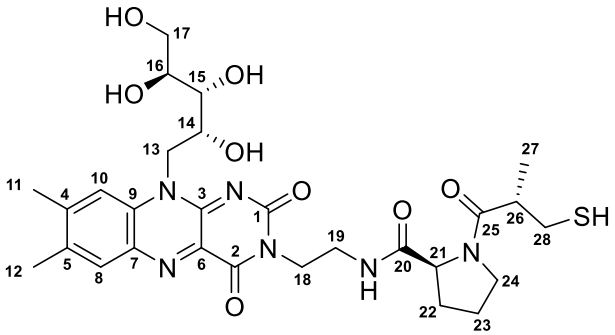

Compound **5** (100 mg, 0.121 mmol) was dissolved in degassed 1M HCl (10 mL) and stirred overnight at 60 °C for 18 h under Ar atmosphere in the dark. The solvent was removed *in vacuo* and the resulting orange residue was recrystallised from ethanol to give an orange solid (66.3 mg, 0.071 mmol, 59%).

^{1}H NMR (500 MHz, DMSO-d_6) δ = 7.95 (s, 2H, **H8**, **H10**), 7.84 (br. t, *J* = 5.2 Hz, -**NH**-) 7.50 (s, 1H, **H10**), 5.14 (br. m, 1H, **H15$_{OH}$**), 4.97 (br. m, 1H, **H13**), 4.89 (br. m, 1H, **H16$_{OH}$**), 4.78 (br. s, 1H, **H14$_{OH}$**), 4.65 (d, 1H, *J* = 12.0 Hz, **H13**), 4.51 (t, *J* = 5.5 Hz, 1H, **H17$_{OH}$**), 4.26 (br. s, 1H, **H14**), 4.20-4.13 (m, 1H, **H21**) 4.07-3.90 (m, 2H, **H24**), 3.65 (m, 3H, **H15**/**16**/**17**), 3.54-3.43 (m, 3H, **H17**, **H18**), 3.26 (m, 2H, **H19**), 2.76-2.54 (m, 2H, **H26**/**28**), 2.49 (s, 3H, **H11**), 2.41 (s, 3H, **H12**), 2.38-2.30 (m, 1H, **H26**/**28**), 2.25-2.05 (m, 1H, **H22**, **H23**), 1.95-1.77 (m, 3H, **H22**, **H23**), 1.05 (m, 3H, **H27**) ppm.

^{13}C NMR (500 MHz, DMSO-d_6) δ = 172.8 (**C25**), 171.8 (**C20**), 159.8 (**C1**), 154.9 (**C2**), 149.5 (**C3**), 146.4 (**C4**), 136.0 (2C, **C5**, **C6**), 134.4 (**C7**), 132.1 (**C8**), 130.8 (**C9**), 117.6 (**C10**), 73.7 (**C15**), 72.9 (**C14**), 69.0 (**C16**), 63.5 (**C17**), 59.5 (**C21**), 47.2 (**C13**), 46.9 (**C24**), 41.2 (**C26**), 40.5 (**C18**), 36.5 (**C19**), 29.2 (**C22**), 27.3 (**C28**), 24.3 (**C23**), 20.9 (**C11**), 18.9 (**C12**), 16.7 (**C27**) ppm.

HRMS (ESI) m/z: $[M + H]^+$ Calcd for $C_{28}H_{39}O_8N_6S_1$ 619.2545; Found 619.2534.

4.2.3 Synthesis of RCPDA

PDA NPs (**PDA-1** or **-2**, 0.1 mg/mL) were suspended in a solution of TRIS buffer (10 mM, pH 8.0, 20 mL) and the solution was sparged with Ar gas for 15 min before adding dropwise a degassed solution of **RFCPT** (1-5 mg per mg of PDA). The mixture was stirred for 18 h under Ar atmosphere and in the dark. The reaction mixture was then centrifuged (15000 rpm for 15 min) and resulting precipitate was washed three times with Milli-Q water by centrifugation (15000 rpm for 15 min). The resulting particles were then resuspended in Milli-Q water to an approximate concentration of 0.2 mg/mL and stored at room temperature.

4.2.4 Homogeneous photoreactions

***General procedure*:** A mixture of substrate (**1-3a**, 10 mM) and flavin photocatalyst (10 mol%) in buffer/MeCN (3:1, v/v, 2 mL) was sparged with Ar gas for 15 min and sealed using airtight septa with an Ar balloon. The reaction mixture was then irradiated with a 450 nm EvoluChem 18W LED (**Figure 4.4**) for 16-18 h using a cooling fan to maintain room temperature. Reaction mixtures were then diluted with Et_2O and filtered through SiO_2 with top a layer of Na_2SO_4 to remove the flavin. Combined washes were then concentrated *in vacuo* and analysed by GC-MS using limonene internal standard or ^1H NMR to determine conversion and yield.

4.2.5 Nanoparticle photoreactions

***General procedure*:** A mixture of substrate (**1-2a**, 1 mM) and **RCPDA** (0.1 mg/mL) in buffer/MeCN (3:1, v/v, 2 mL) was sparged with Ar gas for 15 min and sealed using airtight septa with an Ar balloon. The reaction mixture was then irradiated with a 450 nm EvoluChem 18W LED (**Figure 4.4**) for 24 h using a cooling fan to maintain room temperature. The resulting mixture was extracted using EtOAc (3 x 5 mL), dried over Na_2SO_4 and concentrated *in vacuo*. The resulting residue was re-dissolved in EtOAc (1 mL) to be analysed by GC-MS using limonene internal standard to determine conversion and yield. After analysis, the sample was concentrated *in vacuo* and re-dissolved in IPA/Hexane (1:1, 0.5 mL) and analysed by chiral HPLC using a Chiralcel-OD column for enantioselective excess (*ee*) determination.

4.2.6 LED emission profile

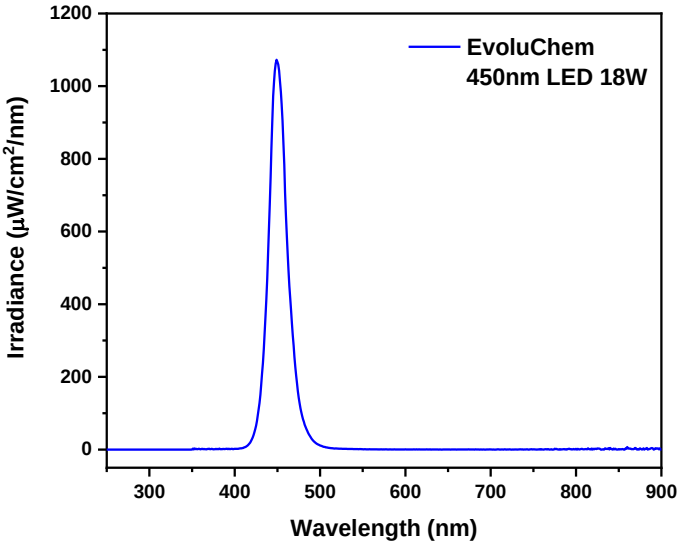

Figure 4.4: Emission spectrum of EvoluChem LED used for photoreactions (450 nm, 18W).

4.2.7 Fluorescence intensity calibration

Two fluorescence intensity calibration curves (A and B) were utilised to approximate flavin wt% loading for **RCPDA** samples. Triplicate dilutions of **RFCPT** in water were measured with 50 µg/mL PDA to account for excitation/emission absorbance by PDA.

Table 4.1: Correlation data from fluorescence calibration A and B. Error was calculated from the standard deviation of triplicate data.

RCPDA	Average Intensity (A.U.) @ λ_{max} (50 µg/mL)	[RFCPT] (µg/mL)	Approximate %wt loading
1	95.84 [A]	0.58 ± 0.05	1.2 ± 0.1
2	150.86 [A]	0.92 ± 0.05	1.8 ± 0.1
3	49.05 [B]	1.87 ± 0.19	3.7 ± 0.4

[A] For **RCPDA-1** and **-2**, calibration A was used with spectrometer excitation and emission slits set at 10 nm:

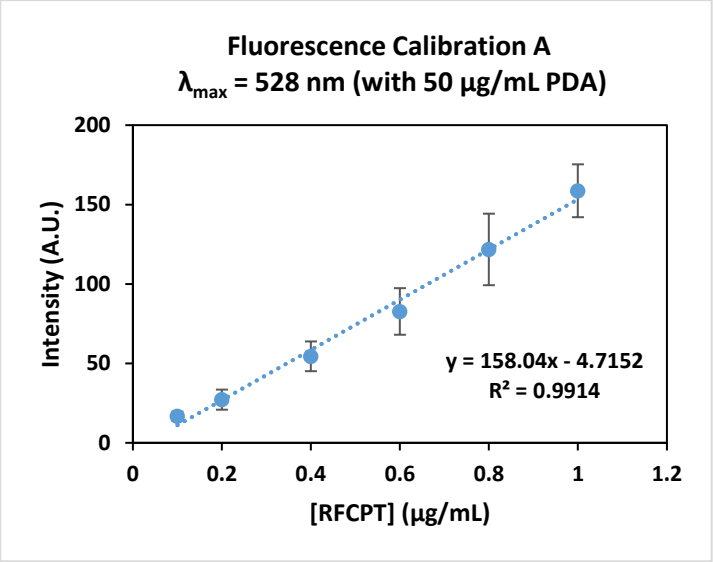

[B] For **RCPDA-3** calibration B was used with spectrometer excitation and emission slits set at 5 nm:

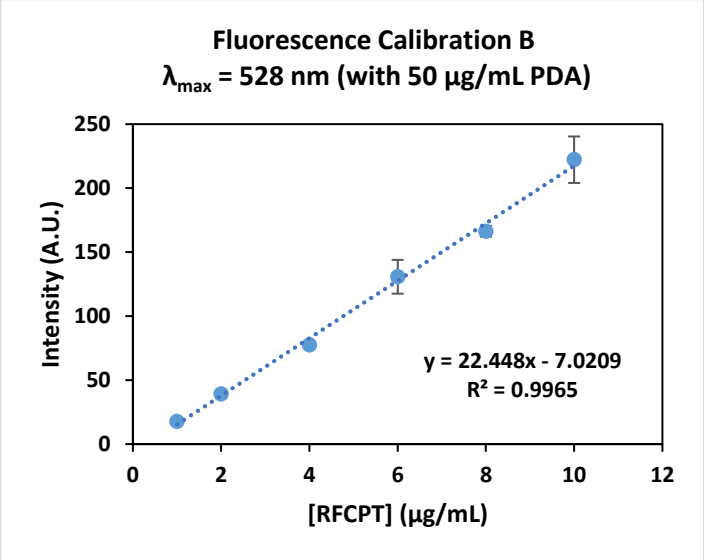

4.3 Results and Discussion

4.3.1 Azoreductase activity

The azo dyes, Amaranth (**AMT**) and Naphthol Blue Black (**NBB**) were chosen as proof-of-concept substrates to initially investigate the reductase activity of **FLPDA** upon blue light irradiation in the presence of a sacrificial electron donor (**Figure 4.5A**). EDTA is commonly used as a sacrificial electron donor to reduce flavins and flavoenzymes,[114,309,394,395] however its oxidation products have been shown to be detrimental to photocatalytic systems by interacting with the catalyst itself.[309,396,397] To avoid this, 3-(*N*-morpholino)propanesulfonic acid (MOPS) buffer at pH 7.5 and 2-(*N*-morpholino)ethanesulfonic acid (MES) buffer at pH 6.0 were chosen as suitable buffer systems as they have shown to be effective electron donors in flavin photobiocatalysis with minimal side reactions or products.[102–104,130,131]

Figure 4.5B and **C** show the kinetic plots of AMT and NBB photoreduction using 25 μg/mL of **FLPDA** as synthesised in **Chapter 2** and **3** using a 5:1 ratio of dopamine to **FLDA**. For both model substrates, activity is slightly increased using MES as the electron donor rather than MOPS, however blank control experiments revealed considerable bleaching in MES pH 6.0 buffer for NBB as shown in **Figure 4.6D.** In the case of AMT there is little bleaching in both buffer systems as shown in **Figure 4.6A** and **B** showing that a lower pH is slightly more optimal for the reduction of these azo species.

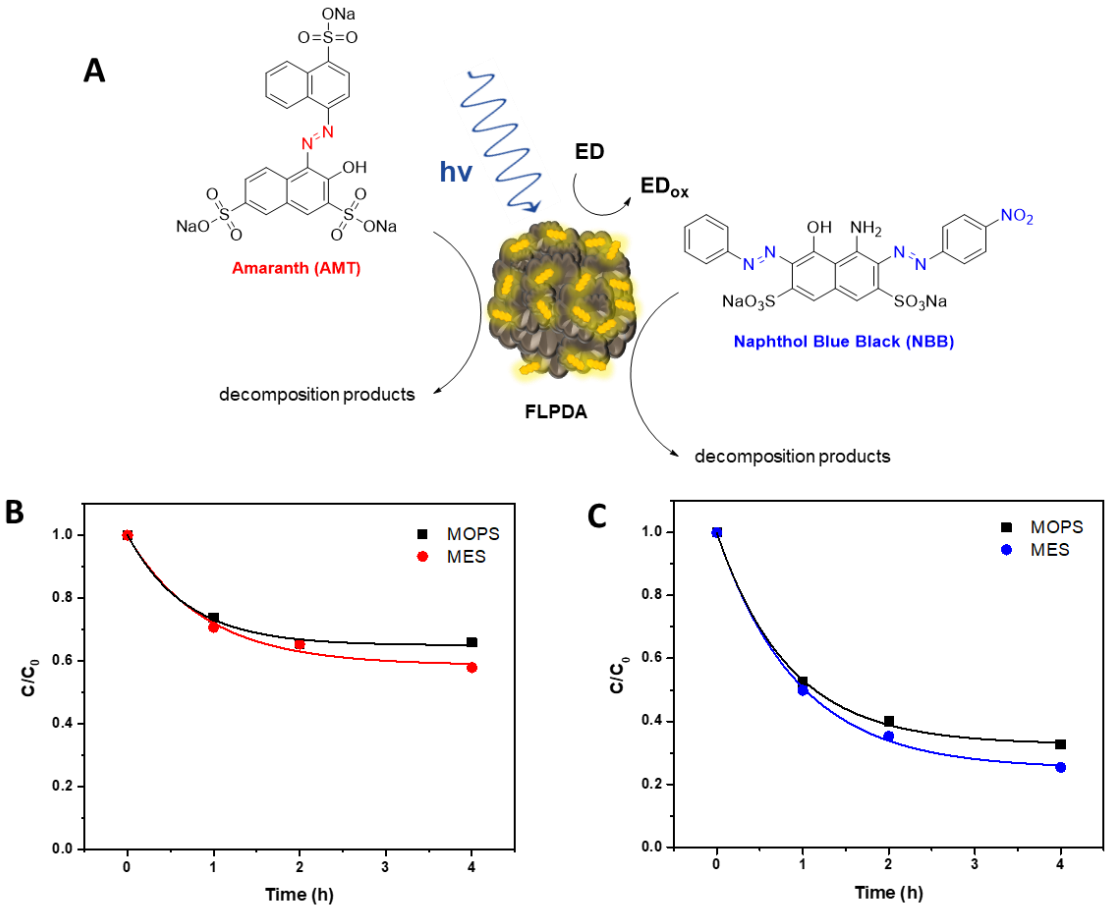

Figure 4.5: (A) Reaction schematic of **AMT** and **NBB** reduction upon blue light irradiation (450 nm) in the presence of FLPDA and an electron donor (ED). (B) Kinetic plot of **AMT** photoreduction (λ_{max} = 520 nm). (C) Kinetic plot of photoreduction **NBB** (λ_{max} = 618 nm). Reaction conditions: **AMT** (0.2 mM) or **NBB** (0.1 mM), **FLPDA** (25 µg/mL) with MOPS buffer (0.1 M, pH 7.5, 2 mL) or MES buffer (0.1 M, pH 6.0, 2 mL), irradiated with a 450 nm LED (18W) at RT for 4 h under Ar atmosphere.

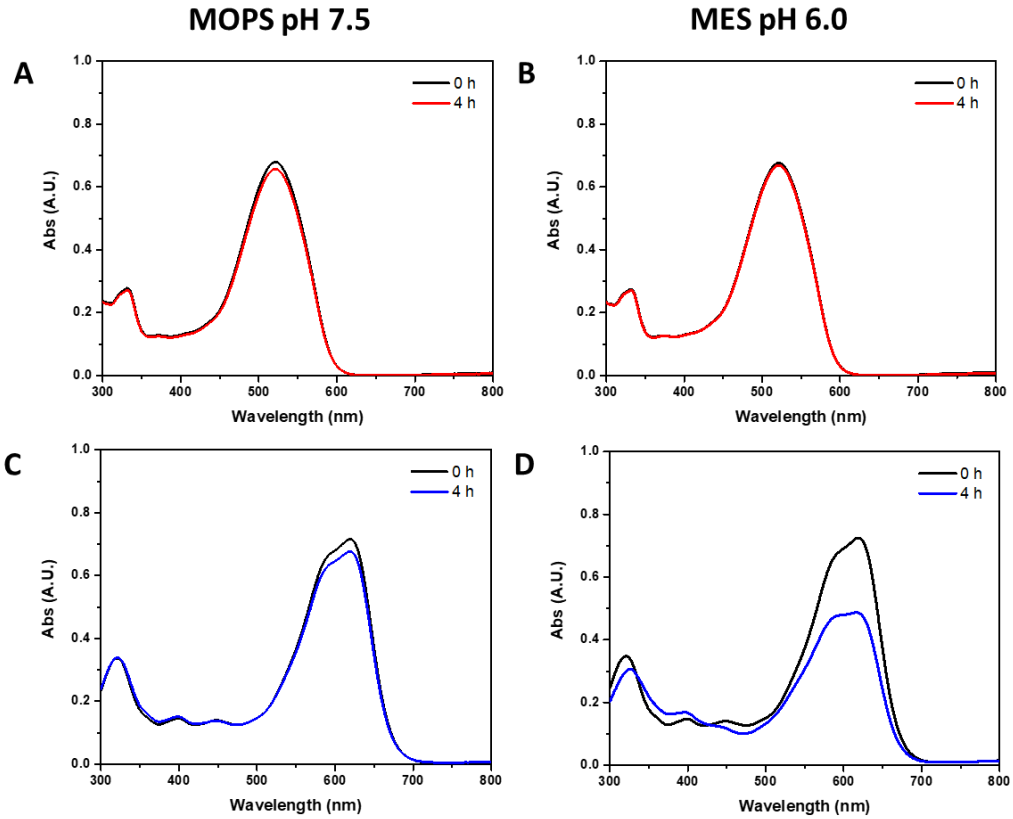

Figure 4.6: UV-Vis spectra of blank control experiments: (A) **AMT** in MOPS buffer and (B) MES buffer; (C) **NBB** in MOPS buffer and (D) MES buffer. Reaction conditions: AMT (0.2 mM) or NBB (0.1 mM) with MOPS buffer (0.1 M, pH 7.5, 2 mL) or MES buffer (0.1 M, pH 6.0, 2 mL), irradiated with a 450 nm LED (18W) at RT for 4 h under Ar atmosphere.

Overall, reaction rates are slow with neither substrate being fully reduced after 4 h even at low substrate concentrations with >10 mol% effective flavin loading. It was therefore decided that a different strategy was necessary to enhance the degradation of the dyes through the anchoring of flavins to a heterogeneous semiconductor such as iron oxide (γ-Fe_2O_3) to be more suitable for water remediation applications. The system has the added advantages of being magnetic for ease of catalyst removal and biocompatibility (work ongoing in collaboration with Samer I. Nehme in the group of Dr. Ljiljana Fruk, Department of Chemical Engineering and Biotechnology, University of Cambridge).[398] Nonetheless, as a proof-of-concept, these results provided encouraging evidence that high potential reduced flavin species could be generated in the presence of PDA using morpholine-based buffers and were able to reduce substrates containing azo/nitro species, which has not been reported by an

artificial flavin photocatalytic system. With this evidence in hand, efforts were then focussed onto investigating ene-reductase activity and future work will involve optimising industrially relevant azo/nitro group reductions using flavin photocatalysis.

4.3.2 Ene-reductase activity

Three typical ene-reductase (ER) substrates were chosen as model compounds to be studied: *N*-pheny-2-methyl maleimide (**1a**), ketoisophorone (**2a**) and α-methyl-*trans*-cinnamaldehyde (**3a**) that can be reduced by ERs to chiral products **1-3b** (**Figure 4.7**).[18]

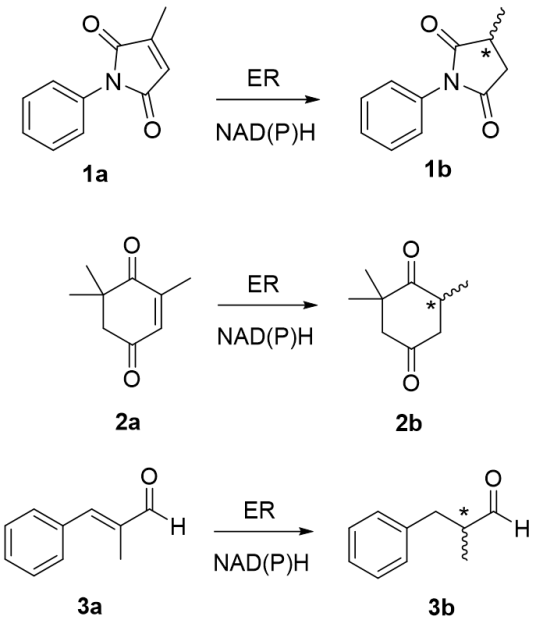

Figure 4.7: Ene-reductase (ER) catalysed bioreduction of *N*-pheny-2-methyl maleimide (**1a**), ketoisophorone (**2a**) and α-methyl-trans-cinnamaldehyde (**3a**).[18]

4.3.2.1 Homogeneous photoreactions

As discussed in **Section 4.3.1**, morpholine-based buffers have recently been shown to enhance photocatalytic activity for enzyme activation.[130,131] To see if this extends to flavin photocatalysis in general, screening of these electron donating buffers was carried out using maleimide **1a** following the reported optimised concentration equivalence of buffer to substrate.[131] It is important to note that 100 equivalents of morpholine buffer was found to be optimal, however 25 equivalents of aliphatic amines (EDTA and TEOA) were used to achieve the same relative activity. A 3:1 ratio of buffer to MeCN was used in our studies to ensure substrate and buffer solubility. The

resulting conversions and yields obtained under these conditions using **RBF** and **RTA** photocatalysts are summarised in **Table 4.2.**

Table 4.2: Buffer screening for homogeneous flavin photoreactions with **1a.**[a]

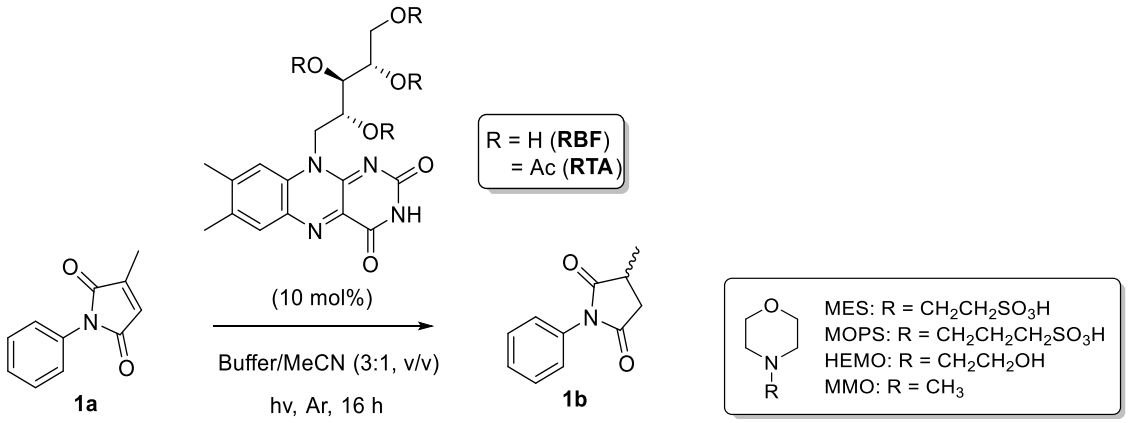

Entry	Buffer	Flavin	Conversion (%)	Yield (%)
1	0.25 M EDTA pH 7.5	RBF	100	1
2		RTA	84	1
3	0.25 M TEOA pH 7.5	RBF	98	3
4		RTA	81	2
5	1 M MES pH 6.0	RBF	76	1
6		RTA	76	1
7	1 M MOPS pH 7.5	RBF	58	6
8		**RTA**	**99**	**32**
9	1 M MMO pH 7.5	RBF	97	7
10		**RTA**	**100**	**28**
11	1 M HEMO pH 7.5	**RBF**	**85**	**23**
12		RTA	77	6

[a] Reaction conditions: **1a** (10 mM) and either **RBF** or **RTA** (10 mol%) in a mixture of buffer and MeCN (3:1, v/v, 2 mL) irradiated with a 450 nm LED (18W) at RT for 16 h under Ar atmosphere.
[b] Conversion determined by GC-MS using calibration curve of **1a** with limonene as the internal standard.
[c] Yield determined by GC-MS using calibration curve of **1b** with limonene as the internal standard.

In the presence of aliphatic amine buffers, EDTA and TEOA (entries 1-4), **1b** was obtained in yields of <5% despite very high conversions, regardless of the flavin photocatalyst. It is therefore apparent that side-reactions occur which consume **1a** but do not lead to the formation of **1b**. The use of a morpholine based buffer greatly improves the yield of **1b**, as shown for entries 8, 10 and 11, however side-reactions still occur limiting the yield of the conversion. Unfortunately, major by-products were not observed using the GC-MS method described in Section 4.2.1 in order to account for the mass balance of these reactions. Optimal reaction conditions were found using **RTA** and MOPS pH 7.5 which resulted in a yield of 32% with quantitative conversion (entry 8) and similar behaviour was also observed with MMO pH 7.5 (entry 10).

It is also apparent that pH plays a role in the enhancing yield of **1b** evidenced by entry 5 and 6 where the use of MES at pH 6 results in much lower conversion and yield compared to MOPS, 4-(2-hydroxyethyl)morpholine (HEMO) and 4-methylmorpholine (MMO) at pH 7.5. The increased efficiency at pH 7.5 could be rationalised through the formation of deprotonated flavin hydroquinone (FL_{hq}^{-}) as the pKa of FL_{hq} in **RBF** is ~6,[399] which facilitates more effective hydride transfer and catalytic turnover. In terms of the flavin photocatalyst used, **RTA** tends to show better activity than **RBF** which is expected due to its greater photostability.[357] However, entry 11 shows that, in the case of HEMO pH 7.5, **RBF** performs more efficiently than **RTA** indicating a possible stabilising relationship between ribityl side chains and the morpholine R group.

A kinetic study using MOPS and **RTA** revealed that yield tends to plateau as conversion increases to >99% (**Figure 4.8**). This provides evidence that side-reactions occur that result in consumption of **1a** that do not lead to **1b**, or there is a catalyst deactivation process that inhibits turnover. For example, photobleaching of **1a** may occur under irradiation which could be enhanced by the flavin photocatalyst that is known to oxidise aromatic amines.[90] Interestingly, previous photocatalytic hydrogenations of *N*-phenylmaleimide derivatives using P25 TiO_2 and UV light showed very low yield (≤5%) for the conversion of **1a** to **1b** which could indicate the substrate has limited photostability.[400]

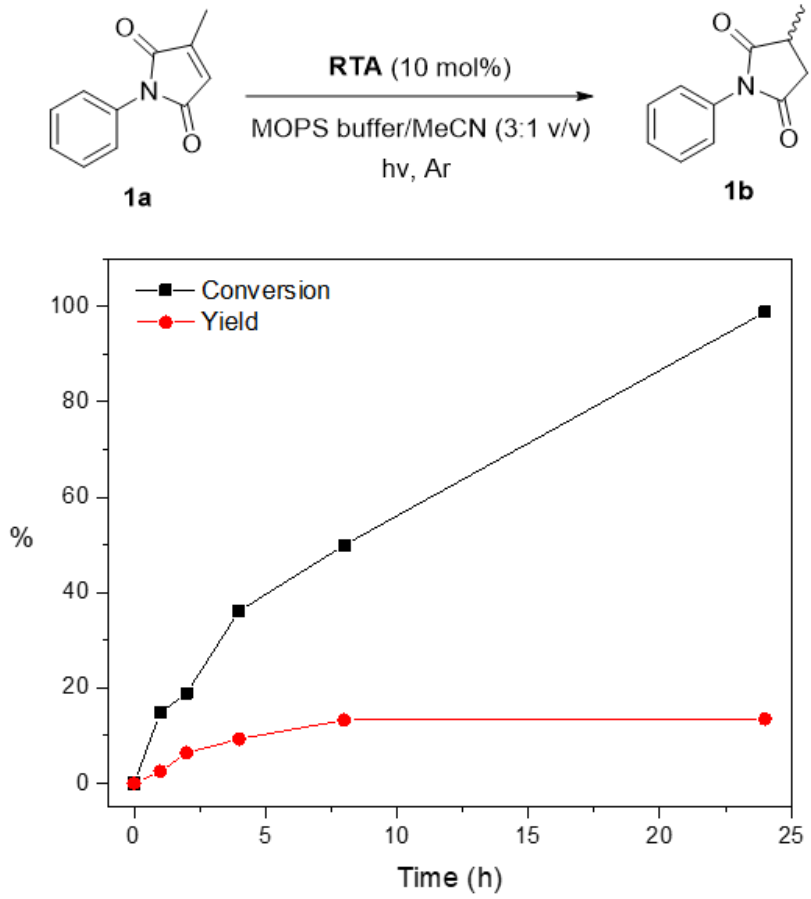

Figure 4.8: Kinetic plot of **1a** (10 mM) photoreduction by **RTA** (10 mol%) in MOPS buffer (1 M pH 7.5) and MeCN (3:1, v/v, 4 mL) mixture over 24 h.

Further control experiments showed that **1b** was not formed in the absence of flavin, MOPS, light or in the presence of O_2 as summarised in **Table 4.3**. Conversion of **1a** occurred in all cases apart from trace amount in the dark (entry 4), further highlighting the substrate's photo-instability. In the case of entry 3 however, where O_2 would be present in the reaction mixture, it can be assumed that photooxidation of the substrate would have occurred (no by-products of considerable concentration were observed *via* TLC or GC-MS). 1-Benzyl-1,4-dihydronicotinamide (BNAH), a common NADH mimic,[34] was employed in the dark to see whether organocatalytic activity could be employed to reduce **1a,** avoiding the use of light. It became apparent however, that the ability of BNAH to initiate the catalytic cycle is perhaps reserved only for enzymes as no product formation or noticeable conversion was observed over a period of 24 h (determined by TLC).

Table 4.3: Control experiments for the photoreduction of **1a** by **RTA**.

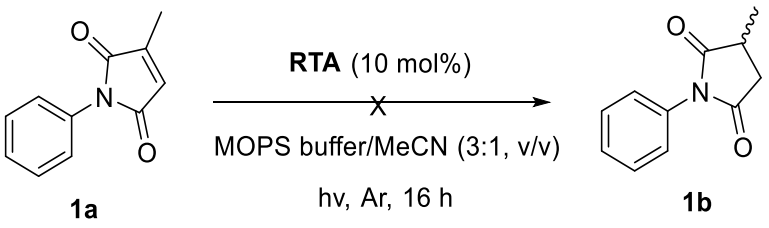

Entry	Change from standard conditions[a]	Conversion[b] (%)	Yield[c] (%)
1	No MOPS	40	0
2	No flavin	54	0
3	Under air	100	0
4	No light	<5	0
5	BNAH (2 equiv.) no light[d]	trace[e]	0[e]

[a] Standard conditions: **1a** (10 mM) and **RTA** (10 mol%) in a mixture of MOPS (1 M, pH 7.5) and MeCN (3:1, v/v, 2 mL) irradiated with a 450 nm LED (18W) at RT for 16 h under Ar atmosphere.
[b] Conversion determined by GC-MS using calibration curve of **1a** with limonene as the internal standard.
[c] Yield determined by GC-MS using calibration curve of **1b** with limonene as the internal standard.
[d] Using KPi buffer (50 mM, pH 7.5) instead of MOPS
[e] Determined by TLC over 24 h

We subsequently applied the optimised reaction conditions to other ER substrates and gratifyingly found that ketoisophorone (**2a**) was photoreduced to **2b** in a good yield of 73% (**Figure 4.9**). Unfortunately, negligible conversion was observed for cinnamaldehyde **3a**. Aldehydes are weak electron withdrawing groups, so it is envisioned that more activating carbonyl moieties such as carboxylic acid, ester or ketone groups may show improved conversion.

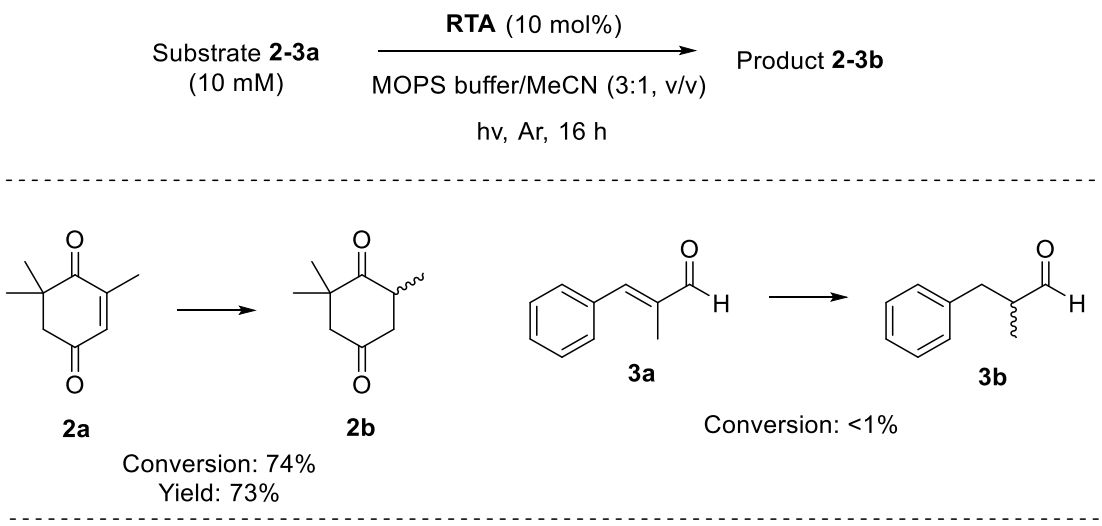

Figure 4.9: Screening of other ER substrates using optimised conditions: substrate (10 mM) and **RTA** (10 mol%) in a mixture of MOPS buffer (1M, pH 7.5) and MeCN (3:1, v/v, 2mL) irradiated with 450 nm LED (18W) for 16 h under Ar atmosphere. Conversion and yield determined by ^{1}H NMR.

These initial data indicated that flavin photocatalysis could be utilised outside of a natural protein make-up to achieve the reduction of activated C=C bonds using an aqueous morpholine-based buffer and MeCN solvent mixture in a homogeneous environment. The extent to which this methodology can be applied is yet to be determined and future work will focus on extensive substrate screening and additional reaction optimisation (effect of co-solvent, other electron donor systems *etc.*). Our main goal was to move towards a flavin-polydopamine nanoparticle system that we hypothesised would show improved catalytic activity with low catalyst loading. In addition, the surface of the nanoparticle could be modified with chiral moieties which we predicted may influence enantioselective product formation.

4.3.2.2 Nanoparticle synthesis and characterisation

We chose riboflavin (**RBF**) as the flavin photocatalyst as it contains an optically active ribityl chain at its N10 position which has been shown beneficial in the discrimination of certain enantiomers when immobilised within an HPLC stationary phase.[401] Conjugation of **RBF** to monodispersed polydopamine nanoparticles (PDA NPs) was chosen as the strategy to introduce flavin moieties to the NPs rather than the co-polymerisation strategy previously explored (**Chapters 2** and **3**). By using N3-modied

flavins we aimed to avoid N10 dealkylation observed with copolymer flavin-polydopamine nanoparticles (**Chapter 3**). The dipeptide, captopril (an ACE inhibitor)[402] was selected as a spacer between the flavin and PDA (**7**, **Figure 4.10**). Captopril has previously been used to synthesise chiral inorganic nanostructures and thanks to its thiol functionality it can be easily conjugated to PDA *via* Michael-addition to quinone moieties.[188,403,404] Therefore a riboflavin-captopril derivative, **RFCPT** was designed and synthesised according to the scheme shown in **Figure 4.10**.

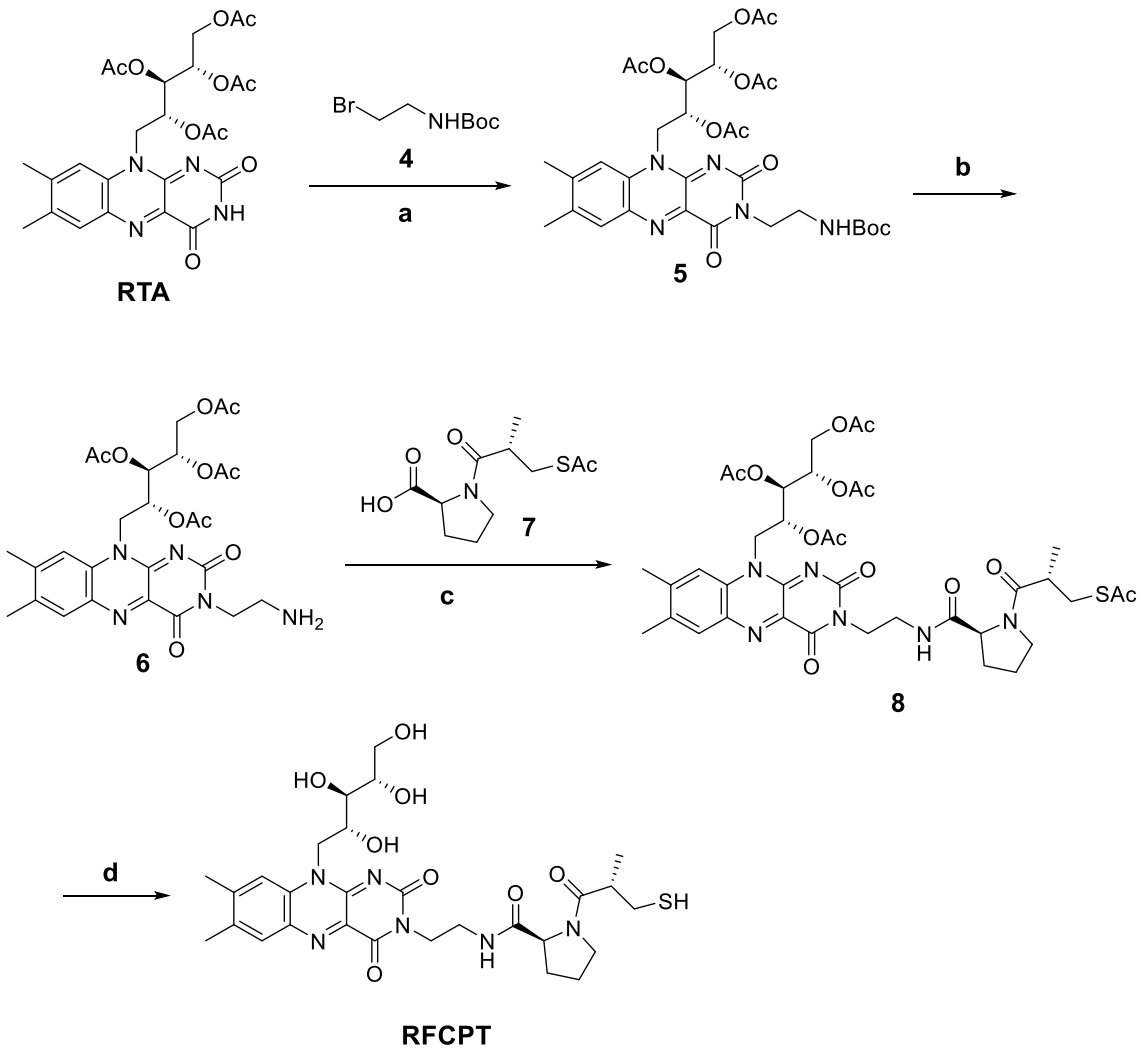

Figure 4.10: Synthesis of **RFCPT**. Reaction conditions: a) Cs_2CO_3, DMF, RT, Ar, dark, 18 h, 84%; b) TFA, DCM, 0 °C – RT, 5 h, Ar, dark, 99%; c) HATU, DIPEA, DMF, RT, 18 h, 84%; d) 1 M HCl, 60 °C, Ar, dark, 18 h, 59%.

First, an amino group was attached to the N3 position of riboflavin tetraacetate (**RTA**) using the NBoc-protected ethyl bromide, **4**. Subsequent

deprotection and amide coupling of acetyl-protected captopril achieved the fully acetylated riboflavin-captopril conjugate **8** in very good yield (84%). Acidic cleavage of acetyl groups resulted in **RFCPT** in fair yield (59%). Finally, riboflavin-conjugated PDA (**RCPDA**) NPs were attained with different flavin loading percentages (wt%) by mixing varied weight ratios of PDA NPs to **RFCPT** in degassed 10 mM TRIS buffer at pH 8.0 as shown in **Figure 4.11**. The reaction was carried out under inert conditions (Ar degassing) in order to avoid thiol oxidation catalysed by the flavin or PDA.[261,405,406]

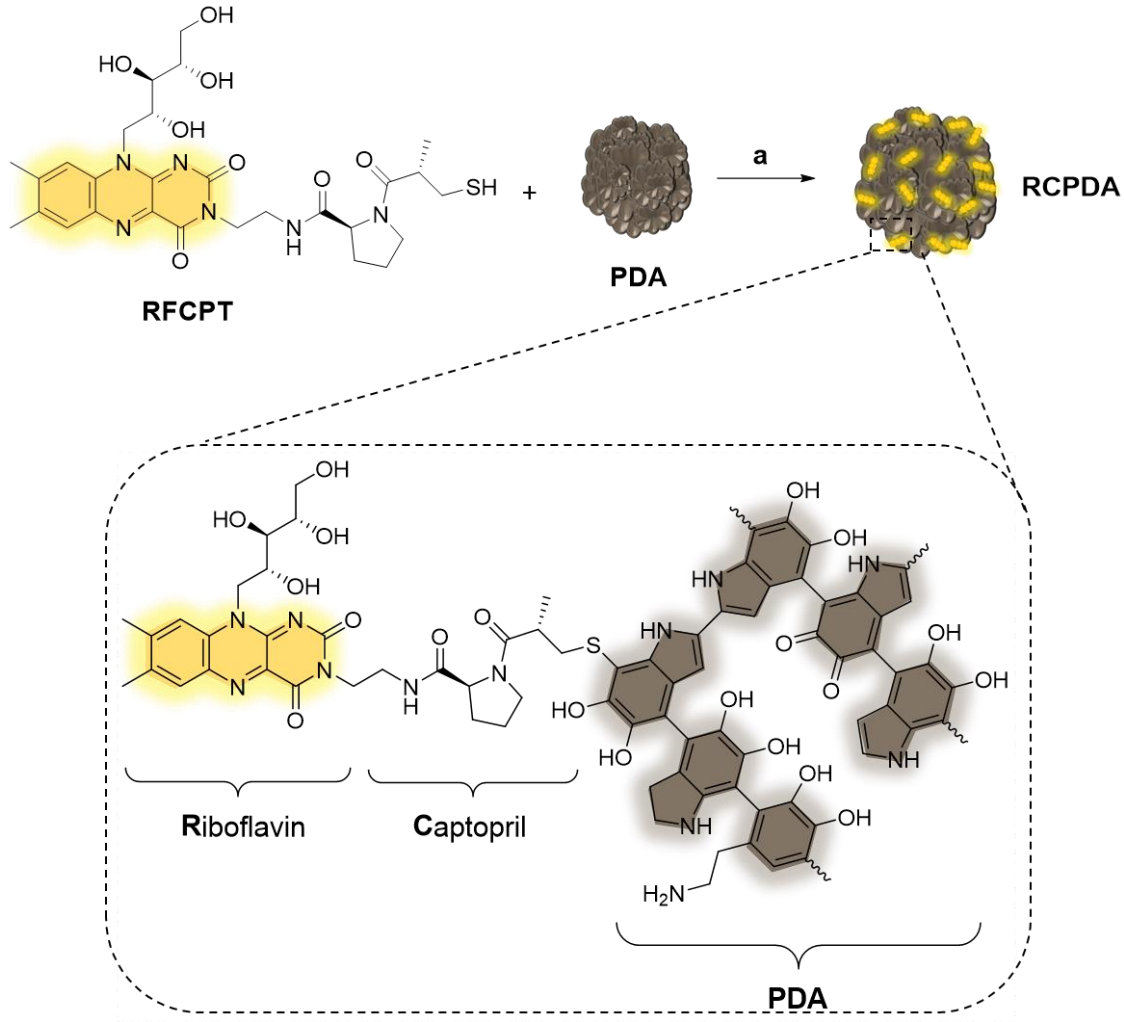

Figure 4.11: Synthesis and structural depiction of **RCPDA**. Reaction conditions: a) TRIS buffer (10 mM, pH 8.0), Ar, dark, 18 h.

Three batches of **RCPDA** NPs with different wt% flavin loadings were synthesised and analysed for light-driven ER activity. In addition, PDA NPs of different sizes were made by the classical Stöber method[204] in order to observe any differences in loading capacity and the resulting photocatalytic activity. **PDA-1** particles were

prepared with an average size (measured by SEM, **Figure 4.12**) of 93.0 ± 14.2 nm, and **PDA-2** being slightly smaller at 82.6 ± 11.5 nm (**Table 3**). Upon addition of **RFCPT** using a 1:1 weight ratio of particle to flavin, relative hydrodynamic sizes of the PDA NPs increased from 214.3 ± 1.8 nm to 244.4 ± 1.6 for **PDA-1** and **RCPDA-1**, with a larger increase observed for **PDA-2** and **RCPDA-2** going from 130.0 ± 0.2 nm to 191.3 ± 1.3 nm. These data provide evidence of successful ligand attachment as the addition of hydrophilic **RFCPT** to the surface of the PDA NPs would be expected to increase the hydrodynamic size of the particle. Furthermore, zeta potential measurements indicated ligand attachment by a positive shift in values showing a change in particle surface charge, although these changes were almost negligible for **RCPDA-1** when compared to **PDA-1**. **RCPDA-3** was prepared using a larger weight excess of **RFCPT** and followed the same trend in value changes in both hydrodynamic sizes and zeta potential. SEM analysis of the **RCPDA** particles revealed only slight changes in particle diameter by attachment of **RFCPT** to the NP surface (**Table 4.4**, **Figure 4.12**).

Table 4.4: Size and zeta potential measurements of PDA and **RCPDA** NPs with their associated wt% loading.

Sample	Synthetic Ratio PDA:RFCPT, wt/wt	Particle Size (nm)[a]	Hydrodynamic Size (nm)[b]	Zeta Potential (mV)[b]	Flavin wt% loading[c]
PDA-1	-	93.0 ± 14.2	214.3 ± 1.8	-35.8 ± 0.6	-
PDA-2	-	82.6 ± 11.5	130.0 ± 0.2	-60.4 ± 0.2	-
RCPDA-1	1:1 (PDA-1)	92.9 ± 15.6	244.4 ± 1.6	-35.4 ± 0.2	1.2 ± 0.05
RCPDA-2	1:1 (PDA-2)	85.5 ± 15.2	191.3 ± 1.3	-37.1 ± 0.6	1.8 ± 0.05
RCPDA-3	1:5 (PDA-2)	88.7 ± 14.1	187.0 ± 3.9	-16.0 ± 3.5	3.7 ± 0.19

[a] Measured by SEM
[b] Measured by DLS
[c] Estimated by fluorescence intensity calibration

Finally, a fluorescence intensity calibration was carried out in order to estimate the wt% loading of flavin (**RFCPT**) on the particles (see **Section 4.2.7** for full

experimental details). This revealed that using a 1:1 weight ratio of **PDA**:**RFCPT** the larger **PDA-1** NPs yielded a lower flavin loading of ~1 wt% (**RCPDA-1**) when compared to the smaller **PDA-2** NPs that had ~2 wt% loading (**RCPDA-2**). Increasing the amount of **RFCPT** to 5 times more than PDA resulted in particles with ~4 wt% flavin loading (**RCPDA-3**).

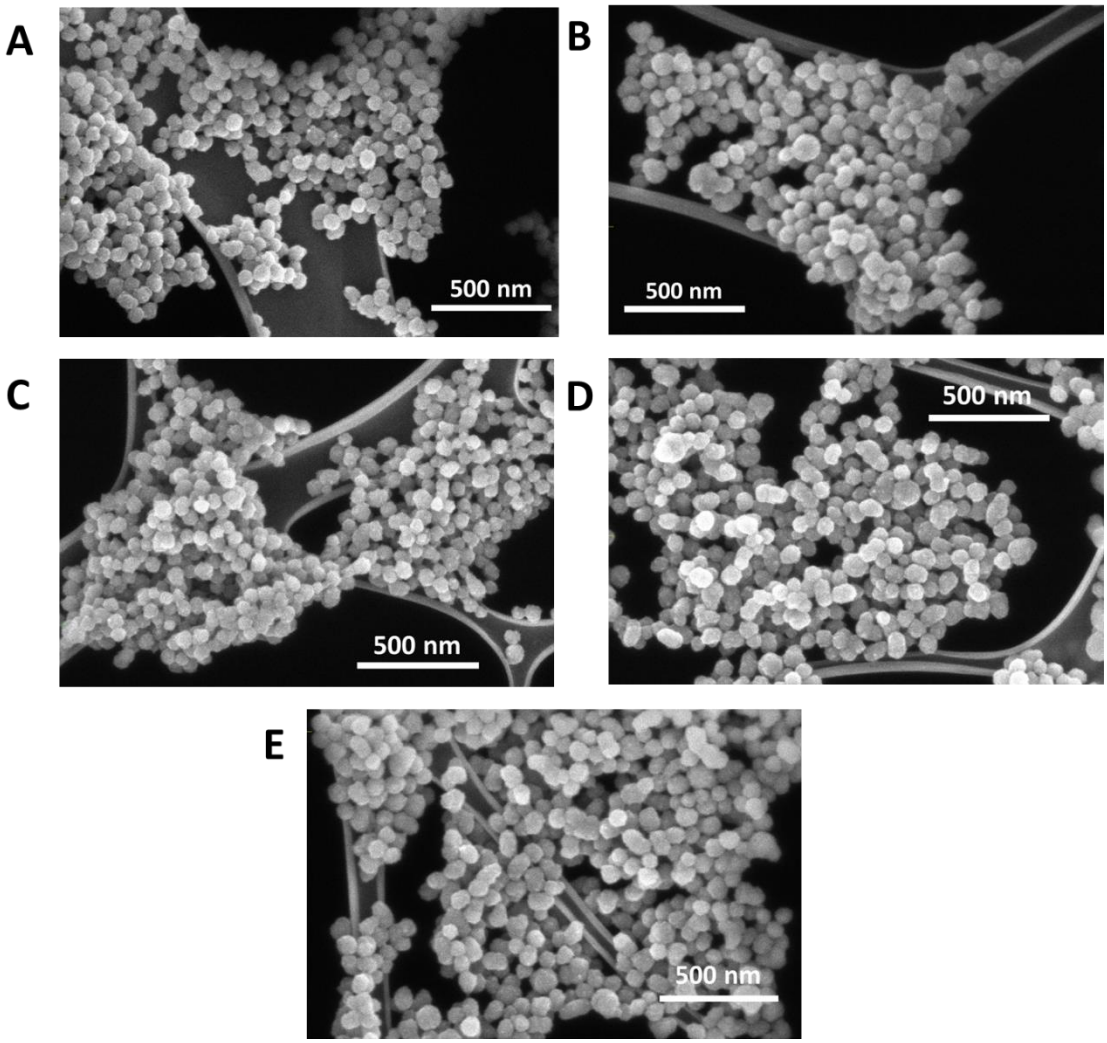

Figure 4.12: SEM images of PDA and **RCPDA** particles. (A) **PDA-1**, (B) **PDA-2**, (C) **RCPDA-1**, (D) **RCPDA-2** and (E) **RCPDA-3**.

The particles were further characterised by UV-Vis and fluorescence spectroscopy as shown in **Figure 4.13**. The UV-Vis spectrum of both **PDA-1** and **PDA-2** show a characteristic broad absorbance profile over the UV-visible range analogous to melanin (**Figure 4.13A**).[407] The absorbance spectrum of **RFCPT** shown in **Figure 4.13B** displays characteristic isoalloxazine absorption bands at λ_{max} = 449 nm and 374 nm corresponding to the $S_0 \rightarrow S_1$ (λ_{max} ~ 442–450 nm) and $S_0 \rightarrow S_2$ (λ_{max} ~ 360–375 nm)

transitions.[2] These bands are red-shifted to 458 nm for $S_0 \rightarrow S_1$ and 378 nm for $S_0 \rightarrow S_2$ transitions in **RCPDA** samples (**Figure 4.13C** and **D**). This red-shift was also observed for the copolymer flavin-polydopamine particles and can be explained by an increase in proton donation and electron-withdrawing inductive effects by PDA. [294,295]

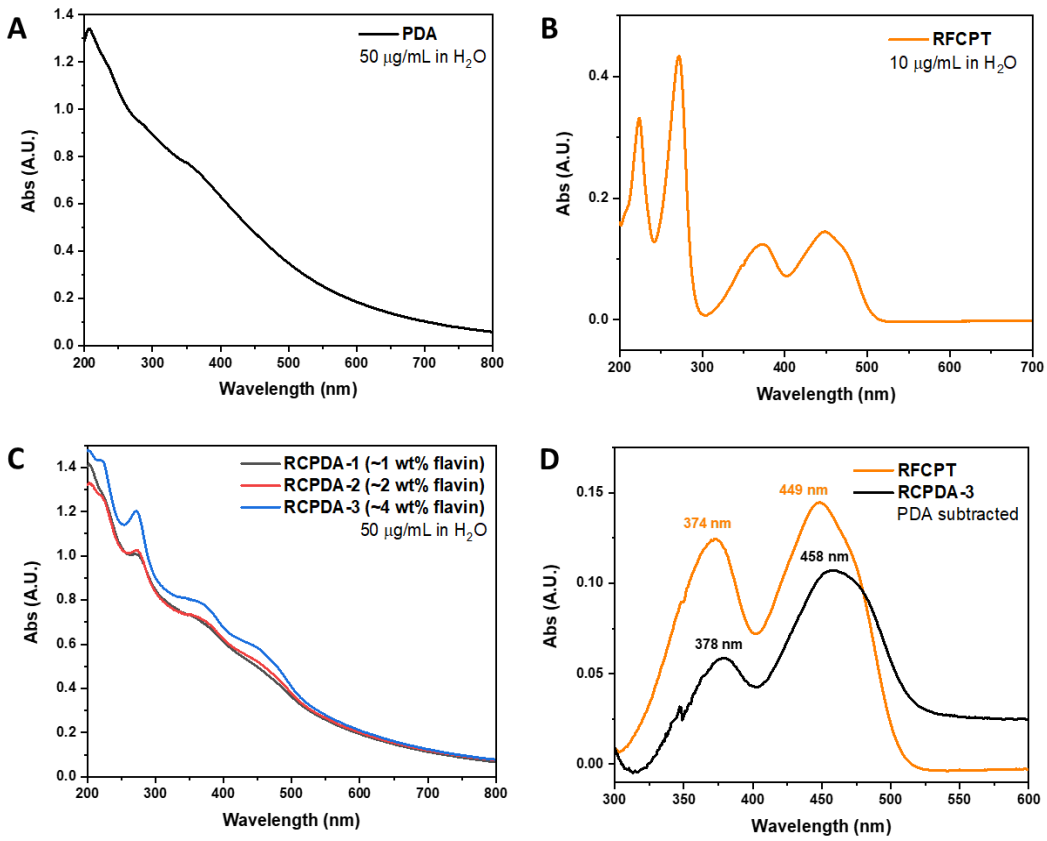

Figure 4.13: UV-Vis spectra of (A) **PDA** NPs, (B) **RFCPT**, (C) **RCPDA** samples and (D) **RFCPT** compared to **RCPDA-3** with PDA absorbance subtracted.

The fluorescence emission spectra of **RCPDA** samples (**Figure 4.14A**) exhibit emission maxima at 528 nm (λ_{ex}= 450 nm) that increase in intensity relative to wt% flavin loading. This value is slightly red-shifted in comparison with **RFCPT** that exhibits an emission maximum at 525 nm (λ_{ex}= 450 nm). An earlier study in which flavin compounds were complexed with melanin similarly showed that flavin emission is red-shifted once complexed, and that there was no significant fluorescent quenching by the polymer.[297] A decrease is observed in the emission intensity of **RFCPT** when PDA is added, which can be corrected by taking into account the relative PDA absorbance at excitation/emission wavelengths as previously seen for copolymer flavin-polydopamine (**Figure 4.14B** and **Chapter 2**). Therefore, all fluorescence calibrations

were performed using PDA and **RFCPT** to determine relative flavin loading in order to account for this absorption decrease (see **Section 4.2.7** for full experimental details).

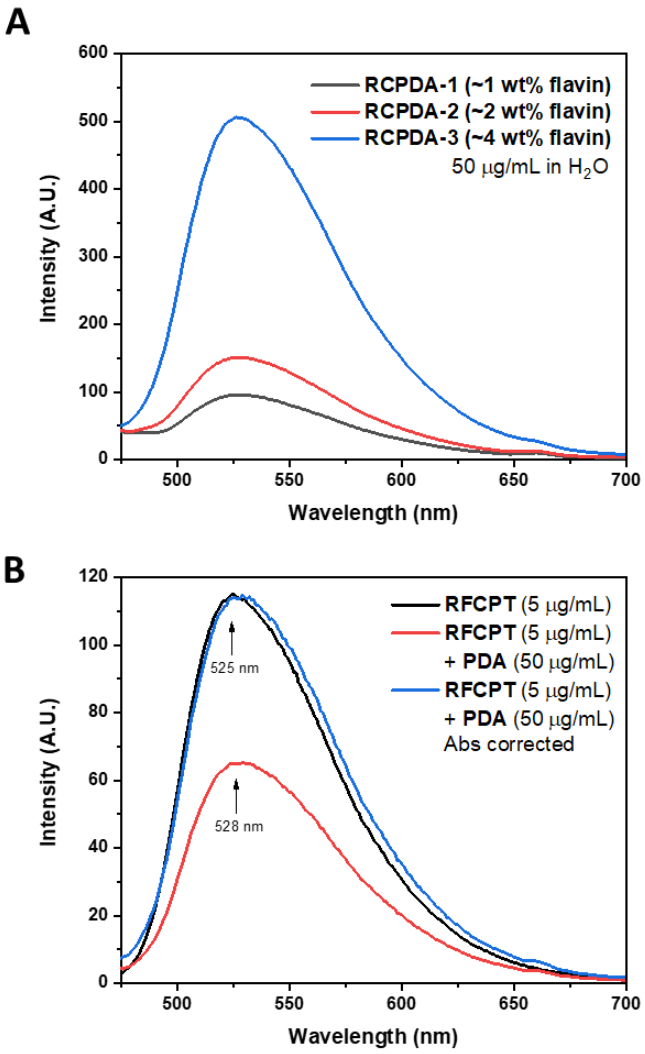

Figure 4.14: Fluorescence intensity spectra of (A) **RCPDA** samples and (B) the comparison intensity profiles of **RFCPT** with PDA added.

4.3.2.3 Nanoparticle photoreactions

The light-driven ER activity of **RCPDA** NPs were then examined by first using **1a** and applying the methodology developed in homogeneous reaction screening (**Section 4.3.2.1**). The 3:1 buffer/MeCN solvent system was kept to ensure substrate solubility which is often found to be a restricting factor in biocatalysis as organic solvents, such as MeCN, denature the enzyme meaning substrate solubility is often limited.[408] Reaction times were increased to account for lower photon absorption efficiency due to the introduction of light-scattering nanoparticles. Despite the substrate showing some photo-instability from this screening, interesting differences in activity were found between the nanoparticle and homogeneous catalyst systems.

Firstly, the morpholine-based buffer systems used previously were screened with **RCPDA** NP samples in the photoreduction of **1a** (**Table 4.5**). The approximate flavin mol% loading in these reactions was kept <1 mol% as this is generally characteristic loading in enzymatic biocatalysis. Despite these amounts being far lower than that used in the homogeneous reaction screening (10 mol%), conversions and yields are relatively comparable or slightly improved between reactions. The photoreactions of **RCPDA-2** and **-3** in HEMO buffer, obtained **1b** in yields of 19% and 20% respectively (entries 8 and 9) with quantitative conversion, whereas the analogous HEMO/RBF homogeneous system yielded **1b** in 23% yield with 85% conversion. This result shows that the covalent immobilisation of the flavin on PDA, greatly improves its catalytic activity, most likely through a favourable flavin-PDA-substrate binding interaction, as previously observed for flavin-polydopamine copolymer particles (**Chapter 2**). MMO proved slightly more effective than the MMO/RBF homogeneous system, raising the yield of **1b** up to 12% (entry 4) compared to 7% with very little catalyst loading. However, MOPS showed poor activity across all **RCPDA** samples like MOPS/RBF with yields <10% (entries 1-3). GC-MS analysis of by-products from the reactions carried out in HEMO buffer, indicated the formation of succinimide **1c** (**Table 4.5**). The mechanism of **1c** formation is unknown but might be attributed to the flavin-photocatalysed oxidation of **1a**/**b** that leads to cleavage of the species.

Table 4.5: Morpholine-based buffer screening for **RCPDA** NP photoreactions with **1a**.[a]

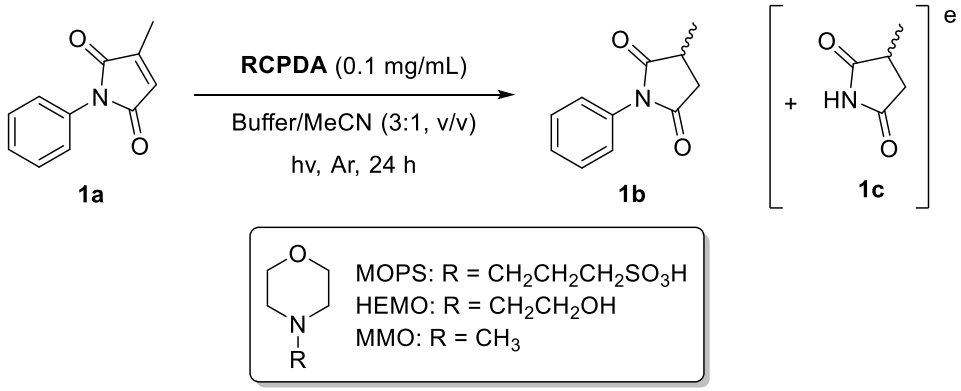

Entry	Buffer	RCPDA	Flavin mol%	Conversion (%)[b]	Yield (%)[c]	ee (%)[d]	Abs. Config.
1	100 mM MOPS pH 7.5	1	0.16	72	3	n.d.	-
2		2	0.32	>95	8	0	-
3		3	0.65	100	7	0	-
4	100 mM MMO pH 7.5	1	0.16	100	12	n.d.	-
5		2	0.32	100	9	0	-
6		3	0.65	100	10	0	-
7	100 mM HEMO pH 7.5	1	0.16	>95	5	n.d.	-
8		2	0.32	100	19	0	-
9		3	0.65	100	20	23	(*R*)

[a] Reaction conditions: **1a** (1 mM) and **RCPDA** (0.1 mg/mL) in a mixture of buffer and MeCN (3:1, v/v, 2 mL) irradiated with a 450 nm LED (18W) at RT for 24 h under Ar atmosphere.

[b] Conversion determined by GC-MS using calibration curve of **1a** with limonene as the internal standard.

[c] Yield determined by GC-MS using calibration curve of **1b** with limonene as the internal standard.

[d] *ee* determined by HPLC using Chiralcel OD column.

[e] By-product observed by GC-MS for reactions in HEMO buffer.

Enantiomeric excess (*ee*) values were obtained for the reactions catalysed by **RCPDA-2** and -**3** using chiral HPLC in order to determine if the chiral linker between flavin and PDA surface has an influence on the stereochemistry of the reaction. Interestingly, the reaction catalysed by **RCPDA-3** in HEMO buffer showed an *ee* of 23%

of the (*R*) enantiomer of **1b** (**Table 4.5**, entry 9). All other reactions showed racemic product formation. This result can be attributed to the larger number of flavin active sites on the PDA surface of **RCPDA-3** compared to **RCPDA-1** or **-2**. Although this is a moderate *ee* value, it is an encouraging proof-of-concept which demonstrates that the inclusion of chiral moities into the design of nanoparticle flavin photocatalysts can influence the stereochemistry of the catalysed reactions. Scale-up of this reaction will show whether this result is reproducible on a larger scale and whether it is a useful methodology for chiral organic synthesis.

Additional control experiments were carried out that confirmed the formation of **1b** was dependent on the presence of an electron donor reagent, flavin and light (**Table 4.6**, entries 1-3). Unexpectedly, conversion of **1a** was observed in the dark experiment (entry 3). This could be a result of a Michael-type reaction between amino residues within PDA and the maleimide or π–π stacking of the compound to PDA that were not extracted in the reaction workup. EDTA and TEOA buffers were also screened but showed very low yields of **1b** as expected from homogeneous optimisation (entries 4 and 5). **RBF** at 1 mol% provided a yield of **1b** at 5% which further exemplified **RCPDA**'s superiority over its homogeneous counterpart (entry 6). Interestingly, the addition of **PDA-2** (0.1 mg/mL, entry 7) to the same reaction improved the yield of **1b**, indicating PDA does indeed have an activating effect on the reaction's pathway, most likely through aromatic electrostatic stabilisation of each reactive component even without covalent immobilisation of the flavin. The *ee* of this reaction was found to be 0% which indicates that the chiral linker used to connect flavin moieties to the PDA surface is required for an enantioselective transformation to occur. Finally, a dark organocatalytic reaction was attempted with **RCPDA-3** with BNAH as the electron donor (2 equiv., entry 8) however the reaction was unsuccessful in the formation of **1b** despite conversion of **1a** but there were no clearly identifiable by-products of considerable concentration observed by GC-MS.

Table 4.6: RCPDA NP control experiments.[a]

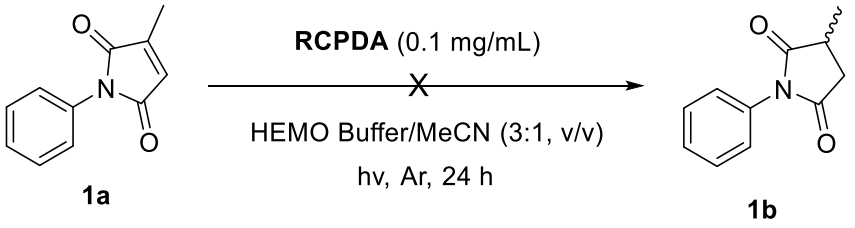

Entry	Change from standard conditions[a]	Conversion (%)[b]	Yield (%)[c]
1	10 mM KPi buffer pH 7.5	100	0
2	PDA-2	70	0
3	No light	40	0
4	25 mM EDTA pH 7.5	100	6
5	25 mM TEOA pH 7.5	100	5
6	RBF (1 mol%)	82	5
7	PDA-2 + RBF (1 mol%)	90	13 (*ee* = 0%)
8	BNAH (2 equiv.), no light[d]	100	0

[a] Standard conditions: **1a** (1 mM) and **RCPDA-3** (0.1 mg/mL) in a mixture of HEMO buffer (100 mM, pH 7.5) and MeCN (3:1, v/v, 2 mL) irradiated with a 450 nm LED (18W) at RT for 24 h under Ar atmosphere.

[b] Conversion determined by GC-MS using calibration curve of **1a** with limonene as the internal standard.

[c] Yield determined by GC-MS using calibration curve of **1b** with limonene as the internal standard.

[d] Using KPi buffer (10 mM, pH 7.5).

The optimal conditions found for **1a** photoreduction were then applied to ketoisophorone (**2a**) in order to see if **RCPDA-3** can be applied to another ER substrate. Under these conditions however, the product **2b** was not detectable by GC-MS after extraction with EtOAc and neither was the starting material (**Figure 4.15**). Additionally, a control experiment containing no **RCPDA-3** showed the same result, indicating that the substrate and/or product are not stable under such reaction conditions and prolonged irradiation. Further experiments should therefore focus on a larger scale (10-20 mM) kinetic study to optimise irradiation times.

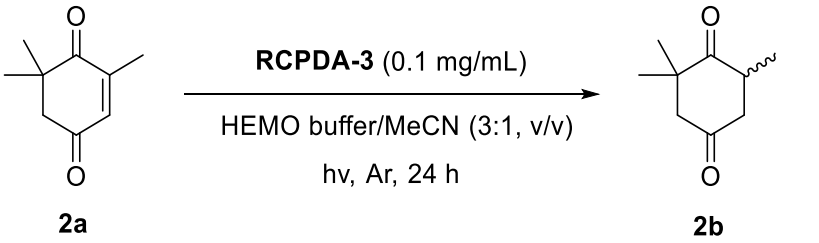

Figure 4.15: Photoreduction of **2a** (1 mM) catalysed by **RCPDA-3** (0.1 mg/mL) in a mixture of HEMO buffer (100 mM, pH 7.5) and MeCN (3:1, v/v, 2 mL). Conversion and yield determined by GC-MS using calibration curves of **2a** and **2b** respectively with limonene as the internal standard.

Overall, **RCPDA** NPs exhibit improved photocatalytic properties when compared to the homogeneous flavin photocatalysts through comparable or enhanced product yield at far lower catalyst loading. Alongside this, enantioselectivity of product formation was also observed, exemplifying for the first time that the addition of chiral moieties within an advanced flavin photocatalyst can direct the stereochemical outcome of the reaction. This small-scale proof-of-concept study indicated the need for a larger scale optimisation of the reaction conditions in order to increase the efficiency and ensure reproducibility of the catalyst. An important comparison would also be the analogous **RTA**-conjugated system to observe any effects of ribityl-protection on overall performance and enantioselectivity.

4.3.2.4 Analysis of RCPDA post reaction

Before an attempt was made to recycle **RCPDA-3** for a subsequent photoreaction, the washed particles and initial reaction supernatant were first analysed by fluorescence spectroscopy to confirm particle integrity. Unfortunately, no fluorescence was observed for the particles but a large emission at λ_{max} = 527 nm (λ_{ex}= 450 nm) was exhibited by the reaction supernatant (**Figure 4.16**). This was a clear indication that flavin species had detached from the particles leaving them inactive. The photodegradation of riboflavin is well understood, ultimately resulting in dealkylated lumiflavin or lumichrome compounds.[311] Photodecomposition products of riboflavin derivatives with N3 conjugation is less widely understood but it has been shown that N3-Me substituted **RTA** displayed very good stability under UV-irradiation in deaerated methanol.[409]

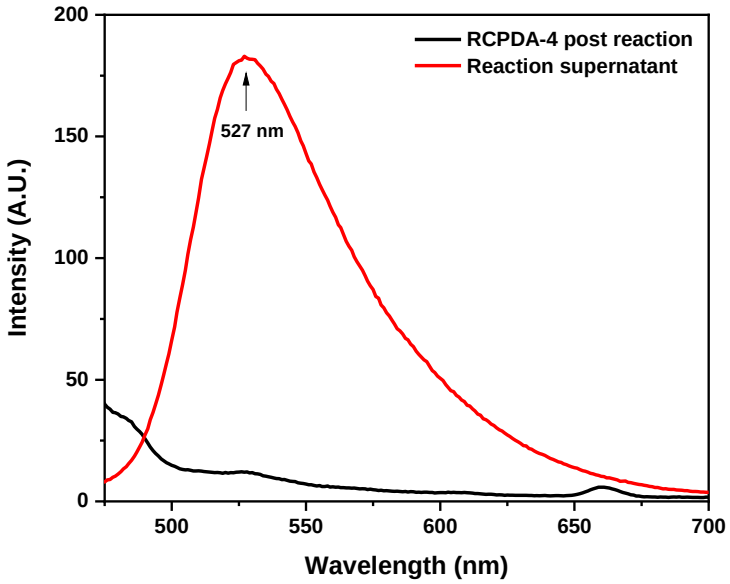

Figure 4.16: Fluorescence emission spectra of **RCPDA-3** particles post reaction and associated reaction supernatant (λ_{ex}= 450 nm).

An ESI mass spectrum of the reaction supernatant was therefore obtained to try and identify major photodecomposition products. Expected photodegradation products such as lumiflavin, lumichrome, **RFCPT** or lumiflavin-captopril were not identified as major mass adducts. Therefore, possible structures and related mass adducts are proposed from the spectra for some major mass peaks observed as shown in **Figure 4.17A** and **B**. In both cases, the evidence points towards flavin species with

PDA-oligomers attached. For m/z ~ 670 a lumiflavin-captopril-leukochrome species is proposed (**Figure 4.17A**) and for m/z ~ 918, a riboflavin-captopril-leukochrome oligomer is proposed (**Figure 4.17B**). Presence of these species indicates that the photodecomposition mechanism of **RCPDA** proceeds through PDA oligomeric units rather than the cleavage of **RFCPT**. This also was evidenced by the observation of a stark reduction in the optical density of the washed particles in solution compared to a solution of fresh particles at the same approximate concentration.

The photodecomposition and photo-induced structural modifications of melanin under exposure to UV-light, as well as blue light, is widely studied to understand melanogenesis, pigment darkening and melanoma formation.[354] The degree to which PDA NPs follow the same photo-induced changes and their dependency on factors such as solvent, pH and temperature is not yet fully understood. However, the use of PDA as a photosensitiser for TiO_2-based photocatalytic CO_2 reduction did result in clear photodecomposition and mass losses when the sample was irradiated with both UV and visible light.[288] One could therefore assume it is very likely that long exposure to blue light, especially in a polar solvent system (H_2O/MeCN) would result in very similar decomposition of **RCPDA**. Indeed, the type of solvent has been shown to affect the stability of other heterogeneous flavin photocatalysts, favouring alcoholic solvent systems over MeCN-based ones.[169] Future work will therefore focus on what effect these reaction parameters have on the stability and activity of **RCPDA** to identify the optimal conditions for photocatalysis.

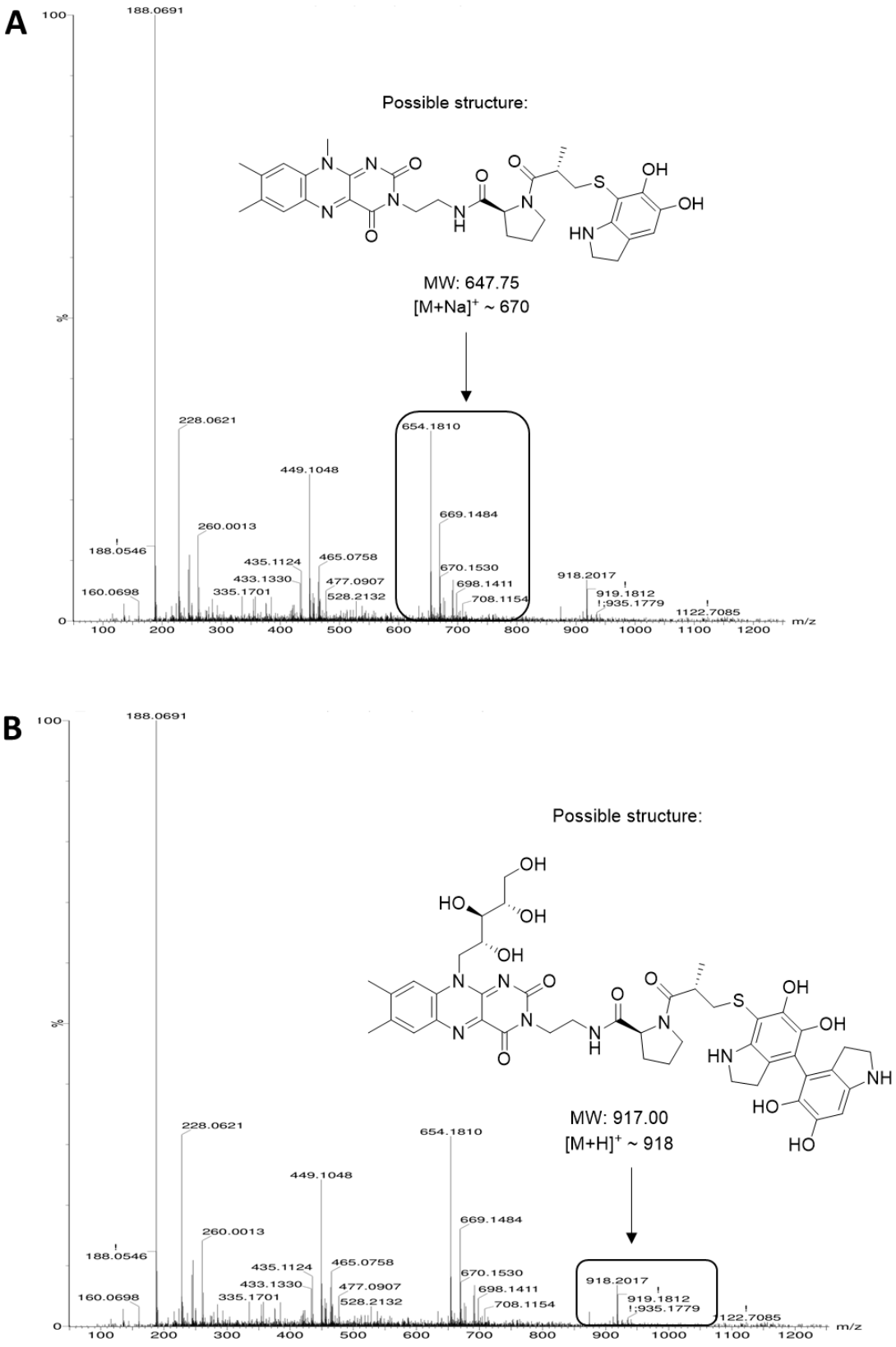

Figure 4.17: HRMS (ESI) spectra of reaction supernatant with two possible structures of photodecomposition products.

4.4 Conclusion

The light-driven reductase activity of flavin-polydopamine (**FLPDA**) has been investigated, at first, through the reduction of azobenzene compounds Amaranth (**AMT**) and Naphthol Blue Black (**NBB**) using copolymer **FLPDA** nanoparticles. Despite the rate of reduction being low for these reactions, it proved that it was possible for flavin moieties to reduce a substrate in the presence of an electron donor whilst being covalently attached to PDA. This encouraged the study of ene-reductase type reactions due to their relevance in producing compounds of industrial interest.

Homogeneous reaction optimisation using riboflavin (**RBF**) and riboflavin tetraacetate (**RTA**) photocatalysts and three typical ene-reductase (ER) substrates revealed activity differences in the presence of certain electron donating buffer systems. For example, **RTA** showed the highest activity in MOPS buffer (pH 7.5) producing succinimide **1b** with a yield of 32% whereas **RBF** showed the best activity in HEMO buffer (pH 7.5) producing **1b** in a yield of 23%. Other ER substrates proved more suitable for this catalytic system, such as ketoisophorine **2a** which was reduced in yield of 73% to the levodione product (**2b**) with **RTA**/MOPS. However, cinnamaldehyde **3a** was not able to be reduced under such conditions.

With this information in hand, a chiral riboflavin-captopril ligand (**RFCPT**) was synthesised to be functionalised onto monodispersed PDA nanoparticles resulting in riboflavin-captopril-PDA (**RCPDA**) nanoparticles. Yields of succinimide **1b** produced by **RCPDA-3** (~4 wt% flavin) were almost equivalent to the homogeneous reaction using **RBF** in HEMO buffer (pH 7.5) at very low catalyst loading (<1 mol%) indicating a clear increase in efficacy through the introduction of PDA NPs. Additionally, enantioselectivity of the catalysed reaction (23% *ee*) was observed which can be attributed to the use of a chiral linkage between flavin and PDA NP surface. This shows for the first time that advanced flavin photocatalysts can be designed to effectively display flavoenzyme-like characteristics.

5 CONCLUSIONS AND FUTURE WORK

5.1 Conclusions

Within this thesis, the combination of photocatalytic flavins and nanostructured polydopamine has been explored through the design and application of copolymer flavin-polydopamine (**FLPDA**) and riboflavin-captopril-polydopamine (**RCPDA**) nanoparticles. Copolymer **FLPDA** was synthesised through the copolymerisation of dopamine and a DOPAC-flavin monomer (**FLDA**) to form particles with the sizes of ~200 nm with large size distribution in samples containing a higher percentage of flavin. Initially, a redox dye system based on oxidation and reduction reactions to afford the pink coloured resorufin (**RF**) was utilised to characterise the photocatalytic activity of the particles. The highest rates in conversion to **RF** were achieved using **FLDPA-5** which contained the largest concentration of flavin moieties (~ 1.0 µmol/mg) for both oxidation and reduction processes. It was also found that **FLPDA-5** performed at a greater efficiency than the homogeneous monomer **FLDA** which was rationalised through an enzyme-like mechanism by using a Michaelis-Menten fit to describe the kinetics of the oxidation reaction. Additionally, the photostability of the system was found to be improved compared to a DOPAC-free flavin compound through charge transfer processes evidenced by fluorescence quenching between the flavin and catechol moieties. Finally, *in vitro* biocompatibility studies of the **FLPDA** particles revealed low cytotoxicity to A549 cells as well as an antioxidative effect which shows **FLPDA** may also be useful in biomedical applications.

Following this initial characterisation, **FLPDA** particles were employed in the photooxidation of indole to form indigo and indirubin dyes which is a characteristic transformation catalysed by flavin-containing monooxygenase enzymes (FMOs). This is the first example of flavin photocatalysis being utilised to produce these valuable dyes

which were produced at a five times greater yield using **FLPDA** than the homogeneous riboflavin (**RBF**) photocatalyst. ROS scavenging experiments were carried out to elucidate **FLPDA**'s photooxidation mechanism, revealing that neither superoxide nor singlet oxygen were solely responsible for indole oxidation. Subsequently, it was discovered that **FLPDA** released less H_2O_2 in the reaction when compared to **RBF** and so, it can be assumed that PDA enables the stabilisation of C4a-hydroperoxy-flavin as a reactive intermediate. This can be used to explain **FLPDA**'s higher product selectivity towards indigo dye formation. The stabilisation of this reactive intermediate further shows the capacity of **FLPDA** to demonstrate enzyme-like mechanism characteristics.

Characteristic flavoenzyme reduction reactions were then explored by first using **FLPDA** to photoreduce two azobenzene dyes. Despite slow reaction kinetics, it was clear that reduced flavin hydroquinone (FL_{hq}) species could be accessed under irradiation in the presence of an electron donor and PDA, which then transfers hydride to a substrate. The reduction of C=C bonds in α,β-unsaturated ketones and aldehydes, characteristic of ene-reductase enzymes (ERs), was then explored. Initially, homogeneous riboflavin (**RBF**) and the more photostable riboflavin tetraacetate (**RTA**) were employed as photocatalyst to optimise reaction conditions by screening various electron donating buffer systems. It was found that **RTA** (10 mol%) performed the best in MOPS buffer (pH 7.5 with MeCN, 3:1 v/v) and was able to reduce 2-methyl-N-phenylmaleimide to 2-methyl-N-phenylsuccinamide (32% yield) and also ketoisophorone to levodione (73% yield). On the other hand, **RBF** performed best in HEMO buffer (pH 7.5 with MeCN, 3:1 v/v) producing 2-methyl-N-phenylsuccinamide in 23% yield. Subsequently, the reactions were performed with PDA NPs bearing chiral riboflavin-captopril surface ligands (**RCPDA**) as the photocatalyst which revealed that HEMO buffer also enabled the highest activity (20% yield of 2-methyl-N-phenylsuccinamide) using very low catalyst loading (<1 mol%). An *ee* value was also determined for this reaction to be 23% which shows, for the first time, that designing chiral components into flavin photocatalyst systems can influence the stereochemical outcome of a catalysed reaction.

Overall, this thesis has extended the known capabilities of flavin photocatalysis by the formulation of nanostructured flavin-conjugated polydopamine which demonstrated enzyme-like catalytic behaviour under irradiation. It is hoped that

this work, along with related future efforts, will help to position the use of flavin photocatalyst systems at the forefront of sustainable catalysis.

5.2 Future work

5.2.1 Light-driven monooxygenase activity of flavin-polydopamine

Future work relating to the photooxidation of indole by **FLPDA** should focus on optimising indigo and indirubin dye formation and selectivity, perhaps by the addition of amino acids such as cysteine which has been shown to increase indirubin yield,[410] or an electron donating buffer system at a particular pH which may enhance activity and photostability further.[131] Additional indole derivatives should also be explored such as nitro- and bromo-substituted indoles to observe any interplay between functional groups, product selectivity and **FLPDA**'s photocatalytic activity. Other FMO type reactions such as Baeyer–Villiger oxidations and sulfoxidations could also be investigated to show the extent of **FLPDA**'s monooxygenase activity. Finally, due to initial evidence of the C4a-hydroperoxy-flavin species through ROS scavenging and H_2O_2 assays (**Section 3.3.4**), further evidence of this species and **FLPDA**'s photocatalytic mechanism should be obtained through NMR and EPR spectroscopy.[411,412]

5.2.2 Light-driven reductase activity of flavin-polydopamine

The initial homogeneous photoreductions of three ER substrates using **RTA** and **RBF** photocatalysts showed that the type of electron donating buffer utilised played a major role on the efficiency and selectivity of the reaction (**Section 4.3.2.1**). Namely, morpholine-based buffer systems showed the best results when compared to the most widely employed electron donors such as EDTA and TEOA. This effect has been described previously in terms of photobiocatalytic systems, however it has not yet been employed in homogeneous photocatalysis to achieve reactions such as azo, nitro, imine, C=O or C=C reduction. This methodology could therefore be applied to this wide range of reductions to show that **RTA** and related derivates can be used as a versatile photocatalysts for reduction reactions. Other electron donors should be investigated such as ascorbate, which has already been shown to be useful in flavin catalysis,[48,413]

and the combination of Lewis acids should increase flavin redox potentials to achieve the reduction of wide range of substrates.[106,107]

Future work relating to ER substrate photoreductions using **RCPDA** should focus on solvent screening with less polar co-solvents (alcohols) in order to analyse the photostability of **RCPDA** and the effect on product yields. The analogous **RTA**-conjugated system should be prepared in order to observe the effects of ribityl-protection on overall performance, stability and enantioselectivity. Enantioselectivity may also be improved by the addition of extra chiral elements to the surface of PDA such as amino acids. Larger scale optimisation up to mmol amounts of substrate should be demonstrated to further display the usefulness of **RCPDA**. Finally, the photodecomposition mechanism of **RCPDA** (and **FLPDA**) should be fully characterised in order to improve the next generation of flavin-PDA hybrids.

6 REFERENCES

[1] C. Walsh, *Acc. Chem. Res.* **1980**, *13*, 148–155.

[2] P. F. Heelis, *Chem. Soc. Rev.* **1982**, *11*, 15–39.

[3] S. GHISLA, V. MASSEY, *Eur. J. Biochem.* **1989**, *181*, 1–17.

[4] D. Leitsch, B. D. Janssen, D. Kolarich, P. J. Johnson, M. Duchêne, *Mol. Microbiol.* **2014**, *91*, 198–208.

[5] K. R. Pryde, J. Hirst, *J. Biol. Chem.* **2011**, *286*, 18056–18065.

[6] S. Masuda, *Plant Cell Physiol.* **2013**, *54*, 171–179.

[7] W. R. Briggs, in *J. Biomed. Sci.*, **2007**, pp. 499–504.

[8] A. R. Cashmore, *Cell* **2003**, *114*, 537–543.

[9] K. Brettel, M. Byrdin, *Curr. Opin. Struct. Biol.* **2010**, *20*, 693–701.

[10] P. Dunlap, *Adv. Biochem. Eng. Biotechnol.* **2014**, *144*, 37–64.

[11] B. Entsch, D. P. Ballou, *Flavins*, **2013**.

[12] V. Massey, *Biochem. Soc. Trans.* **2000**, *28*, 283–296.

[13] C. T. Walsh, T. A. Wencewicz, *Nat. Prod. Rep.* **2013**, *30*, 175–200.

[14] A. Liese, K. Seelbach, C. Wandrey, *Industrial Biotransformations, Second Edition*, **2006**.

[15] A. W. K. Yeung, M. G. Georgieva, A. G. Atanasov, N. T. Tzvetkov, *Front. Mol. Neurosci.* **2019**, *12*, DOI 10.3389/fnmol.2019.00143.

[16] V. F. Batista, J. L. Galman, D. C. Pinto, A. M. S. Silva, N. J. Turner, *ACS Catal.* **2018**, *8*, 11889–11907.

[17] B. A. Sandoval, A. J. Meichan, T. K. Hyster, *J. Am. Chem. Soc.* **2017**, *139*, 11313–11316.

[18] H. S. Toogood, N. S. Scrutton, *ACS Catal.* **2018**, *8*, 3532–3549.

[19] C. K. Winkler, K. Faber, M. Hall, *Curr. Opin. Chem. Biol.* **2018**, *43*, 97–105.

[20] W. J. H. van Berkel, N. M. Kamerbeek, M. W. Fraaije, *J. Biotechnol.* **2006**, *124*, 670–689.

[21] S. A. Baker Dockrey, A. R. H. Narayan, *Tetrahedron* **2019**, *75*, 1115–1121.

[22] S. K. Krueger, D. E. Williams, *Pharmacol. Ther.* **2005**, *106*, 357–387.

[23] I. R. Phillips, E. A. Shephard, *Expert Opin. Drug Metab. Toxicol.* **2017**, *13*, 167–181.

[24] I. R. Philips, A. A. Francois, E. A. Shephard, *Curr. Pharmacogenomics* **2007**, *5*, 292–313.

[25] J. Zhou, E. A. Shephard, *Mutat. Res. - Rev. Mutat. Res.* **2006**, *612*, 165–171.

[26] A. Sib, T. A. M. Gulder, *Angew. Chemie - Int. Ed.* **2017**, *56*, 12888–12891.

[27] S. A. Baker Dockrey, A. L. Lukowski, M. R. Becker, A. R. H. Narayan, *Nat. Chem.* **2018**, *10*, 119–125.

[28] M. J. L. J. Fürst, A. Gran-Scheuch, F. S. Aalbers, M. W. Fraaije, *ACS Catal.* **2019**, *9*, 11207–11241.

[29] C. V. F. Baldwin, R. Wohlgemuth, J. M. Woodley, *Org. Process Res. Dev.* **2008**, *12*, 660–665.

[30] C. Dong, S. Flecks, S. Unversucht, C. Haupt, K. H. Van Pée, J. H. Naismith, *Science (80-.).* **2005**, *309*, 2216–2219.

[31] J. Büchler, A. Papadopoulou, R. Buller, *Catalysts* **2019**, *9*, DOI 10.3390/catal9121030.

[32] N. H. Pham, F. Hollmann, D. Kracher, M. Preims, D. Haltrich, R. Ludwig, *J. Mol. Catal. B Enzym.* **2015**, *120*, 38–46.

[33] A. Angelastro, W. M. Dawson, L. Y. P. Luk, R. K. Allemann, *ACS Catal.* **2017**, *7*, 1025–1029.

[34] T. Knaus, C. E. Paul, C. W. Levy, S. De Vries, F. G. Mutti, F. Hollmann, N. S. Scrutton, *J. Am. Chem. Soc.* **2016**, *138*, 1033–1039.

[35] H. Wu, C. Tian, X. Song, C. Liu, D. Yang, Z. Jiang, *Green Chem.* **2013**, *15*, 1773–1789.

[36] S. H. Lee, D. S. Choi, S. K. Kuk, C. B. Park, *Angew. Chemie - Int. Ed.* **2018**, *57*, 7958–7985.

[37] L. Schmermund, V. Jurkaš, F. F. Özgen, G. D. Barone, H. C. Büchsenschütz, C. K. Winkler, S. Schmidt, R. Kourist, W. Kroutil, *ACS Catal.* **2019**, *9*, 4115–4144.

[38] C. J. Seel, T. Gulder, *ChemBioChem* **2019**, *20*, 1871–1897.

[39] J. A. Maciá-Agulló, A. Corma, H. Garcia, *Chem. - A Eur. J.* **2015**, *21*, 10940–10959.

[40] C. Kemal, T. C. Bruice, *Proc. Natl. Acad. Sci. U. S. A.* **1976**, *73*, 995–999.

[41] C. Kemal, T. W. Chan, T. C. Bruice, *J. Am. Chem. Soc.* **1977**, *99*, 7272–7286.

[42] G. Merényi, J. Lind, *J. Am. Chem. Soc.* **1991**, *113*, 3146–3153.

[43] C. Mazzini, J. Lebreton, R. Furstoss, *J. Org. Chem.* **1996**, *61*, 8–9.

[44] S. I. Murahashi, S. Ono, Y. Imada, *Angew. Chemie - Int. Ed.* **2002**, *41*, 2366–2368.

[45] Y. Imada, H. Iida, S. I. Murahashi, T. Naota, *Angew. Chemie - Int. Ed.* **2005**, *44*, 1704–1706.

[46] S. I. Murahashi, T. Oda, Y. Masui, *J. Am. Chem. Soc.* **1989**, *111*, 5002–5003.

[47] Y. Imada, H. Iida, S. Ono, S. I. Murahashi, *J. Am. Chem. Soc.* **2003**, *125*, 2868–2869.

[48] H. Kotoučová, I. Strnadová, M. Kovandová, J. Chudoba, H. Dvořáková, R. Cibulka, *Org. Biomol. Chem.* **2014**, *12*, 2137–2142.

[49] A. T. Murray, P. Matton, N. W. G. Fairhurst, M. P. John, D. R. Carbery, *Org. Lett.* **2012**, *14*, 3656–3659.

[50] S. Chen, M. S. Hossain, F. W. Foss, *Org. Lett.* **2012**, *14*, 2806–2809.

[51] S. Chen, F. W. Foss, *Org. Lett.* **2012**, *14*, 5150–5153.

[52] S. Y. Jonsson, K. Färnegårdh, J. E. Bäckvall, *J. Am. Chem. Soc.* **2001**, *123*, 1365–1371.

[53] S. Y. Jonsson, H. Adolfsson, J. E. Bäckvall, *Org. Lett.* **2001**, *3*, 3463–3466.

[54] T. Ishikawa, M. Kimura, T. Kumoi, H. Iida, *ACS Catal.* **2017**, *7*, 4986–4989.

[55] H. Iida, R. Demizu, R. Ohkado, *J. Org. Chem.* **2018**, *83*, 12291–12296.

[56] R. Ohkado, T. Ishikawa, H. Iida, *Green Chem.* **2018**, *20*, 984–988.

[57] K. Tanimoto, R. Ohkado, H. Iida, *J. Org. Chem.* **2019**, *84*, 14980–14986.

[58] Y. Arakawa, K. Yamanomoto, H. Kita, K. Minagawa, M. Tanaka, N. Haraguchi, S. Itsuno, Y. Imada, *Chem. Sci.* **2017**, *8*, 5468–5475.

[59] Y. Imada, H. Iida, T. Naota, *J. Am. Chem. Soc.* **2005**, *127*, 14544–14545.

[60] Y. Imada, T. Kitagawa, T. Ohno, H. Iida, T. Naota, *Org. Lett.* **2010**, *12*, 32–35.

[61] M. März, M. Babor, R. Cibulka, *European J. Org. Chem.* **2019**, *2019*, 3264–3268.

[62] S. Shinkai, T. Yamaguchi, O. Manabe, F. Toda, *J. Chem. Soc. Chem. Commun.* **1988**, 1399–1401.

[63] S. -I Murahashi, *Angew. Chemie Int. Ed. English* **1995**, *34*, 2443–2465.

[64] R. Jurok, R. Cibulka, H. Dvořáková, F. Hampl, J. Hodačová, *European J. Org. Chem.* **2010**, 5217–5224.

[65] R. Jurok, J. Hodačová, V. Eigner, H. Dvořáková, V. Setnička, R. Cibulka, *European J. Org. Chem.* **2013**, 7724–7738.

[66] S. Iwahana, H. Iida, E. Yashima, *Chem. - A Eur. J.* **2011**, *17*, 8009–8013.

[67] P. P. Poudel, K. Arimitsu, K. Yamamoto, *Chem. Commun.* **2016**, *52*, 4163–4166.

[68] R. Cibulka, *European J. Org. Chem.* **2015**, *2015*, 915–932.

[69] H. Iida, Y. Imada, S. I. Murahashi, *Org. Biomol. Chem.* **2015**, *13*, 7599–7613.

[70] S. Fukuzumi, K. Yasui, T. Suenobu, K. Ohkubo, M. Fujitsuka, O. Ito, *J. Phys. Chem. A* **2001**, *105*, 10501–10510.

[71] N. A. Romero, D. A. Nicewicz, *Chem. Rev.* **2016**, *116*, 10075–10166.

[72] W. Tong, H. Ye, H. Zhu, V. T. D'Souza, *J. Mol. Struct. THEOCHEM* **1995**, *333*, 19–27.

[73] S. Fukuzumi, S. Kuroda, *Res. Chem. Intermed.* **1999**, *25*, 789–811.

[74] J. Svoboda, H. Schmaderer, B. König, *Chem. - A Eur. J.* **2008**, *14*, 1854–1865.

[75] H. Schmaderer, P. Hilgers, R. Lechner, B. König, *Adv. Synth. Catal.* **2009**, *351*, 163–174.

[76] K. A. Korvinson, G. N. Hargenrader, J. Stevanovic, Y. Xie, J. Joseph, V. Maslak, C. M. Hadad, K. D. Glusac, *J. Phys. Chem. A* **2016**, *120*, 7294–7300.

[77] S. Fukuzumi, K. Tanii, T. Tanaka, *J. Chem. Soc. Chem. Commun.* **1989**, 816–818.

[78] R. Lechner, B. König, *Synthesis (Stuttg).* **2010**, 1712–1718.

[79] J. Dad'ová, E. Svobodová, M. Sikorski, B. König, R. Cibulka, *ChemCatChem* **2012**, *4*, 620–623.

[80] T. Neveselý, E. Svobodová, J. Chudoba, M. Sikorski, R. Cibulka, *Adv. Synth. Catal.* **2016**, *358*, 1654–1663.

[81] R. Lechner, S. Kümmel, B. König, *Photochem. Photobiol. Sci.* **2010**, *9*, 1367–1377.

[82] T. Hering, B. Mühldorf, R. Wolf, B. König, *Angew. Chemie - Int. Ed.* **2016**, *55*, 5342–5345.

[83] J. B. Metternich, R. Gilmour, *J. Am. Chem. Soc.* **2015**, *137*, 11254–11257.

[84] J. B. Metternich, R. Gilmour, *Synlett* **2016**, *27*, 2541–2552.

[85] J. B. Metternich, R. Gilmour, *J. Am. Chem. Soc.* **2016**, *138*, 1040–1045.

[86] J. B. Metternich, D. G. Artiukhin, M. C. Holland, M. Von Bremen-Kuhne, J. Neugebauer, R. Gilmour, *J. Org. Chem.* **2017**, *82*, 9955–9977.

[87] B. O'Leary, B. Duke, J. E. Eilers, E. W. Abrahamson, *Nature* **1973**, *246*, 166–167.

[88] M. März, J. Chudoba, M. Kohout, R. Cibulka, *Org. Biomol. Chem.* **2017**, *15*, 1970–1975.

[89] M. März, M. Kohout, T. Neveselý, J. Chudoba, D. Prukała, S. Niziński, M. Sikorski, G. Burdziński, R. Cibulka, *Org. Biomol. Chem.* **2018**, *16*, 6809–6817.

[90] S. J. S. Düsel, B. König, *J. Org. Chem.* **2018**, *83*, 2802–2807.

[91] L. M. Bouchet, A. A. Heredia, J. E. Argüello, L. C. Schmidt, *Org. Lett.* **2020**, *22*, 610–614.

[92] X. Wu, C. Meng, X. Yuan, X. Jia, X. Qian, J. Ye, *Chem. Commun.* **2015**, *51*, 11864–11867.

[93] N. P. Ramirez, B. König, J. C. Gonzalez-Gomez, *Org. Lett.* **2019**, *21*, 1368–1373.

[94] S. Bloom, C. Liu, D. K. Kölmel, J. X. Qiao, Y. Zhang, M. A. Poss, W. R. Ewing, D. W. C. Macmillan, *Nat. Chem.* **2018**, *10*, 205–211.

[95] N. P. Ramirez, T. Lana-Villarreal, J. C. Gonzalez-Gomez, *European J. Org. Chem.* **2020**, *2020*, 1539–1550.

[96] C. K. Remucal, K. McNeill, *Environ. Sci. Technol.* **2011**, *45*, 5230–5237.

[97] C. Dang, L. Zhu, H. Guo, H. Xia, J. Zhao, B. Dick, *ACS Sustain. Chem. Eng.* **2018**, *6*, 15254–15263.

[98] V. Mojr, E. Svobodová, K. Straková, T. Neveselý, J. Chudoba, H. Dvořáková, R. Cibulka, *Chem. Commun.* **2015**, *51*, 12036–12039.

[99] M. Jirásek, K. Straková, T. Neveselý, E. Svobodová, Z. Rottnerová, R. Cibulka, *European J. Org. Chem.* **2017**, *2017*, 2139–2146.

[100] V. Mojr, G. Pitrová, K. Straková, D. Prukała, S. Brazevic, E. Svobodová, I. Hoskovcová, G. Burdziński, T. Slanina, M. Sikorski, et al., *ChemCatChem* **2018**, *10*, 849–858.

[101] R. Martinez-Haya, M. A. Miranda, M. L. Marin, *European J. Org. Chem.* **2017**, *2017*, 2164–2169.

[102] S. Alonso-De Castro, E. Ruggiero, A. Ruiz-De-Angulo, E. Rezabal, J. C. Mareque-Rivas, X. Lopez, F. López-Gallego, L. Salassa, *Chem. Sci.* **2017**, *8*, 4619–4625.

[103] S. Alonso-de Castro, A. Terenzi, S. Hager, B. Englinger, A. Faraone, J. C. Martínez, M. Galanski, B. K. Keppler, W. Berger, L. Salassa, *Sci. Rep.* **2018**, *8*, DOI 10.1038/s41598-018-35655-2.

[104] S. Alonso-de Castro, A. L. Cortajarena, F. López-Gallego, L. Salassa, *Angew. Chemie - Int. Ed.* **2018**, *57*, 3143–3147.

[105] J. Gurruchaga-Pereda, V. Martínez-Martínez, E. Rezabal, X. Lopez, C. Garino, F. Mancin, A. L. Cortajarena, L. Salassa, *ACS Catal.* **2020**, *10*, 187–196.

[106] S. Fukuzumi, S. Kuroda, T. Tanaka, *J. Am. Chem. Soc.* **1985**, *107*, 3020–3027.

[107] B. Mühldorf, R. Wolf, *Chem. Commun.* **2015**, *51*, 8425–8428.

[108] B. Mühldorf, R. Wolf, *Angew. Chemie - Int. Ed.* **2016**, *55*, 427–430.

[109] G. Tang, Z. Gong, W. Han, X. Sun, *Tetrahedron Lett.* **2018**, 658–662.

[110] W. Zhang, K. L. Carpenter, S. Lin, *Angew. Chemie - Int. Ed.* **2020**, *59*, 409–417.

[111] J. Zelenka, E. Svobodová, J. Tarábek, I. Hoskovcová, V. Boguschová, S. Bailly, M. Sikorski, J. Roithová, R. Cibulka, *Org. Lett.* **2019**, *21*, 114–119.

[112] A. H. Tolba, F. Vávra, J. Chudoba, R. Cibulka, *European J. Org. Chem.* **2020**, *2020*, 1579–1585.

[113] T. Hartman, R. Cibulka, *Org. Lett.* **2016**, *18*, 3710–3713.

[114] V. Massey, M. Stankovich, P. Hemmerich, *Biochemistry* **1978**, *17*, 1–8.

[115] W. R. FRISELL, C. W. CHUNG, C. G. MACKENZIE, *J. Biol. Chem.* **1959**, *234*, 1297–1302.

[116] F. Hollmann, A. Taglieber, F. Schulz, M. T. Reetz, *Angew. Chemie - Int. Ed.* **2007**, *46*,

2903–2906.

[117] A. Taglieber, F. Schulz, F. Hollman, M. Rusek, M. T. Reetz, *ChemBioChem* **2008**, *9*, 565–572.

[118] M. M. Grau, J. C. Van Der Toorn, L. G. Otten, P. Macheroux, A. Taglieber, F. E. Zilly, I. W. C. E. Arends, F. Hollmann, *Adv. Synth. Catal.* **2009**, *351*, 3279–3286.

[119] M. Mifsud, S. Gargiulo, S. Iborra, I. W. C. E. Arends, F. Hollmann, A. Corma, *Nat. Commun.* **2014**, *5*, DOI 10.1038/ncomms4145.

[120] M. Rauch, S. Schmidt, I. W. C. E. Arends, K. Oppelt, S. Kara, F. Hollmann, *Green Chem.* **2017**, *19*, 376–379.

[121] M. K. Peers, H. S. Toogood, D. J. Heyes, D. Mansell, B. J. Coe, N. S. Scrutton, *Catal. Sci. Technol.* **2016**, *6*, 169–177.

[122] J. Kim, S. H. Lee, F. Tieves, D. S. Choi, F. Hollmann, C. E. Paul, C. B. Park, *Angew. Chemie - Int. Ed.* **2018**, *57*, 13825–13828.

[123] D. S. Choi, Y. Ni, E. Fernández-Fueyo, M. Lee, F. Hollmann, C. B. Park, *ACS Catal.* **2017**, *7*, 1563–1567.

[124] S. H. Lee, D. S. Choi, M. Pesic, Y. W. Lee, C. E. Paul, F. Hollmann, C. B. Park, *Angew. Chemie - Int. Ed.* **2017**, *56*, 8681–8685.

[125] M. M. C. H. Van Schie, C. E. Paul, I. W. C. E. Arends, F. Hollmann, *Chem. Commun.* **2019**, *55*, 1790–1792.

[126] L. Schroeder, M. Frese, C. Müller, N. Sewald, T. Kottke, *ChemCatChem* **2018**, *10*, 3336–3341.

[127] V. Massey, P. Hemmerich, *Biochemistry* **1978**, *17*, 9–17.

[128] M. M. C. H. van Schie, S. H. H. Younes, M. C. R. Rauch, M. Pesic, C. E. Paul, I. W. C. E. Arends, F. Hollmann, *Mol. Catal.* **2018**, *452*, 277–283.

[129] F. E. Zilly, A. Taglieber, F. Schulz, F. Hollmann, M. T. Reetz, *Chem. Commun.* **2009**, 7152–7154.

[130] L. C. P. Gonçalves, H. R. Mansouri, E. L. Bastos, M. Abdellah, B. S. Fadiga, J. Sá, F. Rudroff, M. D. Mihovilovic, *Catal. Sci. Technol.* **2019**, *9*, 1365–1371.

[131] L. C. P. Goncąlves, H. R. Mansouri, S. Pourmehdi, M. Abdellah, B. S. Fadiga, E. L. Bastos, J. Sá, M. D. Mihovilovic, F. Rudroff, *Catal. Sci. Technol.* **2019**, *9*, 2682–2688.

[132] D. Sorigué, B. Légeret, S. Cuiné, S. Blangy, S. Moulin, E. Billon, P. Richaud, S. Brugière, Y. Couté, D. Nurizzo, et al., *Science (80-.).* **2017**, *357*, 903–907.

[133] M. M. E. Huijbers, W. Zhang, F. Tonin, F. Hollmann, *Angew. Chemie - Int. Ed.* **2018**, *57*, 13648–13651.

[134] W. Zhang, M. Ma, M. M. E. Huijbers, G. A. Filonenko, E. A. Pidko, M. Van Schie, S. De Boer, B. O. Burek, J. Z. Bloh, W. J. H. Van Berkel, et al., *J. Am. Chem. Soc.* **2019**, *141*, 3116–3120.

[135] Y. Ma, X. Zhang, W. Zhang, P. Li, Y. Li, F. Hollmann, Y. Wang, *ChemPhotoChem* **2020**, *4*, 39–44.

[136] H. J. Cha, S. Y. Hwang, D. S. Lee, A. R. Kumar, Y. U. Kwon, M. Voß, E. Schuiten, U. T. Bornscheuer, F. Hollmann, D. K. Oh, et al., *Angew. Chemie - Int. Ed.* **2020**, *59*, 7024–7028.

[137] K. F. Biegasiewicz, S. J. Cooper, X. Gao, D. G. Oblinsky, J. H. Kim, S. E. Garfinkle, L. A.

Joyce, B. A. Sandoval, G. D. Scholes, T. K. Hyster, *Science (80-.).* **2019**, *364*, 1166–1169.

[138] M. J. Black, K. F. Biegasiewicz, A. J. Meichan, D. G. Oblinsky, B. Kudisch, G. D. Scholes, T. K. Hyster, *Nat. Chem.* **2020**, *12*, 71–75.

[139] B. A. Sandoval, S. I. Kurtoic, M. M. Chung, K. F. Biegasiewicz, T. K. Hyster, *Angew. Chemie - Int. Ed.* **2019**, *58*, 8714–8718.

[140] Y. Nakano, M. J. Black, A. J. Meichan, B. A. Sandoval, M. M. Chung, K. F. Biegasiewicz, T. Zhu, T. K. Hyster, *Angew. Chemie - Int. Ed.* **2020**, *59*, 10484–10488.

[141] Z. C. Litman, Y. Wang, H. Zhao, J. F. Hartwig, *Nature* **2018**, *560*, 355–359.

[142] V. Nandwana, I. Samuel, G. Cooke, V. M. Rotello, *Acc. Chem. Res.* **2013**, *46*, 1000–1009.

[143] I. Tabushi, M. Kodera, *J. Am. Chem. Soc.* **1987**, *109*, 4734–4735.

[144] D. Rong, H. Ye, T. R. Boehlow, V. T. D'souza, *J. Org. Chem.* **1992**, *57*, 163–167.

[145] H. Ye, W. Tong, V. T. D'Souza, *J. Chem. Soc. Perkin Trans. 2* **1994**, 2431–2437.

[146] J. Carroll, M. Gray, K. Bardon, H. Nakade, V. Rotello, *Lett. Org. Chem.* **2005**, *1*, 227–230.

[147] B. J. Jordan, G. Cooke, J. F. Garety, M. A. Pollier, N. Kryvokhyzha, A. Bayir, G. Rabani, V. M. Rotello, *Chem. Commun.* **2007**, 1248–1250.

[148] S. S. Agasti, S. T. Caldwell, G. Cooke, B. J. Jordan, A. Kennedy, N. Kryvokhyzha, G. Rabani, S. Rana, A. Sanyal, V. M. Rotello, *Chem. Commun.* **2008**, 4123–4125.

[149] C. Subramani, G. Yesilbag, B. J. Jordan, X. Li, A. Khorasani, G. Cooke, A. Sanyal, V. M. Rotello, *Chem. Commun.* **2010**, *46*, 2067–2069.

[150] S. M. Butterfield, C. M. Goodman, V. M. Rotello, M. L. Waters, *Angew. Chemie - Int. Ed.* **2004**, *43*, 724–727.

[151] A. K. Boal, V. M. Rotello, *J. Am. Chem. Soc.* **1999**, *121*, 4914–4915.

[152] A. K. Boal, V. M. Rotello, *J. Am. Chem. Soc.* **2000**, *122*, 734–735.

[153] A. Bayir, B. J. Jordan, A. Verma, M. A. Pollier, G. Cooke, V. M. Rotello, *Chem. Commun.* **2006**, 4033–4035.

[154] M. D. Greaves, V. M. Rotello, *J. Am. Chem. Soc.* **1997**, *119*, 10569–10572.

[155] M. D. Greaves, T. H. Galow, V. M. Rotello, *Chem. Commun.* **1999**, 169–170.

[156] V. Mojr, V. Herzig, M. Budíšnský, R. Cibulka, T. Kraus, *Chem. Commun.* **2010**, *46*, 7599–7601.

[157] V. Mojr, M. Buděšínský, R. Cibulka, T. Kraus, *Org. Biomol. Chem.* **2011**, *9*, 7318–7326.

[158] V. T. D'Souza, in *Supramol. Chem.*, **2003**, pp. 221–229.

[159] P. Tomanová, J. Šturala, M. Buděšínský, R. Cibulka, *Molecules* **2015**, *20*, 19837–19848.

[160] Y. Arakawa, R. Kawachi, Y. Tezuka, K. Minagawa, Y. Imada, *J. Polym. Sci. Part A Polym. Chem.* **2017**, *55*, 1706–1713.

[161] Y. Arakawa, F. Sato, K. Ariki, K. Minagawa, Y. Imada, *Tetrahedron Lett.* **2020**, *61*, DOI 10.1016/j.tetlet.2020.151710.

[162] Y. Arakawa, T. Oonishi, T. Kohda, K. Minagawa, Y. Imada, *ChemSusChem* **2016**, *9*, 2769–2773.

[163] Y. Chevalier, Y. Lock Toy Ki, D. le Nouen, J. P. Mahy, J. P. Goddard, F. Avenier, *Angew. Chemie - Int. Ed.* **2018**, *57*, 16412–16415.

[164] T. Sakai, M. Watanabe, R. Ohkado, Y. Arakawa, Y. Imada, H. Iida, *ChemSusChem* **2019**,

12, 1640–1645.

[165] Y. Imada, H. Iida, T. Kitagawa, T. Naota, *Chem. - A Eur. J.* **2011**, *17*, 5908–5920.

[166] Y. Imada, Y. Kugimiya, S. Iwata, N. Komiya, T. Naota, *Tetrahedron* **2013**, *69*, 8572–8578.

[167] Y. Imada, T. Kitagawa, S. Iwata, N. Komiya, T. Naota, *Tetrahedron* **2014**, *70*, 495–501.

[168] J. Špačková, E. Svobodová, T. Hartman, I. Stibor, J. Kopecká, J. Cibulková, J. Chudoba, R. Cibulka, *ChemCatChem* **2017**, *9*, 1177–1181.

[169] M. Kurfiřt, J. Špačková, E. Svobodová, R. Cibulka, *Monatshefte fur Chemie* **2018**, *149*, 863–869.

[170] Y. Arakawa, K. Minagawa, Y. Imada, *Polym. J.* **2018**, *50*, 941–949.

[171] D. Astruc, *Nanoparticles and Catalysis*, **2008**.

[172] J. Jayapaul, M. Hodenius, S. Arns, W. Lederle, T. Lammers, P. Comba, F. Kiessling, J. Gaetjens, *Biomaterials* **2011**, *32*, 5863–5871.

[173] T. P. Thomas, S. K. Choi, M. H. Li, A. Kotlyar, J. R. Baker, *Bioorganic Med. Chem. Lett.* **2010**, *20*, 5191–5194.

[174] A. B. Witte, C. M. Timmer, J. J. Gam, S. K. Choi, M. M. Banaszak Holl, B. G. Orr, J. R. Baker, K. Sinniah, *Biomacromolecules* **2012**, *13*, 507–516.

[175] M. E. Mertens, J. Frese, D. A. Bölükbas, L. Hrdlicka, S. Golombek, S. Koch, P. Mela, S. Jockenhövel, F. Kiessling, T. Lammers, *Theranostics* **2014**, *4*, 1002–1013.

[176] Y. Tsvetkova, N. Beztsinna, M. Baues, D. Klein, A. Rix, S. K. Golombek, W. Al Rawashdeh, F. Gremse, M. Barz, K. Koynov, et al., *Nano Lett.* **2017**, *17*, 4665–4674.

[177] N. Beztsinna, Y. Tsvetkova, M. Bartneck, T. Lammers, F. Kiessling, I. Bestel, *Bioconjug. Chem.* **2016**, *27*, 2048–2061.

[178] C. Y. Wu, Y. C. Chen, *Artif. Cells, Nanomedicine Biotechnol.* **2019**, *47*, 210–220.

[179] Y. Imada, M. Osaki, M. Noguchi, T. Maeda, M. Fujiki, S. Kawamorita, N. Komiya, T. Naota, *ChemCatChem* **2015**, *7*, 99–106.

[180] J. B. Metternich, S. Sagebiel, A. Lückener, S. Lamping, B. J. Ravoo, R. Gilmour, *Chem. - A Eur. J.* **2018**, *24*, 4228–4233.

[181] M. Rochkind, M. Pandiri, M. S. Hossain, F. W. Foss, K. Rajeshwar, Y. Paz, *J. Phys. Chem. C* **2016**, *120*, 16069–16079.

[182] M. Pandiri, M. S. Hossain, F. W. Foss, K. Rajeshwar, Y. Paz, *Phys. Chem. Chem. Phys.* **2016**, *18*, 18575–18583.

[183] P. Dongare, I. MacKenzie, D. Wang, D. A. Nicewicz, T. J. Meyer, *Proc. Natl. Acad. Sci. U. S. A.* **2017**, *114*, 9279–9283.

[184] N. Verma, R. Ananthakrishnan, *J. Phys. Chem. C* **2019**, *124*, 404–415.

[185] J. Willkomm, K. L. Orchard, A. Reynal, E. Pastor, J. R. Durrant, E. Reisner, *Chem. Soc. Rev.* **2016**, *45*, 9–23.

[186] J. W. Tucker, Y. Zhang, T. F. Jamison, C. R. J. Stephenson, *Angew. Chemie - Int. Ed.* **2012**, *51*, 4144–4147.

[187] H. Lee, N. F. Scherer, P. B. Messersmith, *Proc. Natl. Acad. Sci. U. S. A.* **2006**, *103*, 12999–13003.

[188] H. Lee, S. M. Dellatore, W. M. Miller, P. B. Messersmith, *Science (80-.).* **2007**, *318*, 426–430.

[189] M. E. Lynge, R. Van Der Westen, A. Postma, B. Städler, *Nanoscale* **2011**, *3*, 4916–4928.

[190] Y. Liu, K. Ai, L. Lu, *Chem. Rev.* **2014**, *114*, 5057–5115.

[191] M. Liu, G. Zeng, K. Wang, Q. Wan, L. Tao, X. Zhang, Y. Wei, *Nanoscale* **2016**, *8*, 16819–16840.

[192] K. Qu, Y. Wang, A. Vasileff, Y. Jiao, H. Chen, Y. Zheng, *J. Mater. Chem. A* **2018**, *6*, 21827–21846.

[193] M. D'Ischia, A. Napolitano, V. Ball, C. T. Chen, M. J. Buehler, *Acc. Chem. Res.* **2014**, *47*, 3541–3550.

[194] J. Liebscher, R. Mrówczyński, H. A. Scheidt, C. Filip, N. D. Haìdade, R. Turcu, A. Bende, S. Beck, *Langmuir* **2013**, *29*, 10539–10548.

[195] J. H. Ryu, P. B. Messersmith, H. Lee, *ACS Appl. Mater. Interfaces* **2018**, *10*, 7523–7540.

[196] V. Ball, *Front. Bioeng. Biotechnol.* **2018**, *6*, DOI 10.3389/fbioe.2018.00109.

[197] J. Liebscher, *European J. Org. Chem.* **2019**, *2019*, 4976–4994.

[198] Q. Wei, F. Zhang, J. Li, B. Li, C. Zhao, *Polym. Chem.* **2010**, *1*, 1430–1433.

[199] W. Zheng, H. Fan, L. Wang, Z. Jin, *Langmuir* **2015**, *31*, 11671–11677.

[200] F. Ponzio, J. Barthès, J. Bour, M. Michel, P. Bertani, J. Hemmerlé, M. D'Ischia, V. Ball, *Chem. Mater.* **2016**, *28*, 4697–4705.

[201] X. Du, L. Li, J. Li, C. Yang, N. Frenkel, A. Welle, S. Heissler, A. Nefedov, M. Grunze, P. A. Levkin, *Adv. Mater.* **2014**, *26*, 8029–8033.

[202] X. Du, L. Li, F. Behboodi-Sadabad, A. Welle, J. Li, S. Heissler, H. Zhang, N. Plumeré, P. A. Levkin, *Polym. Chem.* **2017**, *8*, 2145–2151.

[203] K. Y. Ju, Y. Lee, S. Lee, S. B. Park, J. K. Lee, *Biomacromolecules* **2011**, *12*, 625–632.

[204] K. Ai, Y. Liu, C. Ruan, L. Lu, G. Lu, *Adv. Mater.* **2013**, *25*, 998–1003.

[205] Y. Liu, K. Ai, J. Liu, M. Deng, Y. He, L. Lu, *Adv. Mater.* **2013**, *25*, 1353–1359.

[206] R. Mrowczynski, *ACS Appl. Mater. Interfaces* **2018**, *10*, 7541–7561.

[207] M. Salomäki, L. Marttila, H. Kivelä, T. Ouvinen, J. Lukkari, *J. Phys. Chem. B* **2018**, *122*, 6314–6327.

[208] T. S. Sileika, H. Do Kim, P. Maniak, P. B. Messersmith, *ACS Appl. Mater. Interfaces* **2011**, *3*, 4602–4610.

[209] Á. Molnár, *ChemCatChem* **2020**, *12*, 2649–2689.

[210] S. Liu, A. Qileng, J. Huang, Q. Gao, Y. Liu, *RSC Adv.* **2017**, *7*, 45545–45551.

[211] X. Yu, G. Cheng, S. Y. Zheng, *Sci. Rep.* **2016**, *6*, DOI 10.1038/srep25459.

[212] T. Zeng, X. Le Zhang, H. Y. Niu, Y. R. Ma, W. H. Li, Y. Q. Cai, *Appl. Catal. B Environ.* **2013**, *134–135*, 26–33.

[213] Y. Ni, G. Tong, J. Wang, H. Li, F. Chen, C. Yu, Y. Zhou, *RSC Adv.* **2016**, *6*, 40698–40705.

[214] Q. Wei, R. Shi, D. Lu, Z. Lei, *RSC Adv.* **2016**, *6*, 29245–29253.

[215] J. Luo, N. Zhang, R. Liu, X. Liu, *RSC Adv.* **2014**, *4*, 64816–64824.

[216] R. Liu, Y. Guo, G. Odusote, F. Qu, R. D. Priestley, *ACS Appl. Mater. Interfaces* **2013**, *5*, 9167–9171.

[217] Y. Zhao, Y. Yeh, R. Liu, J. You, F. Qu, *Solid State Sci.* **2015**, *45*, 9–14.

[218] Y. Song, H. Jiang, B. Wang, Y. Kong, J. Chen, *ACS Appl. Mater. Interfaces* **2018**, *10*, 1792–1801.

[219] G. H. Choi, D. K. Rhee, A. R. Park, M. J. Oh, S. Hong, J. J. Richardson, J. Guo, F. Caruso, P. J. Yoo, *ACS Appl. Mater. Interfaces* **2016**, *8*, 3250–3257.

[220] E. Cao, W. Duan, F. Wang, A. Wang, Y. Zheng, *Carbohydr. Polym.* **2017**, *158*, 44–50.

[221] L. Du, A. Guo, A. Cai, *Micro Nano Lett.* **2018**, *13*, 518–523.

[222] S. Lu, J. Yu, Y. Cheng, Q. Wang, A. Barras, W. Xu, S. Szunerits, D. Cornu, R. Boukherroub, *Appl. Surf. Sci.* **2017**, *411*, 163–169.

[223] J. X. Ma, H. Yang, S. Li, R. Ren, J. Li, X. Zhang, J. Ma, *RSC Adv.* **2015**, *5*, 97520–97527.

[224] J. Xi, J. Xiao, F. Xiao, Y. Jin, Y. Dong, F. Jing, S. Wang, *Sci. Rep.* **2016**, *6*, DOI 10.1038/srep21904.

[225] P. Fu, Z. Xiao, Y. Liu, L. Wang, X. Zhang, G. Li, *ChemistrySelect* **2018**, *3*, 3351–3361.

[226] Y. Liu, G. Li, R. Qin, D. Chen, *Langmuir* **2016**, *32*, 13675–13686.

[227] S. W. Bian, S. Liu, L. Chang, *J. Mater. Sci.* **2016**, *51*, 3643–3649.

[228] J. Zhang, Q. Fang, J. Duan, H. Xu, H. Xu, S. Xuan, *Langmuir* **2018**, *34*, 4298–4306.

[229] Z. Zeng, M. Wen, B. Yu, G. Ye, X. Huo, Y. Lu, J. Chen, *ACS Appl. Mater. Interfaces* **2018**, *10*, 14735–14743.

[230] Z. Wu, H. Lin, Y. Wang, X. Yu, J. Li, Z. Xiong, Y. Wang, Y. Huang, T. Chen, F. Liu, *RSC Adv.* **2016**, *6*, 62302–62309.

[231] A. Ma, Y. Xie, J. Xu, H. Zeng, H. Xu, *Chem. Commun.* **2015**, *51*, 1469–1471.

[232] M. Zhang, G. Li, X. Sun, Y. Jiang, X. Zhang, *J. Mater. Chem. A* **2017**, *5*, 20789–20796.

[233] G. Bakirci, M. Yilmaz, E. Babur, D. Ozden, G. Demirel, *Catal. Commun.* **2017**, *91*, 48–52.

[234] S. Du, Z. Liao, Z. Qin, F. Zuo, X. Li, *Catal. Commun.* **2015**, *72*, 86–90.

[235] S. Du, Y. Luo, F. Zuo, X. Li, D. Liu, *Nano* **2017**, *12*, DOI 10.1142/S1793292017500370.

[236] A. Kunfi, V. Szabó, Á. Mastalir, I. Bucsi, M. Mohai, P. Németh, I. Bertóti, G. London, *ChemCatChem* **2017**, *9*, 3236–3244.

[237] X. Fei, W. Kong, X. Chen, X. Jiang, Z. Shao, J. Y. Lee, *ACS Catal.* **2017**, *7*, 2412–2418.

[238] A. V. Dubey, A. V. Kumar, *RSC Adv.* **2016**, *6*, 46864–46870.

[239] Y. Li, L. Xu, B. Xu, Z. Mao, H. Xu, Y. Zhong, L. Zhang, B. Wang, X. Sui, *ACS Appl. Mater. Interfaces* **2017**, *9*, 17155–17162.

[240] A. Kunfi, Z. May, P. Németh, G. London, *J. Catal.* **2018**, *361*, 84–93.

[241] R. Ma, P. Yang, Y. Ma, F. Bian, *ChemCatChem* **2018**, *10*, 1446–1454.

[242] B. Majumdar, T. Bhattacharya, T. K. Sarma, *ChemCatChem* **2016**, *8*, 1825–1835.

[243] H. Veisi, A. Nikseresht, S. Mohammadi, S. Hemmati, *Cuihua Xuebao/Chinese J. Catal.* **2018**, *39*, 1044–1050.

[244] H. Veisi, P. Safarimehr, S. Hemmati, *J. Taiwan Inst. Chem. Eng.* **2018**, *88*, 8–17.

[245] H. Zhang, J. Luo, S. Li, Y. Wei, Y. Wan, *Langmuir* **2018**, *34*, 2585–2594.

[246] H. Lee, J. Rho, P. B. Messersmith, *Adv. Mater.* **2009**, *21*, 431–434.

[247] Y. Ren, J. G. Rivera, L. He, H. Kulkarni, D. K. Lee, P. B. Messersmith, *BMC Biotechnol.* **2011**, *11*, DOI 10.1186/1472-6750-11-63.

[248] Y. Qu, R. Huang, W. Qi, R. Su, Z. He, *ACS Appl. Mater. Interfaces* **2015**, *7*, 14954–14964.

[249] J. G. Rivera, P. B. Messersmith, *J. Sep. Sci.* **2012**, *35*, 1514–1520.

[250] V. Ball, *J. Colloid Interface Sci.* **2014**, *429*, 1–7.

[251] C. Chao, J. Liu, J. Wang, Y. Zhang, B. Zhang, Y. Zhang, X. Xiang, R. Chen, *ACS Appl. Mater. Interfaces* **2013**, *5*, 10559–10564.

[252] X. Gao, K. Ni, C. Zhao, Y. Ren, D. Wei, *J. Biotechnol.* **2014**, *188*, 36–41.

[253] X. Wu, C. Yang, J. Ge, Z. Liu, *Nanoscale* **2015**, *7*, 18883–18886.

[254] L. Zhang, J. Shi, Z. Jiang, Y. Jiang, S. Qiao, J. Li, R. Wang, R. Meng, Y. Zhu, Y. Zheng, *Green Chem.* **2011**, *13*, 300–306.

[255] J. Luo, A. S. Meyer, R. V. Mateiu, D. Kalyani, M. Pinelo, *ACS Appl. Mater. Interfaces* **2014**, *6*, 22894–22904.

[256] L. Hosta-Rigau, M. J. York-Duran, Y. Zhang, K. N. Goldie, B. Städler, *ACS Appl. Mater. Interfaces* **2014**, *6*, 12771–12779.

[257] L. Wang, Z. Y. Hu, X. Y. Yang, B. B. Zhang, W. Geng, G. Van Tendeloo, B. L. Su, *Chem. Commun.* **2017**, *53*, 6617–6620.

[258] R. Mrõwczyński, A. Bunge, J. Liebscher, *Chem. - A Eur. J.* **2014**, *20*, 8647–8653.

[259] Z. Yang, J. Sun, X. Liu, Q. Su, Y. Liu, Q. Li, S. Zhang, *Tetrahedron Lett.* **2014**, *55*, 3239–3243.

[260] S. Liang, H. Liu, T. Jiang, J. Song, G. Yang, B. Han, *Chem. Commun.* **2011**, *47*, 2131–2133.

[261] Y. Du, H. C. Yang, X. L. Xu, J. Wu, Z. K. Xu, *ChemCatChem* **2015**, *7*, 3822–3825.

[262] A. Vaish, D. J. Vanderah, L. J. Richter, M. Dimitriou, K. L. Steffens, M. L. Walker, *Chem. Commun.* **2015**, *51*, 6591–6594.

[263] S. A. Pawar, A. N. Chand, A. V. Kumar, *ACS Sustain. Chem. Eng.* **2019**, *7*, 8274–8286.

[264] J. E. Mcginness, *Science (80-.).* **1972**, *177*, 896–897.

[265] J. Mcginness, P. Corry, P. Proctor, *Science (80-.).* **1974**, *183*, 853–855.

[266] A. B. Mostert, B. J. Powell, F. L. Pratt, G. R. Hanson, T. Sarna, I. R. Gentle, P. Meredith, *Proc. Natl. Acad. Sci. U. S. A.* **2012**, *109*, 8943–8947.

[267] E. J. Son, J. H. Kim, K. Kim, C. B. Park, *J. Mater. Chem. A* **2016**, *4*, 11179–11202.

[268] W. X. Mao, X. J. Lin, W. Zhang, Z. X. Chi, R. W. Lyu, A. M. Cao, L. J. Wan, *Chem. Commun.* **2016**, *52*, 7122–7125.

[269] X. Zhou, B. Jin, J. Luo, X. Xu, L. Zhang, J. Li, H. Guan, *RSC Adv.* **2016**, *6*, 64446–64449.

[270] Z. Wang, J. Li, F. Tang, J. Lin, Z. Jin, *RSC Adv.* **2017**, *7*, 23535–23542.

[271] R. Liu, L. Dai, C. L. Si, *ACS Sustain. Chem. Eng.* **2018**, *6*, 15756–15763.

[272] C. Wang, Y. Wu, J. Lu, J. Zhao, J. Cui, X. Wu, Y. Yan, P. Huo, *ACS Appl. Mater. Interfaces* **2017**, *9*, 23687–23697.

[273] B. Wang, M. Zhang, W. Li, L. Wang, J. Zheng, W. Gan, J. Xu, *Dalt. Trans.* **2015**, *44*, 17020–17025.

[274] X. Jie, N. Bao, B. Gong, S. Zhou, *Nano-Structures and Nano-Objects* **2017**, *12*, 98–105.

[275] W. Li, G. Zhang, W. Sheng, C. Dong, Y. Dai, C. Li, R. Wang, Y. Shi, X. Guo, X. Jia, *RSC Adv.* **2016**, *6*, 106697–106704.

[276] A. Cai, X. Wang, A. Guo, Y. Chang, *J. Photochem. Photobiol. B Biol.* **2016**, *162*, 486–492.

[277] Z. Yu, F. Li, Q. Yang, H. Shi, Q. Chen, M. Xu, *ACS Sustain. Chem. Eng.* **2017**, *5*, 7840–7850.

[278] J. H. Kim, M. K. Joshi, J. Lee, C. H. Park, C. S. Kim, *J. Colloid Interface Sci.* **2018**, *513*, 566–574.

[279] X. Zhou, B. Jin, J. Luo, X. Gu, S. Zhang, *J. Solid State Chem.* **2017**, *254*, 55–61.

[280] Y. Lv, C. Zhang, A. He, S. J. Yang, G. P. Wu, S. B. Darling, Z. K. Xu, *Adv. Funct. Mater.* **2017**, *27*, DOI 10.1002/adfm.201700251.

[281] A. Xie, K. Zhang, F. Wu, N. Wang, Y. Wang, M. Wang, *Catal. Sci. Technol.* **2016**, *6*, 1764–1771.

[282] J. Tripathy, G. Loget, M. Altomare, P. Schmuki, *J. Nanosci. Nanotechnol.* **2016**, *16*, 5353–5358.

[283] J. H. Kim, M. Lee, C. B. Park, *Angew. Chemie - Int. Ed.* **2014**, *53*, 6364–6368.

[284] M. Lee, J. U. Kim, J. S. Lee, B. Il Lee, J. Shin, C. B. Park, *Adv. Mater.* **2014**, *26*, 4463–4468.

[285] H. J. Nam, B. Kim, M. J. Ko, M. Jin, J. M. Kim, D. Y. Jung, *Chem. - A Eur. J.* **2012**, *18*, 14000–14007.

[286] L. D. M. Torquato, F. A. C. Pastrian, J. A. L. Perini, K. Irikura, A. P. Ana, A. G. S. de Oliveira-Filho, S. I. Córdoba de Torresi, M. V. B. Zanoni, *Appl. Catal. B Environ.* **2020**, *261*, DOI 10.1016/j.apcatb.2019.118221.

[287] J. A. L. Perini, L. D. M. Torquato, K. Irikura, M. V. B. Zanoni, *J. CO2 Util.* **2019**, *34*, 596–605.

[288] T. Wang, M. Xia, X. Kong, *Catalysts* **2018**, *8*, DOI 10.3390/catal8050215.

[289] A. Savateev, M. Antonietti, *ACS Catal.* **2018**, *8*, 9790–9808.

[290] G. A. M. Hutton, B. C. M. Martindale, E. Reisner, *Chem. Soc. Rev.* **2017**, *46*, 6111–6123.

[291] L. Deng, O. Norberg, S. Uppalapati, M. Yan, O. Ramström, *Org. Biomol. Chem.* **2011**, *9*, 3188–3198.

[292] B. Geiseler, L. Fruk, *J. Mater. Chem.* **2012**, *22*, 735–741.

[293] H. Weiner, G. Duester, E. Maser, B. Plapp, *Chem. Biol. Interact.* **2009**, *178*, 1.

[294] A. Kotaki, M. Naoi, K. Yagi, *J. Biochem.* **1970**, *68*, 287–292.

[295] L. N. Mataranga-Popa, I. Torje, T. Ghosh, M. J. Leitl, A. Späth, M. L. Novianti, R. D. Webster, B. König, *Org. Biomol. Chem.* **2015**, *13*, 10198–10204.

[296] A. Kotaki, K. Yagi, *J. Biochem.* **1970**, *68*, 509–516.

[297] A. Kozik, W. Korytowski, T. Sarna, A. S. Bloom, *Biophys. Chem.* **1990**, *38*, 39–48.

[298] G. WEBER, *Biochem. J.* **1950**, *47*, 114–121.

[299] S. B. Smith, T. C. Bruice, *J. Am. Chem. Soc.* **1975**, *97*, 2875–2881.

[300] T. Harayama, Y. Tezuka, T. Taga, F. Yoneda, *Tetrahedron Lett.* **1984**, *25*, 4015–4018.

[301] B. Rieff, S. Bauer, G. Mathias, P. Tavan, *J. Phys. Chem. B* **2011**, *115*, 2117–2123.

[302] L. Fruk, C. M. Niemeyer, *Angew. Chemie - Int. Ed.* **2005**, *44*, 2603–2606.

[303] L. Fruk, V. Rajendran, M. Spengler, C. M. Niemeyer, *ChemBioChem* **2007**, *8*, 2195–2198.

[304] C. Chen, I. Ahmed, L. Fruk, *Nanoscale* **2013**, *5*, 11610–11614.

[305] I. Caballero, M. J. Lafuente, F. J. Gamo, C. Cid, *Anal. Biochem.* **2016**, *506*, 13–21.

[306] F. A. Summers, B. Zhao, D. Ganini, R. P. Mason, *Methods Enzymol.* **2013**, *526*, 1–17.

[307] R. Göstl, A. Senf, S. Hecht, *Chem. Soc. Rev.* **2014**, *43*, 1982–1996.

[308] H. S. Rho, A. T. Hanke, M. Ottens, H. Gardeniers, *PLoS One* **2016**, *11*, e0153437.

[309] P. F. Heelis, B. J. Parsons, G. O. Phillips, J. F. McKellar, *Photochem. Photobiol.* **1979**, *30*, 343–347.

[310] C. Bueno, M. L. Villegas, S. G. Bertolotti, C. M. Previtali, M. G. Neumann, M. V. Encinas, *Photochem. Photobiol.* **2002**, *76*, 385–390.

[311] M. A. Sheraz, S. H. Kazi, S. Ahmed, Z. Anwar, I. Ahmad, *Beilstein J. Org. Chem.* **2014**, *10*, 1999–2012.

[312] J. S. Suk, Q. Xu, N. Kim, J. Hanes, L. M. Ensign, *Adv. Drug Deliv. Rev.* **2016**, *99*, 28–51.

[313] Y. Liu, K. Ai, X. Ji, D. Askhatova, R. Du, L. Lu, J. Shi, *J. Am. Chem. Soc.* **2017**, *139*, 856–862.

[314] S. K. Krueger, D. E. Williams, *Pharmacol. Ther.* **2005**, *106*, 357–387.

[315] J. Zhou, E. A. Shephard, *Mutat. Res. - Rev. Mutat. Res.* **2006**, *612*, 165–171.

[316] D. W. Sullivan, S. E. Gad, in *Encycl. Toxicol. Third Ed.* (Ed.: P. Wexler), Academic Press, Cambridge, Massachusetts, **2014**, pp. 1030–1031.

[317] J. H. Lee, J. Lee, *FEMS Microbiol. Rev.* **2010**, *34*, 426–444.

[318] J. H. Lee, Y. G. Kim, K. H. Baek, M. H. Cho, J. Lee, *Environ. Microbiol.* **2015**, *17*, 1234–1244.

[319] J. H. Lee, T. K. Wood, J. Lee, *Trends Microbiol.* **2015**, *23*, 707–718.

[320] M. Erb, N. Veyrat, C. A. M. Robert, H. Xu, M. Frey, J. Ton, T. C. J. Turlings, *Nat. Commun.* **2015**, *6*, DOI 10.1038/ncomms7273.

[321] N. Mermod, S. Harayama, K. N. Timmis, *Bio/Technology* **1986**, *4*, 321–324.

[322] A. Meyer, M. Würsten, A. Schmid, H. P. E. Kohler, B. Witholt, *J. Biol. Chem.* **2002**, *277*, 34161–34167.

[323] K. E. O'Connor, A. D. W. Dobson, S. Hartmans, *Appl. Environ. Microbiol.* **1997**, *63*, 4287–4291.

[324] A. Singh, N. Singh Chauhan, H. V. Thulasiram, V. Taneja, R. Sharma, *Bioresour. Technol.* **2010**, *101*, 8481–8484.

[325] H. Nagayama, T. Sugawara, R. Endo, A. Ono, H. Kato, Y. Ohtsubo, Y. Nagata, M. Tsuda, *Appl. Microbiol. Biotechnol.* **2015**, *99*, 4453–4470.

[326] G. H. Lin, H. P. Chen, J. H. Huang, T. T. Liu, T. K. Lin, S. J. Wang, C. H. Tseng, H. Y. Shu, *Antonie van Leeuwenhoek, Int. J. Gen. Mol. Microbiol.* **2012**, *101*, 881–890.

[327] G. H. Han, G. H. Gim, W. Kim, S. Il Seo, S. W. Kim, *J. Biotechnol.* **2012**, *164*, 179–187.

[328] Q. Ma, X. Zhang, Y. Qu, *Front. Microbiol.* **2018**, *9*, DOI 10.3389/fmicb.2018.02625.

[329] T. M. Hsu, D. H. Welner, Z. N. Russ, B. Cervantes, R. L. Prathuri, P. D. Adams, J. E. Dueber, *Nat. Chem. Biol.* **2018**, *14*, 256–261.

[330] H. Schmidt, *Chemie Unserer Zeit* **1997**, *31*, 121–128.

[331] R. S. Blackburn, T. Bechtold, P. John, *Color. Technol.* **2009**, *125*, 193–207.

[332] B. Lin, Y. Tao, *Microb. Cell Fact.* **2017**, *16*, DOI 10.1186/s12934-017-0724-7.

[333] S. Li, X. Yang, S. Yang, M. Zhu, X. Wang, *Comput. Struct. Biotechnol. J.* **2012**, *2*, e201209017.

[334] M. T. Reetz, *Tetrahedron* **2002**, *58*, 6595–6602.

[335] G. deGonzalo, M. W. Fraaije, *ChemCatChem* **2013**, *5*, 403–415.

[336] B. König, S. Kümmel, R. Cibulka, *Chem. Photocatal.* **2013**, *3*, 45–66.

[337] X. Jiang, Y. Wang, M. Li, *Sci. Rep.* **2014**, *4*, DOI 10.1038/srep06070.

[338] C. C. Le, M. K. Wismer, Z. C. Shi, R. Zhang, D. V. Conway, G. Li, P. Vachal, I. W. Davies, D. W. C. MacMillan, *ACS Cent. Sci.* **2017**, *3*, 647–653.

[339] R. Cibulka, R. Vasold, B. König, *Chem. - A Eur. J.* **2004**, *10*, 6223–6231.

[340] U. Megerle, M. Wenninger, R. J. Kutta, R. Lechner, B. König, B. Dick, E. Riedle, *Phys. Chem. Chem. Phys.* **2011**, *13*, 8869–8880.

[341] H. H. Kuo, A. G. Mauk, *Proc. Natl. Acad. Sci. U. S. A.* **2012**, *109*, 13966–13971.

[342] M. Linhares, S. L. H. Rebelo, M. M. Q. Simões, A. M. S. Silva, M. G. P. M. S. Neves, J. A. S. Cavaleiro, C. Freire, *Appl. Catal. A Gen.* **2014**, *470*, 427–433.

[343] A. Kumar, S. Kumar, *J. Phys. Org. Chem.* **1998**, *11*, 277–282.

[344] B. Gehauf, J. Goldenson, *Anal. Chem.* **1957**, *29*, 276–278.

[345] H. J. Woo, J. Sanseverino, C. D. Cox, K. G. Robinson, G. S. Sayler, *J. Microbiol. Methods* **2000**, *40*, 181–191.

[346] J. Seixas De Melo, A. P. Moura, M. J. Melo, *J. Phys. Chem. A* **2004**, *108*, 6975–6981.

[347] E. M. J. Gillam, L. M. Notley, H. Cai, J. J. De Voss, F. P. Guengerich, *Biochemistry* **2000**, *39*, 13817–13824.

[348] C. Ganachaud, V. Garfagnoli, T. Tron, G. Iacazio, *Tetrahedron Lett.* **2008**, *49*, 2476–2478.

[349] A. N. Zelentskii, G. V. Fomin, N. V. Kutafina, A. A. Berlin, *Bull. Acad. Sci. USSR Div. Chem. Sci.* **1970**, *19*, 1105–1107.

[350] S. L. H. Rebelo, M. Linhares, M. M. Q. Simões, A. M. S. Silva, M. G. P. M. S. Neves, J. A. S. Cavaleiro, C. Freire, *J. Catal.* **2014**, *315*, 33–40.

[351] K. T. Yong, W. C. Law, R. Hu, L. Ye, L. Liu, M. T. Swihart, P. N. Prasad, *Chem. Soc. Rev.* **2013**, *42*, 1236–1250.

[352] K. M. Tsoi, Q. Dai, B. A. Alman, W. C. W. Chan, *Acc. Chem. Res.* **2013**, *46*, 662–671.

[353] J. Xu, O. Shoji, T. Fujishiro, T. Ohki, T. Ueno, Y. Watanabe, *Catal. Sci. Technol.* **2012**, *2*, 739–744.

[354] S. Ito, K. Wakamatsu, T. Sarna, *Photochem. Photobiol.* **2018**, *94*, 409–420.

[355] Y. Xie, B. Yan, H. Xu, J. Chen, Q. Liu, Y. Deng, H. Zeng, *ACS Appl. Mater. Interfaces* **2014**, *6*, 8845–8852.

[356] V. Massey, S. Strickland, S. G. Mayhew, L. G. Howell, P. C. Engel, R. G. Matthews, M. Schuman, P. A. Sullivan, *Biochem. Biophys. Res. Commun.* **1969**, *36*, 891–897.

[357] R. A. Larson, P. L. Stackhouse, T. O. Crowley, *Environ. Sci. Technol.* **1992**, *26*, 1792–1798.

[358] P. S. Song, E. C. Smith, D. E. Metzler, *J. Am. Chem. Soc.* **1965**, *87*, 4181–4184.

[359] W. Yang, C. Liu, Y. Chen, *Langmuir* **2018**, *34*, 3565–3571.

[360] P. Sai Prathima, R. Bikshapathi, V. J. Rao, *Tetrahedron Lett.* **2015**, *56*, 6385–6388.

[361] M. Tada, M. Kohno, Y. Niwano, *J. Clin. Biochem. Nutr.* **2010**, *46*, 224–228.

[362] R. J. Usselman, I. Hill, D. J. Singel, C. F. Martino, *PLoS One* **2014**, *9*, DOI

10.1371/journal.pone.0093065.

[363] A. Yoshimura, T. Ohno, *Photochem. Photobiol.* **1988**, *48*, 561–565.

[364] E. Silva, P. Barrias, E. Fuentes-Lemus, C. Tirapegui, A. Aspee, L. Carroll, M. J. Davies, C. López-Alarcón, *Free Radic. Biol. Med.* **2019**, *131*, 133–143.

[365] P. Sobrado, *Int. J. Mol. Sci.* **2012**, *13*, 14219–14242.

[366] M. W. Fraaije, A. Mattevi, *Trends Biochem. Sci.* **2000**, *25*, 126–132.

[367] D. Leys, N. S. Scrutton, *Curr. Opin. Struct. Biol.* **2016**, *41*, 19–26.

[368] K. H. Van Pée, E. P. Patallo, *Appl. Microbiol. Biotechnol.* **2006**, *70*, 631–641.

[369] V. Massey, in *Biochem. Soc. Trans.*, **2000**, pp. 283–296.

[370] S. Mahmood, A. Khalid, M. Arshad, T. Mahmood, D. E. Crowley, *Crit. Rev. Biotechnol.* **2016**, *36*, 639–651.

[371] S. A. Misal, K. R. Gawai, *Bioresour. Bioprocess.* **2018**, *5*, DOI 10.1186/s40643-018-0206-8.

[372] R. Stuermer, B. Hauer, M. Hall, K. Faber, *Curr. Opin. Chem. Biol.* **2007**, *11*, 203–213.

[373] C. K. Winkler, G. Tasnádi, D. Clay, M. Hall, K. Faber, *J. Biotechnol.* **2012**, *162*, 381–389.

[374] K. Durchschein, M. Hall, K. Faber, *Green Chem.* **2013**, *15*, 1764–1772.

[375] S. Sarkar, A. Banerjee, U. Halder, R. Biswas, R. Bandopadhyay, *Water Conserv. Sci. Eng.* **2017**, *2*, 121–131.

[376] F. Rafii, C. E. Cerniglia, *Appl. Environ. Microbiol.* **1993**, *59*, 1731–1734.

[377] S. Mendes, A. Farinha, C. G. Ramos, J. H. Leitão, C. A. Viegas, L. O. Martins, *Bioresour. Technol.* **2011**, *102*, 9852–9859.

[378] R. L. Singh, P. K. Singh, R. P. Singh, *Int. Biodeterior. Biodegrad.* **2015**, *104*, 21–31.

[379] F. Figueras, B. Coq, *J. Mol. Catal. A Chem.* **2001**, *173*, 223–230.

[380] D. Friedmann, A. Hakki, H. Kim, W. Choi, D. Bahnemann, *Green Chem.* **2016**, *18*, 5391–5411.

[381] J. Z. Bloh, R. Marschall, *European J. Org. Chem.* **2017**, *2017*, 2085–2094.

[382] H. Schmaderer, M. Bhuyan, B. König, *Beilstein J. Org. Chem.* **2009**, *5*, DOI 10.3762/bjoc.5.26.

[383] R. E. Williams, N. C. Bruce, *Microbiology* **2002**, *148*, 1607–1614.

[384] R. M. Kohli, V. Massey, *J. Biol. Chem.* **1998**, *273*, 32763–32770.

[385] T. N. Burai, A. J. Panay, H. Zhu, T. Lian, S. Lutz, *ACS Catal.* **2012**, *2*, 667–670.

[386] J. Yoon, S. H. Lee, F. Tieves, M. Rauch, F. Hollmann, C. B. Park, *ACS Sustain. Chem. Eng.* **2019**, *7*, 5632–5637.

[387] A. Bachmeier, B. J. Murphy, F. A. Armstrong, *J. Am. Chem. Soc.* **2014**, *136*, 12876–12879.

[388] A. Taglieber, F. Schulz, F. Hollman, M. Rusek, M. T. Reetz, *ChemBioChem* **2008**, *9*, 565–572.

[389] M. C. R. Rauch, M. Pesic, M. M. E. Huijbers, M. Pabst, C. E. Paul, M. Pešić, I. W. C. E. Arends, F. Hollmann, *Biochim. Biophys. Acta - Proteins Proteomics* **2020**, *1868*, DOI 10.1016/j.bbapap.2019.140303.

[390] M. U. Luescher, C. V. T. Vo, J. W. Bode, *Org. Lett.* **2014**, *16*, 1236–1239.

[391] H. P. Li, J. J. Zhang, L. Qin, M. D. Zhao, *Res. Chem. Intermed.* **2013**, *39*, 621–629.

[392] M. Hall, C. Stueckler, H. Ehammer, E. Pointner, G. Oberdorfer, K. Gruber, B. Hauer, R. Stuermer, W. Kroutil, P. Macheroux, et al., *Adv. Synth. Catal.* **2008**, *350*, 411–418.

[393] A. Fryszkowska, H. Toogood, M. Sakuma, J. M. Gardiner, G. M. Stephens, N. S. Scrutton, *Adv. Synth. Catal.* **2009**, *351*, 2976–2990.

[394] G. R. Penzer, *Biochem. J.* **1970**, *116*, 733–743.

[395] R. Traber, H. E. A. Kramer, P. Hemmerich, *Biochemistry* **1982**, *21*, 1687–1693.

[396] B. C. M. Martindale, E. Joliat, C. Bachmann, R. Alberto, E. Reisner, *Angew. Chemie - Int. Ed.* **2016**, *55*, 9402–9406.

[397] Y. Pellegrin, F. Odobel, *Comptes Rendus Chim.* **2017**, *20*, 283–295.

[398] S. I. Nehme, L. Crocker, L. Fruk, *Catalysts* **2020**, *10*, 324.

[399] R. D. Draper, L. L. Ingraham, *Arch. Biochem. Biophys.* **1968**, *125*, 802–808.

[400] D. W. Manley, L. Buzzetti, A. MacKessack-Leitch, J. C. Walton, *Molecules* **2014**, *19*, 15324–15338.

[401] D. Kumano, S. Iwahana, H. Iida, C. Shen, J. Crassous, E. Yashima, *Chirality* **2015**, *27*, 507–517.

[402] C. Odaka, T. Mizuochi, *Clin. Exp. Immunol.* **2000**, *121*, 515–522.

[403] N. Cathcart, P. Mistry, C. Makra, B. Pietrobon, N. Coombs, M. Jelokhani-Niaraki, V. Kitaev, *Langmuir* **2009**, *25*, 5840–5846.

[404] N. Cathcart, V. Kitaev, in *J. Phys. Chem. C*, **2010**, pp. 16010–16017.

[405] I. Yokoe, T. C. Bruice, *J. Am. Chem. Soc.* **1975**, *97*, 450–451.

[406] S. I. Murahashi, D. Zhang, H. Iida, T. Miyawaki, M. Uenaka, K. Murano, K. Meguro, *Chem. Commun.* **2014**, *50*, 10295–10298.

[407] K. Bochenek, E. Gudowska-Nowak, *Acta Phys. Pol. B* **2003**, *34*, 2775–2790.

[408] B. O. Burek, S. Bormann, F. Hollmann, J. Z. Bloh, D. Holtmann, *Green Chem.* **2019**, *21*, 3232–3249.

[409] M. Insińska-Rak, A. Golczak, M. Sikorski, *J. Phys. Chem. A* **2012**, *116*, 1199–1207.

[410] J. Kim, J. Lee, P. G. Lee, E. J. Kim, W. Kroutil, B. G. Kim, *ACS Catal.* **2019**, *9*, 9539–9544.

[411] D. Nohr, R. Rodriguez, S. Weber, E. Schleicher, *Front. Mol. Biosci.* **2015**, *2*, DOI 10.3389/fmolb.2015.00049.

[412] C. Feldmeier, H. Bartling, K. Magerl, R. M. Gschwind, *Angew. Chemie - Int. Ed.* **2015**, *54*, 1347–1351.

[413] Y. Imada, T. Kitagawa, H. K. Wang, N. Komiya, T. Naota, *Tetrahedron Lett.* **2013**, *54*, 621–624.